4th HR-HU and 15th HU geomathematical congress "Geomathematics as Geoscience"	23-25 May, 2012

Conference book

"Geomathematics as geoscience"

Editors:

Tomislav Malvić, János Geiger, Marko Cvetković

Impressum

Publisher: Croatian Geological Society, 2012

For publisher: Jasenka Sremac, president of the Croatian Geological Society

Editors: Tomislav Malvić, János Geiger and Marko Cvetković

Circulation: 50 copies

Copy and distribution: Idendum d.o.o., Rijeka, Croatia

CIP record is available in computer catalogue of National and University Library in Zagreb, Croatia, entry number 806064

ISBN 978-953-95130-6-9

Note

The content of proceedings has not been passed English proof reading by native speaker, and that is why solely the authors are responsible for the quality of language usage.

Organizers

Croatian Geological Society (Hrvatsko geološko društvo)

http://www.geologija.hr

Geomathematical Section (Geomatematički odsjek)

http://www.geologija.hr/geomat.php

Hungarian Geological Society (Magyarhoni Földtani Társulat)

http://www.foldtan.hu/

Geomathematical Section (Geomatematikai Szakosztály)

https://www.smartportal.hu/

Committees

Organizing Committee

Prof. Dr. Tomislav Malvić (chairman, INA & Univ. Zagreb, HR)

Prof. Dr. Janos Geiger (vice-chairman, Univ. Szeged, HU)

Marko Cvetković (vice-chairman, Univ. Zagreb, HR)

Marija Bošnjak (Croatian Natural History Museum, HR)

Ana Majstorović Bušić (INA, HR)

Karolina Novak (INA, HR)

Scientific Committee

Prof. Dr. Janos Geiger (chairman, HU)

Prof. Dr. Tomislav Malvić (vice-chairman, HR)

Prof. Dr. Miljenko Lapaine (Univ. Zagreb, HR)

Prof. Dr. Josipa Velić (Univ. Zagreb, HR)

Kristina Novak Zelenika (INA, HR)

Honorary Committee

Acad. Gyorgy Bardossy (Academy of Science, HU)

Prof. Dr. Jasenka Sremac (president, Croatian Geol. Soc.)

Prof. Dr. Janos Haas (president, Hungarian Geol. Soc.)

CONTENT

Student part

APPENDIX

Non-reviewed abstracts

FOREWORD

Dear readers,

The „Epilogue" of the „New Horizons in Central European Geomathematics, Geostatistics and Geoinformatics" published by GeoLitera in 2011 is closed by the following sentence: " We hope, that this is only the beginning of a new series that will be followed by many others in the future.". In fact, this hope has become reality, as it is demonstrated by this volume which is the proceedings of the 4th Hungarian Croatian and the 15th Hungarian Geomathematical Convent, hosted by the city of Opatija (Croatia).

Four years ago, in 2008, the Division of Geomathematics of the Croatian Geological Society agreed to organize joint meetings with its Hungarian counterpart. Since that time it has been a success story. The actual (4th joint convention) has a special importance, since this is the very first time, when this convent is organized outside of Hungary with the hospitality of the Croatian side.

This volume contains the full overview of 21 oral, 7 poster presentations along with the 5 lectures demonstrate the research activity of the members of IAMG Student Chapter, Szeged. The topics range from theoretical approaches through reservoir modeling and methods used in nuclear remediation as well as the most recent innovations of geoinformatical investigations. Authors listed range from employees of major oil industries of Croatia and Hungary (INA, Industrije Nafte, Croatia, MOL Hungarian Oil and Gas Public Limited Company), representatives of the Lybian Petroleum Institute, as well as Universities (University of Zagreb, University of Szeged, Eötvös Lóránd University of Budapest), National Geological Surveys, and the Eötvös Lóránd Geophysical Institute, Hungary.

Here, we special pointed out five very quality student's submissions, which are presented in special part of the congress. These papers represent the

same quality level and have passed the same review process as all other submissions. However, as the researching on the doctoral studies include often more enthusiasm, risk and new ideas than "regular studies", the committee always considered important to offer students to present their work through special section and to be evaluated in a little bit different way but having in mind mentioned criteria.

In the 2012 we also tried to put more attention on three parts of geomathematics, considering it as the more expanding topic in the future geosciences' researching. Those were the usage of neural networks in geology, digital elevation models and theoretical developments. So, the authors of such papers were asked to give little more extended contribution than others, expecting that readers will be satisfied to find some more data on such topics.

We can hope, that this congress will not only help popularize the use of mathematical, and statistical approaches among geo-professionals of the region, will promote further fruitful collaboration, as well.

We hope to meet you the next year in Hungary.

In Zagreb and Szeged, May 2012

The Editors

Tomislav Malvić, János Geiger and Marko Cvetković

REVIEWED PAPERS

Regular part

Successfulness of inter well lithology prediction on Upper Miocene sediments with artificial neural networks

Marko CVETKOVIĆ[1] and Josipa VELIĆ[1]

[1] University of Zagreb, Faculty of Mining, Geology and Petroleum Engineering, Pierottijeva 6, 10000 Zagreb, marko.cvetkovic@rgn.hr, josipa.velic@rgn.hr

Abstract: Several artificial neural networks were trained on well log curves of spontaneous potential, shallow and deep resistivity from one well for the purpose of lithology prediction in a second well. Data was taken from Upper Miocene intervals from two wells in Kloštar field. Two learning approaches and three methods of prediction were applied. Results show that the best approach for inter well lithology prediction is by training the neural network on a whole well interval. Oppositely, it was trained one neural network for each lithostratigraphic formation in Upper Miocene clastic sediments.

Key words: artificial neural networks, lithology prediction, Pannonian Basin, Miocene, Croatia.

1. INTRODUCTION

Well log data from Kloštar oil and gas Field, located in SW part of the Pannonian Basin (**Figure 1**), was used to test the application of neural networks for lithology prediction in clastic intervals of Upper Miocene sediments. Although prediction of lithology was already proven successful (Cvetković et al., 2009), it was only for 1D prediction, e.g., training of the artificial neural network (ANN) and prediction was successful only if both were made in the same well. Here, the successfulness of 2D prediction will be presented which will be done on a much larger depth interval. Additionally, two types of learning procedures will be made – one for the whole well interval, and one for each clastic Neogene formation individually.

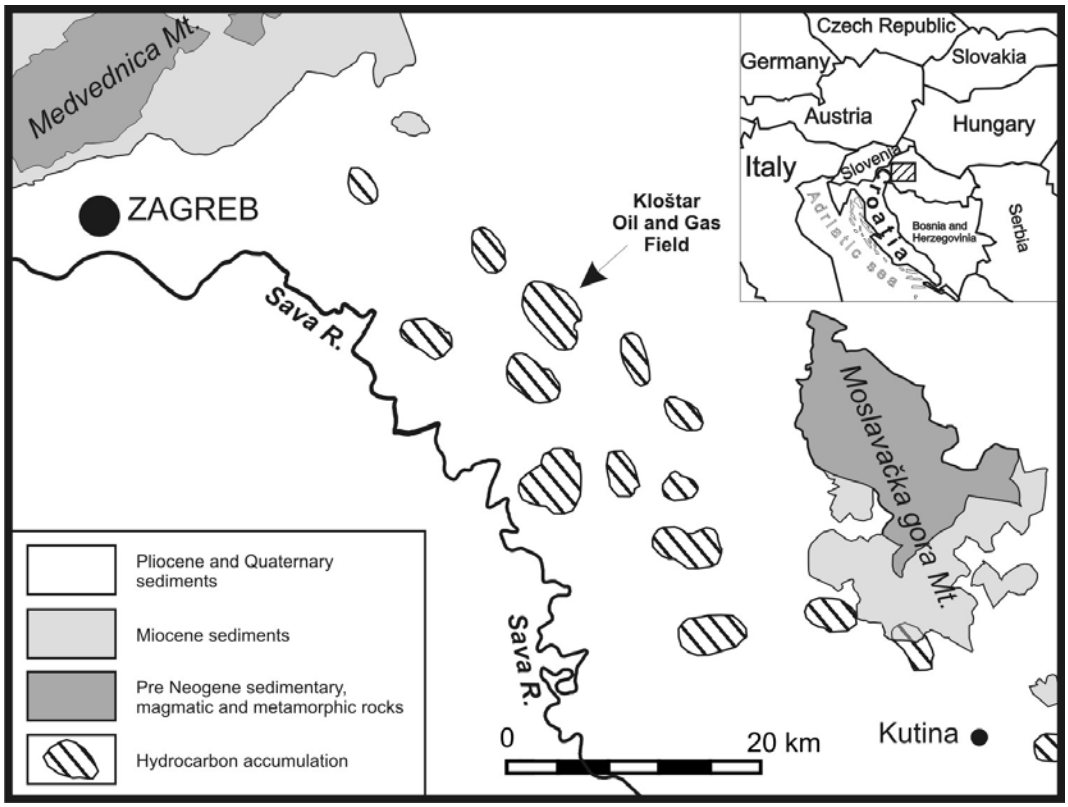

Figure 1: *Location of Kloštar oil and gas Field (Velić et al., 2011)*

2. BASIC GEOLOGICAL SETTINGS

The ANN analysis will be limited only to clastic Upper Miocene intervals which are represented by sediments of Prkos, Ivanić-Grad, Kloštar Ivanić and Široko Polje Formations. These are generally variations of marls and sandstones in Prkos, Ivanić-Grad, Kloštar Ivanić and Široko Polje Formations with sporadic occurrences of breccias and biogenic limestones in the oldest parts of Prkos Formation, and lignites, sand and clays in the youngest interval of Široko Polje Formation. Youngest clastic interval of Lonja Formation (Pliocene, Pleistocene and Holocene) was not included in the analysis because of the small thickness (<150 m) in the selected locations.

3. ARTIFICIAL NEURAL NETWORKS

The basic architecture of neural networks consists of neurons that are organized into layers. A neuron is a basic element of a network that is mathematically presented as a point in space toward which signals are transmitted from surrounding neurons or inputs (**Figure 2**).

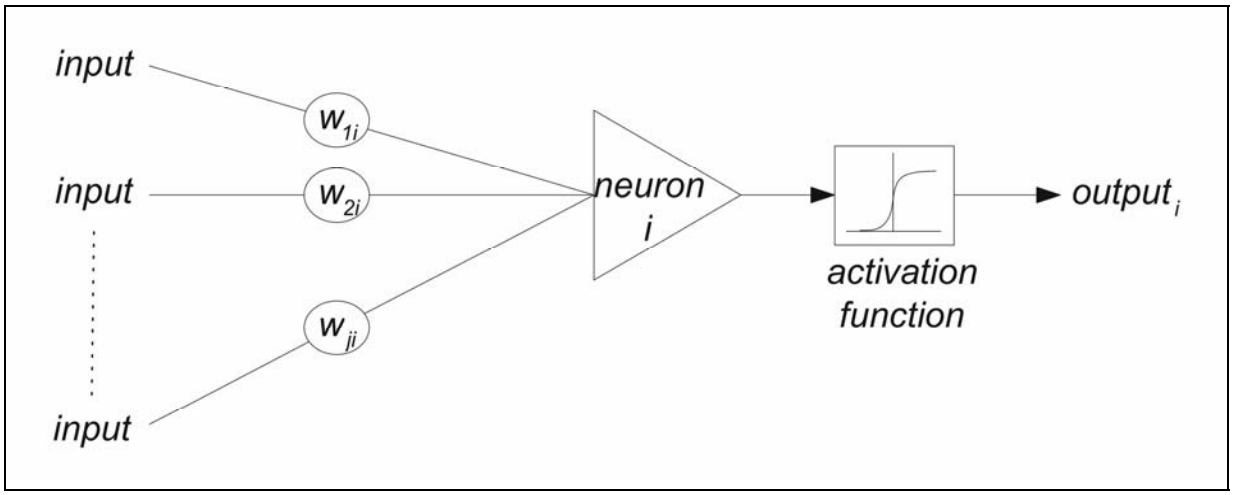

Figure 2: *Basic architecture of an artificial neuron*

The value of a signal on the activity of a neuron is determined by a weight factor multiplied by a corresponding input signal. Total input signal is determined as a summation of all products of weight factor multiplied by the corresponding input signal given by

$$u_i = \sum_{j=1}^{n} (w_{ji} \cdot input_j) \tag{1}$$

where *n* represents the number of inputs for the neuron *i*. If the total input signal has a value more than the sensitivity threshold of a neuron, then it will have an output of maximum intensity. Alternatively, a neuron is inactive and has no output. Value of the output is given by

$$output_i = F(u_i \cdot t_i) \tag{2}$$

where *F* represents the activation function and t_i, the targeted output value of neuron *i*. One can find a more detailed description of neural networks

basics and methods in McCulloch and Pitts (1943), Rosenblatt (1958), and Anderson and Rosenfeld (1988).

For this analysis, only multilayer perceptron (MLP) network was used. The MLP network is based on a backpropagation algorithm that has one or more hidden layers. Also, the network can use a two-phase learning with algorithms such as conjugate gradient descent (Gorse et al., 1997), quasi-Newton (Bishop, 1995), Levenberg–Marquardt (Levenberg, 1944; Marquardt, 1963), quick propagation (Fahlman, 1988), and delta-bar-delta (Jacobs, 1988) all using a program of packages that allow such training. The MLP is more successfully applied in classification and prediction problems (Rumelhart et al. 1986) and is the most often used neural network in solving geological problems. Neural networks have been successfully applied in petroleum geology problems such as determining reservoir properties (e.g., lithology and porosity) from well logs (Bhatt, 2002) and well-log correlation (Luthi and Bryant, 1997). In the Croatian part of the Pannonian Basin, only a few petroleum geology research projects have been performed. In these studies, clastic facies were determined from well logs (Malvić, 2006, Cvetković et al., 2009) and porosity was predicted based on well and seismic data (Malvić and Prskalo, 2007).

4. METHODOLOGY AND ANALYSIS RESULTS

Lithology was firstly manually determined in one well (Klo-105) for the purpose of ANN training based on well log curves of normalised spontaneous potential (SPN), shallow resistivity (R16) and deep resistivity (R64). These were also used as input data for ANN analysis. Two types of data preparations were used. In the first the data was split for each Formation and training was made for each Formation individually. In the second, the whole well interval was used for ANN training. The ANN learning process divides the input data into two groups – the test and validation groups. The first set of data is used for learning purposes while the second one is used

for testing the prediction possibilities of the trained ANN. Accordingly, two sets of performance values are given, one for training and one for test. Performance values range from 0-100 where 100 represents perfect match or 100% of prediction. Most successful ANN for each Formation and for the whole well interval with their properties is presented in **Table 1**.

From the data presented in **Table 1** all neural networks had very low training and test error, less than 7% of maximum training error in the case of Kloštar Ivanić Formation. The next step is employing the trained networks on a new set of data, in this case on the Miocene clastic interval of well Klo-106. Three types of lithology predictions had been applied:

1. Prediction by a single ANN for the whole clastic Miocene interval, labelled LITH A in **Figure 3**,
2. Prediction by a single ANN individually for each formation, labelled LITH B in **Figure 3** and
3. Prediction by an ensemble of ANN's trained on each formation for the prediction on the whole clastic Miocene interval, labelled LITH C in **Figure 3**.

	Type	Train	Test
Whole interval	MLP 3-10-3	97.38641	97.37336
Široko Polje Formation	MLP 3-40-2	99.43228	99.23664
Kloštar Ivanić Formation	MLP 3-19-2	94.02460	93.26923
Ivanić-Grad Formation	MLP 3-10-2	99.65636	100.0000
Prkos Formation	MLP 3-33-2	97.66082	97.05882

Table 1: *Overview of the most successful neural networks for each formation and for the whole Miocene clastic interval*

Even though all ANN's had a very low training error, only the one that was trained in the whole Miocene clastic interval (LITH A in **Figure 3A**) successfully predicted the lithology in the well Klo-106. Individual networks for each Formation, as well as ensemble were only partially successful, only in Kloštar Ivanić Formation (LITH B and C in **Figure 3B**).

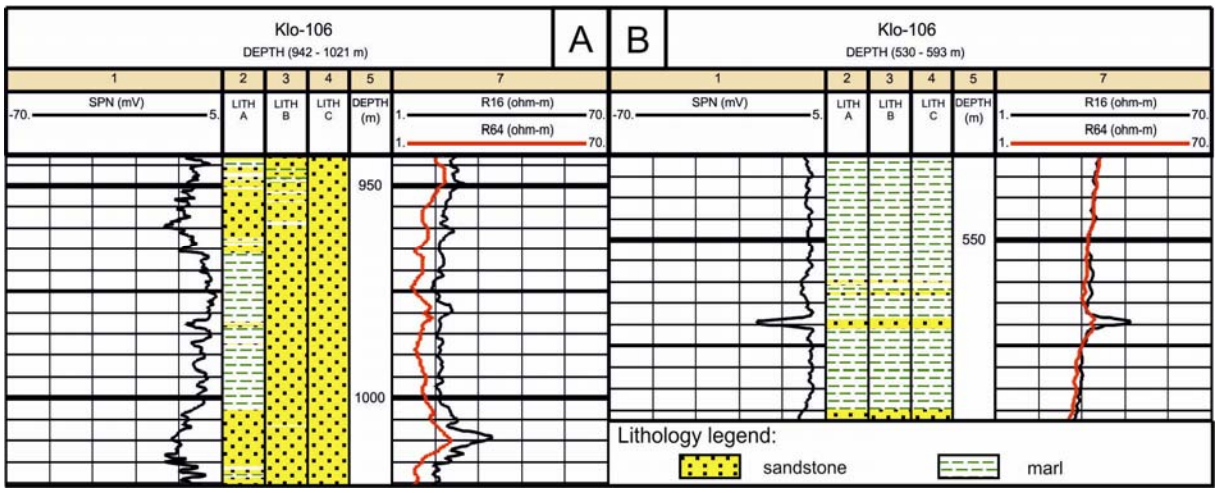

Figure 3: *Well log section showing the poor results of lithology prediction with ANN's trained on a single formation (LITH B) and by an ensemble (LITH C) in Ivanić-Grad Formation (**A**) and successfulness of all three in Kloštar Ivanić Formation (**B**)*

5. CONCLUSIONS

Inter well prediction of lithology via ANN is possible and successful only in the case of an ANN trained on the large interval. Possibly, ANN's trained in each formation were over trained and lost their ability to successfully predict lithology on new data even though their training and testing error were minimal.

6. ACKNOWLEDGEMENTS

This work is part of a research project "Stratigraphical and geomathematical researches of petroleum geological systems in Croatia" (project no. 195-

1951293-0237), financed by the Ministry of Science, Education and Sports of the Republic of Croatia.

Authors would also like to thank INA-Industry of Oil Plc., E&P of Oil and Gas (Zagreb) for the data and Schlumberger and Synergy for supplying academic licenses for Petrel and Interactive Petrophysics to the Faculty of Mining, Geology and Petroleum Engineering in Zagreb.

7. REFERENCES

ANDERSON, J.A. & ROSENFELD, E. (1988): Neurocomputing**:** Foundations of Research. MIT Press, Cambridge, 729 p.

BHATT, A. (2002): Reservoir properties from well logs using neural networks: doctoral dissertation, NTNU, Trondheim, 151 p.

BISHOP, C.M. (1995): Neural Networks for Pattern Recognition, 1st edn. Oxford University Press, New York, 504 p.

CVETKOVIĆ, M., VELIĆ, J., MALVIĆ, T. (2009): Application of neural networks in petroleum reservoir lithology and saturation prediction. Geologia Croatica, 62, 2, 115-121.

FAHLMAN, S.E. (1988): Faster Learning Variations on Back-propagation: An Empirical Study. In: Proceedings of the 1988 Connectionist Models Summer School, Los Altos, 38-51.

GORSE D, SHEPHERD, A. & TAYLOR, J.G. (1997): The new ERA in supervised learning. Neural Networks, 10, 2, 343-352.

JACOBS, R.A. (1988): Increased rates of convergence through learning rate adaptation. Neural Networks, 1, 295-307.

LEVENBERG, K. (1944): A method for the solution of certain problems in least squares. Quardt. Appl. Math., 2, 164-168.

LUTHI, S.M. & BRYANT, I.D. (1997) Well-log correlation using a back-propagation neural network. Math. Geol., 29, 3,, 413-425.

MALVIĆ, T (2006) Clastic facies prediction using neural network (case study from Okoli field). Nafta, 57, 10, 415-431.

MALVIĆ, T & PRSKALO, S (2007): Some benefits of the neural approach in porosity prediction (Case study from Beničanci field). Nafta, 58, 9, 455-467.

MARQUARDT, D.W. (1963): An algorithm for least-squares estimation of nonlinear parameters. J. Soc. Indust. Appl. Math. 11, 2, 431-441.

McCULLOCH, W.S. & PITTS, W. (1943): A logical calculus of ideas immanent in nervous activity. B. Math. Biol., 5, 4, 115-133.

ROSENBLATT, F. (1958): The perceptron: A probabilistic model for information storage and organization in the brain. Psychol. Rev., 65, 6, 386-408.

RUMELHART D.E., HINTON, G.E. & WILLIAMS, R.J. (1986): Learning internal representations by error propagation. In: RUMELHART, D.E., McCLELLAND, J.L. (ed) Parallel Distributed Processing, Vol.1. MIT Press, Cambridge, 381-362.

VELIĆ, J., MALVIĆ, T. & CVETKOVIĆ, M. (2011): Palinspastic reconstruction of synsedimentary tectonics of Neogene and Quaternary sediments in the Kloštar Field (Sava Depression, Pannonian Basin, Croatia). Zeitschrift der Deutschen Gesellschaft für Geowissenschaften, 162, 2, 193-203.

Regional basin depth mapping, supported by parametric interpolation of seismic velocity field

Greg DETZKY, László ZILAHY-SEBESS, László VÉRTESY, Ágnes GULYÁS
Eötvös Loránd Geophysical Institute of Hungary, detzky@elgi.hu

Abstract: The geothermal energy industry has appeared as a new agent among the users most intensively utilising structural geological information. The geo-scientific investigation, previous to geothermal exploitation is based on the same technology as of the CH exploration. In this context a well established knowledge on real geometry of studied basins is similarly substantial. Achieving this aim is impossible without a proper conversion of the most abundant data, the 2D seismic reflection time-sections into the depth. There are many traditional methods for this purpose, involving some kind of direct interpolation. Here we present a new method to be used for calculating of 3D seismic velocity distribution, which is based on 1D approximation of local functions and subsequent spatial interpolation of analytical functions' parameters. These parameters have real geophysical meaning and hence, their mapping beside that being a part of the modelling procedure, inherently can contribute the basin analysis as well.

Key words: seismic velocity, 3D interpolation, time-depth conversion.

1. INTRODUCTION: WHY 3D INTERPOLATION OF SEISMIC VELOCITIES IS NEEDED?

In reflection seismology, the interpretation is traditionally carried out on time sections. This demands joint utilising of information derived from tectonic and stratigraphic elements on the timesections and well data given in depth space. So that the stratigraphic data of wells, and objects from reflection seismics could be brought to relation, the depth data from wells

should be transformed into reflection time or sometimes contrary to this, seismic reflection time into depth. In a better case, the sonic or VSP data are available along wells enabling direct and precise definition of reflection time–depth dependence. When well-log velocity information is not available, it is preferable to obtain interpolated velocity data for well sites, from such other sources as stacking velocity analyses or seismic refraction.

Eventually the integrated structural interpretation results must be presented in depth to use in geological tasks of oil or geothermal resource preparation which demands these data to be given strictly in this dimension. Therefore, a reliable and consistent approximation of velocity field at any point of studied 3D space is a precondition of all the mentioned issues.

2. PARAMETRIC INTERPOLATION

2.1. Proposed Parametric Interpolation Process for Seismic Velocities

In the territories investigated by 2D seismic projects, the most diverse source of velocity data is the set of NMO or DMO velocity functions always available from the conventional velocity analysis phase of the processing. Compared to seismic velocities determined by other direct methods, the stacking velocities have medium accuracy and resolution, but usually provide distributed data on the area, forming a good input for regional interpolation of 3D velocity field.

The parametric interpolation procedure replaces the direct 3D interpolation of velocity samples by a 1D approximation and by a 2D interpolation performed afterwards. In the 1D approximation (Pronin, 2003), unique parameter sets are calculated for a properly chosen analytic function, optimised to best fitting to the functions on original velocity analysis locations.

Good candidate for analytical 1D approximation of seismic velocity fields is a function having finite asymptotic limits and being able to differentiate at any point. The algebraic polynomials are not amongst the best choices because they tend to produce values extremely different from base data ranges even in the close vicinity of the interpolation intervals.

In the second stage of the parametric interpolation the parameter sets of the approximation function instances at different surface points, must be interpolated horizontally (spatially) in 2D. As a result the planar "function space" of the local vertical approximation functions of the 3D velocity space being created, represented by surface parallel grids for each approximation parameter. It makes a consistent estimation of the velocities possible at any 3D point in TWT and location dimension. In the third stage of the whole procedure, a parametrically interpolated velocity field could be used for practical time-depth transformation purposes.

2.2. Mathematical Introduction of an Approximation Function Convenient for Parametric Interpolation of Seismic Velocity Data

Conventional seismic velocity analysis operations of reflection processing flow produce data sequences close to the $V = V_{rms}(T)$ velocities along ascendant reflection time values relating to the surface reference locations of given velocity analyses. Replacing NMO stacking velocities in case of nearly horizontal layers, or DMO stacking velocities in case of dipping layers with V_{rms} velocities yields a satisfying approximation in the exploration works with average requirements (Veeken et al., 2005).

Definition of our particular analytic equation used for 1D approximation of velocity data has been done by just taking the character of the curve shapes without any other consideration. It involved about 2000 real velocity functions, originating from different areas of the Pannonian Basin. According to the experience, the shape of velocity function curves could be

approximated with good fitting by a category of functions provided in **Figure 1**. The general definition

$$V = V_0 + a\frac{bt-\tau}{\sqrt{(bt-\tau)^2+1}} \qquad (1)$$

is the equation (1). This is a form of the derivative of a hyperbole with a vertical axle, extended with proper transformation parameters. The function possesses the aforementioned selection properties, the asymptotic co-domain, overall derivability and simple parameter settings. In the practice, a license-free ActiveX module, (Pronin, 2003) based on the known in geophysics Levenberg-Marquardt-algorithm had been used for the calculations.

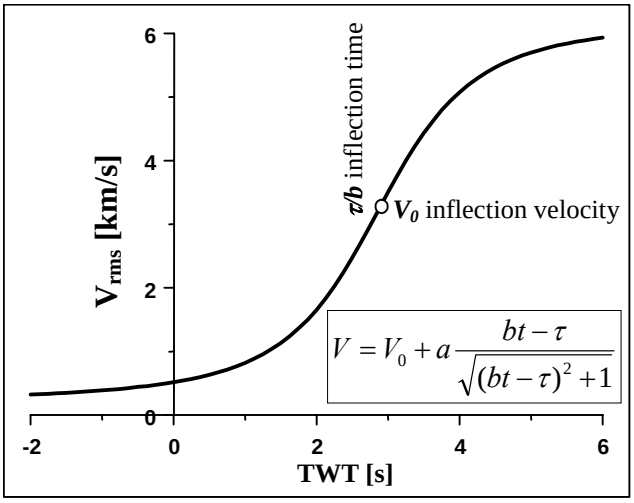

Figure 1: *A Function category suitable for approximation of V_{rms} velocity functions occuring in the Pannonian Basin. Parameters of this curve: V_0=3.2 km/s; a=3 km/s; b=0.7; τ=2 s (more information in the text)*

The parameters of the given approximation function could be assigned to and named by such expressive physical meanings as *inflection velocity V_0*, which is the velocity at the inflection point of the function; *as velocity range a*, which is the difference between the asymptotic and the inflection velocity; *as inflection gradient b*, which is the differential coefficient in the inflection

point; *as inflection time* τ/b, which is the time value of the function at the inflection point measured in dimension of reflection time. At this τ/b time, the gradient of *Vrms* velocity reaches the greatest value *ab*, and the velocity itself is equal to V_0.

2.3. Other useful properties of the selected approximation function

Let a sort of functions is generally defined by the form (1) to be used for the approximation of the input V_{rms} data sequences. Substituting it into the differential counterpart (3) of the well known integral equation (2) describing the interdependency of the interval and the RMS velocities in the continuously variable medium

$$TV^2(T) = \int_0^T v^2(t)dt \tag{2}$$

$$[tV^2(t)]'_t = V^2 + 2tVV' = v^2(t) \tag{3}$$

a more complex but from the viewpoint of numeric computation still sufficiently simple and useful equation can be earned in the following form

$$v^2 = V^2 + 2V\frac{bt}{(bt-\tau)}\left[(V-V_0) - \frac{1}{a^2}(V-V_0)^3\right] \tag{4}$$

The form (4) is an analytical equation defining vertical 1D approximation of the $v = v_{int}(t)$ interval velocity to be referred to at any surface point by 2D interpolation of its parameters. Numerical integration of square root of (4) provides base data in 3D space for the time-depth conversion at any predefined accuracy.

2.4. Testing of the Introduced Approximation Function by Real Data

A batch mode drawing program had been developed for graphical quality control of the approximation. It is jointly plotting the original samples and approximation curves and in such a way provides a good visual checking tool.

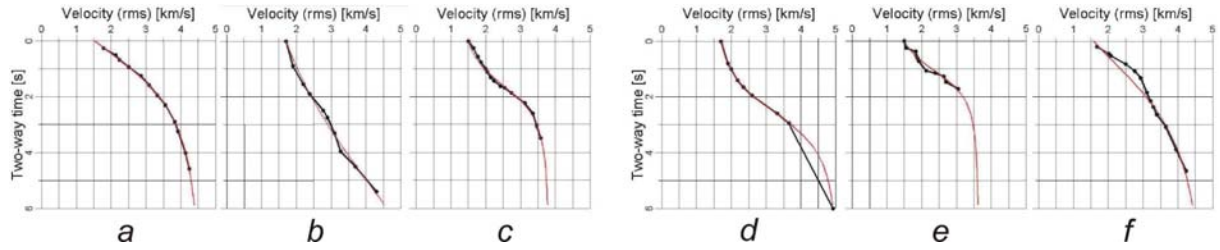

Figure 2: *Typical Vrms function curves and quality of analytical approximation (good fitting: a–convex curve, b–concave curve, c–inflection curve; bad quality fitting: d–missing data, e–uncertain and short input sequence, f–exotic shape)*

An occasional occurrence of bad adaptability of the applied approximation algorithm or the chosen function is very rear. In most of cases the error is less than the sampling uncertainty of velocity analysis itself in the preceding seismic processing. Most of bad quality fits have caused by mistype errors of the input data, and not by stratigraphic extremities. Preserving adequate velocity values by approximation even on short and "noisy" input data indicates the stability of the chosen functions and algorithm (**Figure 2**).

Isoline mapping of the RMS difference between original V_{rms} velocities and approximated values is probably the most convenient way of quality and reliability checking of the interpolated velocity field. Considering the data of test area, the RMS error of approximation is below 30 m/s on most of the area.

3. PRACTICAL APPLICATION OF THE PARAMETRIC INTERPOLATION

3.1. Parametric Mapping

The second computing step of the parametric interpolation is the horizontal 2D interpolation of parameters of 1D approximation functions fitted to vertically spreading original velocity functions. Isoline maps of parameters are useful "side products" of the procedure. Parameters used here could be related to regional distribution of different geological attributes.

Deviation of the vertical velocity gradient from values typical for normal compaction trends is mainly influenced by grain size and mineral content of the sediments (Mészáros and Zilahi-Sebess, 2001). Inflection velocity relating to the depth of the greatest increasing, denotes a zone where in the compaction state, (mainly affecting seismic velocities) the lithostatic effect and age of the rock, (correlating well with depth Meskó, 1994), predominate the effect of the unperfect lithogenesis. The reason for negative inflection-time anomalies may be the uplifting movement periods in the prehistory of the basin evolution.

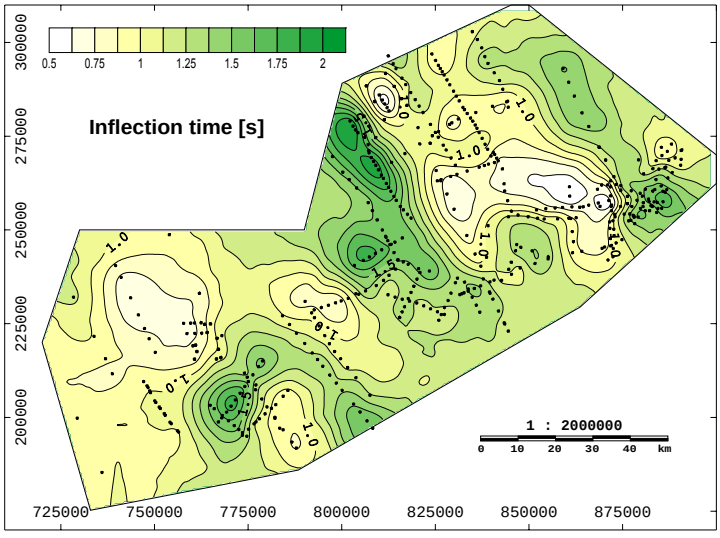

Figure 3: *Parameter map of the 'Inflection time' on the test area*

The same effect was detected using other indicators in some areas of the Pannonian Basin with greater scale (Horváth and Cloetingh, 1996). The ideas above and the isoline map shown by **Figure 3** of the parameter τ/b are provided here just as examples of even more possibilities (Detzky, 2008).

3.2. Time-Depth conversion

In the case of parametric interpolation, the entire interpolated 3D seismic velocity field of an area is represented by horizontally gridded numeric parameters of the 1D (vertical) analytical function. Obvious application of such data set is the conversion to depth of seismic reflection horizons initially given in reflection time. The application result is demonstrated here by the isoline map of the Prepannonian horizon (**Figure 4 right**) converted from the reflection time map (**Figure 4 left**).

Conversion needs the reflection time based 3D interval velocity space. This is available by parametric interpolation in each grid-point according to the equation (4) (in case of the approximation function introduced in chapter 2.2).

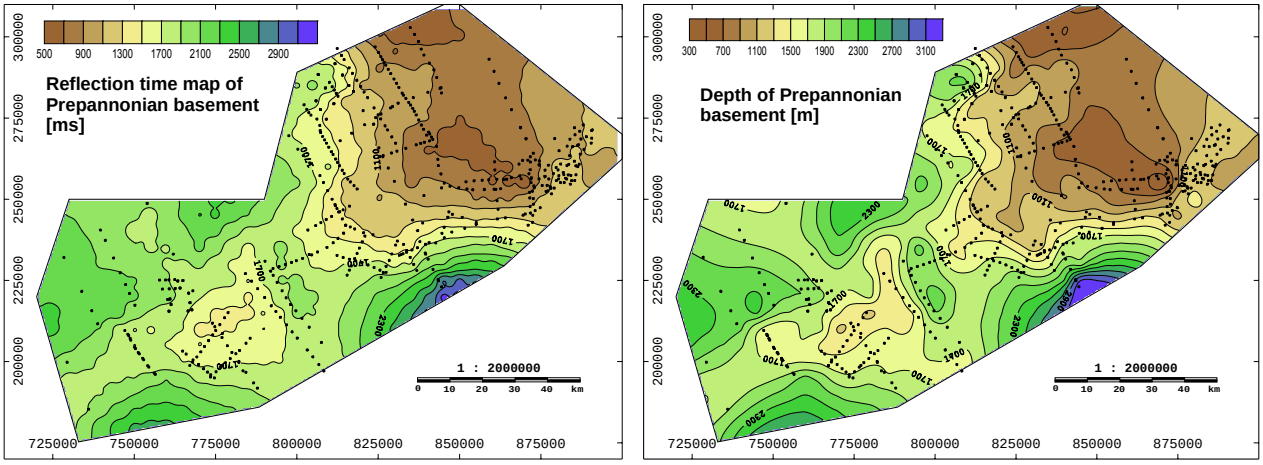

Figure 4: *Reflection time map (left) of the prepannonian basement, compiled from seismic interpretation data of the test area (apx. 1500 km of overall section length) and prepannonian basement depth (right) calculated using velocity field defined by parametric interpolation*

4. CONCLUSION

The parametric interpolation of seismic velocity fields in 3D space is a novel method for to perform seismic time-depth conversion. It has beneficial properties in two special regards compared to other ones:

– It simplifies the calculation originally rising in most cases as 3D problem to a 1D approximation and 2D interpolation executed sequentially.

– It is possible to transfer the usual anisotropy in velocity field by function characteristics to the interpolated result without special mathematical tools, addressed for this particular purpose.

It could be stated that (chapter 2.4) the fitting of approximation function selected for parametric interpolation is possible with such a low level of error (5-50 m/s) which falls in order of accuracy of the original numeric data sets. (It is approved by near 2000 real NMO velocity functions from the Pannonian Basin.)

Parameter maps are useful side products of the parametric interpolation process. These are capable of exploring regional distribution of different geophysical characteristics of the investigated area (chapter 3.1).

Transformation from seismic reflection time to depth based on parametrically interpolated seismic velocity field could serve a result with accuracy adequate to practical requirements.

The demonstrated computing principle of the parametric interpolation has a general nature and it is not necessary to restrict to the interpolation of the 3D seismic velocity fields.

5. REFERENCES

DETZKY, G. (2008): Parametric interpolation of seismic velocity field Geophysical Transactions, 45, 3, ELGI, Budapest.

HORVÁTH F. and CLOETINGH, S. (1996): Stress-induced late-stage subsidence anomalies in the Pannonian basin. Tectonophysics, 266, 287-300.

MESKÓ A. (1994): Rugalmas hullámok a földben (Elastic Waves in Earth – in Hungarian) Academic press, Budapest, 118– 139.

MÉSZÁROS, F. and ZILAHI-SEBESS, L. (2001): Compaction of sediments with great thickness in the Pannonian Basin. Geophysical Transactions,44, 1, ELGI, Budapest.

VEEKEN, P., FILBRANDT, J. and AL RAWAHY, M. (2005): Regional time-depth conversion of the Natih E horizon in Northern Oman using seismic stacking velocities. First Break, 23, August 2005.

URL:

PRONIN, A. (2003): DMFitter ActiveX control http://fitting.datamaster2003.com/

Reliability enhancement of groundwater estimations

Zoltán Zsolt FEHÉR[1,2], János RAKONCZAI[1],
[1]Institute of Geoscience, University of Szeged, H-6722 Szeged, Hungary, [2]e-mail: zzfeher@geo.u-szeged.hu

Abstract: The Danube Tisza Interflow, located in the middle part of Hungary, was afflicted by a serious groundwater level (abbr.: GWL) reduction. This study aims to analyse the spatiotemporal progress of the change taking care with problems that impairing the precision of spatial extrapolation. After preliminary analyses of September GWL datasets, 100 realizations of a sequential Gaussian co-simulation were created applying the Markov II type simple cokriging estimator. Since GWL roughly follows the shape of the relief, DEM-1000 is used as auxiliary data. The expected type grids of e-type estimations can be applied to (1) analyse the trend of absolute groundwater deficit volume, (2) make distinction between areas behaving differently, and (3) continue complex hydrological analyses in the future.

Key words: geostatistics, uncertainty, sequential simulation, auxiliary data, groundwater.

1. INTRODUCTION

Basic thesis in hydrology that multi-year average of the groundwater level (GWL) doesn't show significant changes unless the hydrological elements changes drastically or serious external impacts are taken. The volume, annual distribution and intensity change of precipitation as well as anthropogenic interventions have led to a somewhere excess than 10 meter GWL reduction on the Danube-Tiszainterflow, central Hungary.

Several models and studies were dealt with the water level reduction, but without the consideration of spatial relationships. Nevertheless, groundwater

flows and transport systems are affected by heterogeneity, namely that the spatial continuity of the property changes with distance and direction. Geostatistical approaches are designed to handle spatial characteristics of the site using variograms.

2. METHODS

2.1. Multi Gaussian Approach

Kriging as interpolation method is a trivial way to evaluate the GWL with the consideration of spatial heterogeneity. The results depend only on the geometric structures of the property. The kriged results the best local linear estimation of the expected property in the sense of smallest squared differences, however it has several disadvantages. (1) Kriging behaves as low pass filter, thereby can smooth some small details of the GWL. (2) Estimation error depends only on the data configuration and does not on the input values. (3) Only kriging deviation maps can be created, since estimation error is not quantifiable in the absence of exact water level observation at any grid node.

The results of applied sequential Gaussian simulation give more detailed images (realizations)of the GWL. That is, this method can express the uncertainty of estimations at any grid node. Instead of using static data structure, multiple equiprobable realizations are generated on random data point structures, by continuous inclusion of previously simulated grid nodes. As result of the grid node estimations both the mean and standard deviation is known, but rather than choose the mean at each grid node, SGS takes a random value from this distribution along with its probability level (Deutsch and Journel, 1998; Journel, 1993).

Related grid node estimations of generated realizations set up a statistical distribution. These distributions then determine grid by grid the expected value and standard deviation of the GWL (Deutsch and Journel, 1998).

Preliminary studies (Pálfai, 1994) stated a very strong relationship between topography and water reduction therefore an elevation model as secondary information may improve estimation results. Various methods - kriging with locally varying mean (Goovaerts, 1997), cokriging (Isaaks and Srivastava, 1989), regression kriging (Ahmed and De Marsily, 1987) were developed for incorporating dense secondary information. Among these methods in this study the simple collocated cokriging approach is compared in interpolation and simulation cases.

Simple cokriging and simple Gaussian co-simulation were performed using dense topography as auxiliary data and GWL presented the primary variable. The *NEWCOKB3D* program (Xianlin and Journel, 1999) is used for cokriging and *SGSIM_FC* (Journel and Shmaryan 1999) to perform co-simulations. Both application is open source and available on the homepage of Stanford Centre for Reservoir Forecasting. The applied methods in this study is based on simple kriging (Deutsch and Journel, 1998), with the assumption that the trend component is a constant known mean**.** The kriging equation system is expressed as

$$C * w = D, \qquad (1)$$

where "w" is the kriging weight matrix to be solved, "C" is the covariance matrix between all measured points and "D" for the covariance matrix for the estimated grid node versus any measured points. All covariances are calculated based on the variogram model of the property (Isaaks and Srivastava, 1989).

2.2. Determination of cokriging weights

The *classical Simple Cokriging* approach (Isaaks and Srivastava, 1989) uses the Linear Model of Coregionalization (LMC) namely the above mentioned C and D matrices are extended with auxiliary and cross covariates. Thus not

only the primary data variogram but all auxiliary data variograms and all cross variograms are necessary to determine the covariances. The difficulty of LMC is, that all direct $\gamma_{ii}(h)$and cross $\gamma_{ij}(h)$variogram structures (1) has to be modelled simultaneously using the same variogram structures and (2) must be adequate to all experimental, direct and cross variograms to guarantee positive definiteness and proper regionalized correlation coefficients (Isaaks and Srivastava, 1989). Special case of cokriging is a so called *collocated cokriging*whilesecondary data is known (or previously interpolated) at each node to be estimated. For a situation of strictly collocated cokriging two solutions were developed to ease variogram modelling (Journel, 1999; Xianlin and Journel, 1999; Shmaryan and Journel, 1999). In Markov Model I. (MM 1) the cross variogram is derived from the primary variogram while in Markov Model II. (MM2) the cross covariance is modelled proportional to the secondary variable variogram (Journel, 1999). In this study MM2 was preferable, since (1) topography is more densely sampled; therefore its experimental variogram is more reliable than of the GWL data, and(2) Markov Model 1 is based on the Markov filtering hypothesis (Xianlin andJournel, 1999) in which the conditioning of the auxiliary variable by the collocated primary datum filters the influence of farther primary data. This thesis can't be adapted in our case, since topography data is more densely available than groundwater observations. In case of MM2 the variances and covariances are given by datasets, only the topography variogram and the correlation residual variogram of the GWL is need to be modelled. The cross variogram can becalculated using the following expression:

$$\gamma_{12}(h) = \sqrt{\frac{C_{11}(0)}{C_{22}(0)}} * \rho_{12}(0) * \gamma_{22}(h) = \alpha * \gamma_{22}(h) \qquad (2)$$

where $\gamma_{12}(h)$ is proportional to the direct variogram $\gamma_{22}(h)$ of the topography data with a proportionality coefficient that includes the correlation coefficient

$\rho_{12}(0)$ and the variances of GWL $C_{11}(0)$and topography $C_{22}(0)$variable (Shmaryan and Journel, 1999). The primary variogram covariance function is expressed by the sum of the covariance and covariance residuals (**Eq. 3.**) between the GWL and topography data. Since the secondary variogram is given, only the residual variogram$\hat{\gamma}_R(h)$has to be calculated. The residual variogram can be modeled; (1) using the experimental variogram of the normalized regression residuals for the GWL; or (2) by analytical approaches. (Xianlin and Journel, 1999)

$$\gamma_{11}(h) = \alpha^2 * \gamma_{22}(h) + \hat{\gamma}_R(h) \qquad (3)$$

where $\gamma_{11}(h)$ is the primary variogram$\hat{\gamma}_R(h)$is the residual variogram andα is the angular coefficient of the linear regression curve.

2.3. Procedure of the water level estimation

This procedure includes:

1. Transform GWL and topography datasets to normal scores;
2. Determine linear regression residuals and correlation coefficients between GWL and well elevation data;
3. Compute variograms from normal scores for secondary $\gamma_{22}(h)$ and regression residual $\hat{\gamma}_R(h)$;
4. Create 100 sequential Gaussian co-simulation realizations and perform simple collocated cokriging (**Figure 2d.**)of the GWL using the topography and residual variogram model, along with the correlation coefficient;
5. Back transform the results to original dimensions;
6. Produce expected type estimations (**Figure 2c.**)

3. RESULTS

Given September monthly average GWL time series (above sea level) of 213 observations between 1976 and. These wells represent the GWL fluctuation across the study area. In addition, given a 1000-meter resolution DEM. (**Figure 1.)**.

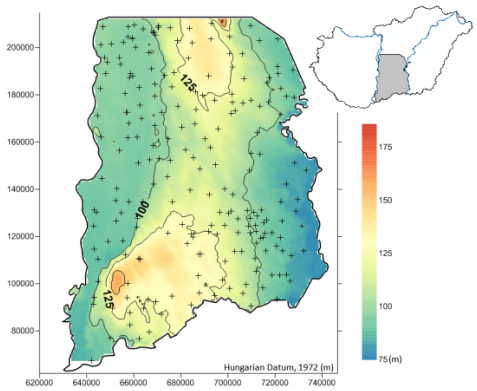

Figure 1:*Well distribution and topography (m.s.l.) of the study area*

The only well that shows outliers systematically was left in the dataset since according to Goovaerts(1997)in environmental applications large values may indicate potentially critical points so they should be removed only if they are clearly proved to be wrong. Exploratory analyses of annual cross-selections established that each annual dataset (1) differs significantly from any theoretical distribution; (2) correlates strongly with the others; (3) the corresponding experimental variograms are quasy similar; (4) correlates significantly with well elevations. A significant difference was revealed between the experimental variogram surface of well elevations and a more densely sampled topography data. This statement along with the strong correlation between GWL data and elevation reveals the unreliability of the existing observation network. As presented before the direct variogram model for DEM (**Eq.4.**), the correlation coefficient and the variogram model of regression residuals (**Eq.5.**) are required for Markov Model 2 to determine the primary and cross variograms.

$$\gamma_{2_2}(h) = 0.1 + 0.53 * Sph\left(\frac{177°}{32000m}\frac{87°}{9697m}\right) + 0.46 * Sph\left(\frac{29°}{31360m}\frac{119°}{9224m}\right) \quad (4)$$

$$\hat{\gamma}_R(h) = 0.38 + 0.46 * Sph(9350m) + 0.16 * Sph(32300m) \quad (5)$$

Contour maps of different approaches show that sequential Gaussian simulation (**Figure 2a.**) whereas highlights local details, it is still significantly determined by the groundwater variogram model applied. Examining on large scale, even application of Ordinary Kriging (**Figure 2b.**) may give better results on the water level but without the consideration of elevation information. Simple Cokriging overestimated and still smoothed the water level but now rough contours of the elevation can be observed (**Figure2d.**). Only sequential co-simulation seems to honour the reality of the inputs (**Figure 2c.**) while results better local estimates than Simple Cokriging (**Figure 3.**).

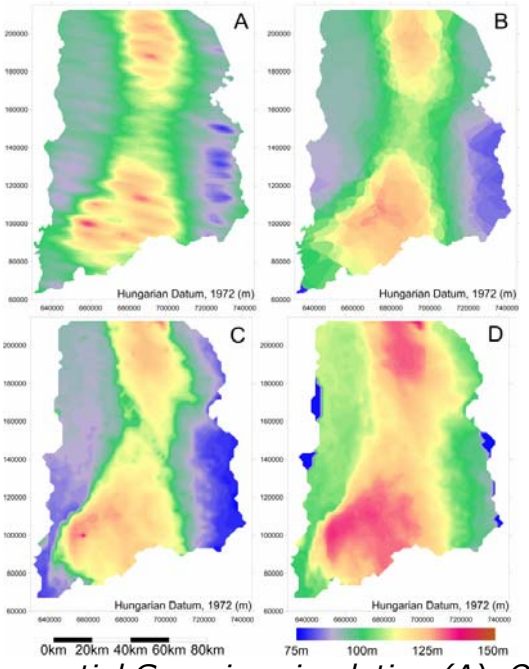

Figure 2: *Results for sequential Gaussian simulation (A), Ordinary Kriging (B), co-simulation with MM2 (C) and Simple Cokriging with MM2 (D)*

Analysis of trends revealed, that neglecting secondary information could lead to overestimation of groundwater change. Furthermore results of simple cokriging drew the attention to the risk of acceptance any singular estimation of a property (**Figure 4.**).

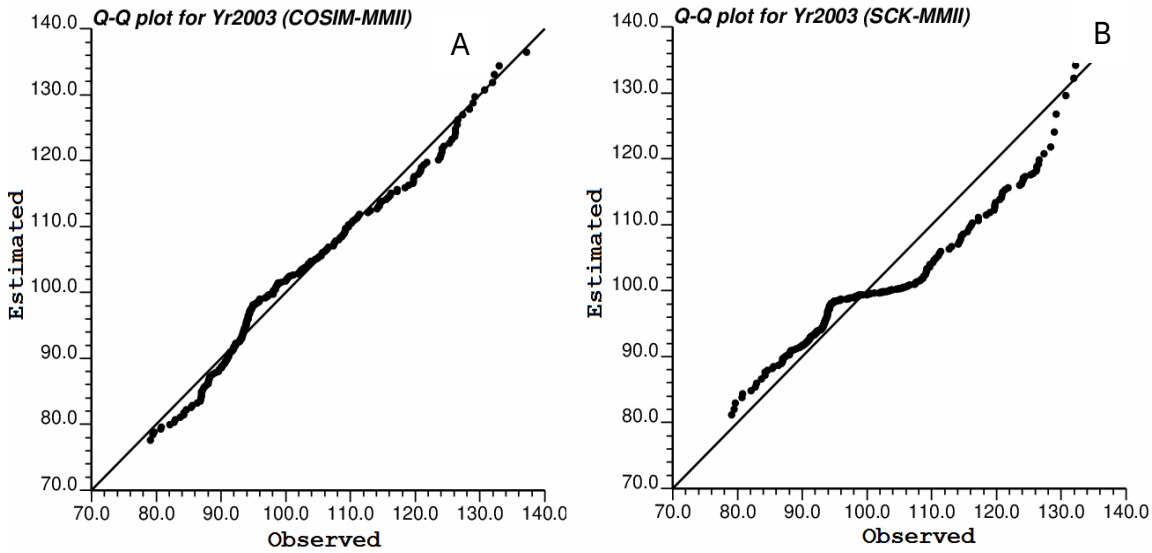

Figure 3:*Comparison of expected vs. observed grid node values for Gaussian Co-simulation with Markov Model 2 (A) and Cokriging with Markov Model 2 (B)*

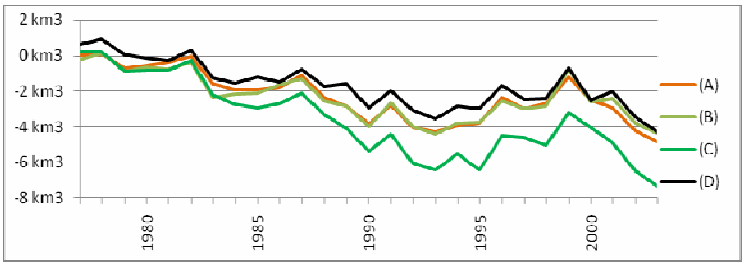

Figure 4: *Calculation of the groundwater volume reduction (km3) using Sequential Gaussian simulation (A), Ordinary Kriging (B), Simple Cokriging (C) and sequential Gaussian co-simulation with Markov Model 2 (D) on the study area*

4. REFERENCES

1. AHMED, S. & DE MARSILY G. (1987): Comparison of geostatistical methods for estimating transmissivity using data on transmissivity and specific capacity. Water Resources Research 23, 9, 1717-1737.
2. DEUTSCH, C. V. &JOURNEL, A. (1998): GSLIB, Geostatistical Software Library and User's Guide, Oxford University Press, New York, 340p.
3. GOOVAERTS, P. (1997): Geostatistics for Natural Resources Evaluation. Oxford University Press, New York, 483 p.
4. ISAAKS, E. H. &SRIVASTAVA M. R. (1989): An Introduction to Applied Geostatistics, Oxford University Press, New York, 561p.
5. JOURNEL, A. (1999): Markov Models for Cross-Covariances. Mathematical Geology, 31, 8, 955-964.
6. PÁLFAII. (1994): Water Management Problems of the Danube-Tisza Interflow (in Hungarian), NagyalföldAlapítványkötetei, Békéscsaba, 126p.
7. SHMARYAN, L. E.&JOURNEL, A. (1999): Two Markov Models and their Application. Mathematical Geology, 31, 8, 965-988.
8. XIANLIN, M. &JOURNEL, A. (1999): An expanded GSLIB Cokriging Program Allowing for two Markov Models, Computers and Geosciences, 25, 6, 627-639.

Application of Bayes' Theorem and entropy sets in the evaluation of uncertainty

Janos GEIGER[1], Judit UDVARHELYI[1]

[1]University of Szeged, Department of Geology and Paleontology. Egyetem u.2, Szeged, Hungary, matska@geo.u-szeged.hu,

Abstract: In this paper we analyzed how the levels of knowledge about mappable geometry of vertically averaged porosity change with the increasing number of wells in a delta-plain reservoir. In this approach Bayesian analysis was sequentially applied to the increasing stets of wells to incorporate a series of new information on vertically averaged porosity. The entropy sets measure how the stability of 2D mapping changes with increasing amount of information. These analyses were performed for porosity sets of distributary mouth bar, channel, channel fringe sands, sheet sands, and interdistributary-bay-filling rock bodies. The result highlighted what levels of knowledge are enough for gaining stable information on the lateral distributions of porosity belonging to these environments.

Key words: Bayes' Theorem, statistical entropy, levele of knowledge, depositional environments.

1. INTRODUCTION

In the recent years, since the general economic crises, there has been a great deal on emphasis the importance of decision analysis under uncertainty. The terms of risk and uncertainty are used to formulate by probabilities. Frequentist definition regards probability as a limited frequency of a particular outcome in a large number of identical experiments. Nevertheless, the practice showed that the initial, or *a priori*, probabilities used to change as new information becomes available. This recognition

developed the so called 'subjective' or 'Bayesian' probability which depends on both the phenomenon and also on the state of knowledge and beliefs of the observer. Therefore, Bayesian probability changes with time (Bárdossy and Fodor, 2004, p.23).

In this paper we analyzed how the levels of knowledge about mappable geometry of vertically averaged porosity change with the increasing number of wells in a delta-plain reservoir. In this approach Bayesian analysis was sequentially applied to the increasing stets of wells. This 'sequential sampling' method was originally suggested by Dowds (1969) and Newendorp (1971). We followed Dowds original idea of using entropy sets to measure how the stability of 2D mapping changes with increasing amount of information. Though, instead of general analysis, we studied how depends this stability on the increasing knowledge of depositional facies and transport directions.

For study area, we chose a well-documented CH-reservoir of the Algyő-Field, Hungary. In this delta-plain formation we analyzed the change of information stability of distributary mouth bar, channel, channel fringe sands, sheet sands, and interdistributary-bay-filling rock bodies with the increasing number of wells.

2.METHODS

2.1 Conditional probability and the Bayes' Theorem

Let *A* and *B* be two events such that $P(B) \neq 0$. Then the conditional probability of A given B, denoted $P(A|B)$, is defined by

$$\mathrm{P}(A|B) = \frac{P(\mathrm{A} \cap \mathrm{B})}{P(B)} \qquad (1)$$

That is, $P(A|B)$ means the probability of *A* given that we know *B* has occurred.

The Bayes' Theorem says that if A and B are two events such that $P(A) \neq 0 \text{ and, } P(B) \neq 0$, then

$$P(B|A) = \frac{P(A|B) \cdot P(B)}{P(A)} \qquad (2)$$

In the Bayesian interpretation, Bayes' theorem links the degree of belief in a proposition *A* before and after accounting for evidence *B*. In this approach $P(A)$, the prior, is the initial degree of belief in, $P(A|B)$, the posterior, is the degree of belief having accounted for, and $\frac{P(B|A)}{P(B)}$ represents the support *B* provides for *A*.

Often, for some partition of the event space $\{A_i\}$, the event space is given or conceptualized in terms of $P(A_i)$ and $P(B|A_i)$. It is then useful to eliminate the unknown $P(B)$ marginal probabilities by substituting the law of total probability.

In that way we have we got that form of Bayes' Theorem which was used in this study:

$$P(A_i|B) = \frac{P(B|A_i) \cdot P(A_i)}{\sum_{i=1}^{n} P(B|A_i) \cdot P(A_i)} \qquad (3)$$

The frequentist interpretation of the above formula is as follows: if an event *B* may occur on the basis of several "causes" $A_1, A_2, \ldots, A_n$ Bayes shows how likely is that A_i was the "cause" when *B* occurred.

2.2 Statistical entropy

The Shannon's statistical entropy is defined in the following simple way (Shannon 1948):

Let Ω be an event space consisting of n events, $\mathcal{A}_i$ $(i = 1, \ldots, n)$, and p_i the probability of event $\mathcal{A}_i$. Then

$$H = -\sum_{i=1}^{n} p_i \cdot \log p_i \qquad (4)$$

with the notion that . $p_i \cdot \log p_i := 0, if\ p_i = 0.$

The entropy H has the following properties:

1. $H = 0$ if $p_j = 1$ and $p_i = 0\ for\ i = 1,2,..,j-1,j+1,\ldots,n$

2. At a given number of states, $H = H_{max}$ *if* $p_i = p_j$ $(i,j = 1,2,\dots,n)$. Thus the maximum entropy of an event space with n event is $H_{max} = \log n$. Consequently for a discretization level n, a standardized measure of the entropy is

3. $$H_{st} = \frac{H}{\ln n} \in [0,1] \qquad (5)$$

4. H increses with the increasing number of events.
5. H is additive, that is it is possible to add up entropy of different event spaces.

2.3 The way of using Bayes' Theorem in the project

2.3.1 General considerations

The studied delta plain reservoir has been penetrated by 500 wells. The temporal expansion and improvement of knowledge in the course of exploration phase can be modeled in the following very simple way.

During the very first time period a small number of well were drilled. This information was summarized in a preliminary map of porosity which can be regarded as a prediction for the future. On this map the five facies were presented by contour intervals of porosity. Their probability forecast for the future can be summarized by their 'geometrical' probabilities.

In the next phase a new sets of wells were drilled. Within a particular facies (porosity contour), say channel, the new wells could reveal any of the five depositional facies. The forecast of the former time period was good-enough if the majority of the new data revealed channel, when channel had been forecasted. That is, using the terminology of Bayes' theorem, the most likely 'cause' of the new channel indication (B in (3)) was that channel had been forecasted ($\mathrm{A_i}$ in (3)). After evaluating the new findings, another improved map was created which provided a new forecast for the future, again. The probability forecast can also be summarized by the 'geometrical' probabilities of the five facies.

With the increasing number of wells, it can be expected that the map-forecasts become more and more stable. That is, on a particular facies forecasted, most of the new wells give the results having been forecasted. That is the probability of e.g. a channel finding given that channel has been forecasted is expected to be 1, and all the other conditional probabilities is assumed to be 0. That is the entropy calculated on each of the forecasted facies (contours) is expected to tend to 0.

Although the above sequence of interpretations look quite straightforward, its reality depends on two assumptions. (1) the transport direction identified by the initial number of wells does not change when incorporating new information (new wells). (2) the scales of the depositional facies assumed at the initial phase do not change with the increase the number of wells. It is quite easy to see that these assumptions are very insupportable, that is both the Bayesian probabilities and the entropies belonging to the depositional facies can be expected to change in time.

2.3.2. Definition of time periods

The 500 wells penetrating the reservoir were subdivided into ten mutually exclusive groups using a random number generator. Each group contained almost the same number of wells. These sets were regarded to represent ten non-overlapping time period.

2.3.3. Definition of depositional facies through porosity cut-offs

The previous sedimentological study has shown that the distributary mouth bar, channel, channel fringe sands, sheet sands, and interdistributary-bay-filling environments can be characterized by different porosity distributions. These distributions can be derived from the porosity histogram along the thresholds of 0.29, 0.28, 0.27, 0.25 and 0.21 respectively (Szilágyi and Geiger, 2012).

2.3.4. Calculation the Bayesian probabilities

Let Fi_i^j sign the porosity set of the j depositional facies in the i time period. In particular, the events to be analyzed are as follows:

Fi_i^1 := porosity set of bay-filling in the $i = 1,2,\dots,10$ time periods

Fi_i^2 := porosity set of sheet sandstones in the $i = 1,2,\dots,10$ time periods

Fi_i^3 := porosity set of channel fringe in the $i = 1,2,\dots,10$ time periods

Fi_i^4 := porosity set of channel sandstones in the $i = 1,2,\dots,10$ time periods

Fi_i^5 := porosity set of mouth bar sandstones in the $i = 1,2,\dots,10$ time periods,

In any fixed time period i, and facies j the *a posteriori* event Fi_i^j (result) belongs to the *a priori* event Fi_{i-1}^j.(cause).

That is

$$P\left(Fi_{i-1}^j \middle| Fi_i^j\right) = \frac{P\left(Fi_i^j \middle| Fi_{i-1}^j\right) \cdot P\left(Fi_{i-1}^j\right)}{\sum_{j=1}^{5} P\left(Fi_i^j \middle| Fi_{i-1}^j\right) \cdot P\left(Fi_{i-1}^j\right)}, for\ i = 2,3,\dots,10 \qquad (6)$$

where $P\left(Fi_{i-1}^j\right)$ means the 'geometrical' probability of the occurrence of the facies j $(j = 1,\dots,5)$ at the time period $(i-1), (i = 2,3,\dots,10)$. This is the forecast coming from the time period $i-1$.

Equantion (6) means how likely is that the predicted geometry of a particular depositional facies at an immediately preceding time period (Fi_{i-1}^j) was the "cause" when the same depositional facies occurred in the actual time period (Fi_i^j). If this probability is high, then there were not any new wells falling in this particular geometry at the time period i which would have changed the contour geometry inherited from $(i-1)$. That is the predicted geometry has been proved to be stable in the mirror of the new wells. In this situation the prediction for this particular depositional facies is called to be precise.

2.3.4. Calculation the entropy

At any fixed time period $i\,(i = 2,3,\dots,10)$ five conditional probabilities are available on a particular facies $j\,(j = 1,2,\dots,5)$ predicted at time $i-1$. For better understanding let i=5 and j=2, that is the 2nd facies (sheet sand) is studied in the 5th time period. The corresponding conditional probabilities are as follows :

$P(Fi_5^1|Fi_4^1)$: the probability of finding bay filling $(j=1)$ facies at the 5th time period $(i=5)$ given that at the immediately preceding time (at the 4th time period) sheet sand was predicted.

$P(Fi_5^2|Fi_4^1)$: the probability of finding sheet sand $(j=2)$ facies at the 5th time period $(i=5)$ given that at the immediately preceding time (at the 4th time period) sheet sand was predicted.

$P(Fi_5^3|Fi_4^1)$: the probability of finding channel fringe $(j=3)$ facies at the 5th time period $(i=5)$ given that at the immediately preceding time (at the 4th time period) sheet sand was predicted.

$P(Fi_5^4|Fi_4^1)$: the probability of finding channel $(j=4)$ facies at the 5th time period $(i=5)$ given that at the immediately preceding time (at the 4th time period) sheet sand was predicted.

$P(Fi_5^5|Fi_4^1)$: the probability of finding mouth-bar $(j=4)$ facies at the 5th time period $(i=5)$ given that at the immediately preceding time (at the 4th time period) sheet sand was predicted.

The above conditional probabilities are defined on a common base (at the 4th time period sheet sand was predicted). That is, they form an event space that is why the entropy can be calculated.

3. RESULTS AND DISCUSSION

The above outlined methods and approaches were performed for each of the ten defined time periods. **Figure 1** shows the corresponding porosity maps. For supporting the stable comparison, they grids were created by the same algorithm (linear kriging).

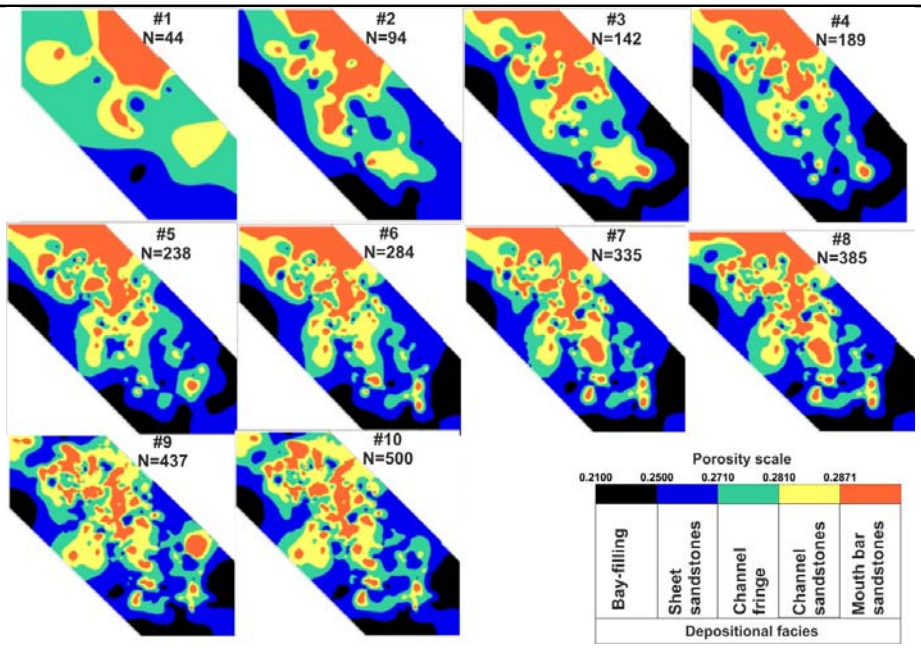

Figure 1: *Maps of porosity/facies of the different time periods.*
Legend: # = Time period, N = number of wells

Figure 2 shows the change of partial entropies of depositional facies with the increasing number of wells. At the bottom the semi-variogram surfaces of the time periods are shown. The shape of the entropy-'functions' are in harmony with the change of the main transport directions/spatial continuity shown by the variogram surfaces.

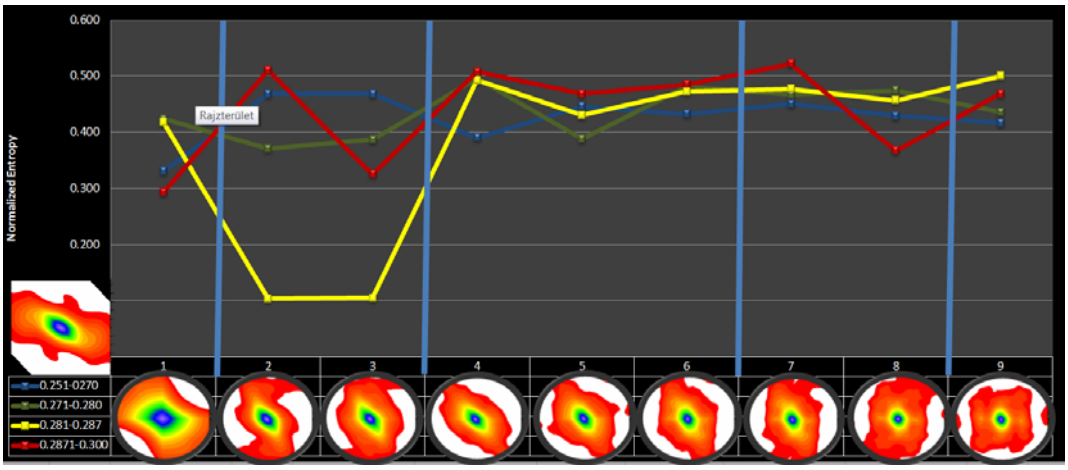

Figure 2: *Shanon's normalized entropies vs. time. At the bottom the variogram surfaces are presented.*

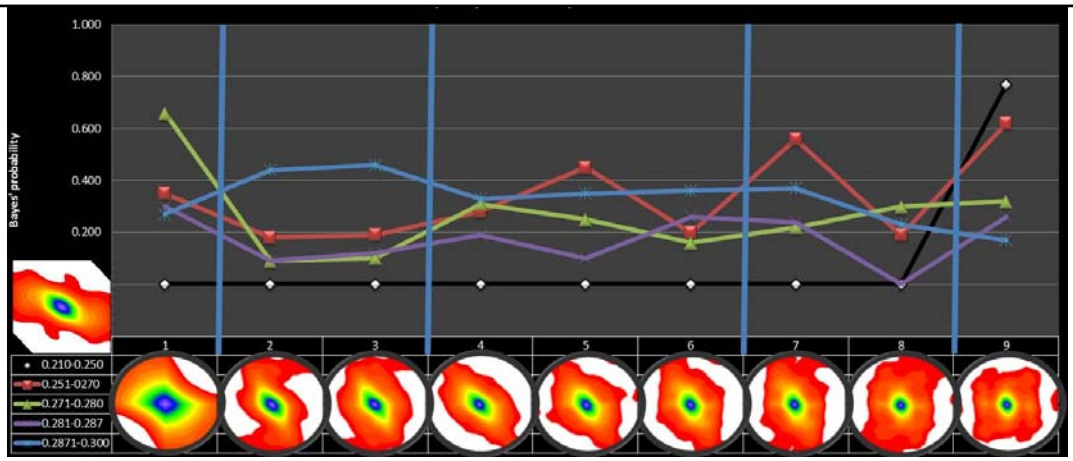

Figure 3: *Bayesian probabilities vs. time. At the bottom the variogram surfaces are presented.*

Figure 3 shows the change of Baysian probabilities with time. It can also be seen, that the shape of the probability-'functions' are in harmony with the change of the main transport directions/spatial continuity shown by the variogram surfaces

The results suggested that the general increase of precision and accuracy of prediction increases with the number of available wells until a new smaller scale of heterogeneity introduced by the increasing number of wells. At this situation both measures fall down and another improving period started. This wavy-like change repeated by the appearance of a new heterogeneity level. Nevertheless, the effect of this process was different on the studied depositional facies.

4. REFERENCES

BÁRDOSSY, Gy. and Fodor, J. (2004): Evaluation of uncertainties and risks in geology, Springer, 27-41.

DOWDS, J. P. (1969): Statistical Geometry of Petroleum Reservoirs in Exploration and Exploitation, Journal of Petroleum Technology, 841-852.

NEWENDORP, P. D. (1972): Bayesian Analysis--A Method for Updating Risk Estimates, Journal of Petroleum Technology, 24, 2, 193-198, DOI: 10.2118/3463-PA.

SHANNON, C. E. (1948): The mathematical theory of communication, Bell Syst. Tech. Journal, 27, 379–423.

SZILÁGYI, Sz. S. and GEIGER, J. (2012): Sedimentological study of the Szőreg-1 reservoir Algyő Field, Hungary: a combination of traditional and 3D sedimentological approaches, Geologica Croatia, 65, 1, 77-90, DOI: 104154/gc.2012.06.

Statistical characterization of clastic sedimentary environments derived by clustering method

Janina HORVÁTH
Department of Geology and Palaeontology, University of Szeged, H-6722, Szeged, Egyetem u. 2-6. Hungary, th.janina@geo.u-szeged.hu

Abstract: In this study an unsupervised neural networks (UNN) algorithm was used to derive such a classification in which groups (clusters) corresponded to depositional sub-environments. The two study areas were: (1) Szőreg-1 reservoir, Algyő Field, SE Hungary; (2) one hydrocarbon field in Sava Depression, N Croatia. The first one represents a delta plain environment, and the other is a deep water turbidity system. Several different statistical techniques were utilized in the interpretation: (i) parametric and non-parametric statistics as tools for exploratory data analysis; (ii) Monte Carlo simulation for increasing the resolutions of histograms; (iii) autocorrelation surfaces to identify the main continuity directions in the geometrical analyses.

Key words: clustering, descriptive statistics, autocorrelation, recognition of sub-environments, Algyő Field, Sava Depression.

1. THE AIM OF THIS STUDY

This study demonstrates an approach for interpretation and identification of generated groups as depositional facies. The applied clustering algorithm can handle simultaneously more point data and even joint more attributes, or property of data points. Therefore the formed clusters are characterized complex and underlying properties which are discovered by exploratory data analyses and visualisation tools.

2. STUDY AREAS

The clustering process was applied for two study area: (1) Szőreg-1 reservoir, Algyő Field, south-eastern Hungary (**Figure 1**); (2) two reservoirs of a hydrocarbon field situated in Sava Depression, northern Croatia (**Figure 2**). In this paper this field is labelled as *"Sava-Field"*.

2.1. Study area-1: Szőreg-1 reservoir, Algyő Field

The Algyő Field is the largest Hungarian hydrocarbon accumulation consisting of several oil and gas bearing reservoirs (**Figure1** after Bérczi, 1988 in Geiger, 2003). The Szőreg-1 oil reservoir with a large gas cap is one of the largest rock bodies within the delta plain record (**Figure 1**). Its average gross thickness is about 35 m, but locally it can be a maximum of 50 m thick, as well. Some earlier work by Geiger (2003) and Sebők-Szilágyi & Geiger (2012) have proved its delta plain origin with significant amount of fluvial channel sedimentation.

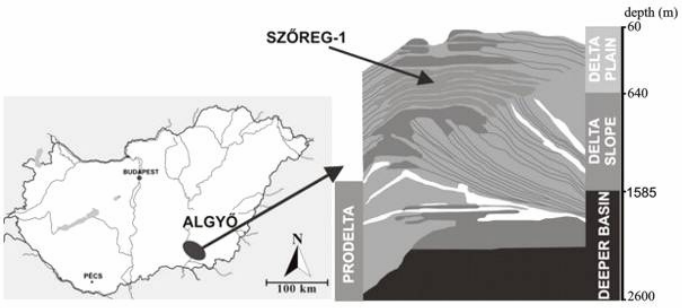

Figure 1: *Location of the study-1 area* ***Figure 2:*** *Location of the study-2 area*

In case of Szőreg-1 reservoir, the UNN clustering method was applied for two depositional facies. They were (1) emerging distributary mouth bar, (2) prograded bifurcation channels and they located one above the other like two *'level'* in the rock body system. The first lies 34-35m below the low-

permeability seal, and the second locates 24-27m below the seal. These depositional facies are selected based on some previously study (Geiger, 2003; Sebők-Szilágyi& Geiger, 2012) in the temporal evolution, the 3D geometry and the geostatistical characters of these sub-environments were presented.

The data set in the first level derived from 290 wells and in the other one case it was 341 wells. The input variable of the UNN clustering algorithm were porosity, hydraulic conductivity and sand content values. The method have been published in Horváth (2011) however that paper contents the applied process for total vertical rock body of the reservoir. That method has modified using well data from two selected level instead of grid data derived kriging.

2.2. Study area-2: Sava-Field

The second study area is located in the Sava Depression, northern Croatia, about 35km to the east of Zagreb (**Figure 2**). The sediments belong to Neogene and Quarterly. Sedimentation was accompanied by influence of pre-Neogene basement palaeorelief, which is a heterogeneous lithological composition.

The lithologically analysed sequence is represented by Upper Miocene marls, silts and sandstones, deposited with turbidity current mechanisms. Sedimentation was through cyclic turbidity flows in lacustrine environments, that area was constantly reducing (Vrbanac, 1996). Sandstones morphology follows depositional currents direction (Saftić et al., 2003) and in the central part of the depression appeared thick, bedded, fine-grained sandy deposits which is bounded in marginal part with basin plain marl sediment. Detritus was redeposited several times before it was finally accumulated (Šimon, 1980; Malvić et al., 2005).

In case of second study field, in this research the UNN clustering method was applied only two reservoirs from the reservoirs sequences (the total

thickness changes between 120-150m) it would be quite large scaled for the model. These located one above the other.

In both of hydrocarbon pool the data came from 79 wells and the inputs were the basic petrophysical parameters (porosity, water saturation, shale volume) and a categorical variable that describes the lithology using a code-number between 0-10 according to the shale content of the sandy deposit. The UNN classification processes have been presented in Horváth & Novak Zelenika (2011).

3. METHODS

In both of study area case, the input variable sets of UNN algorithm were simultaneously from both of level in Szőreg-1, and from both of reservoir in the Sava-Field. This step provided of identification of same clusters if those appears in different levels or reservoirs. The UNN processes managed the several input parameters jointly and divided the data set into clusters. The number of group is initialized.

In the clustering processes was applied for total vertically averaged parameters in any case. The question that the clusters' averages are able to describe duly well the represented facies. On the other hand the formed clusters contents different amounts of elements. Monte Carlo simulation was used for repetitive sampling to increasing of data number and resolutions of histograms. The simulations keep the characteristic of distributions in groups and its properties. This extended set was compared to the set of measured log-values. The comparison based on non-parametric Gamma correlation coefficient. The Gamma coefficients showed the probability of the difference between the sets. According to the comparison the data sets in each cluster were quite significantly similar, only the standard deviation had narrower interval. The exploratory data analyses are based on this extended data set.

In the identification of the clusters, the descriptive statistics and the geometry of mapped clusters aimed. The autocorrelation surfaces of

parameters supported the visualisation of geometry of facies. The spatial patterns of selected variable were analysed by displayed correlation contours which indicates underlying trends to mapping the clusters by the anisotropy of the grid. The axes represent separation distances and rate of axis and/or supplementary axes give a value of anisotropy. The variables with the largest weight in determining of clusters in UNN process were selected to display the autocorrelation. For example in case of second level in Szőreg-1, according to the parameter weighs, the porosity has high weighs. So, it seemed to be a good descriptor. The visualized autocorrelation surfaces of porosity shows the **Figure 3**. Its underlying trends used to the visualisation of the clusters (**Figure 4**). According to the axes of autocorrelation the anisotropy ratio was 0.69 and the angle of direction was 350° (180° is the S-N direction). In the other level case the sand ratio was the adequate parameter to describe the spatial correlation.

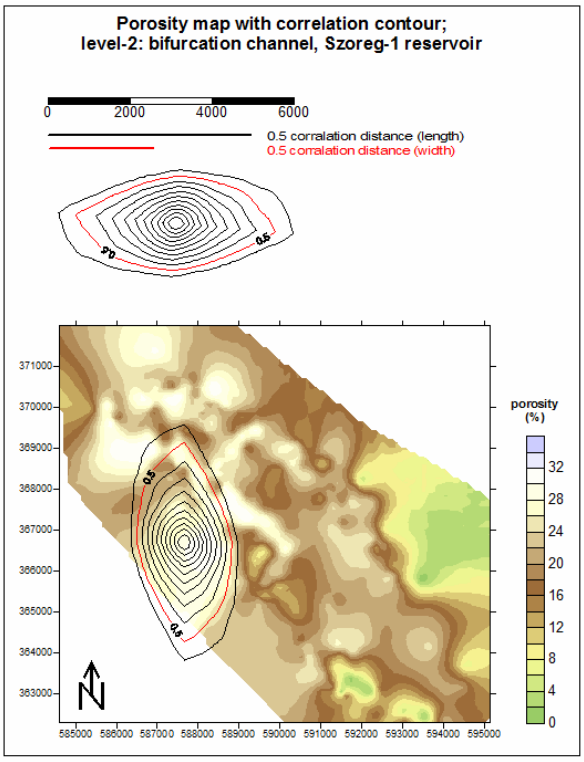

Figure 3: *Porosity map with correlation contour in level 2, Szőreg -1*

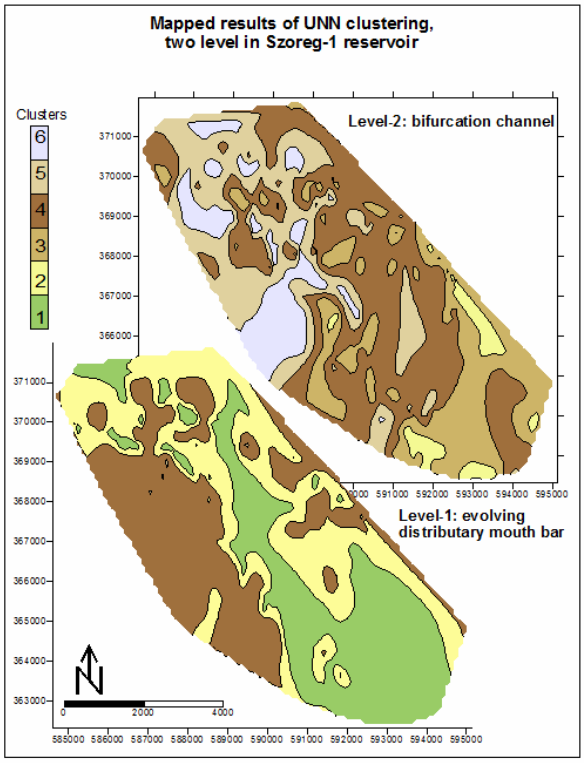

Figure 4: *Results map, Szőreg-1*

4. RESULTS

4.1. Identification of sub-environments, case study-1: Szőreg-1

Cluster-1 represents the interdistributary bay which is characterised predominantly low porosity and sand ratio. This cluster appears only in the lower level when distributary mouth bars involve from two opposite directs and disappear in map of upper level during the progradation.

Cluster 2-3-4: these characterize a distributary mouth bar complex. The bar has poly modal porosity histograms and it divides that to tree sub-areas as outer bar, the marginal part of the bar and the bar crest (central region). The cluster 4 is appears only in the upper level after the bar is extended and in this phase the distributary channel cuts to the bar.

The first two cluster is seems to be not significantly different in porosity and hydraulic conductivity average values however the sand content separated them. The higher sand ratio and the mapped geometry (kidney shape) link to it to the bar but the low porosity values confirm the existence of an isolated group. The fourth and fifth clusters differ from each other in porosity values however the sand ratio cannot separate them. It is represented by the box-plots of porosity and sand ratio. This fact is possible since the channel system (together the cluster 5, 6) has poly-modal porosity histograms where the minor modus coincides with the value of main modus (50-60%) of mouth bar's which formed by the progradation.

results of clustering in both level	Sand ratio	Hydr.cond	Porosity	Cluster	Define of sub-environments *(same colour scale in map)	Deltaic environment	Geometry
	1.907	13.021	3.829	C1	interdistributary bay (deposition from quite water)	bay	
	38.596	20.878	6.121	C2	outer bar	bar	kidney-shaped geometry
	36.427	126.125	16.593	C3	involved distributary mouth bar		
	61.172	147.659	20.708	C4	marginal part of bar (inner)		
	56.069	665.258	25.026	C5	marginal part of involved channels	channel	dendroid geometry
	81.729	1448.889	29.963	C6	bifurcating channel		

Table 1: *Summary Table – Szőreg-1*

Cluster 5-6: These clusters mean the bifurcating channel and its marginal part. The highest porosity values characterises the central part of the channel with dendroid geometry and around it in marginal part has a bit lower but relatively also large porosity value. The sand ratio is similarly high in these clusters. The geometry of the cluster 6 reflects clearly the axis of the channel and shows the direction of progradation from SW to NE direction.

4.2. Identification of sub-environments, case study-2: Sava-Field

The UNN process created four clusters as sub-environments of a deep water turbidite system. **Table 2** shows the averages of groups and sub-environments. In both of case this parameter got the highest weights during the UNN. In the visualisation of the results in both of reservoir the autocorrelation surface of the porosity was used to describe the trends. The **Figure 5** shows the lower reservoirs autocorrelation contours of porosity which define the main and supplementary axes of the anisotropy. To the anisotropy ratio it was used the 0.5 correlation level. Under these conditions the ratio was 0.75 and the angle 40°. The **Figure 6** displays the geometry of groups. The ***cluster 1*** represents the normal basin sedimentation with very low porosity, high shale content. This facies appears around the sandy channels and fan deposit.

results of clustering in both reservoirs (means)	water saturation (%)	Shale volume (%)	Porosity (%)	Cluster	Sub-environments *(same colour scale in map)	turbidity current	lithofacies
	98.88	94.04	1.41	C1	normal basin pelitic sediment	basin	massive marl
	71.02	55.45	13.84	C2	turbidity channel margins	transport zone	laminated sandstones, siltstones and marls
	59.34	34.55	18.16	C3	over bank deposits along the channels		thin sandstones and interrupted siltstones
	52.08	32.13	21.30	C4	central part of channel		massive sandstones

Table 2: *Summary Table – Sava-Field*

The ***clusters 2-3-4*** represent transport zone of the system but it is subdivided into three more sub-classes by clustering. The cluster 4 assigns the geometry of turbidity channels that are linked to higher porosity values and cluster 3 means the overbank deposit along the channels its central part.

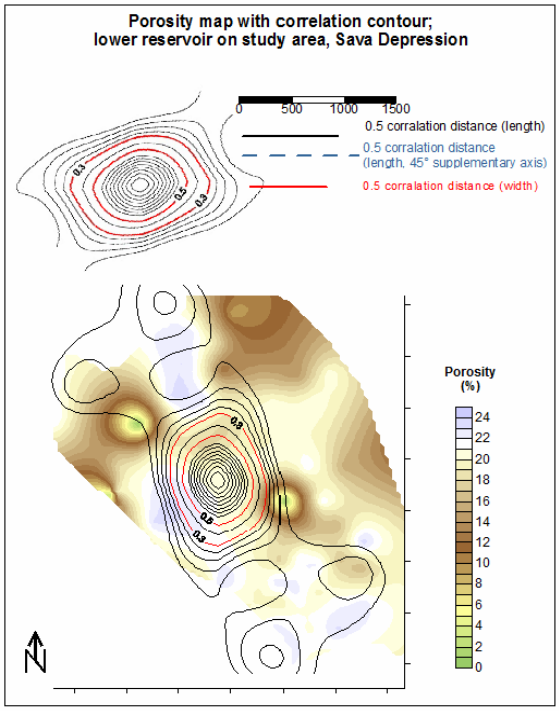

Figure 5: *Porosity map with correlation contour in lower reservoir, Sava-Field*

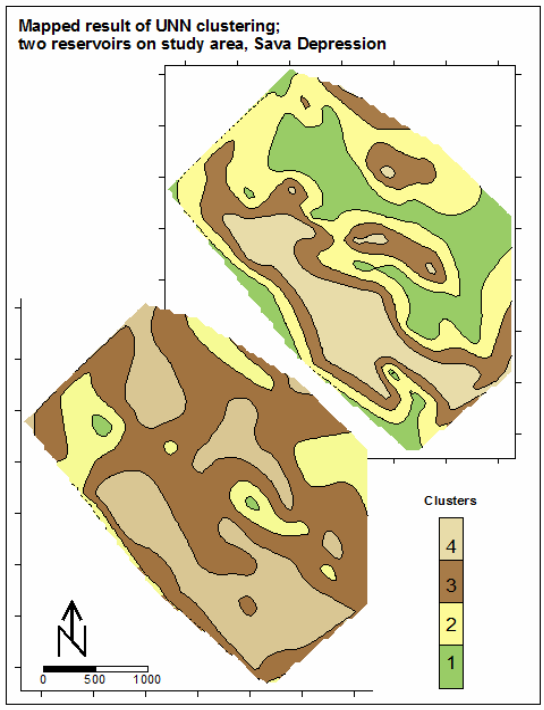

Figure 6: *Results map, Sava-Field*

According to the exploratory analyses the fourth group is a well separated facies especially in the porosity. It is recognized in the box-plot of porosity.

Also it is reflected in histograms of the clusters 3-4 which have similar but shifted histograms. The other hand the geometry is not able to show perfectly and neighbouring the central transport zones. It is fact the total thickness is characterized by large interval. In some wells it reaches the 20-21m therefore the clusters maybe content more turbidite package vertically and the geometry shows amalgamated deposits. It is supported by the sand content, net thickness. In the zone of the fourth cluster, the net thickness reaches the total thickness almost everywhere. Also, the marginal part in transit zone differs clearly from the other two parts which has poly-modal porosity histograms.

According to the mapped clusters (**Figures 6**) it demonstrated the main sediment transport directions (NW-SE) and outlined the main channel and four facies geometry. In fact, those clusters perfectly correspond to lithofacies which are defined as typical for Late Miocene sedimentation in the Sava Depression (Vrbanac at al., 2010). Formerly defined facies of thick-layered massive sandstones (F_1) corresponds to cluster C4. Facies of thin sandstones and interrupted siltstones (F_2) corresponds to C3, facies of laminated sandstones, siltstones and marls (F_3) to cluster C2. Eventually, facies of massive marls (F_4) is cluster C1. The results are in accordance with the previously published models of the depositional history in the Sava Depression (Šimon, 1980; Vrbanac, 1996).

The analysed turbidite flow was taken in a comprehensive analogue system and which is based on Mutti's turbidite systems classification (Mutti, 1985). According to his classification with three aspects, the turbidite current on Sava-Field was defined as interim type of middle and small system in distal part of type-II (transition channel-lobes). It is similar to the type-III (channel-levee complexes) and the facies is dominantly shale on marginal a part of transitional zone which is defined as deposit of channel-levee complexes. Since, the sand/shale ratio is higher than 50% in general and higher than 60% in the central part of transport zone, it is belonged in middle system. In addition to features the extension of the system usually is

several tens of kilometres and thickness of individual strata is between 1-5m and they are often amalgamated. The view of the above the turbidity current in study area can be defined as distal expression of the retrogradation Medium Turbidite Systems.

5. DISCUSSION

Since, the UNN is a tool for divide the rock body in sub-classes which depends on apply of more joint parameters, this clusters are characterized by complex properties. Using the exploratory data statistics, the Monte Carlo simulation for increasing the resolutions of these statistics and applied the autocorrelation surfaces for defining the main continuity direction for the visualisation of geometry, the study demonstrated to the UNN is able to segregate the different sub-environments.

6. REFERENCES

1. BÉRCZI, I. (1988): Preliminary sedimentological investigations of a Neogene depression in the great Hungarian Plain–in: Royden and Horváth (eds.): The Pannonian basin-a study in basin evolution- AAPG Memoir 45, pp. 107-116
2. GEIGER, J. (2003): A pannóniaiújfalui (törteli) formációbanlevőAlgyő-delta fejlődéstörténete – I.: AzAlgyő-delta alkörnyezeteinek 3d modellezése (Depositional history of the PannonianAlgyő-delta (Újfalu Formation). Part one: 3D modeling of the sub-environments of Algyő-delta). Földtani Közlöny, 133, 1, 91-112.
3. HORVÁTH, J. (2011): Define of depositional environment using neural network. Geologia Croatica, 64, 3, 251-258.
4. HORVÁTH, J. & NOVAK-ZELENIKA, K. (2011): Application of clustering methods for identification of palaeoenvironments, case study from Late Miocene sandstones, the Sava Depression. Nafta, 62, 11-12, 365-376.

5. MALVIĆ, T.; VELIĆ, J. & PEH, Z. (2005): Qualitative-Quantitative Analyses of the Influence of Depth and Lithological Composition on Lower Pontian Sandstone Porosity in the Central Part of Bjelovar Sag (Croatia). GeologiaCroatica, 58, 1, 73-85.
6. MUTTI., E. (1985): *Turbidite systems and their relations to depositional sequences.* In: Zuffa, G. G. (ed.): Provenance of Arenites: NATO-ASI Series, D. Reidel Publishing Co., Amsterdam, 65-93.
7. SATFTIĆ B., VELIĆ J., SZTANÓ O., JUHÁSZ, GY. & IVKOVIĆ, Z. (2003): Tertiary subsurface facies, source rocks and hydrocarbon reservoirs in the SW part of the Pannonian basin (Northern Croatia and South-West Hungary). Geologia Croatica, 56, 1, 101-122.
8. SEBŐK-SZILÁGYI, SZ.; GEIGER, J. (2012): Sedimentological study of the Szőreg-1reservoir (Algyő Field, Hungary): a combination of traditional and 3Dsedimentological approaches. Geologia Croatica, 65, 1, 77-90.
9. ŠIMON, J. (1980): Prilog stratigrafiji u taložnom sustavu pješčanih rezervoara Sava-grupe naslaga mlađeg tercijara u Panonskom bazenu sjeverne Hrvatske. PhD dissertation, University of Zagreb, 66 p.
10. VRBANAC, B. (1996): Paleostrukturne i sedimentološke analize gornjopanonskih naslaga formacije Ivanić Grad u Savskoj depresiji. PhD dissertation, Faculty of Natural Sciences, University of Zagreb, 121 p.
11. VRBANAC, B.; VELIĆ, J.; MALVIĆ, T. (2010): Sedimentation of deep-water turbidites in the SW part of the Pannonian Basin. Geologica Carpathica, 61, 1, 55-69.

Environmental Protection by Geothermal Energy Usage: Its Potential and Production in the World and in Croatia

Ivana KAPUSTIĆ*, Danko OMRČEN

INA Plc., Av.V.Holjevca 10, Ivana.Kapustic@ina.hr, Danko.Omrcen@ina.hr

* Author to whom correspondence should be addressed:

E-Mail: Ivana.Kapustic@ina.hr ;

Tel.: +385 1 6451 190

Abstract: Huge geothermal energy potential, generated by slow decomposition of radioactive elements (uranium, thorium, potassium), by chemical reactions or by friction during the movement of tectonic masses lays in the Earth underground. Due its large amount it is represented as renewable source. Heat estimation (estimated in 42×10^{12} W) shows that this energy source is 50 000 times larger than hydrocarbons energy potential. Although development of geothermal energy technologies could provide enough energy supply for the whole mankind, it is still under-represented and in a small percentage used for electricity generation, space heating, greenhouses, swimming pools, for medical purposes, in the fish ponds and in various industrial processes. Although managing this type of energy in Croatia is not a novelty, the realization of own potential is still at unfavorable level. This paper shows cross-section of world resources of geothermal energy, as well as the position of Croatia.

Key words: geothermal potential, renewable energy, geothermal fields in Croatia.

1. BASICS ON GEOTHERMAL ENERGY

Geothermal resources consider both, geothermal water contained in underground reservoirs which are not supplied, as well as the water passing through the underground reservoirs which are supplied by natural or

artificial injection. Based on the geothermal gradient, the first assessments of exploration field perspective are made. For this purpose, maps of geothermal gradients are made, showing the local anomalies.

Although an international standard classification of geothermal resources has not been defined, there are several ways to classify the geothermal resources. There are many different classifications (e.g. Muffler and Cataldi, 1978), but generally classification could be made according to the **Table 1.**

GEOTHERMAL RESOURCE	RANGE (°C)
high-temperature geothermal potential	> 150
medium-temperature geothermal potential	100 - 150
low-temperature geothermal potential	65 - 100
very low-temperature geothermal potential	< 65

Table 1: *Categorization of geothermal resources*

2. GEOTHERMAL RESOURCES AND CONSUMPTION OF GEOTHERMAL ENERGY

From the huge (nearly 35 billion times greater than the amount of today's energy needs) global geothermal potential, only a very small part can be effective (i.e. profitable) exploited, only to a depth of 5000 m. Geothermal water exploitation has been increased over the last 30 years by an approximate rate of 15% per year. As it could be seen from the **Figure 1** installed electrical and thermal power from this renewable energy source grows linearly. Direct consumption of geothermal energy in the last 10 years has been increasing exponentially primarily due to heat pumps.

Today is the world's installed capacity of geothermal power plants around 7000 MW, producing less than 0.5% of total produced electricity, and they are significantly participating among alternative energy sources (Golub et al., 1998). In some countries, geothermal energy is used for thousands of years in the form of spa-medicinal or recreational bathing. Recently it is used also for getting the electricity and space heating, in agricultural

production of flowers and vegetables (to increase yields, heating greenhouses…) (Jelić et al., 2000). The increase of geothermal energy usage is especially connected to rapid jump of oil prices and the increasing demands for the human environment preservation.

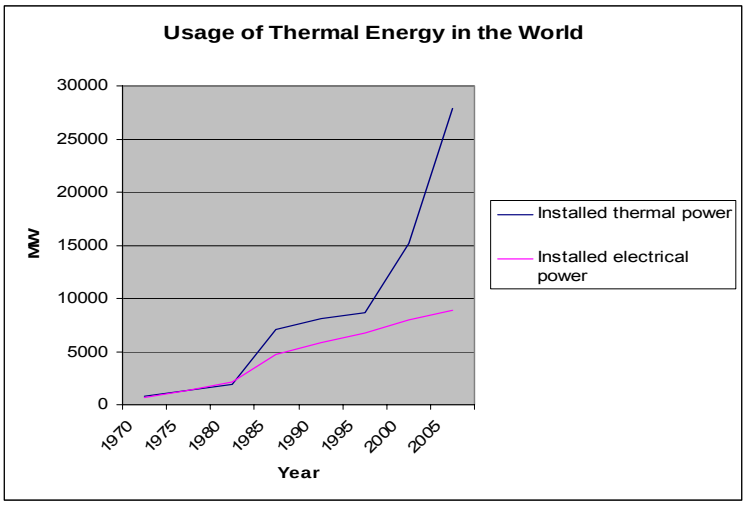

Figure 1: *Usage of geothermal energy in the World (adopted from Živković et al., 2008)*

2.1. Geothermal resources in Croatia

Usage of geothermal water from wells in Croatia started with the accidental discovery of hot water during the construction of oil exploration well on Bizovac area. Exploration drillings at other locations in Croatia also resulted in geothermal water discovery. Bizovac, Zagreb and Ivanić-Grad geothermal fields started with production of geothermal water, which is used for swimming pools water heating (three geothermal fields), heating of complex spaces (Bizovac and Zagreb geothermal fields) and for heating of warehouses, business premises and prefabricated buildings (Zagreb geothermal field). The main geothermal reservoirs are in the fractured Mesozoic and older carbonates rocks, mid Miocene carbonates, under the Pannonian basin and younger clastic sediments, with important geothermal reservoirs in their sandstone sequences (Jelić et al., 2010).

The main geothermal potential in Croatia, indicated by numerous Spas, is in the Pannonian area, where the temperature gradient ranges from 0.03 to more than 0.07°C/m (shown on the **Figure 2**; the average value for Europe is 0.03°C/m) (Bošnjak, 1998). The total geothermal energy potential in Croatia is estimated to be 812 MW heating output and 45.8 MW of electrical power, assuming application in the systems.

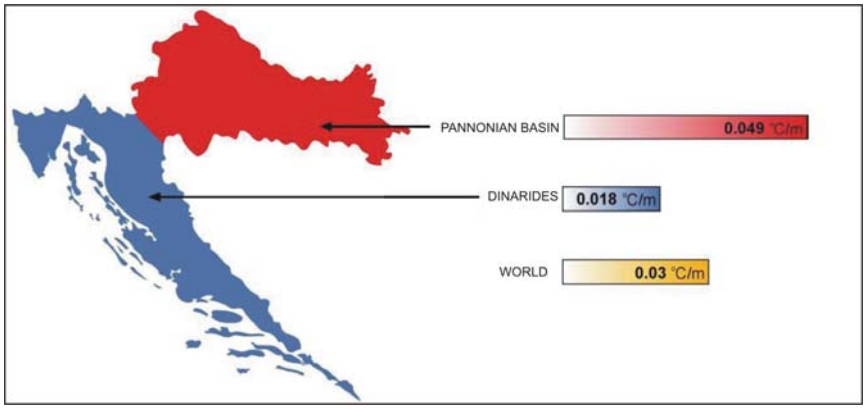

Figure 2: *Geothermal gradients in the Republic of Croatia and the comparison with average world value (taken and adopted from Živković et al., 2008)*

The **Figure 3** shows the current thermal water springs with temperatures below 65 ° C, which can be exploited for balneology purposes.

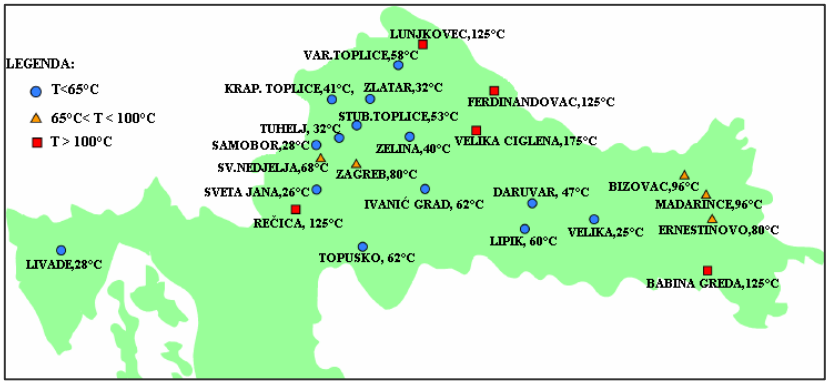

Figure 3: *Geothermal resources in Croatia (taken from Živković et al., 20008)*

According to data given in the Strategy for mineral resources management in the Republic of Croatia (Živković et al., 2008), on the **Figure 4** prediction

for installed geothermal power in Croatia till the year 2030 is given, while the **Figure 5** shows the prediction for installed electrical power from geothermal sources.

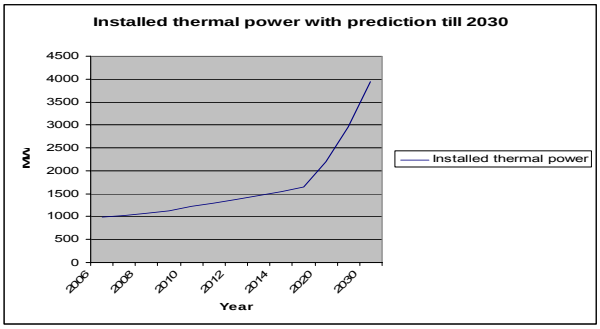

Figure 4: *Prediction for installed geothermal power in Croatia (adopted from Živković et al., 2008)*

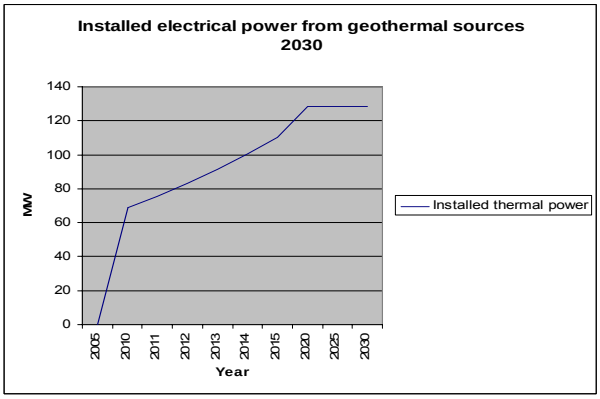

Figure 5: *Prediction for installed electrical power from geothermal sources in Croatia (adopted from Živković et al., 2008)*

3. DISCUSSION AND CONCLUSION

Geothermal energy is used in almost all countries of the world, and the data for some countries are shown in **Table 2**. According to data taken from the http://www.geothermal-energy.org, the paper consider following countries: Austria, Bulgaria, Czech Republic, France, Germany, Hungary, Iceland, Italy, Slovenia, USA, Mexico, Brazil, China, New Zeland and Croatia. As it is seen from the **Table 2**, the greatest usage of geothermal energy (represented by

total thermal installed capacity) belongs to USA, China, Germany, Iceland, France. For this purpose total thermal installed capacity per capita is calculated. Iceland drastically deviates (with 6219.35 installed W per capita). Considering other countries, best results are shown for New Zeland, Austria and Hungary.

COUNTRY	TOTAL THERMAL INSTALLED CAPACITY (MWt)	DIRECT USE (GWh/year)	CAPACITY FACTOR	POPULATION
AUSTRIA	662.85	1,035.6	0.18	8,192,880.00
BULGARIA	98.3	380.6	0.44	7,385,367.00
CROATIA	67.48	130.3	0.22	4,494,749.00
CZECH REP.	151.5	256.1	0.19	10,235,455.00
FRANCE	1,345.00	3,591.7	0.30	60,876,136.00
GERMANY	2,485.4	3,546.00	0.16	82,060,000.00
HUNGARY	654.6	2,713.3	0.47	9,981,334.00
ICELAND	1,862.00	6,767.5	0.42	299,388.00
ITALY	867.00	2,761.6	0.36	58,133,509.00
SLOVENIA	104.17	315.7	0.35	2,010,347.00
UK	186.62	236.1	0.14	60,609,153.00
USA	12,611.46	15,710.1	0.14	**298,444,215.00**
MEXICO	155.82	1,117.5	0.82	107,449,525.00
BRAZIL	360.1	1,839.7	0.58	188,078,227.00
CHINA	8,898.00	20,931.8	0.27	1,321,367,270.00
NEW ZELAND	393.22	2,653.5	0.77	4,076,140.00

Table 2: *Total installed thermal capacity for certain countries (data taken from http://www.geothermal-energy.org)*

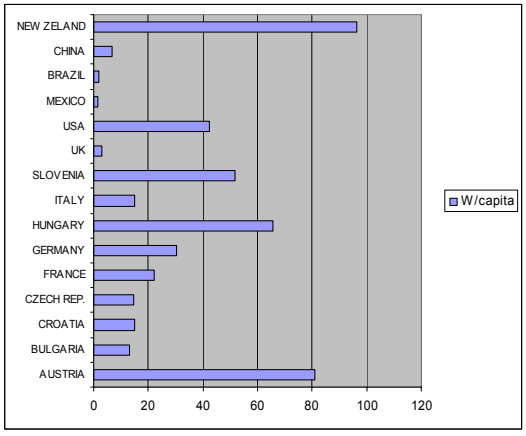

Figure 6: *Total installed thermal capacity for certain countries*

Considering our geothermal potential, it can be stated that Croatia slightly uses its own geothermal potential. Generally, there are two regions in Croatia in geological and geothermal respect, but geothermal resources capable for direct usage refer to the northern part of Croatia.

Direct utilization in the country is mainly for heating swimming pools and spas along with recreational centres, as well as space heating. There are 20 spas and five geothermal fields above 100°C that are using geothermal energy. The five high temperature geothermal fields are being considered for combine heat and electrical energy production and may be started in 2010.

There are many ecological advantages of this kind of energy source; the geothermal process does not produce by-products which pollute the environment, there is no used water discharging because the water returns to the reservoir through the injection well. Geothermal power plants occupy minimum space per produced megawatt… On the other hand, it is about reliable energy source, because there is no interruption of production due to weather, natural disasters or political influence, which can prevent transport of other types of fuels (Golub et al., 1998).

In accordance with the general orientation towards ecologically acceptable renewable energy resources proclaimed in the Strategy of the Energy Development of the Republic of Croatia, a significant growth of the geothermal energy usage is planned. In the first phase the growth will be based on the total exploitation of the existing geothermal wells together with some new wells, appropriate for high temperature and long-term production. Beside development in the direct heat segment, the planned construction of some power plant should bring Croatia into the group of countries producing electricity from geothermal sources (Jelić et al., 2010).

REFERENCES

BOŠNJAK, R. (1998): GEOEN – Program korištenja geotermalne energije: osnovni rezultati i buduće aktivnosti [GEOEN – Program of Geothermal Energy Utilization : Basic Results and Further Activities]. Hrvatske vode, 6, 25, 363-369.

GOLUB, M., KOLIN, I., JELIĆ, K., SALOPEK, B., RAJKOVIĆ, D., KOŠĆAK, S., SEČEN, J., ČUBRIĆ, S., PRAVICA, Z., KULENOVIĆ, I., MIOĆEV, D., STANIŠIĆ, L. & GRABOVSKI, K. (1998): GEOEN - Program korištenja geotermalne energije - prethodni rezultati i buduće aktivnosti [*GEOEN – Program of Geothermal Energy Utilization – Previous Results and Further Activities*]. Energetski institut «H.P.», Zagreb, 124 p.

JELIĆ, K., GOLUB, M., KOLBAH, S., KULENOIĆ, I. & ŠKRLEC, M. (2010): Croatian Geothermal Resources Updates in the Year 2009. World Geothermal Congress 2010, Bali, Indonesia, Proceedings, 25-29.

JELIĆ, K., ČUBRIĆ, S., PAVIČIĆ, H. & BOŠNJAK, R. (2000): Geothermal Energy Potential and Utilization in the Republic of Croatia. –In: IGLESIAS, BLACKWELL, HUNT, LUND & TAMANYU (eds.): World Geothermal Congress 2000, Tokyo, Proceedings, 237-246.

MUFFLER, L.P.J. & CATALDI, R. (1978): Methods for regional assessment of geothermal resources. Geothermics, 7, 53-89.

ŽIVKOVIĆ, S. A., KRASIĆ, D., DEKANIĆ, I., GOLUB, M., NUIĆ, J., RAJKOVIĆ, D., SAFTIĆ, B., SEČEN, J., VELIĆ, J., VRKLJAN, D., GALIĆ, I., KARASALIHOVIĆ SEDLAR, D., BOHANEK, V., KUREVIJA, T., MARKOVIĆ, S., MAROS, M., HRNČEVIĆ, L., PEĆINA, D., STRAHOVNIK, T., SVRTAN, M., VIDIĆ, D., KOTUR, V., KIRIN, D., GLOBAN, M., ŠOLAR, S. V., ŠINKOVEC, B. & KREBEL, K. (2008): Strategija gospodarenja mineralnim sirovinama Republike Hrvatske [*Mineral resources management strategy of the Republic of Croatia*]. Faculty of Mining, Geology and Petroleum Engineering ,University of Zagreb, Zagreb, 417 p.

3D FE modelling of gravity-driven rock-deformation field, cavity effect, and sensitivity of extensometric measurement systems

Márta KIS, Greg DETZKY, András KOPPÁN

Eötvös Lóránd Geophysical Institute of Hungary, Columbus str. 17-23, H-1145 Budapest,

kis.marta@mfgi.hu

Abstract: In geodynamics, monitoring of long period near-surface deformations of the Earth-crust is mostly performed by extensometry using equipments with different principles, capable for monitoring the variations even in 10^{-11} order. Using the observations wide spectra of natural physical processes of the Earth can be analysed. In this paper 3D finite element modelling has been performed to analyse the gravity-driven rock deformations. Authors calculated deformation fields of a simple-geometry 3D cavity, which are caused by variable gravity loads. Results of a method development are presented where the sensitivity of a given or planned system arrangement against a particular geometric property and a cavity effect rate caused by the unique cavity system embodying the equipment and distorting the real rock-deformations are characterized by the proposed formulas. Dependence of the sensitivity of a measurement system and the cavity effect, on distinct elastic properties, in categorized models has also been investigated.

Key words: 3D FEM, extensometer, sensitivity, cavity effect

1. THEORETICAL BACKGROUND

As the extensometer equipments are usually established in natural or artificial caves, galleries, tunnels, wells under the surface in order to minimize environmental influences (changes in temperature, air pressure, humidity...), one has to take into account the distorting effect of the cavity

system itself on the real rock deformations. The so-called **cavity effect** covers the phenomena that a rock matrix with a unique cavity system deforms differently than it would be filled with rock materials. This causes an inhomogeneity problem in the observation system (**Figure 1**). The cavity effect is one of the most important factors influencing the absolute accuracy of rock deformation measurements.

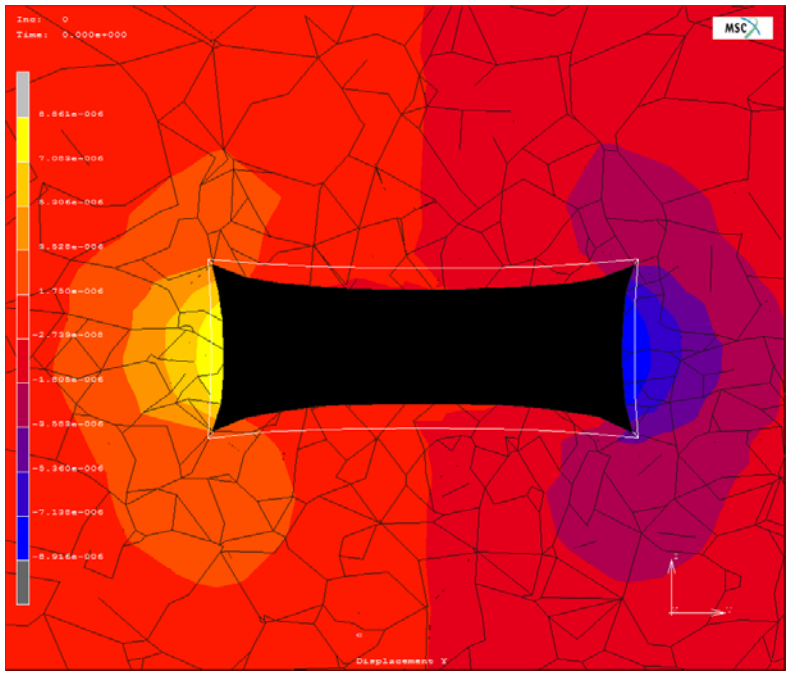

Figure 1: *Relative deformation around a cavity in horizontal plane (displacements are increased by the factor of 2000, colour scale for X-displacements (Kis et al., 2011)*

The calculation of the real cavity effect influencing the accuracy of the deformation measurements cannot be done analytically. In actual practice generally various installation rules are considered in the designing phase to decrease the effect (Mentes, 1997). As the cavity effect is different at various measurement places and arrangements, for the consistent comparison and processing of datasets from different observatories this effect needs to be corrected. In this paper authors propose a method based on 3D FEM for this purpose.

Results of the method can be utilised not only for estimating the cavity effect for a given arrangement, but then again for characterising the

sensitivity of the measurement system. Accordingly, results can be exploited in the planning phase of a measurement system.

2. METHOD

In this paper authors investigate the deformation fields as strain response functionsfor variable gravity loads in case of intact and cavernous 3D rock models with different elastic properties. For the qualitative and quantitative characterisation of the cavity effect and sensitivity authors proposed different parameter fields, described bellow.

As the different processes to be measured induce extremely small amounts of mechanical rock deformations, the nonlinearities caused by the possibly complex geometry of cavities and the slightly nonlinear elastic rock properties can be ignored to a close approximation. Based on this condition all the materials in our models are considered to have linear continuum mechanical behaviour defined by the generalized Hook's law

$$\varepsilon_{ij} = \frac{1}{E}[\sigma_{ij}(1+\nu) - \nu\delta_{ij}\sigma_{kk}], \quad \sigma_{kk} = \sigma_x + \sigma_y + \sigma_z$$

whereε is the strain tensor, σ is the stress tensor, *E* is the Young's modulus, ν is the Poisson's ratio and δ_{ij} is the Kronecker delta. Based on the Hooke's law there is a linear proportionality between the strain and the mechanical load (stress).

In order to characterise the sensitivity and the cavity effectauthors introduced two quantities, the 'Differential Cavity Effect' (DCE**)** and the 'Cavity Effect Ratio' (CER). Let the total deformational displacement resulted bythe 3D FEM, depending on material properties and the load be written as

U*=*G*+*D *U, G, D: (nx3) matrices where i=1..n (n is the number of the nodes in the 3D FE model) and j=1…3 (components in the direction of x, y and z axis)*

where **G** is the global, position dependent displacement related to the long-range effect of the global geological structure enclosing the cavity system (or the local target area)and **D** is the local displacement component related

to the domain part of the cavity system (or target area) (Kis and Detzky, 2008, 2009).

Let the **'Differential Cavity Effect' (DCE)**be defined as a difference of total deformation displacements in a *C*avernous$^{(C)}$and in a congenial *I*ntact$^{(I)}$model (which is identical to the cavernous model except that places of cavities are filled with rock materials)

$$\boldsymbol{DCE = U^C - U^I = G^C - G^I + D^C - D^I = D^C - D^I.} \quad (\boldsymbol{G^C - G^I = 0})$$

The **DCE** differential displacement field is suitable only for a qualitative characterisation related to a particular material, because it depends from the material properties and the amount of the load. At the same time this quantity contains only the anomalous component of the total deformation field caused by the cavity.

Let's define the **'Cavity Effect Ratio' (CER)** as the ratio of relative displacements of the intact and the cavernous model, where those are related to a previously chosen local referential point (node) with index r. This referential point can be considered as the base (fixation) point of a virtual extensometer.

$$CER_{ij} = \frac{D^I_{ij} - D^I_{rj}}{D^C_{ij} - D^C_{rj}}$$

where j=1…3 (direction of x, y and z axis), $1 \leq r \leq n$, i=1,...,n but $i \neq r$. CER_{rj} were chosen as 1 (Kis et al., 2011).

It can be seen that extensometric axial values of CER field comprises the multiplying correction factor for the equipment concerning every node as a possible sensor point. The value of the CER is dependent only from the Poisson's ratio and the reference point. Because the numerator and denominator of the CER equally depend on the elastic modulus and the load, the above parameter field is suitable for quantitative characterisation of the cavity effect, invariantly to the above mentioned variables.

The correction factor CER can be given by 3D FE modelling for the place of observations. Henceforth the measured relative displacement data series can

be corrected, and the datasets from different measuring places can be conformed.

3. NUMERICAL RESULTS

For the investigation of sensitivity and cavity effect, a 3D cavity model was used with simple geometries. Nodal displacements were calculated by Marc Mentat 3D FE modelling software applying variable gravity loads. The cavity model shown in **Figure 2** is surrounded by a rock block, the size of which is approximately one order bigger then the cavity itself. Our model calculations correspond to the theoretical considerations and pointed out the independence of **CER** parameter field from the load and the elastic modulus. At the same time, its dependence upon the Poisson-ratio can be numerically given by repeated modelling (**Figure 3**).

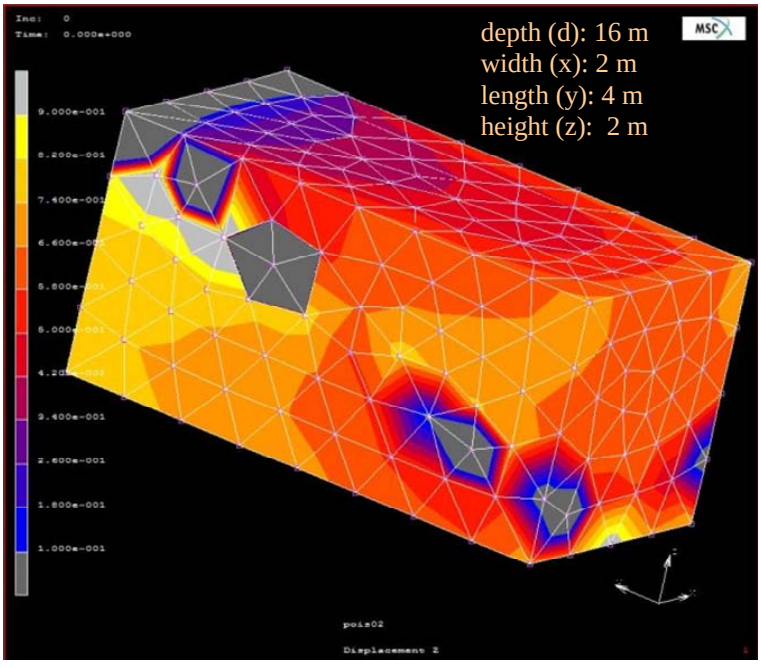

Figure 2: *The cavity model applied in the calculations, with the extensometric-axial component distribution of the correction factor CER (Reference point is signed by '*'.The values of CER are instable in the zone where the relative axial deformation is close to 0, owing to the ratio nature.)*

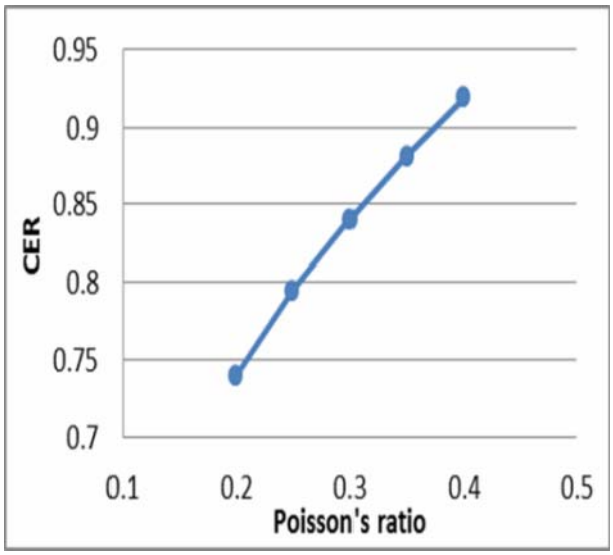

Figure 3: *Dependence of* ***CER*** *upon the Poisson-ratio*

By the help of relative displacement distribution (**RD**) calculated for the surface of the cavity the sensitivities of various arrangements can be analysed (**Figure 4**, normal vertical gravitational load, **RD** axial component). Responses for tidal-order gravity loadwith different (x, y, z) directions were also analysed (**Figure 5**, **RD** distribution on the surface of the cavity).

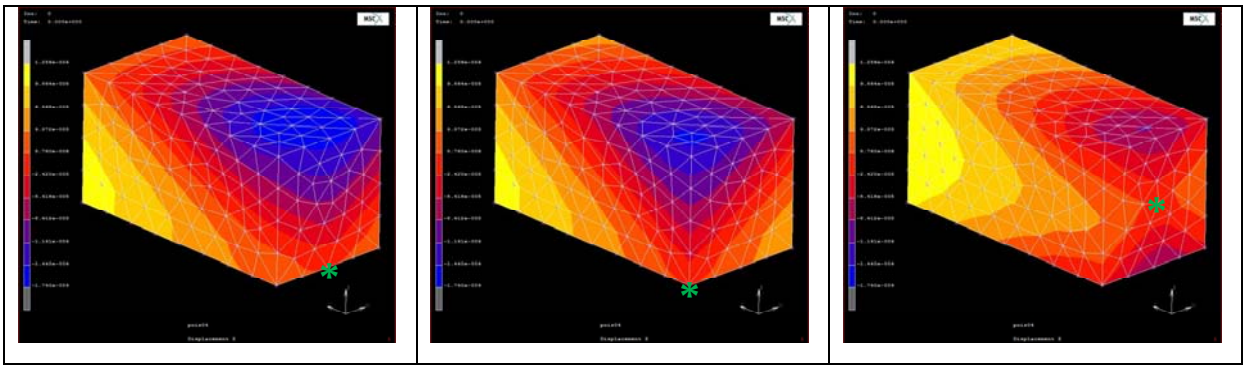

Figure 4.*Investigation of sensitivity and installation-alternatives*

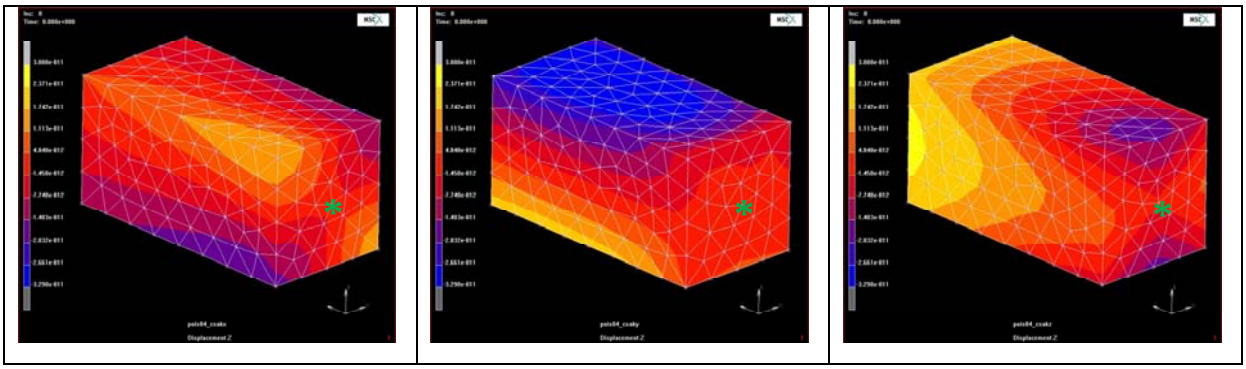

Figure 5: *Investigations of model answers for tidal gravity load in x, y and z directions*

4. CONCLUSIONS

* Planning of extensometer arrangements can be supported by the spatially distribution of the **CER**and **RD**parameter fields introduced in this paper, where the reference points are considered as possible fixation points of the equipment. The zones of maximum values of these parameter fields shape the potentially most sensitive equipment directions.
* The correction factor **CER**against the cavity effect can be calculated for the place of observationsby the proposed method. Henceforth the measured data series of different observatories can be conformed and processed together.
* *The **CER** field is independent from the elastic modulus and the load. The dependence from the Poisson's ratio must be given by series of modelling.*

5. REFERENCES

KIS, M. & DETZKY, G. (2008). Correction improvement for a geophysical extensometric system using finite elementmodelling. 21st CODATA International Conference, Scientific Information for Society Today to the Future, 5-8 October 2008, (Best-poster award).

KIS, M. & DETZKY, G. (2009): Correction improvement for a geophysical extensometric monitoring system by FEM. Proceedings of VPD 2009 Conference, 12-13 May 2009, München.

KIS, M., DETZKY, G. & KOPPÁN A. (2011): 3D finite element modelling for the estimation of the cavity effect, in the application of planning extensometer system. BGS2011, 6th Congress of Balkan Geophysical Society, 3-6 October 2011, Budapest.

MENTES, Gy. (1997): Continuous measurement methods for observing geodynamical environmental and industrial deformations. Academic doctoral thesis, MTA GGKI, Sopron.

Explorative statistical analysis of water chemistry data obtained from the southern part of Lake Fertő (Hungary)

Norbert MAGYAR[1]*, Mária DINKA[2], Gyula KUTRUCZ[3]

[1]Eötvös Loránd University, Department of Physical and Applied Geology, H-1117 Budapest, Pázmány Péter stny. 1/C, magyarnorbert87@gmail.com

[2]Danube Research Institute Hungarian Academy of Sciences Research Centre of Ecology, H-2163 Vácrátót, Alkotmány u. 2-4., dinka.maria@okologia.mta.hu

[3]Hydrometeorological Station of the North-Danubian Water Authority, H-9241 Fertőrákos, kutrucz.gy@t-online.hu

Abstract: The aim of the present study was to distinguish and compare areas with different chemical properties within the Hungarian part of Lake Fertő/Neusiedler See and to determine the parameters that influence the similarity of its sampling locations. Uni- and multivariate data analyses were applied to the data of 15 parameters the majority of which were chemical, with some biological for the time period 1994-2010 from 14 sampling sites. The sampling locations were first clustered then grouped. Four groups could be distinguished: open water, areas in front of the reed belt, channels within the reed belt, and a single sampling site within the reed stands. Using Wilks' λ distribution it was determined that most of the main ions, pH, dissolved oxygen and chemical oxygen demand have a greater effect on the formation of cluster groups than calcium and those parameters standing in close relation to the nutrient cycle. The results clearly show that Lake Fertő cannot be considered to be one homogenous system.

Keywords: cluster analysis, Lake Fertő, spatial variability, water quality, Wilks' λ distribution.

1. INTRODUCTION

Conserving the water quality of surface waters is such an important aim that national borders should perhaps be disregarded in its pursuit. A good example is Lake Fertő/Neusiedler See, which is situated on the Hungarian-Austrian border. However, even today its monitoring is conducted separately by the two countries. The datasets obtained from monitoring are highly complex in most cases. As a result, these are often difficult to interpret and draw meaningful conclusions from. The application of multivariate statistical methods, e.g. cluster analysis (CA) and discriminant analysis (DA), could help in easing these problems. There are tools which are commonly used to analyze water quality data, to describe the quality of the water body the data originated from and to optimize monitoring (Zhou et al. 2007). Using these methods on the time series of the Hungarian part of Lake Fertő the lake's heterogeneity (mosaic structure) was examined, and the question was raised of whether it would be possible to distinguish areas with different chemical properties within the lake also, that of which parameters are the ones that mostly determine the grouping of the sampling sites and what kind of differences could be observed between these groups.

2. THE STUDY AREA

Lake Fertő is Europe's western-most and largest steppe lake, with a surface area of 309 km^2. It is an extremely shallow, well-mixed lake with regulated outflow and large water level fluctuation (Dokulil and Herzig, 2009). Taken as a whole, 54% of the lake is covered by reeds, while regarding only the Hungarian side (75 km^2), the coverage is 85%. Many inner ponds are located on the lake's Hungarian side (Dinka et al., 2004). Lake Fertő is a wetland (which is one of the most endangered ecosystems). Accordingly it is protected by many international conventions, such as UNESCO biosphere

reserve, IUCN's[1] protection zone or World Heritage status (Dinka et al., 2004). The lake's water balance is unstable. Most of its input comes from precipitation, besides which the Wulka and the Rákos streams provide input. Its output is mainly via evaporation. The air is almost constantly in motion, and because of the orographic effects the dominant wind direction is NW, which is followed by the SE direction as far as strength is concerned. Sediment is stirred up at wind speeds of 2 m s^{-1} or more (Löffler, 1979).

3. MATERIALS AND METHODS

The sampling and the lab work was performed by the Hydrometeorological Station of the North-Danubian Water Authority. Monthly sampling is carried out from April to October or November. The data analysis was conducted on the data from the time interval 1994-2010, 14 sampling sites (SS) (**Figure 1A**). Regarding the SS, there are several representing the open water (Nos. 2, 4, 14), one near the reeds (No. 1), one from an inner pond (No. 5), one from each channel (direction N-S, Nos. 6-9; direction E-W, Nos. 10-13) and one from within the reeds (No. 3).

The sampled parameters which suited the conditions of the methods applied[2] are the following: pH, dissolved O_2 (DO), chemical oxygen demand – potassium-permanganate (COD^p), total phosphorus (TP), NO_2-N, NO_3-N, K^+, Na^+, Ca^{2+}, Mg^{2+}, Cl^-, SO_4^{2-}, CO_3^{2-}, HCO_3^- (mg l^{-1}), chlorophyll-a (chl-a) (µg l^{-1}). Specifically, there were 92 time points, yielding 19,320 data altogether.

The methods applied were cluster analysis (using Ward's method, and squared Euclidean distance; Kovács et al., 2006, 2008, 2012) and Wilks' lambda distribution to determine which parameter influences the cluster groups conformation the most (Hatvani et al., 2011). In this method the smaller the value of lambda ($0 > \lambda < 1$) for a certain parameter, the more it

[1] International Union for Conservation of Nature and Natural Resources

[2] Parameters have to be measured at all sampling sites at all investigated time points

determines the cluster groups. As a verification tool, discriminant analysis was used. All of these methods were applied to z-scale standardized data. To aid the visualization of the differences between the cluster groups box-and-whiskers diagrams were used (Hatvani et al., 2009).

4. RESULTS AND DISCUSSIONS

4.1. Spatial variations in water quality

CA was conducted on 92 time points and 15 parameters in order to group the similar SS for every point in time. Each group thus obtained received a code and these codes were clustered again to obtain the most characteristic groups for the whole time interval (**Figure 1B**).

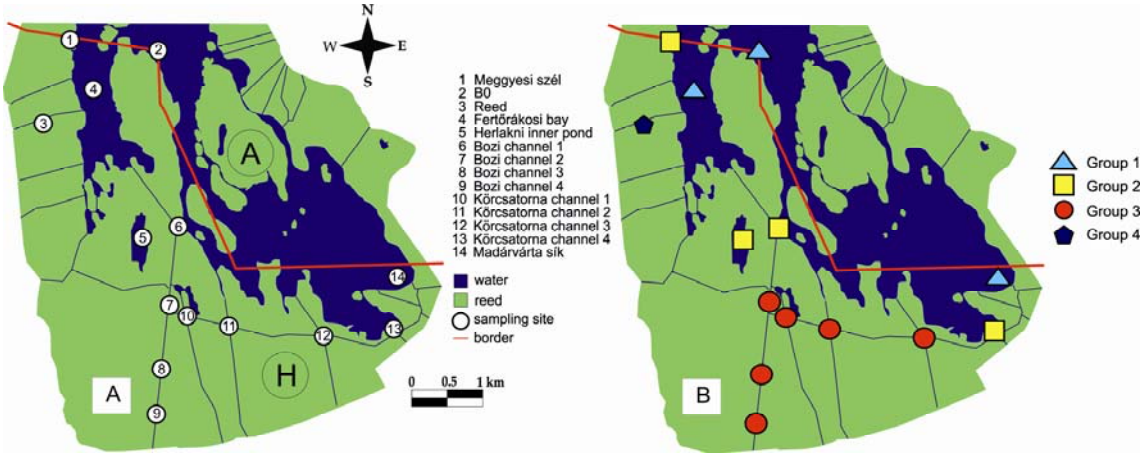

Figure 1: *The location (A) and groups (B) of the sampling sites*

Four groups could be distinguished. First one covered the open water area, the second the sedimentation zone in front of a certain the reed belt (including the SSs located in the channels, which displayed resemblance to the open water, and the inner pond). The third group contained the SSs of the channels, while the fourth contained the sole SS from within the reed stands. Discriminant analysis pointed out that the original groups were correctly identified in 70.3% of the cases. Naturally, this value does not reach 100.0% because at certain sampling events unusual events such as

extreme wind and water level conditions affected the groups conformation. This value confirms that the water quality of Lake Fertő varies significantly over time and space.

4.2. Parameters influencing the grouping of the sampling locations

For each cluster result a Wilks' lambda distribution was calculated. The average values were as follows: pH (0.16), DO (0.19), HCO_3^- (0.20), Cl^- (0.21), CO_3^{2-} (0.21), Mg^{2+} (0.22), K^+ (0.22), COD^p (0.22), Na^+ (0.25), SO_4^{2-} (0.25), Ca^{2+} (0.37), chl-a (0.39), TP (0.46), NO_3-N (0.46), NO_2-N (0.48).
As a next step, the obtained Wilks' λ quotients (92 x the number of parameters) were clustered, and two groups were obtained. The main anions and cations (except Ca^{2+}) with pH, COD^p and DO (average 0.21) influenced the formation of the cluster groups the most. Parameters in close relation to the nutrient cycle and calcium, however, had a smaller influence (average 0.43).

4.3. Differences between the groups

The groups obtained from the 92 time points were compared using boxplots. The median of pH, DO and CO_3^{2-} in the open water (cluster group (G) 1) was higher than the one in the channels (G3) or in the reed stands (G4) (**Figure 2A**, **B, C**). All three displayed a similar pattern.
In the case of pH, the phenomenon behind the change in its values is the chemical, biological processes in the reed belt producing humic substances, which originate mostly from the decomposition of reed detritus (**Figure 2A**). The pH of the waters near the shore increases gradually towards the deeper water, after seeping through the reed belt. The water of the lake is much more alkaline in the deeper sections.
Regarding DO (**Figure 2B**) in the open water (G1), because of the frequent mixing and low nutrient input, the oxygen conditions are good. On the

contrary, in the reed channels (G3) oxygen concentrations are low or in certain cases anaerobic conditions may even occur (Dinka and Szeglet, 2001). The lack of mixing and the oxidization of organic substances decreases dissolved oxygen content. The median of DO is much higher at the sole SS in the reed stands (G4) than at the SSs in the channels. This may have happened because in the surroundings of G4 the reed stands degraded, so given the lack of shelter from the frequent NW winds allows the water here to be stirred up more frequently than in the channels.

CO_3^{2-}, because of its pH dependence (Daniel, 1999), behaves similarly to it in all the groups (**Figure 2C**). The median of pH oscillates around 8.49, which is almost at the critical threshold for carbonate ions to be present. This oscillation caused carbonate concentrations to reach the highest values in the open water (G1) and the lowest in the channels (G3).

COD^p increases gradually from G1 to G4 (**Figure 2D**). However this increase is influenced by the vicinity of the reeds. In G4 the water is shallow, the diurnal temperature fluctuation is high, and both of these influence the biological processes.

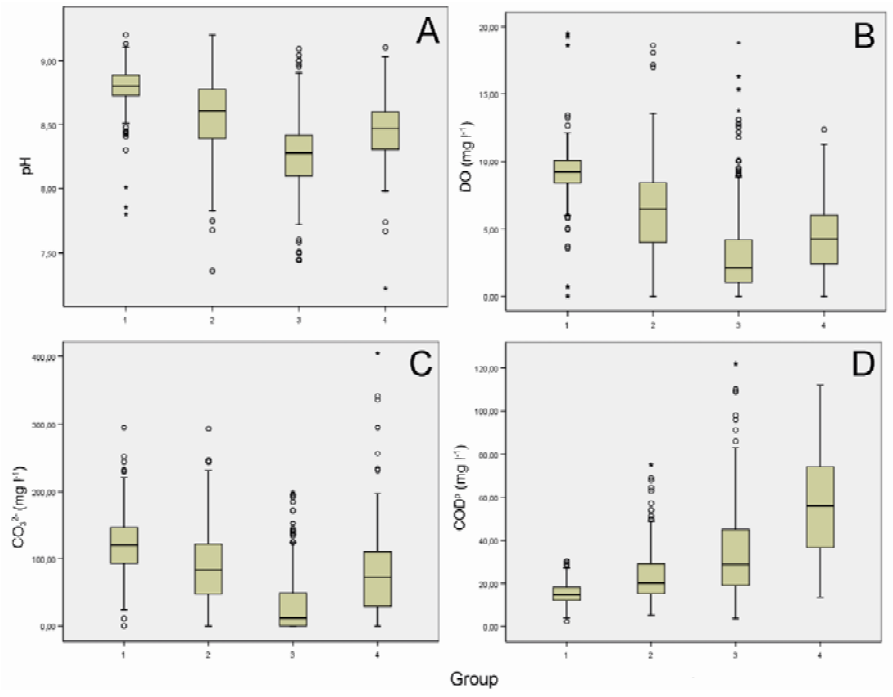

Figure 2: *Box-and-whiskers plot: pH (A); DO (B); CO_3^{2-} (C); COD^p (D)*

5. CONCLUSIONS

This study emphasises the fact that multivariate data analysis methods can be optimal tools in evaluating complex environmental datasets, as in the case of Lake Fertő. With CA, the most representative pattern of SS was determined, resulting in four groups (open water, sedimentation zone in front of the reed, channels, reed stands).

Using Wilks' lambda distribution it was pointed out that the main ions, pH, COD^p and DO, determine the formation of the cluster groups the most, while calcium and nutrient content (TP, NO_2-N, NO_3-N) and chl-a were less relevant. Boxplots highlighted significant differences between the distinguished areas.

It can be stated that the water quality of the Hungarian part of Lake Fertő varies both in time and space. This is reflected in its fragmented water surface, which is the basis for its diversity.

6. ACKNOWLEDGMENTS

We the authors would like to thank the Hydrometeorological Station of the North-Danubian Water Authority in Fertőrákos for providing the datasets; furthermore we would like to thank the colleagues working at the Department of Physical and Applied Geology for the stimulating discussions.

7. REFERENCES

DANIEL, J. J. (1999): Introduction to Atmospheric Chemistry. Princeton University Press, New Jersey, 264 p.

DINKA, M. & SZEGLET, P. (2001): Some characteristics of reed that indicate different health between vigorous and die-back stands (Phragmites

australis/CAv./TRIN ex STEUDEL). Verh. Internat. Ver. Limnol., 27, 3364-3369.

DINKA, M., ÁGOSTON-SZABÓ, E., BERCZIK, Á. & KUTRUCZ, GY. (2004): Influence of water level fluctuation on the spatial dynamic of the water chemistry at Lake Fertő/Neusiedler See. Limnologica, 34, 1–2, 48–56.

DOKULIL, M. T. & HERZIG, A. (2009): An analysis of long-term winter data on phytoplankton and zooplankton in Neusiedler See, a shallow temperate lake, Austria. Springer Science Aquat. Ecol., doi: 10.1007/s10452-009-9282-3.

HATVANI, I. G., KOVÁCS, J., KORPONAI, J. & KOVÁCSNÉ, SZ. I. (2009): A Kis-Balaton Vízvédelmi Rendszer (KBVR) hosszú távú fizikai, kémiai és biológiai paramétereinek elemzése [*Analysis of long term physical, chemical and biological data series of the Kis-Balaton Water Protection System – in Hungarian*]. Hidrológiai Közlöny, 89, 6, 15-18.

HATVANI, I. G., KOVÁCS, J., KOVÁCSNÉ, SZ. I., JAKUSCH, P. & KORPONAI, J. (2011): Analysis of long-term water quality changes in the Kis-Balaton Water Protection System with time series-, cluster analysis and Wilks' lambda distribution. Ecological Engineering, 37, 4, 629-635.

KOVÁCS, J., CZAUNER, B., KOVÁCSNÉ, SZ. I., BORSODI, A. & RESKÓNÉ, N. M. (2008): A Balaton eltérő vízminőséggel rendelkező térségeinek változásai és a mért vízminőségi idősorok mintázatai 1985-2004 között [*Changes in the different water quality areas of Lake Balaton and the pattern of its data series (1985-2004) – in Hungarian*]. Hidrológiai Közlöny, 88, 6, 172-174.

KOVÁCS, J., KOROKNAI, ZS. & KOVÁCSNÉ, SZ. I. (2006): A Balaton környezeti állapotának vizsgálata többváltozós adatelemző módszerekkel. -In: SZENDREI, G. (ed.): Magyarország környezetgeokémiai állapota [*Analysis of the ecological state of Lake Balaton using multi variate data analysis. - In: Environmental-geochemical state of Hungary –in Hungarian*]. Innova Print Kft., Budapest, pp. 111-117.

KOVÁCS, J., TANOS, P., KORPONAI, J., KOVÁCSNÉ, SZ. I., GONDÁR, K., GONDÁR-SŐREGI, K., HATVANI, I. G. (2012): Analysis of Water Quality Data for Scientist. -In: VOUDOURIS, K., VOUTSA, D. (eds.): Water Quality Monitoring and Assessment, InTech Open Access Publisher, Rijeka, pp. 65-94.

LÖFFLER, H. (1979): Neusiedlersee: The limnology of a shallow lake in Central Europe, Monogr. Biol. 37. Dr W.Junk Publishers, The Hague, Boston, London, 543 p.

ZHOU, F., LIU, Y. & GUO, H. (2007): Application of multivariate statistical methods to water quality assessment of the watercourses in Northwestern New Territories, Hong Kong. Environ. Monit. Assess., doi: 10.1007/s10661-006-9497-x.

Minimum dataset and spatial distribution for possible mapping of Sarmatian deposits, SW part of CPBS

Ana MAJSTOROVIĆ BUŠIĆ INA-Oil industry, Oil & Gas Exploration and Production, Sector for Geology and Reservoir Management, Šubićeva 29, 10000 Zagreb, e-mail: ana.majstorovic@ina.hr

Abstract: In the palaeogeographic sense, the largest part of Central Paratethys is represented by the Pannonian Basin System (PBS). The southwestern part of that system includes the North Croatian depressions (CPBS). During the Sarmatian (13.0–11.5 Ma) transtensional tectonics were replaced by transpressional. The importance of alluvial fans significantly decreased because regression started, sea level was lowered and salinity was reduced. The studied area belongs to the south-western marginal part of the PBS and the Central Paratethys. There are a few problems with mapping Sarmatian deposits, because it is difficult to distinguish Badenian/Sarmatian/Pannonian boundaries. Since the sampling grid is irregular, mapping by computer software is not favourable and variogram analysis would not be realistic. The best way of mapping this type of area is mapping by "hand", but also only the marginal part close to present mountains.

Key words: Sarmatian, mapping, minimum data, SW part of CPBS.

1. INTRODUCTION

During the Sarmatian (Middle Miocene) the sedimentary basins of Northern and Central Croatia belonged to the south-western part of the Central Paratethys Sea (Pavelić, 2002). Temporary connections and disconnections with the palaeo-Mediterranean realm led to peculiar palaeo-environmental characteristics and sedimentation in Paratethys (RÖGL, 1998).

In the geotectonical sense, the largest part of Central Paratethys is represented by the Pannonian Basin System (PBS). The PBS is surrounded by the Alps, Carpathian and Dinarides mountains. The southwestern part of the PBS includes the North Croatian Basin and the Northern Bosnia region (Pavelić, 2002).

This paper analyzes the arrangement of varied data point, "weighted" with different sources (outcrops and well data), small numbers of data and also by subjective selection of data point along presumed border of the Sarmatian depositional environment. In this paper only SW part of Sava Depression as the one part of the North Croatian Basin is described.

2. SHORT EVOLUTION HISTORY OF THE ANALYSED AREA

The sediments of the Neogene and Quaternary systems in the southwestern part of the PBS are divided into three sedimentary megacycles, which are separated by regional markers (Velić et al., 2002; Velić, 2007). The general time scale of different tectonical styles and depositional events is shown in Figure 1 (Malvić & Velić, 2011).

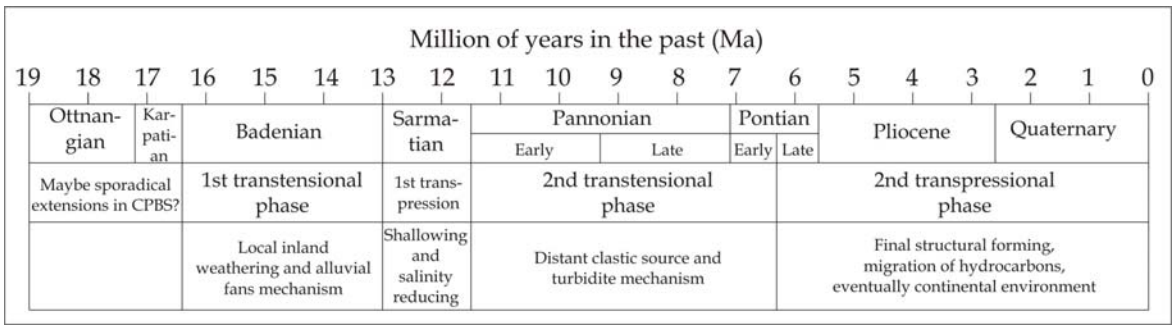

Figure 1: *The main tectonical and depositional events in CPBS during Neogene and Quaternary (from Malvić & Velić, 2011)*

The first megacycle is characterized by a heterogeneous lithological composition, consisting of marine syn-rift and early post-rift sediments of Middle Miocene age. The second depositional megacycle was active in the Late Miocene and is characterized by sandstone, marly sandstone, sandy

marl, and marl lithofacies. The third megacycle is of Pliocene-Quaternary age and is composed of sand, clay, and gravel with some sporadic lenses of lignite or peat (Velić et al., 2002).

During the Sarmatian (13.0–11.5 Ma) transtension tectonics were replaced by transpression. The importance of alluvial fans significantly decreased because regression started (Malvić & Velić, 2011), sea level was lowered and salinity was reduced.

3. ANALYSED LOCALITIES

The studied area belongs to the south-western marginal part of the Pannonian Basin System (PBS) and south-western part of Central Paratethys. Based on published papers (Vrsajko et al., 2005, 2006; Šikić, 1995) short overview of Sarmatian deposits in the analysed area is given. Based on general geological map (Šikić et al. 1979) some outcrops on Sv. Nedelja Mts. were located and describe. Data form two wells were also included.

Locality 1- "Trzunove pećine" (Figure 2) are represented with biocalcarinites (Figure 3). These deposits are composed of numerous skeletal and other fragments. Fossils association mostly contains foraminifers *Elphidium flexuosum grilli, Elphidium hauerinium* and fragments of molluscs *Musculus sarmaticus, Pirinella picta* etc. (Šikić, 1995). This facies suggests deposition within high-energy shallow- water environment of reduced salinity.

Locality 2 – "Podsusedsko Dolje" (Figure 2) is represented with clays and marls which are horizontally bedded and almost laminated. Sometimes these sediments are massive. Sands occur as thin intercalations within this group of sediments. A rich fossil association is found in the marls. The *Elphidium–Protelphidium–Porosononion* foraminiferal association is an important palaeoecological characteristic of the marls. The whole fossil association documents generally reduced salinity within Sarmatian environments (Vrsaljko et al., 2006).

Localities 3, 4, 5 and **6** are in the Svetonedeljski breg (Figure 2). In the area of Svetonedeljski Breg Sarmatian sediments can be found, dominated by distinctly laminated marls. Occasionally and especially in the lower part of the Sarmatian deposits, metre-thick sand beds are observed. Sandstones consist of biogenic detritus, mainly re-deposited from Badenian rocks (Vrsaljko et al., 2005).

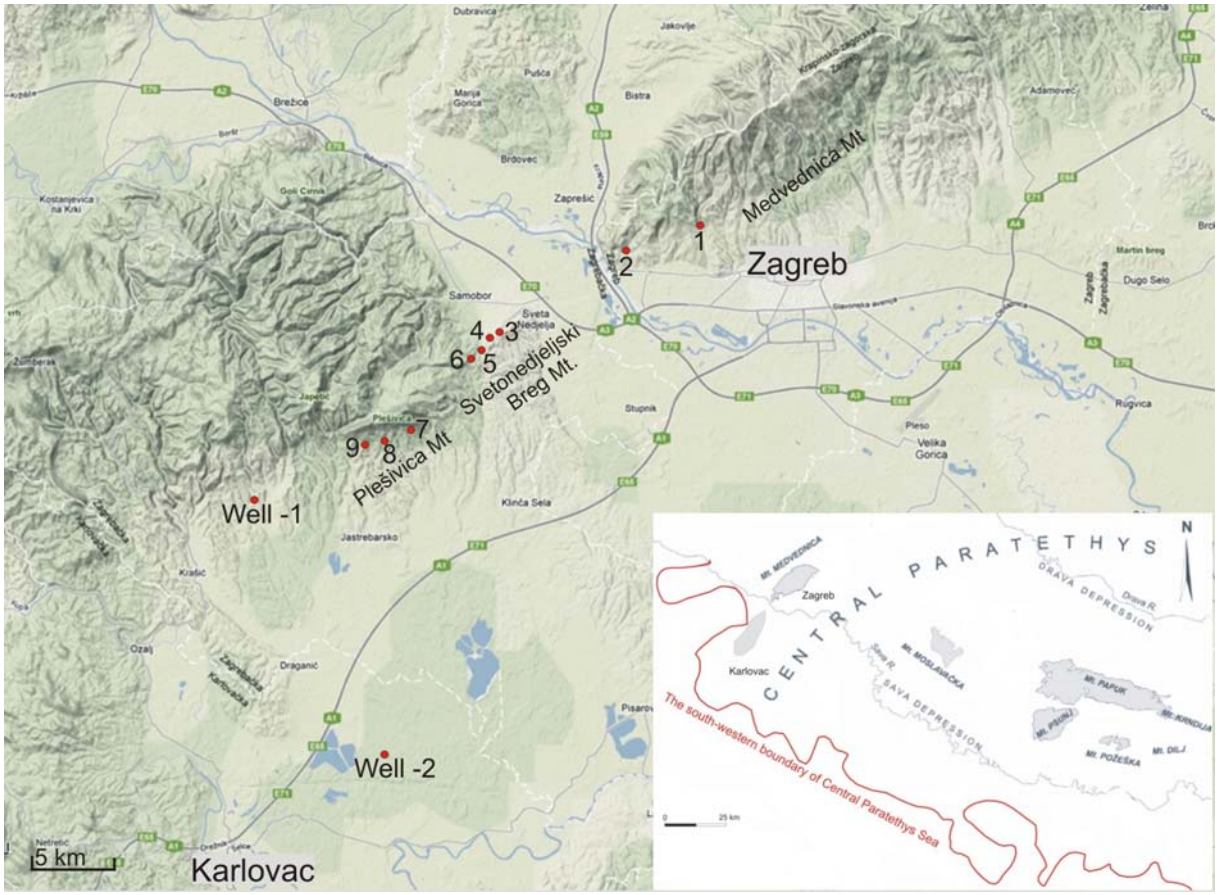

***Figure 2**: Localities – 1- Trzunove pećine; 2- Podsusedsko Dolje; 3,4,5,6- Svetonedeljski Breg area; 7,8, 9- the slopes of Plešivica Mt.(map taken and modified from Google maps; the south-western boundary of Central Paratethys Sea is modified after Pavelić et al, 2003, taken from Ćorić et al. 2009).*

Localities 7, 8 and **9** are observed on the slopes of Plešivica Mt. (Figure 2). The Lower Sarmatian is mainly composed of marls and clays, with sporadically with cm-thick intercalations of calcarenites and conglomeratic sandstones. The middle parts of the Sarmatian are characterized by the

presence of varve-like laminated marls and clays, with scarce intercalations of sandstones. Rhytmites composed of laminites, limestones and sandstones comprise the upper parts of the Sarmatian, while in the uppermost ten metres layers of marls and clays dominate, varying in thickness from millimetres to centimetres (from Vrsaljko et al., 2005).

Well-1 - from cutting samples and cored interval (interval 416-122 m) in the Sarmatian deposits, thicknesses about 100 m was determined.

Well-2 - based on cores from two intervals (intervals 1392–1394 m and 1462–1467 m) Sarmatian laminated marls were determined. The thickness of the Sarmatian sediments is approximately 80 m (from Vrsaljko et al., 2005).

Figure 3: *Calcitic marl blocks outcrop (vertical scale about 10 m, Zagreb, Trzinove pećine locality, Medvednica Mt., altitude 264.4 m) [photo Majstorović Bušić, 2011].*

4. DISCUSION AND CONCLUSION

There are a few problems with mapping Sarmatian deposits. Thickness mapping from the wells in the central part of the Sava Depression is not possible, because it is difficult to distinguish Badenian/Sarmatian/Pontian

boundaries. Sarmatian is rarely determined with a clearly defined top and bottom facies. One of the problems is insufficient number of paleontological analyses and well cores of this interval. Despite numerous outcrops along depression margins, mapping of outcrops is also difficult. The disadvantage is inability of measuring total thickness. Also, Badenian/Sarmatian/Pannonian boundaries are often covered with vegetation and difficult to determine.

According to Pavelić (2002) south-western margins of the Parathetys Sea area were defined. The closest wells to the boundary with proven Sarmatian deposits are Well-1 and Well-2. Approximate thickness in Well-1 is 100 m and in Well-2 80 m. Sarmatian sediments belong to shallow shelf area and south-west boundary is located south from mentioned wells.

Possible explanation of differences in the depth of the Sarmatian sediments in those two wells is that whole Sarmatian sedimentation basin has been continuously sinking during 2nd transtension phase. Well-1 is located very close to Plešivica Mt. while Well-2 is located more to the deeper basin. There is also a fault very close to the Plješevica Mt., that could lowered area that belongs to Well-2 playing role of syn-sedimentary fault.

Since the sampling grid and small number of data point is irregular, mapping by computer software is not favourable and variogram analysis would not be realistic. Thickness mapping of the outcrops also does not represent true total thickness. So, the best way of mapping geological variables in the Sarmatian rocks in analysed area is mapping by "hand", especially because collected data cover only SW and W margin of Sarmatian depositional palaeo-environment in the Sava Depression.

5. REFERENCES

ĆORIĆ, S., PAVELIĆ, D., RÖGL, F., MANDIC, O., VRBAC, S., AVANIĆ, R., JERKOVIĆ, L. & VRANJKOVIĆ, A. (2009): Revised Middle Miocene datum for initial marine flooding of North Croatian Basins (Pannonian Basin System, Central Paratethys). Geologia Croatica, 62, 1, 31-43.

MALVIĆ, T. & VELIĆ, J. (2011): Neogene Tectonics in Croatian Part of the Pannonian Basin and Reflectance in Hydrocarbon Accumulations. In: SCHATTNER, U. (ed.): New Frontiers in Tectonic Research: At the Midst of Plate Convergence, InTech, Rijeka, 352 p.

PAVELIĆ, D. (2002): The south-western boundary of Central Paratethys. Geologia Croatica, 55, 1, 83-92.

PAVELIĆ, D., AVANIĆ, R., KOVAČIĆ, M., VRSALJKO, D. & MIKNIĆ, M. (2003): An Outline of the Evolution of the Croatian Part of the Pannonian Basin System.– In: VLAHOVIĆ, I. & TIŠLJAR, J. (eds.): Evolution of Depositional Environments from the Palaeozoic to the Quaternary in the Karst Dinarides and the Pannonian Basin. 22nd IAS Meeting of Sedimentology, Opatija – Sept. 17–19, 2003, Field Trip Guidebook, Zagreb, 155–161.

RÖGL, F. (1998): Palaeographic consideration for Mediterranean and ParatethysSeaways (Oligocene to Miocene). Annales des Naturhistorischen Museum, Wien, 99A, 279–310.

ŠIKIĆ, K . (1995): Geološki vodič Medvednice, Institut za geol. istraž. & Ina–Industrija nafte d.d. Naftaplin , Zagreb, 199. p.

ŠIKIĆ, K., BASCH, O. & ŠIMUNIĆ, A. (1979): Osnovna geološka karta 1:100 000. Tumač za list Zagreb l33-38. Institut za geol. istraž., Zagreb, Savezni geol. Zavod, Beograd, 81 p.

VELIĆ, J., WEISSER, M., SAFTIĆ, B., VRBANAC, B. & IVKOVIĆ, Ž. (2002): Petreloleum-geological characteristics and exploration level of the three Neogene depositional megacyclus in the Croatian part of the Pannonian basin. Nafta, 53, 6-7, 239-249.

VELIĆ, J. (2007): Geologija ležišta nafte i plina. (ed. Zorić, I.).- University of Zagreb, Zagreb, 342 p.

VRSALJKO, D., PAVELIĆ, D. & BAJRAKTAREVIĆ, Z. (2005): Stratigraphy and Palaeogeography of Miocene Deposits from the Marginal Area of Žumberak Mt. and the Samoborsko Gorje Mts. (Northwestern Croatia). Geologia Croatica. 58, 2, 133-150.

VRSALJKO, D., PAVELIĆ, D., MIKNIĆ, M., BRKIĆ, M., KOVAČIĆ, M., HEĆIMOVIĆ, I., HAJEK-TADESSE, V., AVANIĆ, R. & KURTANJEK, N. (2006): Middle Miocene (Upper Badenian/Sarmatian) Palaeoecology and Evolution of the Environments in the Area of Medvednica Mt., (North Croatia). Geologia Croatica, 59, 1, 51-63.

Stochastical categories in the probability of success (POS) calculation

Tomislav MALVIĆ*[1,2], Josipa VELIĆ[2], Marko CVETKOVIĆ[2]

[1]INA Plc., Šubićeva 29, 10000 Zagreb, tomislav.malvic@ina.hr

[2] University of Zagreb, Faculty of Mining, Geology and Petroleum Engineering, Pierottijeva 6, 10000 Zagreb, josipa.velic@rgn.hr , marko.cvetkovic@rgn.hr

Abstract: Geological risk of existence of hydrocarbon reservoir is calculated on deterministical, stochastical or expert-opinion way. The most often term for numerical result is 'Probability Of Success' (abbr. POS) of hydrocarbon discovery. In all cases it included adding of probability values to categories that define hydrocarbon system. Here is described hybrid model, based on the most often deterministical approach that is, up to now, applied in the Croatian hydrocarbon provinces in the Pannonian Basin System. The term "hybrid" is applied because deterministical estimation of one category is replaced with stochastical calculations. As result, some geological events can be estimated with several values, what eventually give several probabilities of hydrocarbon reservoir existence. This is advantage of classical deterministical approach.

Key words: geological risk, determinism, stochastic, Pannonian basin, Croatia.

1. INTRODUCTION

Calculation of geological risk is well-established tools for estimation of possible reservoir in plays, prospects or reservoirs. Using of that calculation is well described in the areas of the Sava and Drava Depressions (Hernitz et al., 2000; Malvić & Rusan,2007, 2009; Vrbanac et al., 2010). The term 'play' in those papers is generally defined as an stratigraphical unit in the range of

stage or sub-stage where hydrocarbon production already exist and 'prospect' as vertical surface projection of potential reservoir borders. It was a little different then definition given by Rose (2001) or White (1992) where 'play' is generally defined as an operational unit characterised by several prospects and/or fields and 'prospect' is an economic unit. However, those are similar approaches where classical deterministical calculation of POS can be equally applied.

Mathematically, deterministical calculation of POS is simple multiplication of several, the most often five, geological categories probabilities. Furthermore, each category is defined with several geological events where each of them also has own probability, what means that calculation of category probability is the same procedure as POS calculation. Although result is single numerical value, the probability values of events are not always exactly defined. In fact, only exact and discrete source of values for POS calculation are probability tables, like one shown on **Figure 1**. Such tables are subjective in meaning that each event probability is colloquial considered and officially accepted only in one team, company, institute etc. If it is published (e.g., Malvić & Rusan, 2007, 2009) also can be cited from others, but most of them always stay as internal documents. However, the events can be completely estimated from expert opinion, what means that single person or team will completely have freedom and responsibility for given values. Such process is biased and often subdued to benchmarking, i.e. corrections after new data (especially wells) appeared. This way is not discussed here.
However, it is obvious that the most of geological events (e.g., **Figure 1**) can be estimated with several probabilities selected from possible range, like it is often applied in Monte Carlo methods. However, in POS calculation number of available data if larger than in Monte Carlo, what asks for more reliable estimation of range values.

TRAP	RESERVOIR	SOURCE ROCKS	MIGRATION	PRESERVATION OF HYDROCARBONS	
Structural	**Reservoir type**	**Source facies**	**HC shows**	**Reservoir pressure**	**'p'**
Anticline and **buried hill** linked to basement	**Sandstone**, clean and laterally extended; **Basement** granite, gneiss, gabbro; **Dolomites** with secondary porosity; Algae reefs with significant secondary porosity, due karsting or other subaerial processes exposure	**Kerogene** type **I and/or II**	**Production** of hydrocarbons	**Higher** than hydrostatic	**1.00**
Faulted anticline	**Sandstones,** rich in silt and clay; **Basement** with secondary porosity, limited extending; **Algae reefs**, filled with skeletal debris, mud and marine cements	**Kerogene** type **III**	Hydrocarbons **in traces**; **New gas** detected >10%	**Approximately** hydrostatic	**0.75**
Structural nose closed by fault	**Sandstone** including significant portion of silt/clay particles, limited extending;	**Favourable palaeo-facies** organic matter sedimentation	**Oil** determined **in cores** (luminescent analysis, core tests)	**Lower** than hydrostatic	**0.50**
Any "positive" faulted structure, margins are not firmly defined	**Basement rocks**, including low secondary porosity and limited extending	**Regionally known** source rock facies, but not proven at observed locality	**Oil** determined **in traces** (lumin. anal., core tests)		**0.25**
Undefined structural framework	Undefined reservoir type	Undefined source rock type	Hydrocarbon are not observed		**0.05**

Stratigraphic or combined	Porosity features	Maturity	Position of trap	Formation water	
Algae reef form	**Primary** porosity **>15%** **Secondary** porosity **>5%**	Sediments are in **catagenesis phase** ("oil" or "wet" gas-window)	**Trap** is located in proven **migration distance**	**Still aquifer** of field-waters	**1.00**
Sandstones, pinched out	**Primary** porosity **5-15%** **Secondary** porosity **1-5%**	Sediments are in **metagenesis phase**	**Trap** is located **between two source rocks** depocentres	**Active aquifer** of field-waters	**0.75**
Sediments changed by **diagenesis**	**Primary** porosity **<10** **Permeability <1x10**(-3)** micrometer**2	Sediments are in **early catagenesis phase**	**Short migation pathway** (<=10 km)	**Infiltrated aquifer** from adjacent formations	**0.50**
Abrupt changes of petrophysical properties (caly, different facies)	**Secondary** porosity **<1%**	Sediments are in **late diagenesis phase**	**Long migration pathway** (>10 km)	**Infiltrated aquifer** from surface	**0.25**
Undefined stratigraphic framework	Undefined porosity values	Undefined maturity level	Undefined source rocks		**0.05**

Quality of cap rock	Data sources	Timing	
Regional proven cap rock (seals, isolator)	Geochemical analysis on **cores and fluids**	**Trap** is **older than** matured **source** rocks	**1.00**
Rocks without reservoir properties	Analogy with **close located geochemical**	**Trap** is **younger than** matured **source** rocks	**0.75**
Rocks permeable for gas (gas leakage)	**Thermal modeling** and calculation (e.g. Lopatin, Waples etc.)	**Relation** between trap and source rocks is **unknown**	**0.50**
Permeable rocks with locally **higher silt/clay content**	**Thermal modeling** at just a **few locations**		**0.25**
Undefined cap rock	Undefined data sources		**0.05**

Figure 1: *This is an example of relevant database prepared for the Bjelovar subdepression and can be mostly unchanged applied in all Croatian depressions (after Malvić & Rusan, 2007, 2009)*

If we accept statement that subsurface is deterministically defined, but our knowledge is only partially and highly depend on number and kind of data,

then some events of the potential reservoir can be estimated stochastically. The most used stochastical tools in geology are geostatistical simulation methods applied on reservoir variables like porosity, thickness and depth (Novak Zelenika & Malvić, 2011). Such approach can be regularly applied for several events in POS calculation (e.g., Malvić, 2009) and be set up as standard part of this procedure.

2. BASIC THEORY 'POS' CALCULATION AND SELECTION OF 'STOCHASTICAL' EVENTS

Generally, the hydrocarbon plays or prospects are deterministically analysed by several independent geological categories. The most often those are: (1) structures, (2) reservoirs, (3) migration, (4) source rocks and (5) preservation of hydrocarbons (e.g., Malvić & Rusan, 2007, 2009; White, 1992). The most category values can be evaluated from well-files, well logs, seismic, cores and geological interpretations or the comprehensive regional papers (e.g., Velić et al., 2012). Based on those data it can be easily selected value from probability table valid for Bjelovar Subdepression and the most of Croatian part of the Pannonian Basin System (**Figure 1**).

Such defined values make possible to calculate 'POS' for any consider play or prospect by **Equation 1**: POS = p (structures) x p (reservoir) x p (migration) x p (source rocks) x p (preservation). However, let to observe some events, even subcategories, which are defined with numerical values. Those are obviously subcategory 'Porosity features' (in the category 'Reservoir'), but also 'Quality of cap rocks' ('Trap') that can be estimated using permeability data and 'HC shows' ('Migration') that can be defined directly using percentage of new gas detected. Those give three subcategories that can be defined via ranged values, i.e. numerically and consequently be calculated spatially by geostatistical stochastical maps.

The first testing of such approach had been done in the Badenian part of gas-condensate reservoir in the Stari Gradac-Barcs Nyugat Field (Malvić,

2009). The reservoir is of massive type, trapped with combined structural-stratigraphic closure, with very complex lithology divided in four lithofacies (but single hydrodynamic unit). The clastites of Badenian were the best sampled and also show regularity of porosity distribution regarding depositional model clearly defined with strike NW-SE (Malvić, 2006). It meant that it was possible to map reservoir porosity with numerous stochastical realisations and got the range of possible values. In fact average porosity had been calculated for each 'Original Gas in Place' (OGIP) volume and the minimal OGIP corresponded to 3.1%, media to 3.2% and maximum to 3.53%. Those values were considered as three possible inputs for 'Porosity feature' subcategory what could result in three POS values. In presented case (Malvić, 2009) the categories were estimated as follows: **Structures:** Trap is faulted anticline (p=0.75); Quality of cap rock is regionally proven (p=1.00); **Reservoir:** Coarse-grained sandstones (p=1.00); Primary porosity **three values (3.1; 3.2; 3.53)**<5% (p=0.50); **Source rocks**: Kerogen type II (p=1.00); **Migration:** Proven production (p=1.00); Position of trap (p=1.00); Trap is older than mature source rocks (p=1.00); **HC preservation:** Higher than hydrostatic (p=1.00); Still aquifer (p=1.00). The total POS=0.5 x 0.75 = 0.375. Although three 'Porosity feature' values had been used, all of them belonged to the same event and resulted in unique POS. However, the principle of using of stochastic in deterministical calculation is clearly and correctly presented.

3. DISCUSSION AND CONCLUSION

Reservoir space is always characterised with uncertainties, due to limited number of available data. Evaluation of possible new hydrocarbon discoveries in always connected with their 'POS' values in the range 0-1. The methodology for such calculation in the Croatian part of the Pannonian Basin System is well established and published. However, some of subcategories can be expressed numerically (**Figure 2**). The 'Porosity feature' is always

defined with numerical values, what directly define the selection of relevant geological events with corresponding probability (**Figure 1**). However, the subcategories 'HC shows' and 'Quality of cap rock' can be also indirectly transformed in numerical values if 'HC shows' is expressed with percentage of new gas or percentage of observed oil traces in cores or recovered quantities. The same statement is valid for cap rock where sealing properties can be represented with exact permeability ranges that define particular geological events (**Figure 1**).

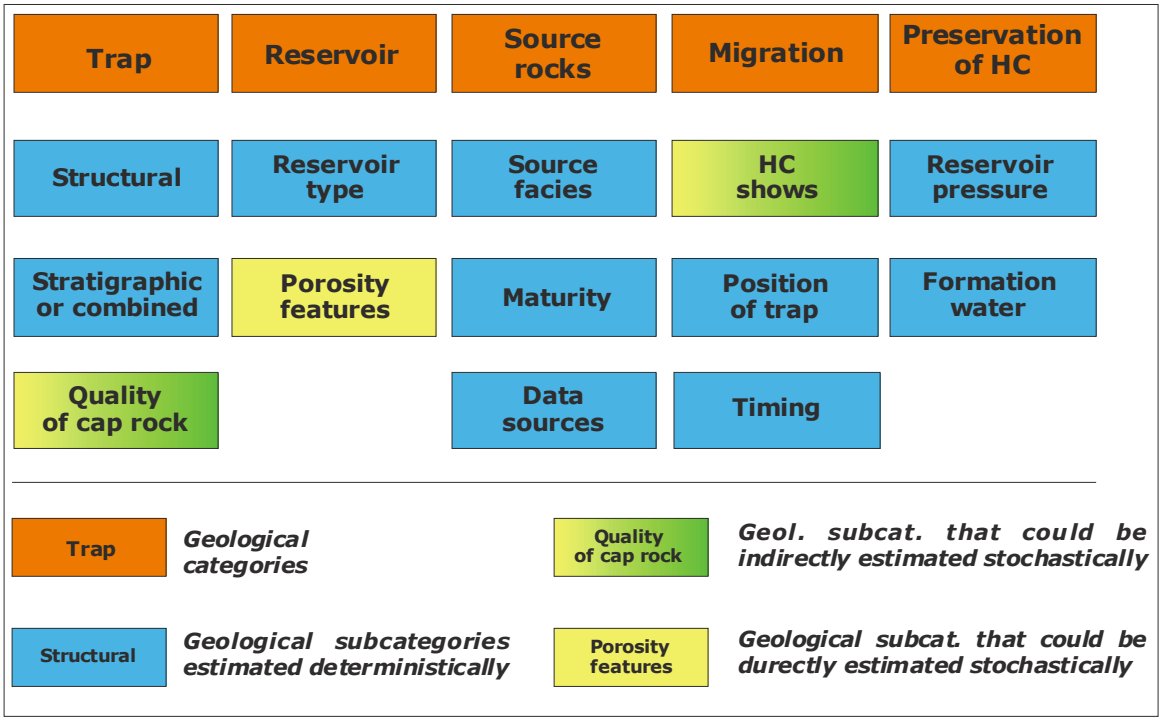

Figure 2: *This is an example of relevant database prepared for the Bjelovar subdepression and can be mostly unchanged applied in all the Drava depression (after Malvić & Rusan, 2007, 2009)*

Consequently, those subcategories can be estimated through stochastical simulation(s). If from results of all three subcategories are selected minimum, median and maximum realisation as outcomes, it leads to 27 possible combination for POS. It is way how in deterministical calculation can be introduced also stochastical algorithms and help to reach POS value expressed through range.

4. REFERENCES

HERNITZ, Z., BOKOR, N. & MALVIĆ, T. (2000): Probability evaluation of new hydrocarbon discoveries in selected parts of the Sava and Drava depression, Croatia. Nafta, special issue, 144-155.

MALVIĆ, T. (2009): Stochastical approach in deterministic calculation of geological risk - theory and example. Nafta, 60, 12, 651-657.

MALVIĆ, T. (2006): Middle Miocene Depositional Model in the Drava Depression Described by Geostatistical Porosity and Thickness Maps (Case study: Stari Gradac-Barcs Nyugat Field). Rudarsko-geološko-naftni zbornik, 18, 63-70.

MALVIĆ, T. & RUSAN, I. (2009): Investment Risk Assessment of Potential Hydrocarbon Discoveries in a Mature Basin (Case Study from the Bjelovar Sub-Basin, Croatia). Oil and Gas European Magazine, 35, 2, 67-72.

MALVIĆ, T. & RUSAN, I. (2007): Potential hydrocarbon discoveries in Bjelovar subdepression, Croatia. Search and discovery, article no. 10133, AAPG/Datapages Inc. available at http://www.searchanddiscovery.net/, Tulsa.

NOVAK ZELENIKA, K. & MALVIĆ, T. (2011): Stochastic simulations of dependent geological variables in sandstone reservoirs of Neogene age: A case study of Kloštar Field, Sava Depression. Geologia Croatica, 64, 2, 173-183.

ROSE, P. R. (2001): Risk analysis and management of petroleum exploration ventures. AAPG, Methods in Exploration Series, 12, 164 p.

SMOLJANOVIĆ, S. & MALVIĆ, T. (2005): Improvements in reservoir characterization applying geostatistical modelling (estimation & stochastic simulations vs. standard interpolation methods), Case study from Croatia, *Nafta*, 56, 2, 57-63.

VRBANAC, B., VELIĆ, J. & MALVIĆ, T. (2010): Deterministical calculation of probability of hydrocarbon saturated reservoirs in the Sava Depression,

Croatia. –In: Organising Committee (eds.): Proceedings of IAMG 2010, IAMG, Budapest, p. 11.

VELIĆ, J., MALVIĆ, T., CVETKOVIĆ, M. & VRBANAC, B. (2012): Reservoir geology, hydrocarbon reserves and production in the Croatian part of the Pannonian Basin System. Geologia Croatica, 65, 1, 91-101.

WHITE, D. A. (1992): Selecting and assessing plays. In: STEINMETZ, R. (ed.): Business of Petroleum Exploration: Treatise of Petroleum Geology, Chapter 8, AAPG, Tulsa, 87-94.

DIGITAL ELEVATION MODEL BASED MORPHOMETRIC ANALYSIS OF MEDVEDNICA MOUNTAIN AREA

Bojan MATOŠ[1], Neven TRENC[2],Bruno TOMLJENOVIĆ[1],
[1]Faculty of Mining, Geology and Petroleum Engineering, *Pierottijeva 6, Zagreb, Croatia, (e-mail: bojan.matos@rgn.hr),*
[2]State Institute for Nature Protection, *Trg Mažuranića 5, Zagreb, Croatia.*

Abstract: Quantification of recent neotectonic activity using morphometric analysis of digital elevation models represents one of the most prosperous tools in modern tectonic geomorphology. With extrapolation of morphometric parameters of hypsometric curve, longitudinal river profiles and trunk channel steepness obtained by morphometric analysis of digital elevation model (DEM) of Mt. Medvednica we were able to discriminate possible tectonically active drainage areas. Basically, active areas/drainage areas are *Dedina*, *Poljanica* and *Trnava.* Furthermore there is necessity to conduct another set of morphometric methods as well as field observations in order to verify or disallow results as in Medvednica mountain area first obstacle in conducting DEM based morphometric analysis is great lithological heterogeneity.

Key words: Medvednica Mt., DEM, hypsometric curves, longitudinal valley profiles, concavity index.

1. INTRODUCTION

Relief based morphometric analysis aimed to recognize geomorphologic indicators of recent tectonic activity comprises methods which are able to recognize and quantify interaction between active tectonic processes and consequent landform development (Keller & Pinter, 2002).The basic goal of morphometric analysis of Medvednica mountain area was to extract and quantify parameters (geomorphic indices) that may be useful for identifying

locations of on-going tectonic activity, together with previous results from geomorphologic, geodetic, seismotectonic and neotectonic investigations of this area (Hećimović, 1984; Prelogović et al., 1998; Tomljenović et al., 2008; Herak et al., 2009).

2. GEOLOGICAL AND GEOMORPHICAL SETTING

Mt. Medvednica lies at a „triple junction" between the Eastern/Southern Alps, Internal Dinarides and Pannonian basin in northern Croatia (Tomljenović et al., 2008). It is composed of strongly deformed and partly metamorphosed stratigraphic and pre-Neogene tectonic units, which together with their Pannonian basin covering sequences (**Figure 1**) experienced a polyphase deformation history during the Neogene and Quaternary (Prelogović et al., 1998; Tomljenović & Csontos, 2001). On-going tectonic activity in this area is well documented by historical seismicity and several catastrophic earthquakes with the intensity of VII-VIII° MSC (Herak et al. 2009). Besides strong damage of buildings, occurrence of liquefaction and mud volcanoes observed in the surrounding valley of Sava River, no data on surface rupture or deformation in landscape directly related to particular seismic events were reported so far. However, Pinter (2005) suggested that the landscape development in the Pannonian basin area is in many cases controlled by fault-related growth structures and/or growing anticlines in hanging walls of blind faults. Nowadays, these hidden structures could be recognized by calculation of different geomorphometric parameters extracted from digital elevation models, following a methodology that was proved as reliable in many cases worldwide (e.g. Delcaillau et al., 2006).

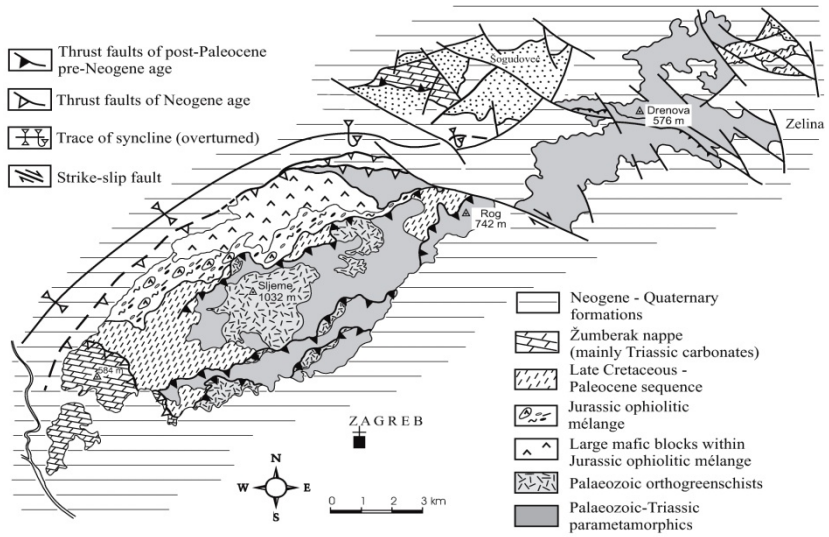

Figure 1: *Main tectonic and stratigraphic units of Medvednica. Simplified geologic map (Tomljenović et al., 2008).*

3. METHODOLOGY

Input set of point data with x,y,z coordinates was acquired from the Croatian Geodetic Survey based on extrapolation from detailed topographic maps **(DTM)** 1:25 000. DEM raster was modeled and analyzed using software package *ESRI ArcMap Version 9.3.1.* Resulted DEM raster has horizontal and vertical cell resolution of 25 m, which is furthermore processed and analyzed using ***ArcMap Version 9.3.1., Mathlab*** software and special geomorphologic ***ArcMap*** extension ***StPro*** (Whipple et al., 2007) in order to gather quantitative morphometric parameters.

4. MORPHOMETRIC UNITS

In most tectonically active areas the most sensitive landscape feature sensitive on active tectonic processes (folding and faulting) is drainage network (Keller & Pinter, 2002; Pérez-Peña et al., 2009). In morphometric analysis there were delineated 36 drainage areas with drainage network like fundamental morphometric units (**Figure 2** and **Table 1**).

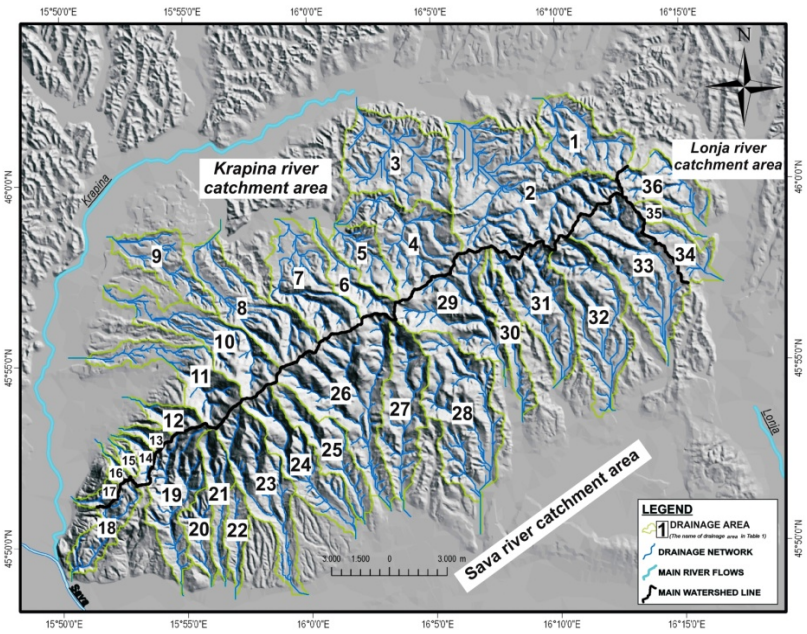

Figure 2: *DEM map of Medvednica mountain area with main river catchment areas and numbered delineated drainage areas (see Table 1 for drainage area's name).*

Extraction of morphometric units was conducted using ***ArcHydro 1.1*** extension with methodology described in Taraboton (1997) and Peckham & Jordan (2007). Taking into account distribution of relative relief as well as dip and orientation of slopes, study area was divided in three main sectors (**Figure 2**). The first sector was derived at NW slopes of Medvednica area comprising 17 drainage areas making part of greater Krapina river basin. The second and third sectors were delineated at SE slopes of Medvednica area composed of 16 drainage areas making part of greater Sava river basin. The last 3 drainage areas were delineated at the NE marginal zone of SE slopes making part of Lonja river basin.

No.	Catchment area	Area (km^2)	Trunk channel L(km)	Elevation (m) min.	Elevation (m) max.	Max. slope (°)	Hi	Zmax	ΔI/L	σ (%)	ksn (max.)	ksn (avg.)	ksn group
1	ŽITOMIRKA	13,73	6,96	165,00	445,39	35,18	0,26	0,627	0,218	67,80	38,46	16,38	1
2	BISTRICA	40,31	11,23	160,00	575,63	44,58	0,33	0,503	0,258	57,40	62,71	26,56	1
3	PINJA	21,81	8,27	160,00	480,00	32,85	0,17	0,569	0,326	62,60	51,39	18,97	1
4	BURNJAK	18,85	9,14	196,44	610,00	37,87	0,28	0,475	0,294	54,20	24,74	16,89	1
5	GORNJA STUBICA	7,32	5,45	195,46	630,00	34,58	0,27	0,397	0,268	48,20	57,69	28,96	1
6	SLANI POTOK	6,12	7,49	190,00	716,08	40,63	0,43	0,318	0,229	40,20	55,84	35,71	1
7	RIJEKA	16,30	10,47	180,00	833,98	45,58	0,32	0,379	0,392	40,40	102,35	42,21	2
8	VIDAK	17,66	11,85	160,00	890,00	50,80	0,32	0,431	0,286	52,80	89,03	43,29	2
9	JAMNO	9,71	7,22	140,00	325,00	28,36	0,30	0,351	0,286	37,20	21,31	13,63	1
10	BISTRA	16,13	12,11	150,00	1017,11	43,44	0,31	0,489	0,238	57,20	147,78	50,82	2
11	DEDINA	13,27	10,23	135,00	1031,33	44,33	0,33	0,471	0,324	58,80	115,03	50,65	2
12	POLJANICA	3,32	4,57	159,46	810,00	39,24	0,48	0,306	0,418	37,00	97,29	65,23	2
13	DUBOVEC	1,83	2,77	180,00	584,83	40,93	0,46	0,268	0,267	30,00	57,88	38,55	2
14	NOVAČAK	2,33	3,81	170,77	585,00	41,75	0,49	0,173	0,505	19,00	48,15	35,52	2
15	VOLOVEC	1,24	2,23	165,12	585,00	39,48	0,54	0,234	0,430	27,00	67,03	47,62	3
16	JABLANOVEC	1,15	2,60	150,00	600,00	40,48	0,69	0,288	0,435	30,60	120,39	61,14	3
17	IVANŠČAK	1,74	2,67	140,45	600,00	41,19	0,54	0,296	0,237	31,00	93,20	54,06	3
18	BIZEKI	7,01	7,36	130,24	600,00	40,34	0,48	0,204	0,653	16,00	116,77	43,84	3
19	VRAPČAK	14,58	10,31	127,87	860,00	44,12	0,35	0,388	0,342	46,60	74,96	44,96	3
20	KUSTOŠIJA	5,38	5,24	130,00	515,00	43,74	0,32	0,365	0,242	43,40	37,20	25,06	3
21	VELIKI POTOK	7,15	8,72	128,32	870,00	43,69	0,37	0,357	0,297	44,20	74,79	46,72	4
22	KUNIŠČAK	4,65	5,82	123,46	460,00	31,88	0,32	0,344	0,305	43,60	38,82	22,13	3
23	MEDVEŠČAK	17,21	12,21	116,29	1030,00	41,60	0,33	0,390	0,355	48,40	112,02	47,19	4
24	BLIZNEC	14,19	10,49	150,00	1030,70	43,86	0,31	0,389	0,356	48,60	104,63	45,39	4
25	ŠTEFANOVEC	10,38	9,58	152,25	985,00	39,22	0,29	0,391	0,258	48,40	116,61	48,03	4
26	TRNAVA	27,92	10,72	151,07	961,46	48,50	0,40	0,470	0,319	52,80	139,44	57,39	4
27	ČUČERJE	15,52	11,18	150,00	740,41	39,26	0,28	0,399	0,206	49,60	66,33	31,40	1
28	KOSTANIČ	24,60	12,81	130,00	700,00	39,42	0,23	0,477	0,319	59,20	50,11	22,78	1
29	KAŠINA	17,67	8,34	180,00	740,59	43,35	0,33	0,465	0,206	56,40	60,20	31,78	1
30	BLAGUŠA	7,45	9,26	160,00	490,15	43,16	0,35	0,348	0,275	38,60	35,25	19,04	1
31	GLAVINČICA	16,36	8,67	150,00	543,53	44,35	0,33	0,379	0,366	47,60	46,31	23,36	1
32	NESPEŠ	20,11	11,21	125,44	570,00	40,81	0,26	0,460	0,176	56,40	43,28	21,08	1
33	ZELINA	21,76	11,28	140,00	555,93	42,21	0,33	0,390	0,423	49,40	52,81	25,86	1
34	TOPLIČICA	6,03	5,39	121,41	371,54	32,07	0,25	0,498	0,197	60,00	52,69	16,04	1
35	KALINEC	2,72	4,13	130,00	474,83	36,84	0,41	0,399	0,308	42,20	64,11	33,05	1
36	OREŠČAK	9,35	6,12	130,08	476,66	43,14	0,40	0,378	0,216	45,80	56,01	27,43	1
	mean value	12,30	8,00	150,67	674,87	40,63	0,36	0,391	0,312	45,79	72,02	35,52	2

***Table 1**: Numbered delineated drainage areas with extrapolated morphometric parameters.*

5. MORPHOMETRIC PARAMETERS

5.1. Hypsometric curves

Basin hypsometric curves represent distribution of surface area and total values of surface heights inside studied drainage area, i.e. distribution of relative surface area below(above) certain surface height (Pérez-Peña et al., 2009 and references therein). Derived shape of hypsometric curves give information about erosional stage of drainage areas as they are outcome of interaction between tectonic activity, lithological heterogeneity and climatic condition (Huang & Niemann, 2006). Keller & Pinter (2002) suggested that convex, S and concave shape of hypsometric curves are typical for basins in young, mature and final (old) erosional stages, respectively. Shapes of hypsometric curves are approximated by hypsometric integral:

$$Hi = \frac{h_{mean} - h_{min}}{h_{max} - h_{min}} \quad (1)$$

where are: $\mathbf{H_{mean}}$ *average value of surface heights in drainage area*; $\mathbf{h_{min}}$ & $\mathbf{h_{max}}$: *minimal and maximal values of surface heights in drainage area.*

Hypsometric integral values are in range between **0** and **1.** Values closer to 1 are typical for young erosional stage areas and values closer to 0 are specific for mature or final (old) erosional stage areas (Strahler, 1952; Keller i Pinter, 2002; Pérez-Peña et al., 2009; Ruszkiczay-Rüdiger et al., 2009). To compute hypsometric curves and hypsometric integral for studied drainage areas we used ***CalHypso*** extension intended to *ESRI ArcMap 9.3* (for details see in Pérez-Peña et al., 2009).

5.2. Longitudinal river profiles

In most cases, longitudinal river profiles have smooth shaped curves like outcome of balance between bedrock erosion and tectonic uplift (Schumm et al., 2000; Bull, 2009). According to Snow and Singerland (1987) and Ruszkiczay-Rüdiger et al. (2009) the shape of normalized longitudinal river profiles in the absence of active tectonics become more concave along trunk channel which is in correlation with stream age. Certainly, stream has to be in the steady state in relation to the climatic conditions, uplift rate and the erosion coefficient, which has to be uniform in the whole length of the stream. Any deviation of longitudinal river profile from typical shape suggests resistant channel bedrock or tectonic activity (Rãdoane et al., 2003). In Medvednica area comparison was made between delineated drainage areas using their normalized longitudinal river profiles following procedure described in Ruszkiczay-Rüdiger et al. (2009). Moreover, following statistical parameters for longitudinal river profiles were extrapolated (**Table**

1): *maximal concavity (Z_{max}), distance from the source ($\Delta l/L$) and concavity indicator (σ).*

5.3. Trunk channel steepness

The relation between the channel steepness and contributing drainage basin can be described by the power function (Howard and Kirby 1983):

$$S = k_s A^{-\theta} \qquad (2)$$

Where ***S*** is the channel slope, ***A*** the area of the contributing watershed which is actually a proxy for the discharge, θ –concavity index and k_s is steepness index. The value of θ connects incision rate with channel steepness and reflects catchment hydrology with channel specific incision process (Wobus, 2006). The value of k_s in the streams that are in dynamic equilibrium reflects the relation between the uplift and erosion. It has higher values in the areas of uplift. If function (2) is shown in the ***log A-log S*** coordinate system it is represented by a line whose slope is the concavity index θ, and the intercept on the y axis is the steepness index. Lithological boundaries or other changes of rock properties can induce changes in the shape of longitudinal profiles and special caution has to be taken in the interpretation of the data (Wobus et. al., 2006). Also, it has to be pointed out that power law relation between the contributing watershed and channel steepness is not valid (1) in the uppermost part of the stream, (2) in cases where the critical watershed area is smaller than 10^6 m^2 (as colluvial mechanisms predominate over discharge) and (3) in the lower part of the stream where stream channel is not incised in bedrock and alluvial sedimentation predominates (Wobus et al., 2006).

6. RESULTS

6.1. Hypsometric curves

The resulting (***H_i)*** values for studied drainage areas range between ***0.17*** and ***0.69*** (**Table 1**)**.** Two groups of drainage areas were delineated based on hypsometric curve shape and ***H_i*** values. The first group comprises basins with ***H_i*** values in range from 0.17-0.37 and the second one with ***H_i*** values in range from 0.40-0.69. According to *Strahler (1952)* values of ***$H_i \geq 0.60$*** constitute limiting value between young and mature erosional stage areas. Hence, it follows that ***Jablanovec, Volovec, Novačak, Ivanšćak, Poljanica, Dubovec and Bizeki*** catchments in the SW part of Medvednica are all in a young erosional stage while all other studied catchments are in mature to final(old) erosional stage.

6.2. Normalized river profiles

Normalized longitudinal river profiles and extrapolated statistical parameters were used in recognition of vertical deformations in delineated drainage areas based on procedure described in Ruszkiczay-Rüdiger et al. (2009). Calculated statistical values of concavity indicator ***(σ)*** range between 16 i 67.80 %, maximal concavity ***(Z_{max})*** between 0.17 i 0.63 and distance from the source ***($\Delta l/L$)*** between **0.18** and **0.65 (Table 1).** With graph correlation using maximal concavity ***(Z_{max})*** and distance from the source ***($\Delta l/L$)*** parameters, there was possibility to make comparison between delineated drainage basins as well as to recognize similarities between them. Furthermore, it was recognized clustering of drainage areas following procedure suggested by Holbrook & Schumm (1999) and Ruszkyczay-Rüdiger et al. (2009).

First cluster **P1** gathered ***Poljanica, Novačak, Volovec, Jablanovec and Bizeki*** drainage areas. Basic properties of **P1** cluster are lower values of maximal concavity (***Z_{max}-0.173-0.306)*** and its position in regards to distance from the source ***(ΔI/L-0.418-0.653)***. Based on their position in relation to equilibrium state features **(Figure 3)**, and their lithological uniform substrate, there is opinion that mentioned drainage areas are in non-equilibrium steady state as a result of active tectonic deformation. In relation to cluster **P1**, clusters **P2** and **P3** represent other drainage areas **(Figure 3)** which are considered as being in mature to old (final equilibrium) erosional stages as evidenced by medium to high values of maximal concavity (***Z_{max}-0.268-0.627)*** and its position (in the upper reach of stream) with respect to the distance from the source ***(ΔI/L-0.176-0.423)***.

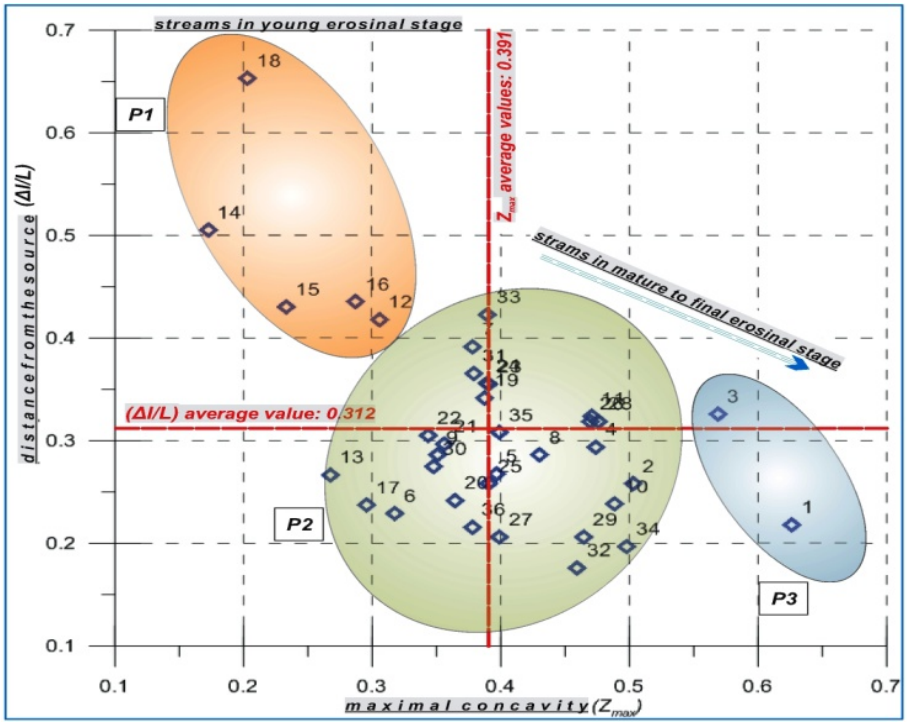

Figure 3: *Distance of maximal concavity from the source plotted against maximal concavity of normalized river profiles (see Table 1 for drainage area names).*

6.3. Trunk channel steepness

In this initial phase of investigation the main emphasize is on the analysis of the general spatial distribution of the k_{sn} values and in the lesser extent on the interpretation and analysis of particular stream profiles. The data were overlapped with the geological map 1:100.000 and preliminary interpretation of possible causes of k_{sn} variation in relation to tectonic activity and lithology was performed (**Figure 4**). The max and min values of normalized steepness index k_{sn} were calculated and analyzed (**Table 1**) enabling grouping of streams geographically. In the NE part *(Group 1)* of the Medvednica on the NW slopes and on the SE slopes *(from Cucerje to Kalinec)* streams have relatively low k_{sn} values, which may indicate the relatively low activity and uplift.

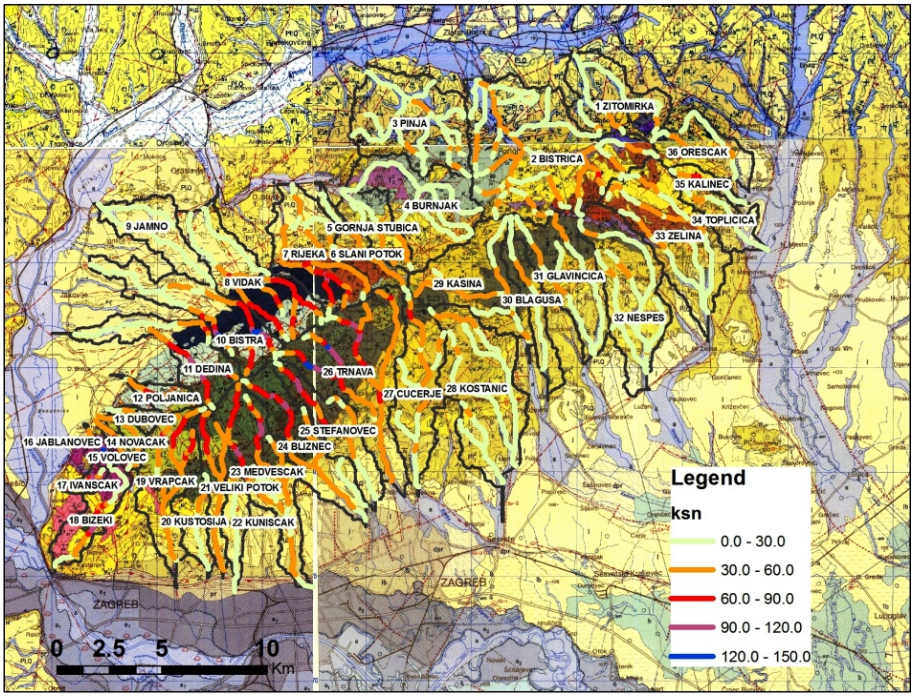

Figure 4: *Auto generated K_{sn} values for drainage areas overlapped with geological map of studied area using StPro extension.*

Streams in the central part of the NW slopes of the Medvednica *(Group 2) (from Rijeka to Dedina)* show an increased k_{sn} values as they entered the more resistant basalts and spilite rocks. The profiles showed knick points that mostly correspond to the lithological boundaries. Of particular interest are streams ***Poljanica*** and ***Dedina*** that are incised in rocks of the Medvednica Jurassic ophiolitic mélange tectonic unit but have higher k_{sn} values then the neighbouring streams incised further to the east in the same lithological unit. This difference could indicate a higher uplift rate in this area. *Group 3* comprises streams in the SW part of the NW slope of the Medvednica that is a karstic area characterized by secondary porosity and equation 1 may not be applicable since relation between stream discharge and watershed area is not consistent. The last group, *Group 4* represent streams in the central part of the SE slopes of Medvednica that flow trough ortho- and para-metamorphic bedrock and have consistently high values of the k_{sn}. The highest k_{sn} was in the more resistant orthometamorphite rocks. In this relatively large and lithological uniform area the stream ***Trnava*** has the highest values of the k_{sn}, thus indicating possible location of tectonic activity and uplift in this area.

7. CONCLUSION

On the Medvednica mountain area first obstacle in conducting DEM based morphometric analysis is lithological heterogeneity and variation within almost all of the drainage areas. Based on calculated morphometric parameters (H_i, *maximal concavity-*Z_{max}, *distance from the source -*$\Delta l/L$, *concavity indicator (*σ*) and* k_{sn}*)* results are speaking in favor of several tectonically possible active areas/drainage areas: *Dedina*, *Poljanica, Dubovec, Novačak, Volovec, Jablanovec, Ivanšćak, Bizeki* and *Trnava.* Excluding drainage areas who pass through predominantly karstic area we can conclude that the possible tectonically active areas are drainage basins of **Dedina, Poljanica and Trnava.** This conclusion is not mandatory as our

DEM based morphometric analysis is first time used in Medvednica mountain area. Furthermore there is necessity to define another set of morphometric methods which should verify or disallow our results.

ACKNOWLEDGEMENTS: This morphometric research was financially supported by the Ministry of Science, Education and Sports of the Republic of Croatia *(Project CROTEC, grant no. 195-1951293-3155)*

8. REFERENCES

BULL, W.B. (2009): Geomorphic Responses to Climatic Change. *Blackburn Press, New Jersey, 326 p.*

DELACAILLAU, B., CAROZZA, J.M., LAVILLE, E. (2006): Recent fold growth and drainage development: the Januari and Chandigarh anticlines in the Siwalik foothills, northwest India. *Geomorphology, 76, 241-256.*

HEĆIMOVIĆ, I. (1984): Strukturno-geomorfološka istraživanja između Medvednice, Ivanščice i Kalnika. *Geološki vjesnik, 37, Zagreb, 33-40.*

HERAK, D., HERAK, M., TOMLJENOVIĆ, B. (2009): Seismicity and earthquake focal mechanisms in North-Western Croatia. *Tectonophysics, 465, 212-220.*

HOLBROOK, J., SCHUMM, S.A. (1999): Geomorphic and sedimentary response of rivers to tectonic deformation: a brief review and critique of a tool for recognizing subtle epirogenic deformation in modern and ancient settings. *Tectonophysics, 305, 287–306.*

HOWARD, A.D. & KIRBY, G. (1983): Channel changes in badlands: *Geological Society of America Bulletin, v. 94, p. 739–752, doi: 10.1130/0016-7606(1983)94<739:CCIB>2.0.CO;2.*

HUANG, X.J., NIEMANN, J.D. (2006): An evaluation of the geomorphically effective event for fluvial processes over long periods. *J. of Geophysics Res.–Earth Surf. 111, F03015.*

KELLER, E.A., PINTER, N. (2002): Active Tectonics; Earthquakes, Uplift and Landscape, *2nd edition. Prentice-Hall, Upper Saddle River, New Jersey, 362 p.*

PÉREZ-PEÑA, J.V., AZAÑÓN, J.M., AZOR, A. (2009): CalHypso: An ArcGIS extension to calculate hypsometric curves and their statistical moments. Applications to drainage basin analysis in SE Spain. *Computer & Geosciences, 35, 1214-1223.*

PECKHAM, R., JORDAN, G. (2007): Digital elevation modeling. Development and applications in a policy support environment. *Springer Verlag, Berlin, ISBN: 978-3-540-36730, 313 p.*

PINTER, N. (2005): Applications of tectonic geomorphology for deciphering active deformation in the Pannonian Basin, Hungary. In: Fodor, L. and Brezsnyánszki, K. (eds): *Occasional Papers of the Geol. Inst. of Hungary, 204 , 45-51.*

PRELOGOVIĆ, E., SAFTIĆ, B., KUK, V., VELIĆ, J., DRAGAŠ, M., LUČIĆ, D. (1998): Tectonic activity in the Croatian part of the Pannonian basin. *Tectonophysics 297, 283-293 p.*

RĂDOANE, M., RĂDOANE, N., DUMITRIU, D. (2003): Geomorphological evolution of longitudinal river profiles in the Carpathians. *Geomorphology, 50, 293-306.*

RUSZKICZAY-RÜDIGER, Z., FODOR, L., HORVÁTH, E., TELBISZ, T. (2009): Discrimination of fluvial, eolian and neotectonic features in a low hilly landscape: A DEM-based morphotectonic analysis in the Central Pannonian Basin, Hungary*. Geomorphology, 104, 203-217 p.*

SCHUMM, S.A., DUMONT, J.F., HOLBROOK, J.M. (2000): Active Tectonics and Alluvial Rivers. *Cambridge University Press, Cambridge. 276 p.*

SNOW, R.S. AND SINGERLAND, R.L. (1987): Mathematical modeling of graded river profiles. *Journal of Geology, 95, 15-33.*

STRAHLER, A.N. (1952): Hypsometric (area–altitude) analysis of erosional topography. *Bulletin of the Geological Society of America, 63, 1117–1142.*

TARBOTON, D. (1997). A new method for the determination of flow directions and upslope areas in grid digital elevation models. *Water Resources Research, 33(2), 309-319.*

TOMLJENOVIĆ, B., CSONTOS, L. (2001): Neogene-Quaternary structures in the border zone between Alps, Dinarides and Pannonian Basin (Hrvatsko zagorje and Karlovac Basin, Croatia*). International Journal of Earth Sciences (Geologische Rundschau), 90, 560-578.*

TOMLJENOVIĆ, B., CSONTOS, L., MÁRTON, E., MÁRTON, P. (2008): Tectonic evolution of northwestern Internal Dinarides as constrained by structures and rotation of Medvednica Mountains, North Croatia. *Geological Society, London, Special Publications v.298, 145-167*.

WOBUS, C., WHIPPLE, K.X., KIRBY, E., SNYDER, N.P., JOHNSON, J., SPYROPOLOU, K., CROSBY, B.T., AND SHEEHAN, D. (2006): Tectonics from topography: Procedures, promise, and pitfalls, in, Willett, S.D., Hovius, N., Brandon, M.T., and Fisher, D.M., eds., Tectonics, Climate, and Landscape Evolution: *Geological Society of America Special Paper 398, p. 55–74, doi: 10.1130/2006.2398(04)006.2398(04)10.1130/2*

WHIPPLE, K.X., WOBUS, C., CROSBY, B., KIRBY, E., AND SHEEHAN, D. (2007): New tools for quantitative geomorphology Extraction and interpretation of stream profiles from digital topographic data: *Geological Society of America Annual Meeting Short Course*, 28 October 2007.

Ordinary Kriging Mapping of the Upper Pannonian Reservoirs in the Ivanić Field

Karolina NOVAK*, Živka MAŠINA
INA Plc., Av.V.Holjevca 10, Zagreb, Croatia
* Author to whom correspondence should be addressed:
E-Mail:karolina.novak@ina.hr;
Tel.: +385 1 6450 729

Abstract: Based on the results of laboratory tests and numerical simulation, in the period 2001-2006 Enhanced Oil Recovery (EOR) pilot project on of the Ivanić oil Field was performed. The pilot project results proved feasibility of the EOR project. In the same time it will be used as a very efficient method for carbon dioxide sequestration. Reservoir determination and distribution of its variables are very important for information on possibility of gas injection and oil recovery and their dependence. Considering the data on porosity, depth and reservoir thickness, given by the log analysis of the "Gamma 3" and the "Gamma 4" reservoirs of the Ivanić oil Field, Ordinary Kriging maps are constructed.

Key words: Ordinary Kriging, Upper Pannonian reservoirs, Ivanić Field.

1. RESEARCH AREA-THE IVANIĆ OIL FIELD

The Ivanić Field (**Figure 1**), situated in the vicinity of the Croatian Capital in north-western part of the Sava depression, covers mostly the area of the Sava River alluvial plain. The longer axis of the asymmetrical brachianticline field structure is of northwest-southeast direction.

Figure 1: *Schematic map of Ivanić Field location in the Croatian part of the Pannonian Basin System and schematic well net (taken from Malvić, 2008)*

2. GEOLOGICAL SETTINGS

The main oil reservoirs belong to the Late Pannonian age, and are faulted in several tectonic blocks. Informal lithostratigraphic units with the main oil reservoirs are called the Gamma "series" (**Figure 2**).

Lithologically, reservoir sandstones are predominantly composed of mica and quartz grains, with minor clay mineral content. Although entire "series" can reach several dozen meters, compaction did not reduce reservoir's porosities in the deeper parts. This is in accordance with observations published by Malvić et al. (2005) saying that sandstones of this age (Upper Miocene) and mineral composition will only show influence of compaction when the depth difference between two points in the same lithostratigraphic unit is greater than 400 meters.

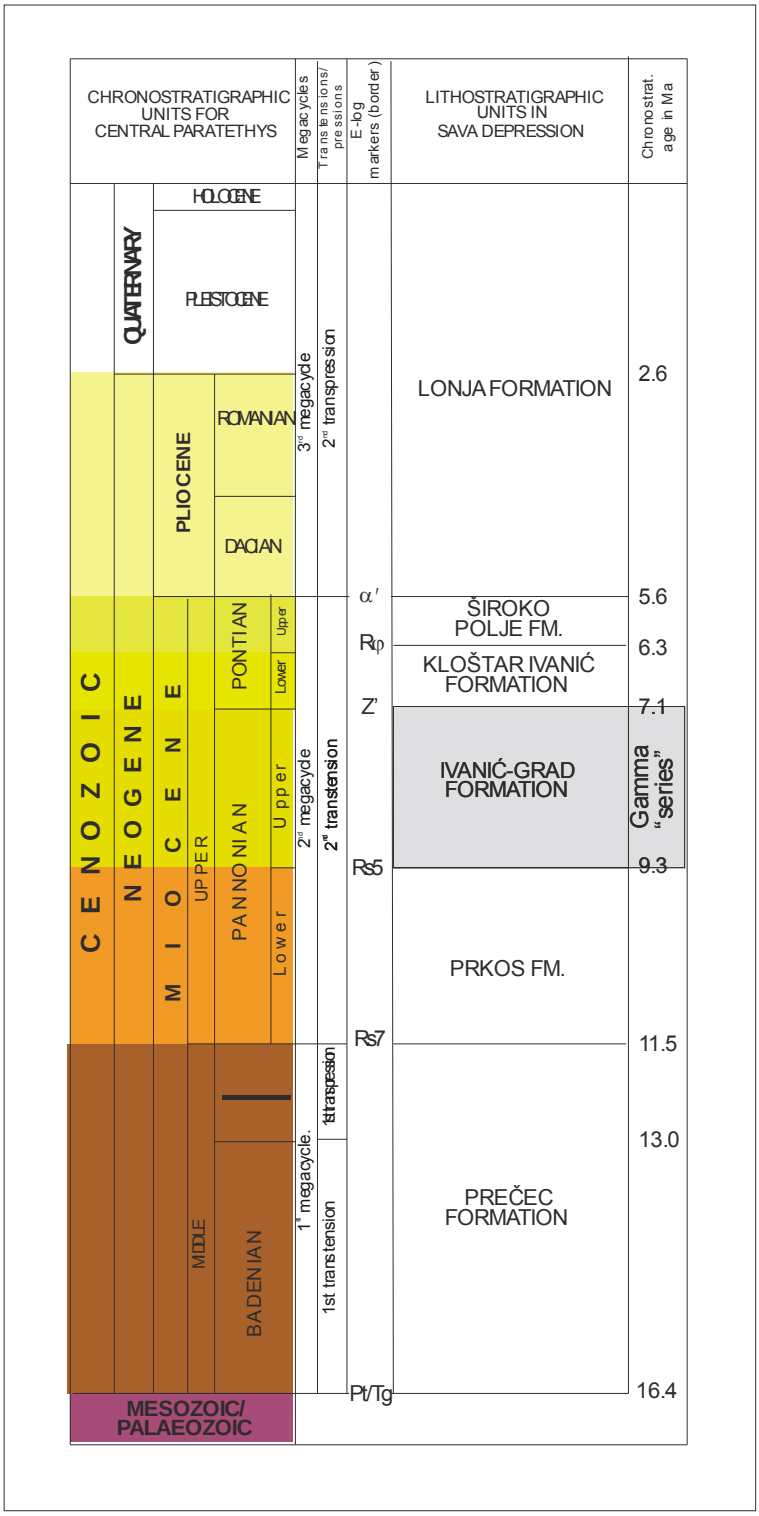

Figure 2: *Lithostratigraphic and chronostratigraphic units in the Ivanić Field, with position of Gamma "series" reservoirs*

Gamma „series" consists of 8 sandstone intervals: Gamma 5, Gamma 4, Gamma 3, Gamma 2/1, Gamma 2/2, Gamma 2/3, Gamma 2/3, Gamma 2/4, Gamma 2/5. The shale/marl layer divides the „series" on two hydrodynamic units. This paper will show the results of porosity, thickness and depth maps obtained by Ordinary Kriging in Gamma 3 and Gamma 4 reservoirs.

3. SHORT FACTS ABOUT PRODUCTION AT THE IVANIĆ FIELD

Production from the Ivanić Field has been constantly ongoing for more than 40 years. After initial production under gas driven regime, water flooding should have been used till the year 2032 (the year of economical end of life) (Novosel, 2009). However, by such a production regime about 60% of geological reserves would remain within the reservoirs, which is the reason why this field is chosen as the one of the most favourable candidates for applying tertiary recovery methods, i.e. EOR recovery based on the injection of CO_2 (e.g. ,Vrbošić et al., 2003; Perić and Kovač, 2003; Novosel, 2009).

4. MAPPING BY ORDINARY KRIGING

Estimation by Kriging is given through following equation (Malvić, 2008a):

$$z_K = \sum_{i=1}^{n} \lambda_i \cdot z_i \qquad (\mathbf{1})$$

Where are: z_K – estimated value; λ_i – weighted coefficient at the "i" location; z_i – true value at the "i" location.

Kriging was used for the purpose to create the maps of porosity, thickness and depth of the Gamma 3 and the Gamma 4 reservoirs. The porosity map of Gamma "series" is previously published in Malvić (2008), but for different dataset. Input data for this method are the point data given in the ASCII

format which was used in making variogram. Porosity, thickness and depth maps of Gamma 3 (**Figure 3a, b, c**) and Gamma 4 (**Figure 4a, b, c**) reservoirs of the Ivanić Field were interpolated by the Surfer8™ software.

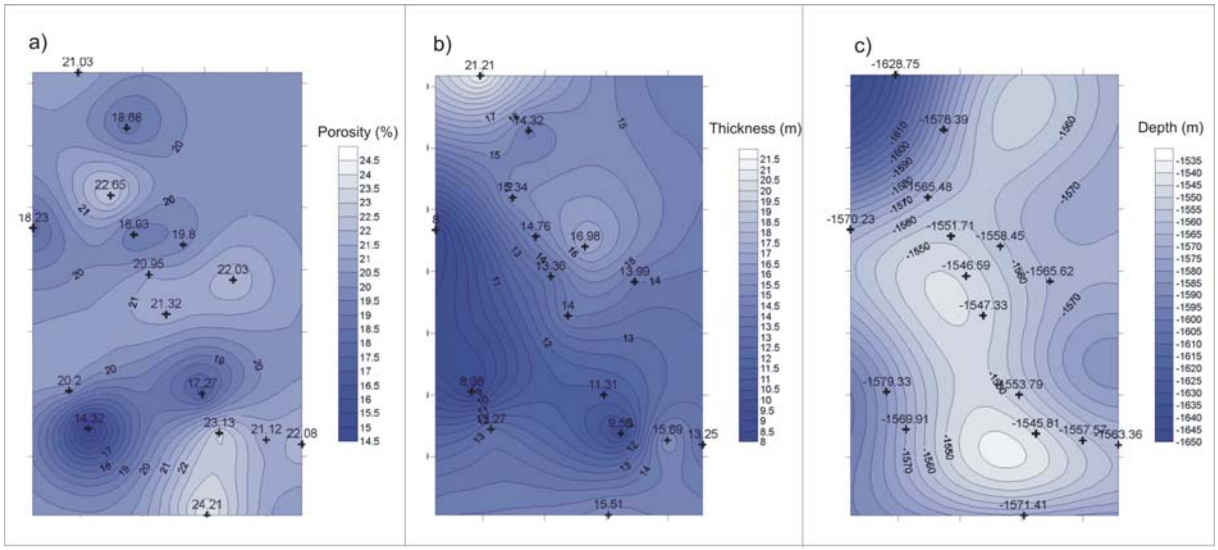

Figure 3: *Kriging map for variables (a) „porosity", (b)" thickness ", (c) „depth" in the Gamma reservoir, the Ivanić Field*

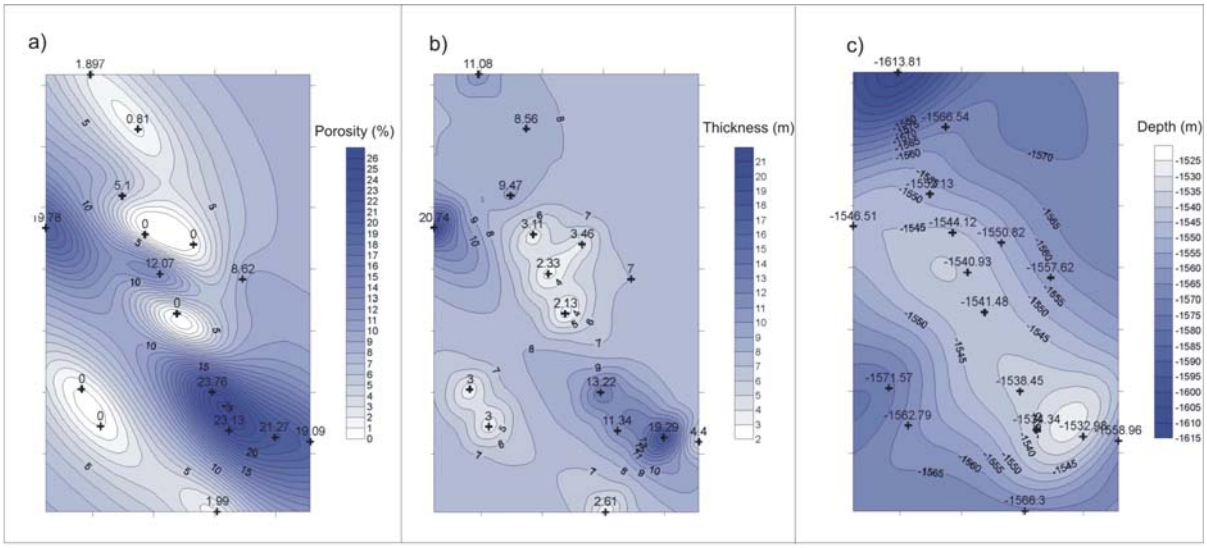

Figure 4: *Kriging map for: a) „porosity", b)" thickness ", c) „depth" for the Gamma 4 reservoir, the Ivanić Field*

5. DISCUSSION AND CONCLUSION

Maximum porosity of the Gamma 3 reservoir is located at the north-western, central and south-eastern part of the map (**Figure 3a**). Area between the central and south-eastern part shows minimum porosity. Minimum thickness of the Gamma 3 reservoir (**Figure 3b**) occurs at the western part. Thickness increasing is in the north-east direction, while the maximum values are reached at the north-west. On the depth map of the Gamma 3 reservoir (**Figure 3c**) at he north-east, central part, as well as at the north-west, the shallowest areas can been seen. The map shows the depth maximum at the north-western part.

The Kriging porosity map of the Gamma 4 reservoir (**Figure 4a**) clearly indicates several areas of maximum porosity, mostly located along the NW-SE axis, which corresponds to the present-day anticlines, i.e. the top of the hydrocarbon traps. Also, the areas of maximum porosity are associated with the channel sandstones with the smallest clay component. The sandstones were deposited mostly as parallel laminated sands (or Bouma sequence "Tb") of sub-lake turbidites active in Upper Miocene. The marginal parts with porosities of lower than 15% and especially 10%, belong to lithofacies of marlitic sandstones and sandy marlstones, and have lower permeabilities. The identification of lithofacies borders, made possible from porosity maps. For similar reservoir lithology it is published in Novak Zelenika and Malvić (2011) and Novak Zelenika et al. (2010). is crucial for the prediction of oil-water contact, especially during the late stage of water flooding, and consequently for planning the injection of water and CO_2. The porosity (**Figure 4 a**) and the thickness (**Figure 4 b**) maps of the Gamma 4 reservoir show some similarity. Thickness maximum values are located at the western and south eastern parts. At the depth map (**Figure 4c**) the shallowest part occurs at the southeast, while the anticline structure of the northwest–southeast direction is clearly stressed. Thickness and porosity

maps of the Gamma 4 reservoir indicates the depositional channel of northwest-southeast direction, meaning that the hugest material deposited in the central part of the channel (maximum thickness and porosity). The depth map shows that the former channel was subsequently tectonically raised.

6. REFERENCES

MALVIC, T., J. VELIC & Z. PEH (2005): Qualitative-quantitative analyses of the influence of depth and lithological composition on Lower Pontian sandstone porosity in the central part of Bjelovar Sag (Croatia). Geologia Croatica, 58, 73-85.

MALVIĆ, T. (2008a) Primjena geostatistike u analizi geoloških podataka [Application of Geostatistics in Geological Data Analysis-in Croatian]. INA, SD istraživanje i proizvodnja nafte i plina, Zagreb, 103 p.

MALVIĆ, T. (2008): Production of Porosity Map by Kriging in Sandstone Reservoirs, Case Study from the Sava Depression. Kartografija i geoinformacije, 9, 12-19.

NOVAK ZELENIKA, K., MALVIĆ, T., GEIGER, J. (2010): Kartiranje gornjomiocenskih pješčenjačkih facijesa metodom indikatorskog kriginga [Mapping of the Late Miocene sandstone facies using indicator kriging]. Nafta, 61, 5, 225-233.

NOVAK ZELENIKA, K. & MALVIĆ, T. (2011): Stochastic simulations of dependent geological variables in sandstone reservoirs of Neogene age: A case study of Kloštar Field, Sava Depression. Geologia Croatica, 64, 2, 173-183.

NOVOSEL, D. (2009): Učinak ugljičnog dioksida u tercijarnoj fazi iskorištavanja naftnih ležišta polja Ivanić ivanić [The effect of the carbon dioxide on the tertiary exploration phase of the Ivanić oil field]. –Unpub. PhD Thesis, Faculty of Mining, Geology and Petroleum Engineering, University of Zagreb, Zagreb, 162 p.

PERIĆ, M. & KOVAČ, S. (2003): Simulacijska studija procesa povećanja iscrpka nafte (EOR-procesa) istiskivanjem ugljik-dioksidom primjenom višekomponentnog modela COMP III [Simulation Study of Enhanced Oil Recovery Process by CO_2 Injection Applying a Multi-component COMP III]. Naftaplin, 1, 13-25.

VRBOŠIĆ, A., ŠKRLEC, M., NOVOSEL, D. & IVANOVIĆ, K (2003): Naftno polje Ivanić 1963.-2003. [The Ivanić Oil Field 1963-2003]. Naftaplin, 1, 1-4.

Cut-offs definition in Indicator Kriging mapping, case study Lower Pontian reservoir in the Sava Depression

Kristina NOVAK ZELENIKA

INA-Oil Industry Plc. Exploration and Production of Oil and Gas, Sector for Geology and Reservoir Management, Šubićeva 29, 10000 Zagreb, kristina.novakzelenika@ina.hr

Abstract: Turbidites were dominant clastic transport mechanism in the Croatian part of the Pannonian Basin System during the Early Pontian. Most of transported detritus had been eroded in the Eastern Alps and re-deposited several times before the suspended materials entered the Sava Depression. Due to long transport only medium and fine grained sands and silts (Tb - Td Bouma sequences) reached the Sava Depression. In the calm period, when turbiditic currents were not active, marls were deposited. Indicator Kriging technique is most often used for lithofacies mapping, where mapped variable (in this case porosity) is transformed into 0 or 1, based on certain cut-off. Definition of the cut-off values depends mostly on the experience. In this paper it was presented how to use core and log data to define proper cut-offs for describing different lithofacies. Obtained maps are probability maps and one of them clearly show turbiditic channel and material transport direction.

Key words: Indicator Kriging, cut-offs, lithofacies definition, Lower Pontian reservoir, Sava depression.

1. INTRODUCTION

Sedimentation area in time of the Pannonian Basin extension in Croatia were marginal parts of the Medvednica, Papuk, Psunj Mt. and the lowest parts of the Sava, Drava, Slavonia-Srijem and Mura Depressions (e.g. Vrbanac, 1996; Malvić, 2003).

Turbidites were dominant clastic transport mechanism in the Croatian part of the Pannonian Basin System (CPBS) during the Late Pannonian and Early Pontian (e.g. Vrbanac, 1996; Rögl, 1996, 1998).

Although, there are some theories that local mountains, which were uplifted above lake level during the Early Pontian, gave some material, it was proven that most of transported detritus had been eroded in the Eastern Alps, deposited in lake (lacustric) environments through present-day depressions located in Slovenia and Hungary, and due to gravitational instability, transported to the Mura Depression (Croatia). From that point, turbiditic material had been re-deposited several times before the suspended materials entered the Save Depression. This material reached numerous re-activated strike-slip faults inside the Sava Depression. Due to long transport it was logically to conclude that only the medium and fine grained sands as well as silts (Tb - Td lithofacies) reached the Sava Depression. In the calm period, when turbiditic currents were not active, marls, as typical calm deep water sediments, were deposited.

In reservoir characterization, mapping of the lithofacies is important for getting insight to sedimentary environments, shapes and boundaries of hydrocarbon reservoirs. Indicator Kriging is a technique which is most often used for lithofacies mapping. It is based on indicator transformation of the input data (based on different cut-offs) into 0 or 1, depending on presence or absence of the certain lithofacies. Obtained maps show probabilities that mapped variable is lower than the cut-off, and with a proper cut-off selection it is possible to map turbiditic channel or to observe material transport direction.

2. DEFINING SANDSTONE AND MARL LITHOFACIES BASED ON CORES

Definition of the different lithofacies was based on cores examination. There were just two of the selected wells which have both, log and core data of the Lower Pontian sandstones. Clarification was subjective and grain size played

main role. If coarse and medium grained material was dominate, core was declared as sandstone, and of course the opposite if fine grained material was dominant it represented silty or marly sandstones. Cores of a pure marls were not found. Examined cores and their lithological definition is given in **Figure 1**.

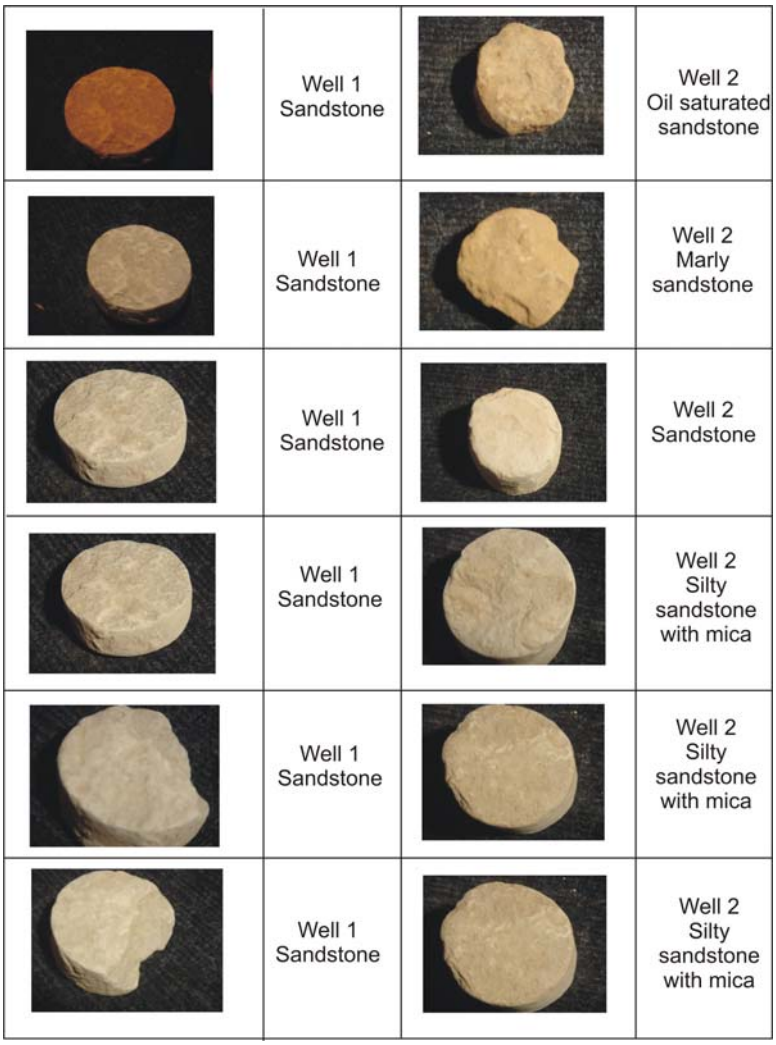

***Figure 1**: Examined cores of the Lower Pontian reservoirs*

3. INPUT DATA AND CUT-OFFS DEFINITION

Input data for Indicator Kriging mapping were well log porosities measured in 20 wells of the Lower Pontian reservoir (**Table 1**). They were compared with core porosities from two wells (**Table 1**). Base for Indicator Kriging

mapping is indicator transformation of the input data. That means that the mapped variable (i.e. porosity in this case) should be transformed into 0 and 1 based on certain cut-off. According to Novak Zelenika et al. (2010) recommended number of cut-offs for this kind of mapping is 5-11.

Well	Reservoir	Average log porosity (%)	Average core porosity (%)
Well 1	Lower Pontian reservoir	23.3	15.8
Well 2		22.0	21.2
Well 3		19.9	
Well 4		19.5	
Well 5		19.6	
Well 6		21.1	
Well 7		20.5	
Well 8		20.1	
Well 9		21.2	
Well 10		17.9	
Well 11		19.2	
Well 12		13.8	
Well 13		5.5	
Well 14		19.7	
Well 15		18.2	
Well 16		21.8	
Well 17		18.1	
Well 18		18.5	
Well 19		19.6	
Well 20		18.4	

***Table 1**: Input well data*

For many statistical analyses, especially for geostatistical mapping (e.g. Isaak and Srivastava, 1989; Deutsch and Journel, 1997), normal distribution is mathematical base for the proper use of descriptive statistics, which includes variance, mean, mod, median etc. Variogram, which is a basis for kriging mapping, is derived from the variance. That means that normal distribution is also condition for a variogram as a representative tool. Many of geostatistical methods, as the first step, perform normal transformation of data wherever it is possible. So, Novak Zelenika et al. (2011) proved that the best way for cut-off definition is to group the data into several classes so

that they approximately follow normal distribution pattern. **Figure 2** represent normally distributed porosity classes subsequently applied as cut-offs for indicator transformation of the Lower Pontian reservoir.

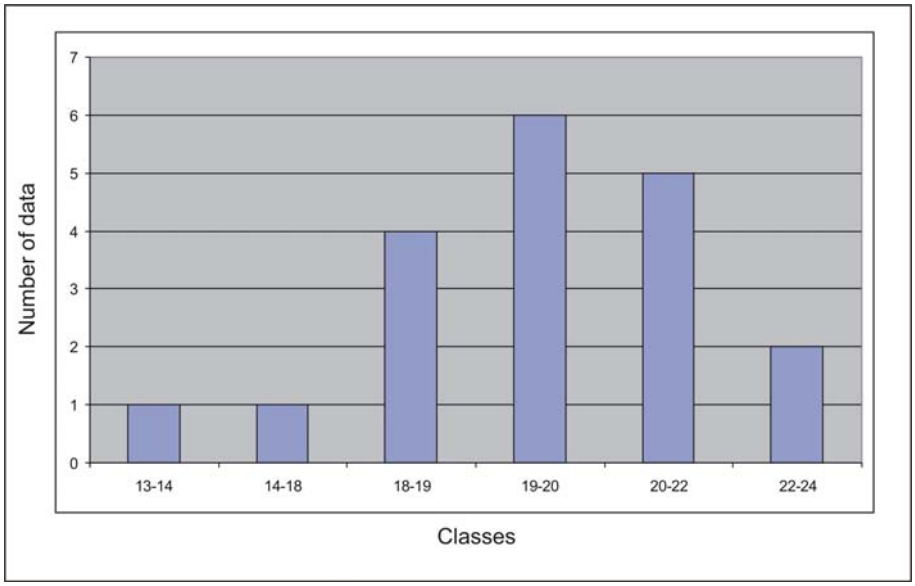

***Figure 2**: Normally distributed porosity classes within the Lower Pontian reservoir*

4. LITHOFACIES DEFINITION BASED ON CUT-OFF VALUES

Empirical experience shows that sandstones in this type of reservoir have porosity between 15 and 25 %. Most of the well log measurements cover the main part of the reservoir, which is sandstone by lithology, but it is also the most abundant part. Since chosen wells are equally distributed on the reservoir area, it is logical that most of the well log measurements are from the sandstone. On the other hand, one well shows extremely low log porosity value (5.5 %). Such low porosity directly points to marl, i.e. to Te Bouma sequence. Well 12 has porosity value 13.8 %, which indicates marls, sandy marls and marly sand intercalation and represents Tc Bouma sequence. As there was just one measurement in Tc interval and one in Te, which is not the highest porosity value in marl (also concluded by experience) and does not represent border between Te and Td lithofacies, it was not possible to define borders between Te and Td or Tc and Td intervals.

For that reason it was decided to map Tc and Tb intervals with a goal of finding border between them, and to exclude Well 13 as outlier (Novak Zelenika et al., 2010). The lowest (13.8 % from the Well 12) and the highest (23.3 % from the Well 1) porosities (**Table 1**) defined minimum and maximum cut-off for the indicator mapping.

5. OBTAINED RESULTS

Results of Indicator Kriging mapping are probability maps which show probability that the mapped variable is lower than the certain cut-off. For every cut-off value map was created (**Figure 3**).

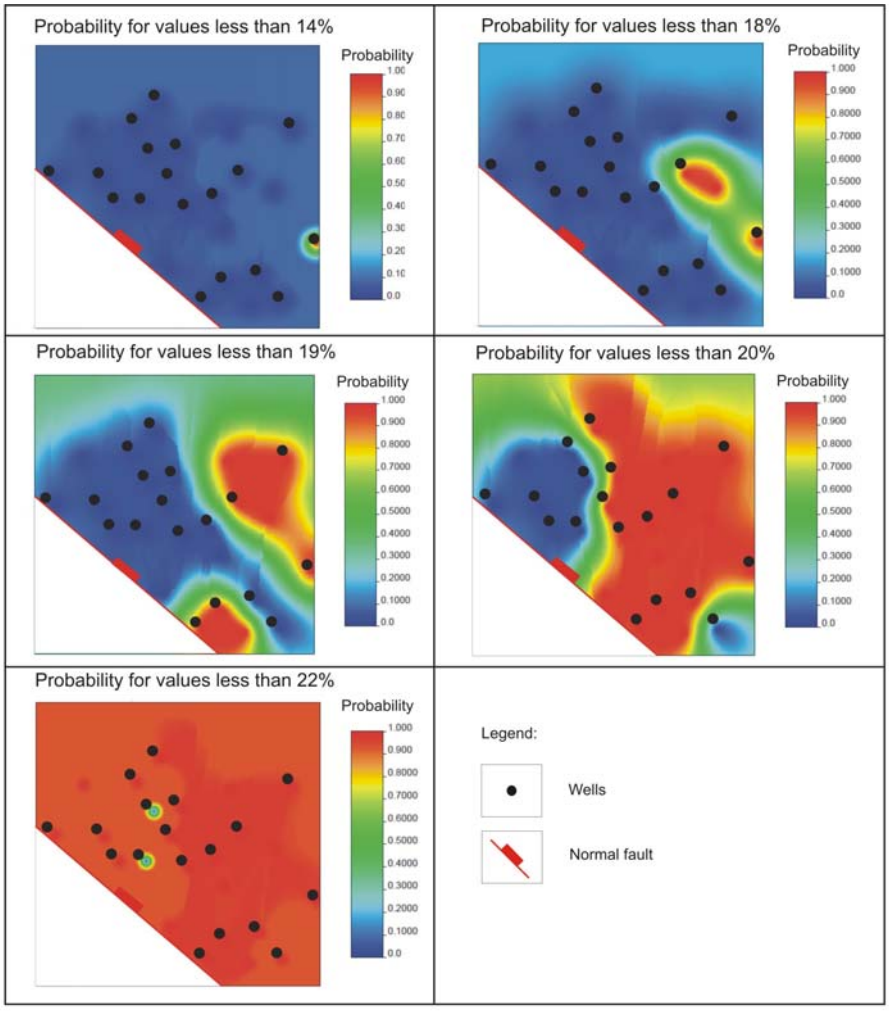

***Figure 3**: Probability maps for porosity cut-offs (Novak Zelenika et al., 2010)*

Material transport direction (N-S and NW-SE) and a turbiditic channel (blue colour on the map) is very well observed in the 19 % cut-off probability map (**Figure 3**). The blue colour on the map shows 0% probability that porosity is lower than 19%. Since turbiditic channel is the best seen in probability map for 19% of porosity it could be assumed that this value is actually border between Tc and Tb sequence.

6. CONCLUSION

Defining cut-off values is the hardest part in Indicator Kriging mapping because it depends mostly on the experience. With too many classes of the mapped variable, time needed for mapping drastically increases. Such approach also asks for large number of point data - more than 30. On contrary, less than 5 cut-offs can result in the loss of some important geological features. Although normality is not the condition for Indicator Kriging mapping, definition of classes that approximately follow normal distribution is useful, because it makes possible to calculate the descriptive statistics of such data and improve interpretation of indicator maps. It is also very important to try to map certain cut-offs which are borders between different lithofacies. In this case turbiditic channel and material transport direction could be observed in maps.

7. REFERENCES

DEUTSCH, C.V. & JOURNEL, A.G. (1997): GSLIB: Geostatistical Software Library and User's Guide, 2nd edn. Oxford University Press, New York, 369 p.

ISAAKS, E. & SRIVASTAVA, R. (1989): An Introduction to Applied Geostatistics. Oxford University Press Inc., New York 580 p.

MALVIĆ, T. (2003): Vjerojatnost pronalaska novih zaliha ugljikovodika u bjelovarskoj uleknini [Oil-Geological Relations and Probability of

Discovering New Hydrocarbon Reserves in the Bjelovar Sag - *in Croatian and English*]). -Unpub. PhD Thesis, Faculty of Mining, Geology and Petroleum Engineering, University of Zagreb, Zagreb, 123 p.

NOVAK ZELENIKA, K., MALVIĆ, T. & GEIGER, J. (2010): Mapping of the Late Miocene sandstone facies using Indicator Kriging. Nafta, 61, 5, 225-233.

NOVAK ZELENIKA, K., VELIĆ, J., MALVIĆ, T. & CVETKOVIĆ, M. (2011): Geological Variables Fitting in Normal Distribution and Application in Indicator Geostatistical Methods. -In: MARSCHALLINGER, R. & ZOBL, F. (eds.): IAMG 2011 Conference "Mathematical Geosciences at the Crossroads of Theory and Practice", Salzburg, Proceedings 245-251.

RÖGL, F. (1996): Stratigraphic Correlation of the Paratethys Oligocene and Miocene. Mitteilungen Ges. Geol. Bergbaustudenten Österreich, 41, 65-73.

RÖGL, F. (1998): Palaeographic Consideration for Mediterranean and Paratethys Seaways (Oligocene to Miocene). Ann. Naturhist. Mus. Wien, 99A, 279-310.

VRBANAC, B. (1996): Paleostrukturne i sedimentološke analize gornjopanonskih naslaga formacije Ivanić grad u savskoj depresiji [Palaeostructural and sedimentological analyses of Late Pannonian sediments of Ivanić Grad formation in the Sava depression - *in Croatian*]. Unpub. PhD Thesis, Faculty of Natural Sciences, University of Zagreb, Zagreb, 303 p.

Geostatistical modelling of turbiditic rock bodies in the Hungarian part of Pannonian Basin, Szolnok Formation.

Mátyás SANOCKI, Sándor TÓTH

MOL Plc., 1117 79th Budafoki út, msanocki@mol.hu, satoth@mol.hu

Abstract: Modelling of Pannonian sl. sediments is a very complex task because of the heterogeneity of the rock sequences. The inner facies and petrophysical structure of these reservoirs can only be described by defining highly detailed 3D models. The object based facies modelling is one of the most advanced method for modelling turbidite sequences, well describes the intrabody petrophysical structure. The conceptual model of the local depositional environment and sediment influx directions (vectorfields) were either based on the seismic interpretations or upon conceptual models derived from sequence thickness investigations. In the object based facies model the shape and size distribution of the turbidite bodies were scaled from both literary data and from object based experimental pilot models. Spatial distribution of petrophysical parameters within the turbidite bodies are defined by intrabody grain size distribution trends of which are driven by the energy of depositional settings. These effects can be modelled with multi direction intrabody porosity trends (vertical, body along, normal to body). Authors verify the above described workflow on validated modelling of 3 individual oil/gas fields from different sub-basins of the Pannonian Basin.

Key words: Szolnok Formation, nonclassical turbidites, heterogeneity, object based modelling, intrabody structure.

1. IMPORTANCE OF TURBIDITE MODELLING

During the oil&gas exploration in Hungary significant coarse-grained deep water sediments was found and the understanding of their nature led to the

understanding of the delta complex of Lake Pannon. Over the years they proved to be major hydrocarbon and water reservoirs.

Within the revealed deep basins (e.g., Derecske, Békés, Makó, Győr, Zalatárnok depressions) the first stage of the basin filling started with the deposition of deep water distal fans, slowly progarding toward the basin centre, followed by proximal sand lobes, as the sediment source and depositional base come closer to each other. Thus, gravity flows rushing down the permanently closer slopes formed sediments like distal and later proximal turbidites and connecting distributary channels. These sequences often achieve significant thickness, and they form what we call Szolnok Formation within the Pannonian basin. Conceptual model of the Pannonian delta complex can be seen on **Figure 1**, with the areal extent of the Szolnok Fm. on **Figure 2**.

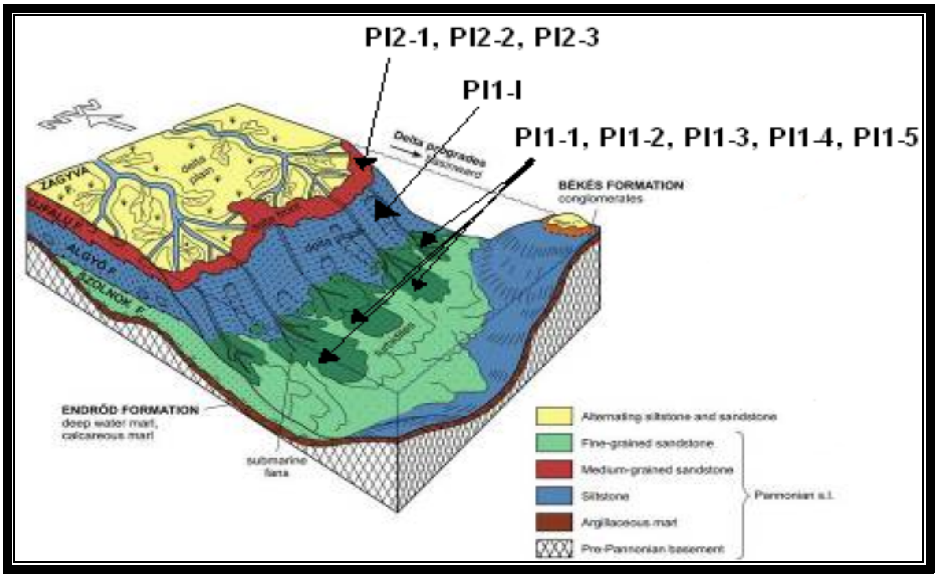

Figure 1: *Conceptual model of the Pannonian deltaic depositional environment (modified after Bérczi and Juhász , 1998)*

In this paper, authors show an integrated workflow applicable on 3D modelling of Szolnok Formation turbidites. This conception and workflow was validated on several Hungarian oil&gas Szolnok Formation turbidite reservoirs from different sub-basins, with successful history match.

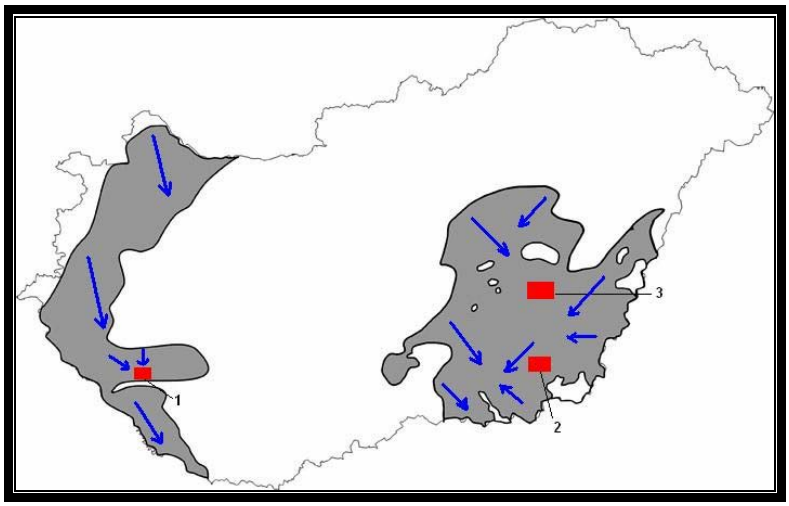

Figure 2: *Areal extent of Szolnok Formation in Hungary. Arrows represent approximate sediment influx. Red labels mark studied sub-basins (Modified after Juhász et al., 1998).*

2. SEISMIC BASICS

Base and top of Szolnok Formation can be interpreted routinely upon seismic facies. Highly diverse lithology (both laterally and vertically) leads to strong amplitudes and easy lateral tracking of reflexions. Lower inflection point of klinoforms also helps to provide formation top.

Inner structure can be revealed by seismic attribute analysis. Direct correlation between attribute maps and petrophysical parameters is challenging, however vectorfields always can be drawn showing turbidite flow directions. **Figure 3** shows a possible flow lines overlying total amplitude map of a Békés Basin turbidite reservoir. Note the spatial correlation between the sweet spot and the distal fan system.

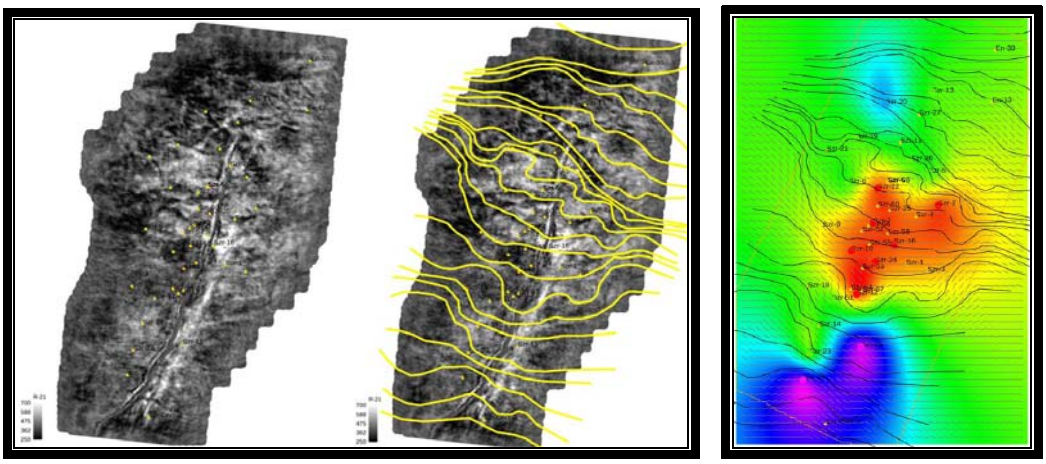

***Figure 3**: Seismic total amplitude map with flow polygons and resulting stickplot overlying deterministic permeability map based on well test data*

3. ISOCHORE INVESTIGATION

Isochore mapping of turbidite sequences need special practice, because thanks to the vertical heterogeneity driven thickness variability, sequence thicknesses are usually below the seismic interpretation limit (10-100 metres per sequence, 20-30 metres are most common). Isochore maps based on well picks can reveal bigger structure of each sequence, so approximate location of distributary channels and lobes can be defined upon well data. In figure 4 gross thickness maps of three consecutive turbidite sequences can be seen from a reservoir in Zalatárnok sub-basin. Colour coding is similar, and prograding system easily can be seen from left to right (bottom to top). Depositional direction is changing after the first turbidite sequence. Anisotropy direction in variograms of petrophysical parameters also change in the same way. This thickness map can give the modeller a concept of the lateral relative intensity (sand content) and depositional directions as well.

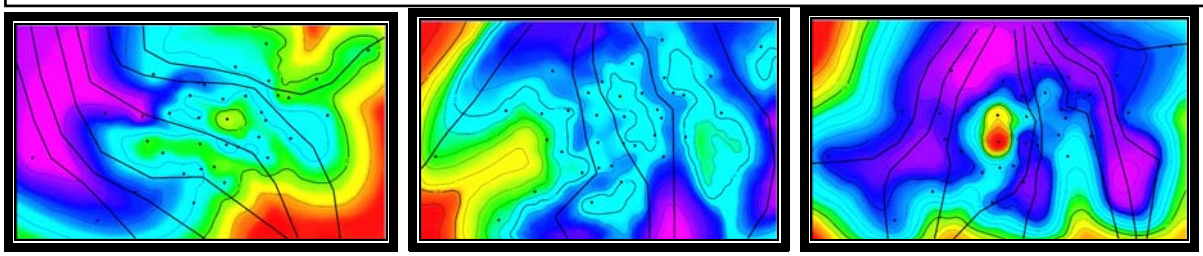

***Figure 4**: turbidite sequence thicknesses with depositional flow lines (Lower-left, Mid-centre, Upper-right)*

4. FACIES MODELLING

Facies modelling is best performed by object based modelling of each turbidite lobes. Industry softwares for 3D modelling provide solution for the facies modelling workflow and allow the modeller to do comprehensive geostatistics over facies data. Our now standardized workflow contains:

- Drawing flow lines and create vectorfield of depositional direction upon thickness maps and, if available, upon seismic attributes
- Create stochastic traditional pixel based (indicator) facies model
- Compute expected value from pixel based facies model realizations
- Make and investigate average sand content in above listed expected value parameter
- bodylog classification - each parasequence is coded individually within each sequence
- run object based faces modelling integrating all available information (VPC, vectorfield, bodylog, body shape and size distributions)

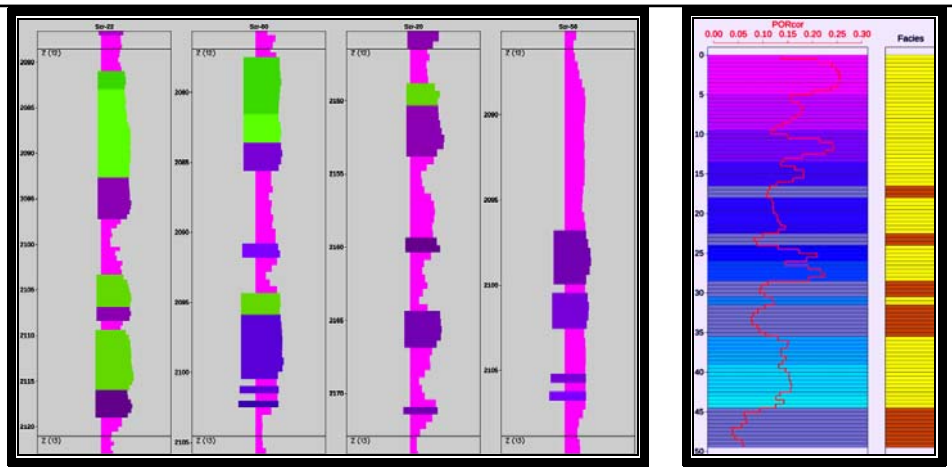

Figure 5: *bodylogs of turbidite bodies in nearby wells in a Békés Basin turbidite reservoir. Colour coding marks the different turbidite events (parasequences) The scattered nature of sand bodies doesn't allow modellers to rely on simple pixel based modelling, because connectivity can not be described well.*

A common but crucial question is how we define the size distributions of the turbidite lobes, because from the wells we only know the vertical (thickness) parameters of the bodies. The lateral dimensions of turbidite bodies are dependent on a large number of factors including the dimensions of the turbidity flow, the grain-sizes in the flow, slopes and degree of confinement. Thus, the dimensions are highly variable in different depositional settings and basins. (Bouma, 1962) Literature states some correlation between the thickness vs. elongation vs. width of the turbidites, but Szolnok Formation turbidites can not be measured directly in the surface. After literature we guess, that thickness/length ratio should be in a range of 1:100 to 1:1000. In other basin worldwide most turbidite sand bodies considered to be several km to several 10's of km long. (Dutton and Barton, 2001; Hauge et al., 2003)

In this example the lengths of the turbidites were assumed to vary between 1 and 5 km and the widths were up to 1 km as seen on **Figure 6.** These estimates were mainly based on an analysis of the well data, which suggest significant lateral discontinuity. There are also other ways to investigate whether our conception was good or bad. If we overestimate the size, bodies

will be bigger then they should fit properly within the wells, and resulting model will contain bodies with jagged, noisy, scattered artefacts, and model will run only with high rugosity settings. This can lead to underestimate of sand within the most densely drilled area, which is easy to recognize. If modelled bodies are too small, we can loose connectivity, which we should know from the well tests and production history. This question will also appear in chapter 5.

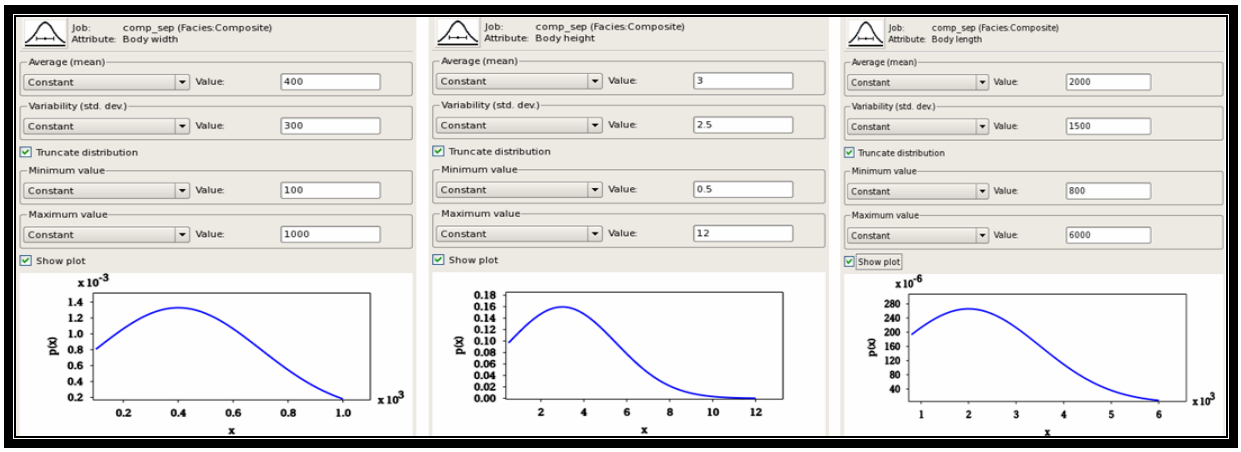

Figure 6: *size distributions of the turbidite lobes in a Békés Basin example*

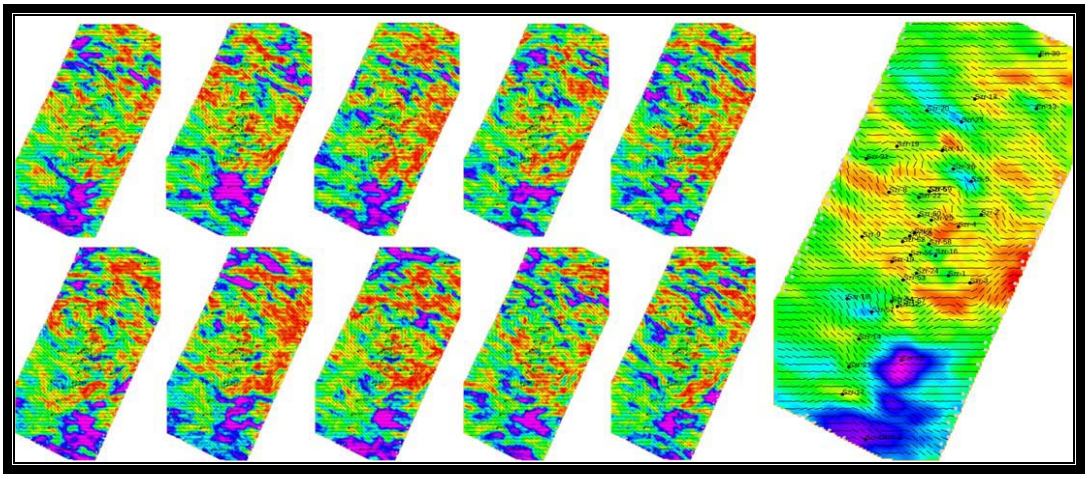

Figure 7*: Creating expected value from pixel based facies model realizations. Resulting map is used as relative intensity map for object based modelling.*

5. PETROPHYSICAL PROPERTIES

Object based facies modelling count every single turbidite body individually incorporating their geometric parameters and orientation as well. Thus it's possible to measure and model intrabody petrophysical (e.g., porosity) trends vertically and laterally as well, as **Figure 8** shows. Otherwise petrophysical modelling itself rely on the classic sequential Gaussian simulation, just pre-simulation trend removing can also be made individually within the facies bodies, after removing common trends compactional and depositional trends. (Zakrevsky, 2011; Hauge et al., 2003) This approach helps to confirm the body size distributions we have chosen before, because intra-body lateral along and lateral normal trends can only be seen if we have set up body size distributions properly. Otherwise no visible trends are present, and we need to recalculate body size distributions prior to have a good trend.

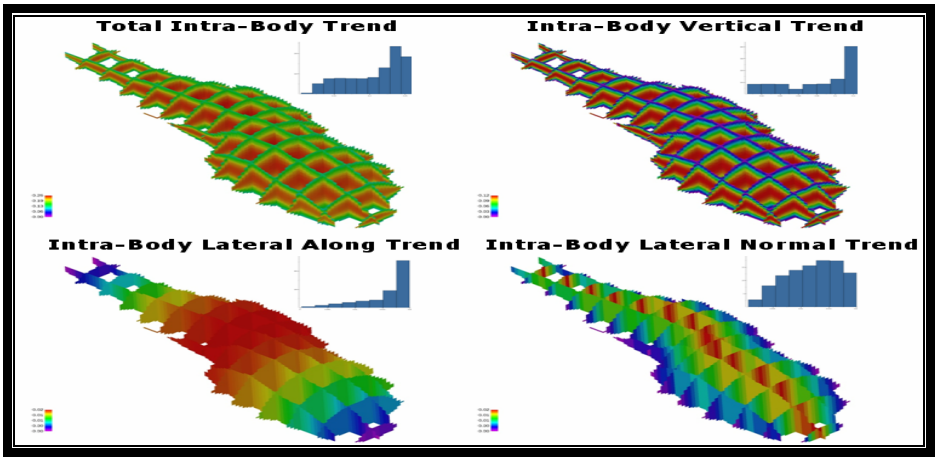

Figure 9: *3D intrabody trend analysis*

Bimodal porosity distribution of turbidite sand bodies is a common problem when modelling such environments with traditional facies models. When using intrabody trends we can easily set these trends up to reflect the bimodal distribution, which as a superposition of the intrabody porosity

trends, as seen in **Figure 9** and **Figure 10** respectively. Within a multi-zone model, which describes consecutive turbidite sequences we often see a trend in the changing of the intrabody porosity-trends. This is not just due to the compaction but the change in the paleo environment, as sediment influx changes between the sequences. (Gysi and Tóth, 2011)

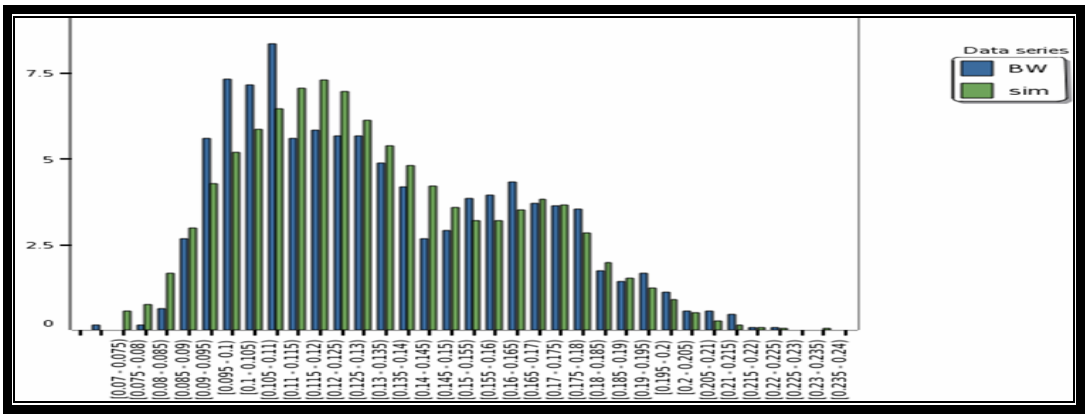

Figure 10: *Bimodal porosity distribution of a turbidite reservoir. Blue is for well data, green is for P50 case of simulation*

8. CONCLUSIONS

Modelling of Pannonian sl. sediments is a very complex task because of the heterogeneity of the rock sequences. The inner facies and petrophysical structure of these reservoirs can only be described in highly detailed 3D models. The object based facies modelling is one of the most advanced method for modelling turbidite sequences, of which describes well the intrabody petrophysical structure

The models should be divided to zones in addition to bigger sedimentation events, e.g. turbidite megacycles/sequences. Each cycle should be modelled separately but taking into account the continuity between them. Each cycle typically represent separate hydrodynamic units.

The reservoir engineers were able to achieve a good history match after minimal modifications and reasonable time which confirmed the model's consistency. In case of the classical approach a comparable result was only

achieved after serious modifications which often where difficult to explain by a natural system. On the other hand, the object-based facies model facilitates to analyse and capture intra-body trend, which could not been discovered and reproduced in the traditional approach model.

9. REFERENCES

BOUMA A.H. (1962): Sedimentology of some Flysch deposits: A graphic approach to facies interpretation, Elsevier, Amsterdam, 168 p.

GYSI, M. and TÓTH, S. (2011): Object-based modelling in a turbidite type reservoir. In: Geiger, J., Pal-Molnar, E., Malvić, T. (Eds.): New horizons in Central European geomathematics, geostatistics and geoinformatics, Geolitera, Szeged, 47-59.

JUHÁSZ GY. (1998): A magyarországi neogén mélymedencék pannóniai képződményeinek litosztratigráfiája. In: Bérczi I., Jámbor Á. (Eds.): Magyarország geológiai képződményeinek rétegtana. MOL Rt., MÁFI, Budapest, 469-484.

JUHÁSZ GY., POGÁCSÁS GY., MAGYAR I. and VAKARCS G. (2006): Integrált-sztratigráfiai és fejlődéstörténeti vizsgálatok az Alföld pannóniai s.l. rétegsorában. Földtani Közlöny, 136, 1, 51-86.

DUTTON S.P., BARTON M.D., (2001): Diagenesis and reservoir quality of turbidite sandstones in the Bell Canyon Formation, Delaware Basin, Texas: Geological Society of America, Abstracts with Programs, 33, 36–37.

HAUGE R., SYVERSVEEN A. R., MACDONALD A. C. (2003): Modelling Facies Bodies and Petrophysical Trends in Turbidite Reservoirs. SPE paper 84053

ZAKREVSKY K.E. (2011): Geological 3D modelling. EAGE publications, Houten, 261 p.

Pseudo-random sweep optimisation for vibratory measurements in built-up area

Péter SCHOLTZ

Eötvös Loránd Geophysical Institute, 17-23 Columbus, 1145 Budapest, Hungary,

scholtz@elgi.hu

Abstract: Optimised pseudo-random sequences are calculated and tested for the purpose of reducing possible damage to buildings by vibratory sources during seismic reflection acquisitions. The common linear sweeps used at vibratory measurements cause resonance in infrastructure, hence the potential for damage increases. Pseudo-random sweep signal can be a natural choice to decrease resonance effects, but the sequences produced by simple random number generators have disadvantages. In this paper an optimisation process is employed and behaviours are set for producing pseudo-random sweep signals to achieve satisfactory results. Analysis of optimum sweep examples shows that the peak energy is increased, while side-lobe energy is decreased compared to a simple pseudo-random sweep. Field tests reveal, that the peak particle velocity values are reduced substantially along with possible damage, while correlated records are of similar quality to a linear sweep driven record, which cannot be said about a simple pseudo-random sweep generated one.

Key words: pseudo-random, peak particle velocity, resonance, seismic sweep.

1. INTRODUCTION

The vibroseis method, where a ground-coupled device (i.e. usually a hydraulic seismic vibrator) generates vibration on the surface, took over most of the seismic reflection land operations. Unfortunately, even this way

of seismic wave generation has enough power in the vicinity of buildings to produce fractures in plastering or structural damage to walls, fundaments, etc. This is partly due to resonance effects, because the frequency band employed by the vibratory acquisition technique (typically 6-100 Hz) contains the resonance frequencies of buildings, too. Also, the common sweep is a linearly varying frequency sinusoid, where relatively long time is spent at each frequency component helping the build-up of constructive energy.

To overcome the problems, found by using a simple linear sweep, different sweep designs are suggested (Cunningham, 1979; Strong, 2003), where the application of pseudo-random sweeps is offering an ideal solution. Pseudo-random sweeps are used in simultaneous acquisitions, too, where source separation is enhanced by the orthogonal sequences (Krohn et al., 2008; Sallas et al., 2008). On **Figure 1** the linear and a simple pseudo-random sweep record are shown. The linear sweep driven waves generates higher peak particle velocity values due to resonance effects.

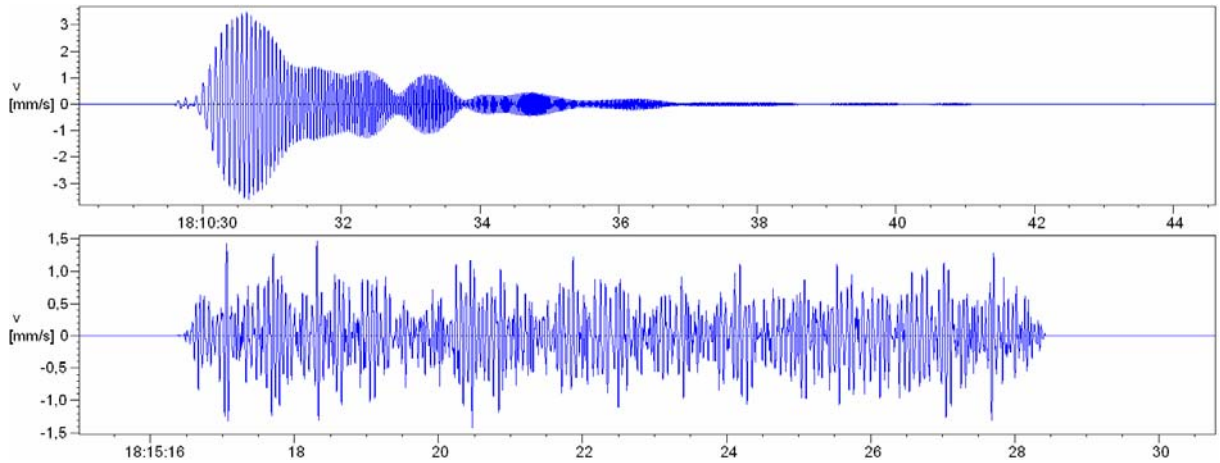

Figure 1: *Particle velocity records of linear (upper image) and simple pseudo-random (lower image) sweeps driven vibrations*

Unfortunately, a simple random number generator produced sweep has unwanted features. The frequency response is not smooth enough in the required frequency band, the total seismic energy is reduced and the

autocorrelation function of the sweep has stronger side-lobes (Burger et al., 1992; Strong, 2003). Fortunately, there are plenty of variations in pseudo-random sweeps, hence one can choose the optimum solution. In Iranpour et al. (2009) optimum sweeps are produced to have non-correlating sequences to be used in simultaneous seismic acquisition techniques. The authors have used a Simulated Annealing based algorithm to search for the optimum design. In this paper we use a similar technique, where the optimum pseudo-random sweep sequence has to satisfy the needs of our special seismic measurement: the aim is to cause the least damage to nearby buildings, while maintaining the common procedure as much as possible. Here we define the criteria and highlight the calculation method. Through examples the behaviour of such sweeps is shown and finally some field tests are presented to verify the idea.

2. OPTIMISED PSEUDO-RANDOM SWEEPS

The common pre-processing step in the vibroseis technique is the correlation of the theoretical sweep signal with the geophone recordings. This step will produce an impulse like signal. The main requirements from such a correlation result are that the arrival peaks should have maximum, the side-lobe amplitudes should be minimum (not to interfere with other seismic arrivals) and should have a band-limited, flat amplitude response (or follow a function to enhance certain bands). These are the basic requirements for pseudo-random sweeps, too. If we use a random number generator and produce the time sequence, these criteria will not be met. This is the case with the sweep generator programs given by the manufacturers to calculate sweeps for the vibrator electronics. As a result the simple pseudo-random sequences are not used in practice. The optimisation procedures described by Iranpour et al. (2009) can be deployed or other methods can be considered to generate optimised pseudo-random sequences. Their simple global optimisation procedure calculates cost functions and updates the

sequences by minimising the total cost function. The update is driven by a cooling scheme and carried out during several thousand iterations and perturbations.

But whatever the optimisation procedure is, the main task is to define the requirements. In our work we have followed two strategies. The first one is using the principles of the current field practices. The main goal was to find an optimum pseudo-random sweep, where the autocorrelation of the pseudo-random sweep should match, as much has possible, the common sweep's autocorrelation (i.e. the linear sweep's) used at other parts of the survey (where there is no sensitive infrastructure nearby). In this case, after pre-processing (i.e. field correlation), the seismic records have similar characteristics, though the actual sweeps have been changed during the acquisition. As a result resonance effects are reduced, the optimum pseudo-random sweep can be used at higher drive levels, with more simultaneously run vibrators, closer to sensitive buildings, with less number of sweepings at lower risk to cause damage. The other strategy was to replace the correlation procedure by deterministic deconvolution. In that case the side-lobe energy is less of a concern. Those results are discussed in a separate paper.

3. OPTIMUM PSEUDO-RANDOM SWEEP BY MATCHING AUTOCORRELATIONS

In the optimisation procedure we define a cost function, where different weights are given to the predefined criteria:

1. Maximise the total energy of the sweep (i.e. zero lag value of the autocorrelation function);
2. Maximise the main peak (zero lag) to side-lobe ratio;
3. Maximise the match between the autocorrelation function of the optimised pseudo-random sweep and a common linear sweep.

The numeric calculations were carried out on a T=12 sec long, dt=2 msec sample rate, 6-90 Hz sweep. The tapers at each end were 0.3 sec long cosine type. As a reference the same parameters are used in a linear sweep design.

In **Figure 2** the time sequence (upper part), the time-frequency distribution (middle part) and the dB scaled autocorrelation function of the final optimised pseudo-random sweep (bottom part, red curve) are shown. For comparison the autocorrelations of a linear sweep and a simple pseudo-random sweep are also shown (bottom part, blue and green curve). The side-lobe values are lower for the optimised sweep, there is up-to a -20 dB gain relative to the simple case. Also, the central part of the autocorrelation function perfectly matches the behaviour of the linear sweep's autocorrelation (around the zero lag), proving the success of the optimisation.

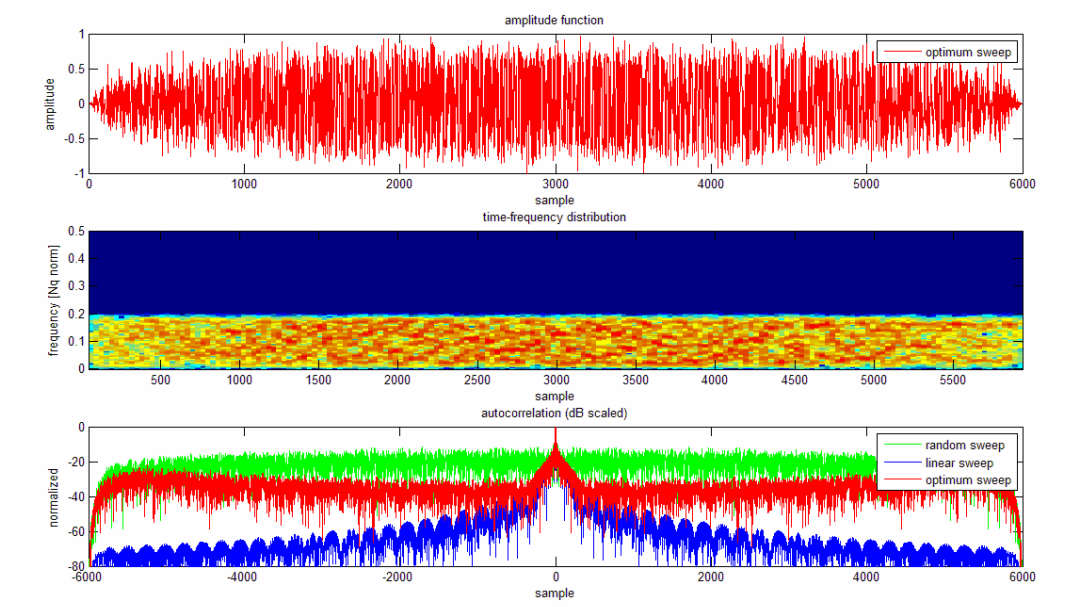

Figure 2: *Time sequence (upper part), time-frequency distribution (middle part) and dB scaled autocorrelation function of the optimised pseudo-random sweep (bottom part, red curve). As a reference the autocorrelations of a linear sweep and a simple pseudo-random sweep are also shown (bottom part, blue and green curve).*

In **Figure 3** some time and frequency domain close-ups are shown. The colours are representing the different sweeps again: red is for the optimised, green is for the simple pseudo-random and blue is for the linear sweep. The upper and the lower left corner images show the autocorrelations around the zero lag. Here the actual energy levels can be compared, where the linear sweep has the highest, the simple pseudo-random has the lowest and the optimised pseudo-random is in between (gained some during the process). The upper right image shows again the central part of the autocorrelation functions in normalised dB scale. Here the goodness of fit between the autocorrelations of the linear and the optimised pseudo-random sweeps can be observed (the blue curve is hardly visible, since the red curve covers it). The lower right image shows the autocorrelation functions in frequency domain (amplitudes). The simple pseudo-random (green) sweep exhibits a rapidly changing behaviour. The optimised sweep has a much lower variation and a higher total energy (though less smooth and has lower energy, than the linear sweep's autocorrelation).

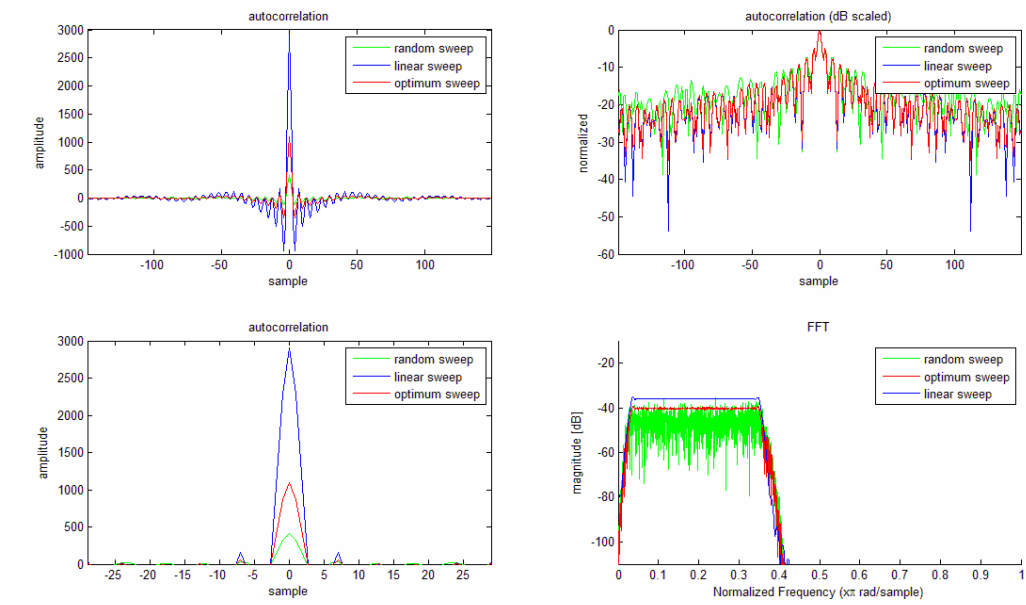

Figure 3: *Comparison of different autocorrelation functions: red is the optimised, green is the simple pseudo-random and blue is the linear sweep. The upper and the*

lower left corner images show the autocorrelations around the zero lag. The upper right image shows the central part in normalised dB scale. The lower right image shows the autocorrelation functions in frequency domain (amplitudes).

4. FIELD TESTS

We have carried out a field test to compare the different sweeps via the analysis of the recorded seismic signals. There were several types of sweeps used in the tests, but here we show only three of them:

1. Linear sweep (T=12 sec, dt=2 msec, 6-90 Hz, 0.3 sec cosine taper);
2. Pseudo-random sweep, generated by the software given by the manufacturer of the vibrator electronics (T=12 sec, dt=2 msec, 6-90 Hz, 0.3 sec cosine taper);
3. Optimised pseudo-random sweep, where the optimisation target was to match the autocorrelation function of the linear sweep (T=12 sec, dt=2 msec, 6-90 Hz, 0.3 sec cosine taper).

On **Figure 4** parts of correlated records are shown from the same seismic line with different sweeps. From left to right: on the left is the linear sweep; in the middle is the off the shelf pseudo-random sweep; on the right is the optimised pseudo-random sweep. The sweep designs followed the requirements of a common oil exploration project. The records reveal several clearly distinguishable reflection surfaces, though the middle record shows very noisy characteristics due to the cross-correlation side-lobes. By the optimisation process, the application of the pseudo-random sweep, this kind of noise is highly eliminated, only late arrivals (with weak energy) are buried under the earlier arrivals' correlation noise (not seen in the figure). Since the optimisation was weighted towards the matching of the autocorrelation functions, the total energy contained in the pseudo-random sweep was about the third of the linear sweep. This leads to some S/N degradation, but could be improved by enhancing the energy component in the cost function.

The resonance effects are reduced as shown by **Figure 1** and the reduction has reached the factor of 5 in general. Also, the vibrators work better in producing the low frequencies (Sallas et al., 2008). This benefit was seen in our tests as well. There are concerns about the use of pseudo-random sweeps. One example is the harmonic distortion, which is due to the non-linear behaviour in the hydraulics and mechanics of the vibrator, the vibrator-ground coupled system. In case of linear sweeps this effect was studied by Saragiotis et al. (2010), but their method is not applicable here, since that harmonic energy separation does not work in this case. There is a need for further studies in this area.

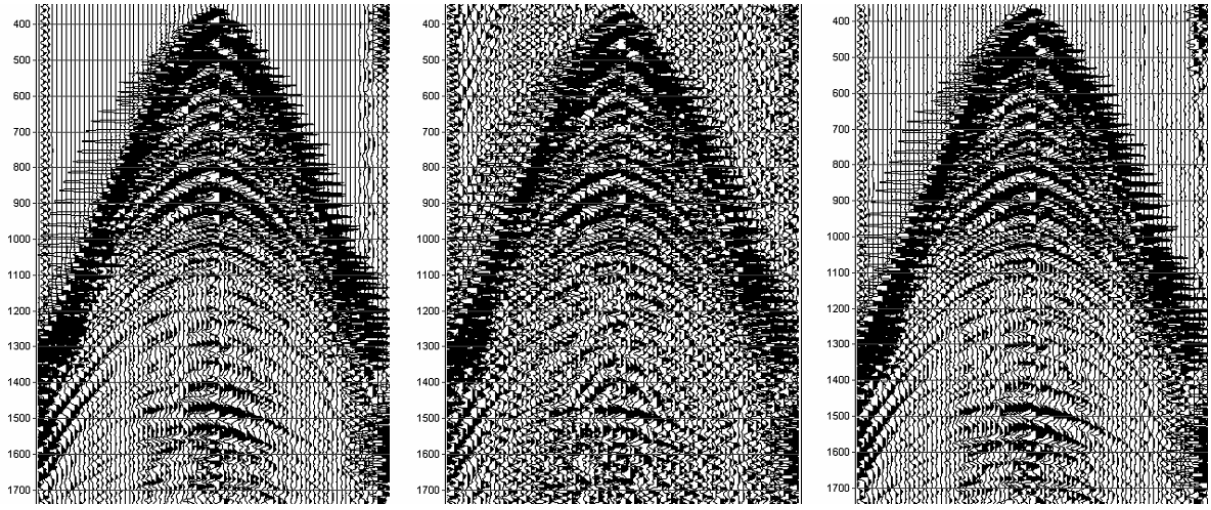

Figure 4: *Parts of correlated 3D seismic reflection records from the same seismic line with different sweeps. From left to right: linear sweep, off the shelf pseudo-random sweep, optimised pseudo-random sweep driven vibrations.*

5. CONCLUSION

We have shown that optimised pseudo-random time sequences can be used successfully in seismic reflection measurements, where the aim is to have less potential for damage to nearby buildings during vibratory wave generation. An optimisation process can generate sweeps, which have reduced side-lobe energy compared to a simple off the shelf random number generator, hence multiple arrivals are not buried in correlation noise. Also the optimisation process can accommodate satisfactorily the request for a

match between the central zone of the autocorrelation functions (seismic wavelet after pre-processing) of a common linear sweep and an optimised pseudo-random time sequence. This makes possible the mixed use of the two sweeps as required by the need for reducing resonance during a seismic acquisition campaign without further processing differences. Field tests revealed, that in this particular case the PPV values are reduced by 5 times, compared to a linear sweep, hence the time spent at a vibrator point can be decreased by a similar factor, enhancing productivity, while maintaining PPV limits to avoid damage to buildings.

6. ACKNOWLEDGEMENTS

This work was inspired by the discussions with Kambiz Iranpour during the European Marie Curie Host Fellowships (no. MTKD-CT-2006-042537). The field tests were carried out by the support of Acoustic Geophysical Services.

7. REFERENCES

BURGER, P., BALIGUET, P. and NAUDOT, J.C. (1992): New vibrator control concept offers industrial use of pseudo-random sweeps in populated areas. 54th EAEG Meeting, Paris

CUNNINGHAM, A.B. (1979): Some alternative vibrator signals. Geophysics, 44, 1901-1921.

IRANPOUR, K., ERIKSSON, S. and HOERLIN, C. (2009): Generating Sweep Sequences. United States Patent no. 20090052278

KROHN, C.E. and NEELAMANI, R. (2008): Simultaneous sourcing without compromise. EAGE Vibroseis Workshop, Prag

SALLAS, J.J., GIBSON, J.B., FOREST, L., WINTER, O., MONTGOMERY, R. and NAGARAJAPPA, P. (2008): Broadband vibroseis using simultaneous pseudorandom sweeps. 78th SEG meeting, Las Vegas, Nevada, USA, Expanded Abstracts, 100–104.

Saragiotis, C., Scholtz, P. and Bagaini, C. (2010): On the accuracy of the ground force estimated in vibroseis acquisition. Geophysical Prospecting, 58, 69–80.

Strong, S.R., (2003): Numerical modelling of pseudo-random seismic sources. Honours Thesis, University of Queensland.

Integrated Fractured Reservoir characterization of the Nubian sandstones, Southeast Sirt Basin, Libya

O. SLIMAN and K. BERGIG
Libyan Petroleum Institute, P.O.BOX 6431 Tripoli, Libya,
e-mail: omarslmn@yahoo.com & kabergig@yahoo.com

Abstract: The Lower Cretaceous Nubian Formation is the most important oil bearing formation in the Sirt Basin. It is composed mainly of non- marine sediments and subdivided into three members; Lower Nubian Sandstone, Upper Nubian Sandstone, and Middle Nubian vary colored shale separating the two sandstone members. The study area is located in the eastern part of Sirt Basin, and it has been carried out from the Upper Nubian Formation. The available data used in this study includes the cores, petrophysical analysis data, and wire-line logs. The studied section consists of sandstone, light brown-gray; mostly medium grained locally becomes coarse to very coarse with scattered granules towards the channel base, locally highly argillaceous and micaceous. It exhibits abundant trough cross bedding, clamping ripples, flat lamination, deformed bedding, and minor syn-sedimentary fault. This section is locally organized into fining- upward sequences and it is interpreted as fluvial sediments deposited in both meandering and braided stream. The examined core cut in the upper member sandstone for natural fracturing only (excluded induced fractures) in this study is comprised of 168 feet in length and 4-inch diameter of non-oriented cores, between depths 10280 and 10448 feet (3133.19-3184.39 meters) from core 5 to 10. The natural fracturing was recorded feet by feet (each 0.305 meter) relative to the core axis, 84 fractures have been recorded including both macro, and micro fractures. These fractures occur in varying degrees of concentration throughout this interval. The analyses are correlating with the petrophysical data and the results obtained from wire-line log.

Key words: Nubian Sandstone, fractured places, well log analysis.

1. INTRODUCTION

Detection of fractured places and estimation of their characteristics are essential for fractured reservoir characterisation because of the major roll of the natural fracture system on the reservoir recovery. Here two methods are used in integration mode for fracture detection and description in the selected depth interval from the upper Nubian Sandstone in the Sirt Basin: (1) Using core description including fracture (type, length, orientation, density) and core measurements (horizontal permeability, vertical permeability and porosity); (2) Well log analysis by probabilistic methods to reveal fracture places.

This integration will finally yield a striplog which summarised all the results and information from different sources (geology, engineering data) verses depth for the processed interval. In addition, the fractured zones are statistically analysed by using (Ross diagram, frequency histogram, crossplots) in order to identify the different fracture categories depending on the orientation and aperture.

2. METHODOLOGY

2.1. Fractures detection using core description and core measurements

The cored section of the selected interval was studied sedimentologically and the natural fractures were recognized and recorded related to the core axis. Including the following: (a) A graphic image of natural fractures only; (b) Mode of fracture opening or closed; (c) Fracture orientation, i.e. dip angle related to datum; (d) Fracture geometry, i.e. planner, steeped …. etc.; (e)

Fracture dimensions - Visible fracture (length, width, aperture width) and top and bottom depths of occurrence.

The recognized fractures were statistically analyzed applying (histogram, rose diagram) technique and classified into four distinct sets: (1) Steeply dipping and vertical fractures (80-90 degree dip); (2) Moderately dipping fractures (45-79 degree dip); (3) Gently dipping fractures (10-40 degree dip); (4) Bedding plan parallel fractures (0-9 degree dip).

2.2. Fracture detection by well logs using probabilistic methods

In the selected interval the following logs are taken into account: ρb, Φn, Δt, Pe, CGR, SGR, Cal, for both of statistical lithology analysis and the fracture detection. Among these logs the Δt, Pe, Cal are considered to be fracture-sensitive and can be used for fracture detection where the Pe and Cal are qualitatively utilised and the Sonic Δt, compressional log is quantitatively analysed depending on the circumstances that Sonic Δt, compressional is sensitive for : porosity, shaliness, fracture and rugosity . The analysis for fracture detection is made by long-far spaced and long-near spaced sonic logs in an integrated mode with the results of statistical lithology analysis where the fracture places could be identified by means of an indicator called sonic fracture indicator (FrI-Δt) which is established by log values and answer as explained by (Barlai and Kelemen, 2000).

3. RESULTS AND DISCUSSION

3.1. Fracture Types

The recognized fractures in the studied interval were divided into four distinct fractures sets **(Table 1)**, depending on the result of frequency distribution of natural fractures attitude, which analyzed for population of 84 fractures including both macro and micro-fractures (78 and 6 respectively)

Figures 1 and **2**.

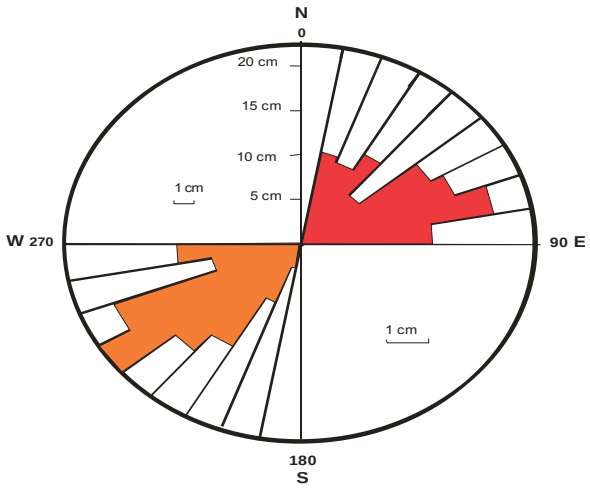

Figure 1: *Frequency with mean length, Frequency with percentage*

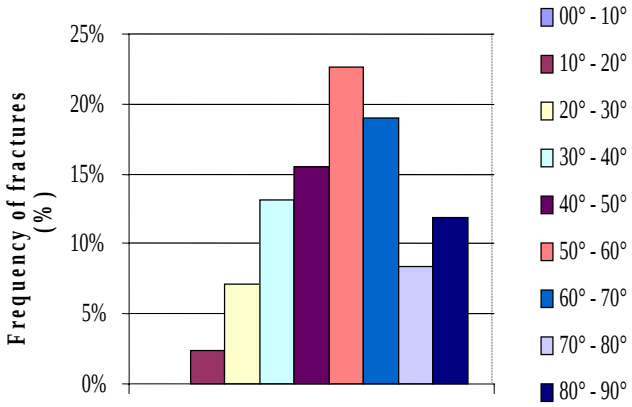

Figure 2: *Frequency of the fractures*

3.1. Steeply Dipping and Vertical Fractures

This set is consist of (13) individual fractures which represents 15% of the total fractures. With length varies between 3 and 40 cm. and thickness are mostly between 1mm and 3mm. The main cement developing in these fractures is carbonate with minor amount of pyrite (**Figure 3**).

Figure 3: *Examples of secondary mineralization cemented fractures (A-left, carbonate; B-right, pyrite)*

3.2. Moderately Dipping Fractures

These fractures constitute the dominant set occurring in these intervals which is (52) individual fractures and it represents 62% of the total fractures. They are categorized as cemented, partly cemented and closed fractures. Lengths vary between 1 and 56 cm. and the thickness is mostly between 1 and 10 mm. The main cements included in these fractures are carbonate with minor pyrite and mixed cements (**Fig.3**). Locally, the fracture void space is occupied by carbonate and pyrite cement, although cementation is incomplete and leaves fracture porosity (aperture).

3.2.1. Gently Dipping Fractures

Nineteen (19) individual fractures of this class were recorded in varying frequencies from different intervals. They are mostly cemented by carbonate and pyrite and the other healed by clays. Fracture length varies between 3 cm. up to 29 cm. and thickness is mostly between 1mm and 13mm.

3.2.2. Bedding Plane Parallel Fractures

No fracture has been recorded within this class.

Dip angle	No	**%**	**Fracture type**				**Cement type**				**Length rang (cm)**	**Width rang (mm)**
			Ce	Cl	O/C	Mi	Ca	Py	Ca/Py	Cy		
0 - 9º	0	0										
10º - 44º	19	23	12	7	-	-	8	3	-	1	3 - 29	1 - 13
45º - 79º	52	62	25	19	2	5	23	2	3	1	1 - 56	1 - 10
80º - 90º	13	15	5	6	1	1	4	1	1	-	3 - 40	1 - 3
Total	84	100	42	32	3	6	35	6	4	2		

Table 1: *Summary of the natural Fracture Distribution*

CODES - Fracture Type: Ce - Cemented, Cl – Closed, O/C - Partly open/partly cemented, Mi – Microfractured. Cement Type: Ca – Carbonate, Py - Pyrite, Ca/Py - Mixed cement, Cy - Clay healed.

4. DETECTION OF FRACTURED ZONES

In the striplog (**Figure 4**) results obtained from the used methods of fracture analysis are shown where the first track from the left consist of two curves. The upper shaded one represents the caliper delta= (Borehole size-Bit size), the deflection of this curve indicates the rugosity (**Figure 5**) which can used qualitatively to predict fracture places. Regarding to the zero value of this curve in front of the shale places this gives the reason that the curve deflection not because of borehole enlargement caused by shale wash out, especially in our case where the drilling fluid was oil base mud. The second curve within this track is photoelectrical index which is sharply affected by the presence of barite in the drilling mud the values of this log are in good correlation to the deflection of caliper delta it shows high reading in the rugosity places where it assumed that barite precipitated and concentrated in fracture surfaces.

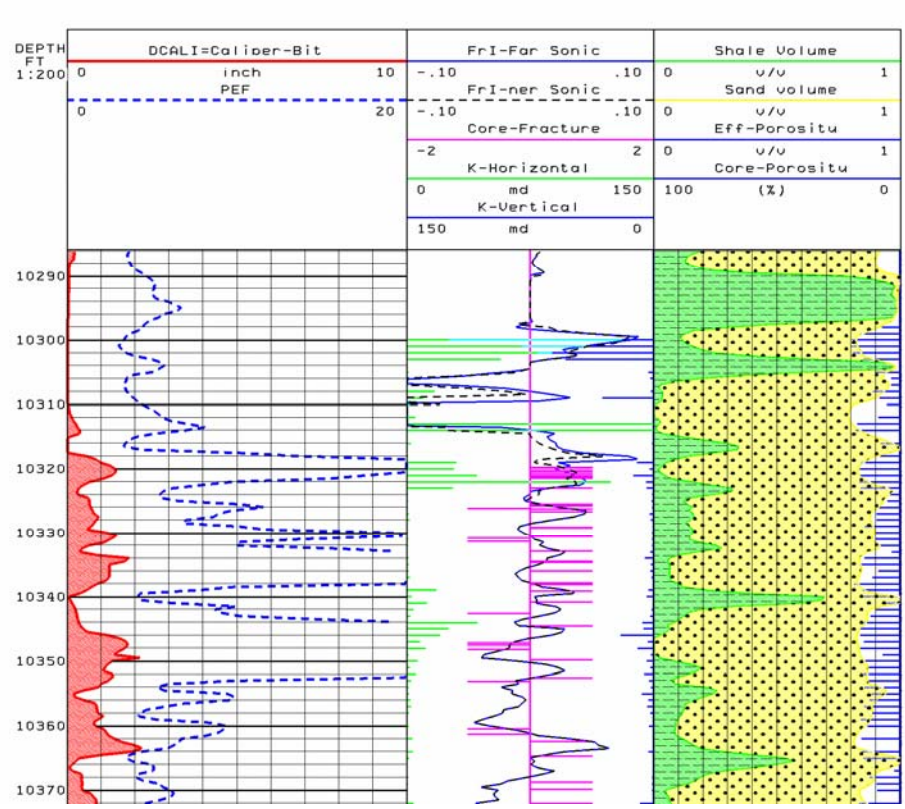

Figure 4: *Composite striplog of fracture places detection and lithology analysis*

The second track composite of several fracture indicator: from above the sonic long –far and near spaced indicator which are shown by tow overlapping curves indicate two cases of fracture development, the positive deflection from the zero base line belongs to brecciated places and negative deflection belongs to sub vertical fracturing. Then the fracture places recognized from core description traced verses depth as sticks directed from the base line to left as cemented fractures and to the right as macro, micro-fractures. The last fracture indictor with-in this track is represented by the values of the vertical and horizontal core permeability traced verse depth as sticks where the horizontal K increases to the right and the vertical K increases to the left. The lowermost track shows the result of lithology analysis made by means of statistical methods of the FlexInLOG, four well logs were applied CGR, ρb (corrected for rugosity), Φn, Δt (corrected for rugosity), by using rock model of four rock components: effective porosity, fraction volume of sand, fraction volume of shale, fraction volume of silt. The

results are presented in this track verse depth; it is easily observed that all the fractured places were developed in intervals of low shale fraction volume.

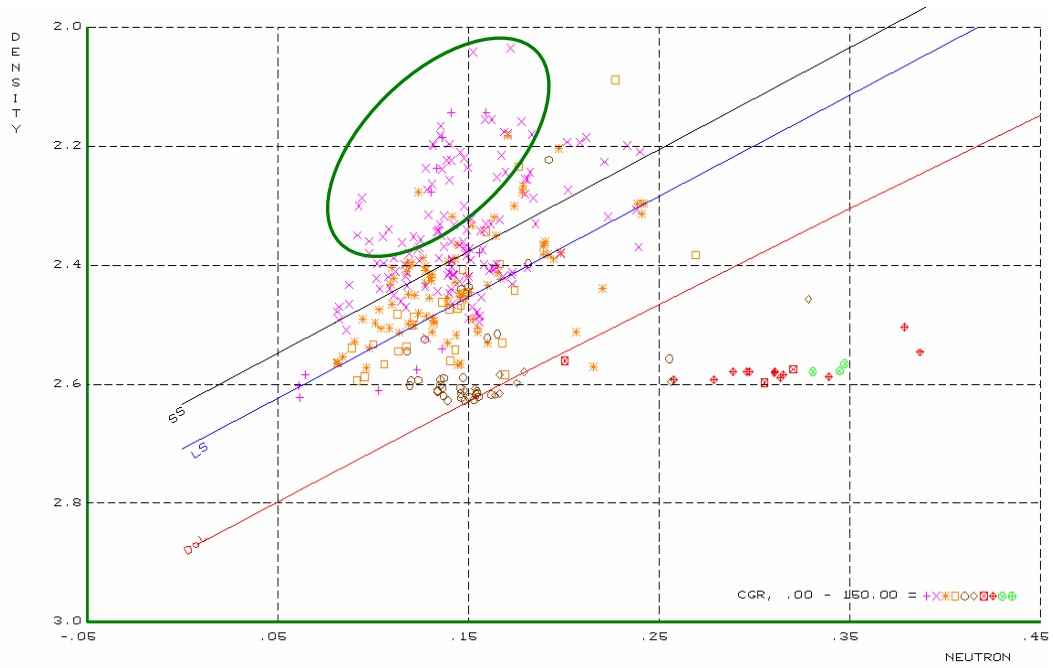

Figure 5: *Crossplot Density verses Neutron shows the rugosity places*

5. CONCLUSION

1. Depending on the fracture intensity the processed interval could be divided in to three zones: upper zone 10300-10390 feet (3139.3-3166.72 metres), middle zone 10390-10420 feet (3166.72 -3175.86 metres) and lower zone 10420-10448 feet (3175.86 -3184.39 meters) eliminating the shale intervals.
2. The value of vertical and horizontal core permeability shows good agreement with the fracture types.
3. The results of lithology analysis by FlexInLOG methods show good correlation with the core description (rock composition and fracture places).

6. REFERENCES

1. KULANDER B.R., DEAM S.L. & WARD B.J. (1990): Fractured Core Analysis, Am. Assoc. Petrol. Geol.Serise No. 8, 88 p.
2. BARLAI Z. & KELEMEN Z. (2000): Structure of FleInxLOG SOTWARE, Libyan Petroleum Institute unpublished document.

Bošković-Laplace's and Related Methods of Adjustment

Martina TRIPLAT HORVAT, Miljenko LAPAINE
University of Zagreb, Faculty of Geodesy, Kačićeva 26, Zagreb, Croatia,
mthorvat@geof.hr, mlapaine@geof.hr

Abstract: In this paper the Bošković-Laplace's method for determining the best linear relation based on measured data is shown. Also, there are related methods of fitting of the straight line described by minimizing the L_1-, L_2- and L_∞-norm. Application of these methods is illustrated on the Bošković's example on nine lengths of the meridian arcs.

Key words: Ruđer Bošković, Bošković-Laplace's method, linear approximation, fitting the straight line, adjustment.

1. INTRODUCTION

Bošković-Laplace's method is the method of estimating errors of measurements and the mathematical elimination of their influence on the final measurement result (Lapaine, 2012). Besides Bošković-Laplace's method, the Least Squares Method, also known as L_2-norm adjustment method, is often applied. In this paper, apart from Bošković-Laplace's method, the description of adjustments according to L_1-, L_2- and L_∞-norms will be shown for comparison purpose.

2. METHODS OF ADJUSTMENT

2.1. Bošković-Laplace's Adjustment Method

Under the assumption that the Earth has the shape of an ellipsoid due to its rotation, the lengths of short arcs can be approximated by a linear function, from which the first Bošković's condition (Stigler, 1986) is fulfilled:

$$L_i + v_i = a + b\sin^2\varphi_i \qquad \text{(i=1, 2,..., n)} \qquad (1)$$

where is

a – the length of a meridian degree at the equator

b – the excess of a degree at the pole over one at the equator

L_i – the length of an arc at location *i*

φ_i – the latitude of the midpoint of the arc at location *i*

v_i – the corrections of the length of a meridian degree

The expression (1) can be written as follows:

$$y_i + v_i = a + bx_i \qquad \text{(i=1, 2,..., n)} \qquad (2)$$

where *a* and *b* are the parameters which need to be estimated.

One of the problems that Bošković dealt with was determining the values of the parameters *a* and *b*, which are "the most appropriate" for *n* linear equations (2). Bošković formed two additional conditions to find the most appropriate values of coefficients *a* and *b*. Bošković's second condition is: the sum of positive corrections should be equal to the sum of the negative ones (by their absolute value). In other words:

$$\sum_{j=1}^{m} v_j^+ = -\sum_{k=1}^{u} v_k^- \Leftrightarrow \sum_{i=1}^{n} v_i = 0 \qquad (3)$$

In expression (3), v_j^+ are positive corrections, and v_k^- are negative ones. From expressions (2) and (3) follows

$$\sum_{i=1}^{n} (a + bx_i - y_i) = 0 \qquad (4)$$

According to the third condition the sum of the absolute values of all corrections should be as little as possible. Analytically, the third condition can be written as:

$$\sum_{i=1}^{n} \left| a + bx_i - y_i \right| = \sum_{i=1}^{n} \left| v_i \right| = \min . \qquad (5)$$

The required solution will give the pair (*a,b*) for which expression (5) takes the minimum value. From (4) it is easily obtained

$$a = \bar{y} - b\bar{x} \qquad (6)$$

where we denoted

$$\bar{x} = \frac{\sum_i x_i}{n} \text{ and } \bar{y} = \frac{\sum_i y_i}{n} \qquad (7)$$

In other words, the second condition shows that the Bošković's best fitting line passes through the centroid (barycentre) of the set of points. If the expression (6) is inserted in expression (5) it is clear that coefficient *b* should be determined such that

$$\sum_{i=1}^{n} \left| (y_i - \bar{y}) - b(x_i - \bar{x}) \right| = \min \qquad (8)$$

To determine the parameter *b* an explicit equation does not exist. The geometric procedure of Bošković's method is shown in detail in several papers on the example on five meridian degrees (Varićak, 1910; Eisenhart, 1961; Stigler, 1986; Farebrother, 1999; Triplat Horvat et al., 2011).

Bošković's method is considered to be a distinct method, and at the same time the first method of adjustment, which has induced further studies to elaborate the problems of adjustment (Čubranić, 1961). Today, this method is mainly used in modified form, primarily based on Bošković's third

condition and most often denominated as L_1-norm method of adjustment (Sneeuw, Krumm 2010).

2.2. L_1-norm Method of Adjustment

The general principle of L_1-norm method of adjustment states

$$\| \mathrm{v} \|_1 = \sum_{i=1}^{n} | v_i | = \min. \tag{9}$$

This problem has a long history, dating back even before the introduction of Least Squares Method. The method was first mentioned in the Laplace's paper in 1786, and it was first systematically analyzed by Edgeworth in 1887. A detailed historical report can be found in the paper published by Farebrother in 1987. Modern systematic study of this problem was published in the late 1950s paper by Motzkin and Walsh (Watson, 2000).

Let there is

$$S(a,b) = \sum_{i=1}^{n} \left| y_i - a x_i - b \right| = \sum_{i=1}^{n} \left| v_i \right| = \min \tag{10}$$

Let us imagine $S(a,b)$ as a surface above the plane (a,b) which is piecewise continuous and straight (linear). With this property, the minimum can be achieved only in an intersection of straight lines $y_i = a x_i + b$ in the plane (a,b). The implication is the following simple algorithm for solving the problem of minimum (11). All straight lines in (a,b)-plane should be intersected in pairs, which gives

$$a = \frac{y_k - y_j}{x_k - x_j} \tag{11}$$

and

$$b = \frac{x_k y_j - x_j y_k}{x_k - x_j} \qquad \text{(k=1,…, n-1; j=i+1,…, n)} \qquad (12)$$

The required solution is the pair (*a,b*) defined by (11) and (12) for which expression (10) takes the minimum value. In special cases there can be multiple solutions (Späth, 1973). The problem can also be solved by the linear programming method (Marshall, 2002; Amiri-Simkooei, 2003).

2.3. L_2-norm Method of Adjustment (Least Squares Method)

Besides the Bošković's Adjustment Method, several methods were developed later, from which the Least Squares Method is the most significant and the most used one today. It is known as L_2-norm estimation. The Least Squares Method was developed, simultaneously and independently of each other, by Adrien-Marie Legendre (1752-1833) and Johann Carl Friedrich Gauss (1777-1855).

Unlike Bošković's condition (5) where the sum of absolute values of all corrections should be as minimum as possible, Gauss and Legendre set the condition that the sum of squared corrections is minimal. The basic principle of adjustment with L_2-norm can be written as follows:

$$\| \mathbf{v} \|_2 = \sum_{i=1}^{n} v_i^2 = \min. \qquad (13)$$

Thus, it is necessary to find such *a* and *b* to be

$$S(a,b) = \sum_{i=1}^{n} (y_i - ax_i - b)^2 = \sum_{i=1}^{n} v_i^2 = \min \qquad (14)$$

It is known that the required solution is obtained by solving the system of two linear equations with the two unknowns *a* and *b*, and with that procedure it is obtained

$$a = \frac{\sum_i (x_i - \bar{x})(y_i - \bar{y})}{\sum_i (x_i - x)^2} \quad (15)$$

$$b = \bar{y} - a\bar{x} \quad (16)$$

2.4. L_∞-norm Method of Adjustment (Chebyshev norm)

By the application of L_∞-norm or Chebyshev's approximation the maximum distance between data and approximation function is minimized, wherefrom the name minimax approximation is derived (URL1).

Detailed historical contribution of these methods, and the methods which it is derived from, can be found in a paper published by Farebrother in 1987. Spatial functional analogy was studied by Chebyshev in 1850s, and derived from the analysis related to the steam engines. That is why the continuous and discrete problems bear his name today (Watson, 2000). The basic principle of adjustment using L_∞-norm can be written as follows:

$$S(a,b) = \max_i |y_i - ax_i - b| = \max_i |v_i| = \min \quad (17)$$

From the references (Späth, 1973) we can assume that a and b should be selected in such way that for the three values taken from the $x_1,\ldots, x_n$ the value of $|y_i - ax_i - b|$ with alternating signs takes the maximum value for all possible abscissa triplets. The corresponding triplets are called alternants. Here is the following simple algorithm. It should solve, $\binom{n}{3}$ altogether, the systems of linear equations (k=1,..., n-2; j=i+1,..., n-1; l=j+1,..., n)

$$ax_k + b + \frac{1}{p_k}\lambda = y_k$$

$$ax_j + b - \frac{1}{p_j}\lambda = y_j \quad (18)$$

$$ax_l + b + \frac{1}{p_l}\lambda = y_l$$

and determine the triplet indices (k, j, l), for which |λ| takes the maximum value. The corresponding values (*a,b*) that applies (35) minimize (34). The system (35) can be solved in a closed form. With

$$\gamma = \left[\frac{x_j - x_l}{p_k} + \frac{x_k - x_l}{p_j} + \frac{x_k - x_j}{p_l} \right] \tag{19}$$

it applies

$$\lambda = \frac{1}{\gamma}\left[y_l(x_k - x_j) + y_j(x_l - x_k) + y_k(x_j - x_l) \right]$$

$$a = \frac{1}{\gamma}\left[\frac{y_j - y_l}{p_k} + \frac{y_k - y_l}{p_j} + \frac{y_k - y_j}{p_l} \right] \tag{20}$$

$$b = \frac{1}{\gamma}\left[\frac{x_j y_l - x_l y_j}{p_i} + \frac{x_i y_l - x_l y_i}{p_j} + \frac{x_i y_j - x_j y_i}{p_l} \right].$$

3. APPLICATION

Nine measurements of the meridian arc length and the corresponding latitudes (Maire and Boscovich, 1770) are shown in the second and fourth column of the Table 1. The values n Table 1 in the third column were calculated from those in the second column.

Let y_i be measured length of meridian degrees and x_i squared sinus of corresponding latitudes, then the measurements function, assuming that each meridian degree can generally be approximated by $a + bx_i$ can be written as follows $y_i + v_i = a + bx_i$. By introducing the values from Table 1 the

result is the equation system of corrections which are the basis for the adjustment procedure for all methods described in the second chapter:

$$v_1 = a + 0{,}0000 \cdot b - 56750$$
$$v_2 = a + 0{,}3014 \cdot b - 57037$$
$$v_3 = a + 0{,}3995 \cdot b - 56888$$
$$v_4 = a + 0{,}4651 \cdot b - 56975$$
$$v_5 = a + 0{,}4953 \cdot b - 57069$$
$$v_6 = a + 0{,}5000 \cdot b - 57028$$
$$v_7 = a + 0{,}5465 \cdot b - 57091$$
$$v_8 = a + 0{,}5762 \cdot b - 57074$$
$$v_9 = a + 0{,}8389 \cdot b - 57422$$

Using adjustment, the corrections of measurements, the estimations of true values of the meridian arc length and the unknowns *a* and *b* need to be determined. Table 2 shows the results of adjustment with all previously described methods, and the Figure 1 graphically displays the straight lines and their equations.

Place of the measured meridian degree	Latitude of the measured degree	$\sin^2\varphi$	Arc length [toise]
Quito	00° 00'	0,0000	56 750
Cape of Good Hope	33° 18'	0,3014	57 037
Maryland-Delaware	39° 12'	0,3995	56 888
Rome	43° 00'	0,4651	56 975
Piedmont	44° 44'	0,4953	57 069
France	45° 00'	0,5000	57 028
Austria	47° 40'	0,5465	57 091
Paris	49° 23'	0,5762	57 074
Lapland	66° 20'	0,8389	57 422

Table 1: *Nine measured meridian degrees and their latitudes (the values in the second and fourth columns are taken from Maire and Boscovich 1770)*

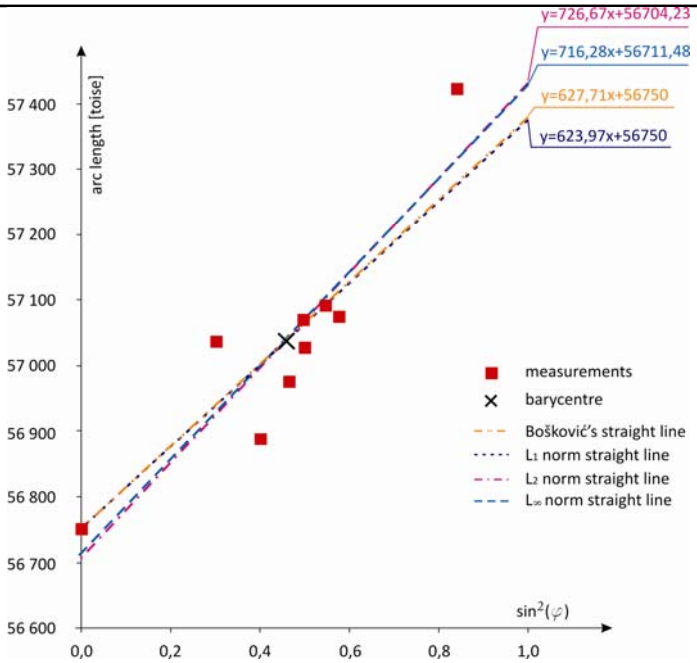

Figure 1: *Regression straight lines and their equations*

Name of points	Corrections of measurement			
	Bošković's method	**L_1 norm**	**L_2 norm**	**L_∞ norm**
Quito	0	0	-45,77	-38,52
Cape of Good Hope	-97,79	-98,94	-113,76	-109,63
Maryland-Delaware	112,75	111,28	106,53	109,63
Rome	62,96	65,21	67,20	69,62
Piedmont	-8,06	-9,95	-4,86	-2,75
France	35,86	3,99	39,56	41,62
Austria	2,03	0,00	10,35	11,93
Paris	37,69	35,53	48,93	50,20
Lapland	-145,43	-148,55	-108,18	-109,63
$\Sigma(v^2)$	50165,48	49867,46	46691,37	46791,45
$\Sigma(-v)$	-251,29	-257,43	-272,56	-260,53
$\Sigma(+v)$	251,29	216,00	272,56	283,00
$\Sigma\|v\|$	502,58	473,44	545,13	543,53
$\Sigma(v)$	0,00	-41,43	0,00	22,47
$\max\|v\|$	145,43	148,55	113,76	109,63

Table 2: *Corrections of measurements*

5. CONCLUSION

Bošković-Laplace's method for determining the best linear relationship on the basis of measured data is comparable with similar methods based on minimizing the corrections of measurements with L_1-, L_2- and L_∞-norms. On the given example of adjustment on nine meridian degrees all these methods give results that differ very little from each other.

6. REFERENCES

AMIRI-SIMKOOEI, A. (2003): Formulation of L_1 Norm Minimization in Gauss-Markov Models, Journal of Surveying Engineering, Vol. 129, No. 1, 37-43.

ČUBRANIĆ, N. (1961): Geodetski rad Ruđera Boškovića, Zavod za višu geodeziju AGG fakulteta, Zagreb.

EISENHART, CH. (1961): Boscovich and the Combination of Observations. In: Ed. Lancelot Law Whyte: Roger Joseph Boscovich S.J., F.R.S., 1711-1787, Studies in His Life and Work on the 250th Anniversary of His Birth, George Allen & Unwin Ltd., London.

FAREBROTHER, R. W. (1999): Fitting Linear Relationships: A History of the Calculus of Observations 1750-1900. Springer, New York.

LAPAINE, M. (2012): Bošković-Laplaceova metoda. In: Leksikon Ruđera Boškovića, Ed. A. Bogutovac, Leksikografski zavod Miroslav Krleža, Zagreb.

MAIRE, CH., BOSCOVICH, R. J. (1770): Voyage astronomique et géographique, dans l'État de l'Église, entrepris par l'ordre et sous les auspices du pape Benoit XIV, pour mesurer deux dégrés du méridien, & corriger la Carte de l'État ecclésiastique. N. M. Tilliard, Paris.

MARSHALL, J. (2002): L1-norm pre-analysis measures for geodetic networks, Journal of Geodesy, Earth and Environmental Science, Vol. 6-7, No. 76, 334-344.

SNEEUW, N., KRUMM. F. (2010): Lecture Notes Adjustment Theory, Geodätisches Institut, Universität Stuttgart.

SPÄTH, H. (1973): Algorithmen für elementare Ausgleichs-modelle, R. Olden-bourg Verlag München, Wien.

STIGLER, S. M. (1986): The History of Statistics: The Measurement of Uncertainty before 1900. The Belknap Press of Harvard University Press, Cambridge, Massachusetts and London, England.

TRIPLAT HORVAT, M., LAPAINE, M., TUTIĆ, D. (2011): Application of Bošković's Geometric Adjustment Method on Five Meridian Degrees, On the Occasion of 300th Anniversary of the Birth of Ruđer Josip Bošković, KoG, Journal of Croatian Society for Geometry and Graphic, No. 15, 67-74.

VARIĆAK, V. (1900): Matematički rad Boškovićev. Rad JAZU, knjiga 181, 75-208, Zagreb.

WATSON, G. A. (2000): Approximation in normed linear spaces, Journal of Computational and Applied Mathematics, Vol. 121, 1-36.

URL1: The Data Analysis BriefBook, Internet version, http://rd11.web.cern.ch/RD11/rkb/AN16pp/node29.html, 15.03.2012.

Free and open-source porous media simulator

Zeljka TUTEK,
University of Zagreb, Faculty of Geodesy, Kaciceva 26, 10000 Zagreb, Croatia,
e-mail: zeljkat@geof.hr

Abstract: Recently funded Open Porous Media (OPM) initiative is dedicated to the development of a wide range simulators for flow and transport in porous media built on modern software principles which are released under the most popular license for free software called GNU General Public License (GPL). It was initially supported by five research groups in Norway and Germany. With ease of use, high performance and easy extensibility, it tries to attract more users from outside and to integrate academic and industrial partners and potential end users. One of such simulators DuMu^X (**DU**NE for **mu**lti-{phase, component, scale, physics, ...} flow and transport in porous media) is presented. It uses the DUNE, the Distributed and Unified Numerics Environment, a modular toolbox for solving partial differential equations (PDEs) with grid-based methods.

Key words: porous media simulator, open source, software.

1. OPEN POROUS MEDIA (OPM) INITIATIVE

The principal objective of the Open Porous Media (OPM) initiative (http://www.opm-project.org/) is to provide a long-lasting, efficient, and well-maintained, open-source software for flow and transport in porous media which should: have functionality supporting multiple application areas, handle industrially relevant cases, be easy to extend with new functionality, be built on open source code principles and have a relatively low user threshold. The motivation is to provide a means to unite industry and public research on simulation and to accelerate the technology transfer

from academic institutions to professional companies by making new research results available as free software of professional standard.

2. DuMu^{X}

One of the OPM components is **DuMu^{X}** (short for **DU**NE for **mu**lti-{phase, component, scale, physics...} flow and transport in porous media).

2.1 General characteristics

The DUNE module DuMu^{X} (**Figure 1**) is a simulator for the non-isothermal compositional multiphase fluid flow and transport processes in porous media (Flemisch et al., 2011). Its development started in the 2007 at the University of Stuttgart (Flemisch et al., 2007). It was first released in July 2009. The stable and documented version 2.1 of the code is fully available on the webpage www.dumux.org. With an enhanced user-friendly interface it tries to attract more users from outside of the developers group. But they are still required to have the profound knowledge of advanced C++ programming techniques.

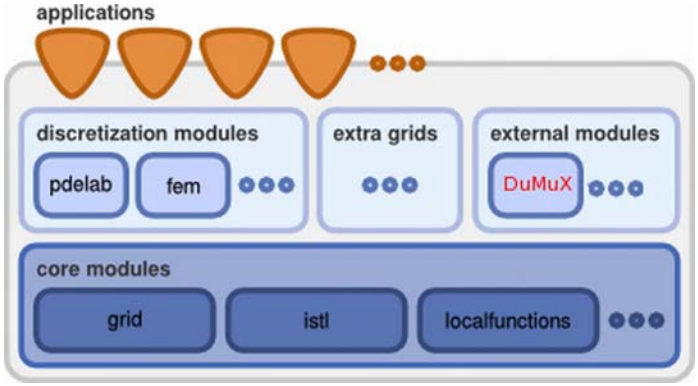

Figure 1: *DUNE (http://www.dune-project.org) – the backbone of DuMu^{X}*

DuMu^{X} provides a generic framework for easy and efficient implementation of new physical and mathematical models for porous media flow problems. Through the *property system* the user sets the parameters at compile time

in order to: select one of the many implemented *model concepts*, define the material properties and the constitutive relations (extendable *material system*), choose the coupled fully-implicit or the decoupled semi-implicit approach (*simulation control*) and specify the spatial and temporal discretization method (*numerical scheme)*.

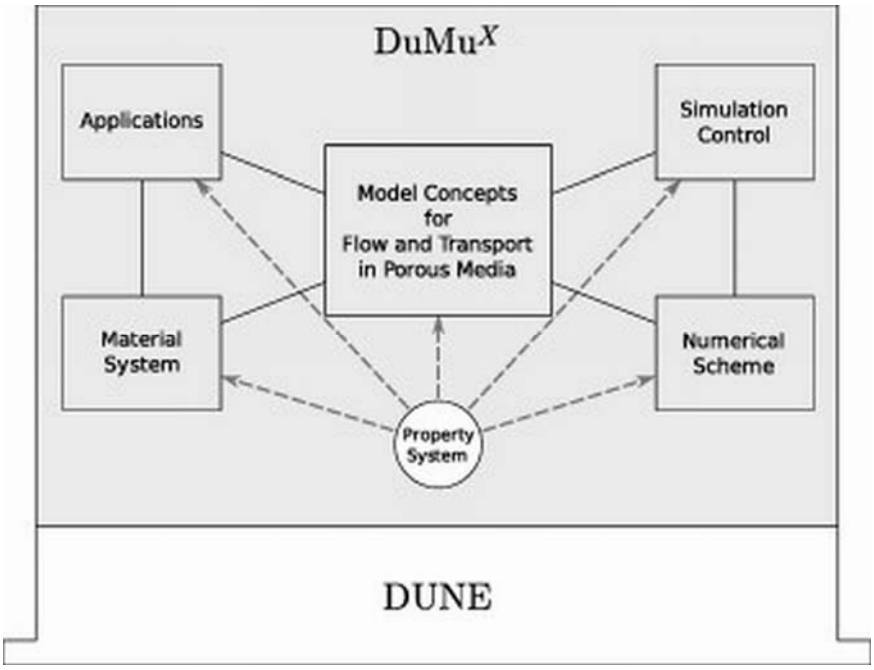

Figure 2: *Modularity of DuMu^X (Flemisch et al., 2011)*

DuMu^X inherits modular design (**Figure 2**) and functionality from DUNE modules and shares its main principles: separation of data structures and algorithms by abstract interfaces and efficient implementation of these interfaces using generic programming techniques. DUNE allows the use of a wide range of different grids, linear and nonlinear solvers, space and time discretization as well as parallelization of computationally demanding code without knowledge of the underlying implementation and data structures, i.e. with a little programmer's effort. DuMu^X depends on the DUNE core modules: *dune-common* (basic classes), *dune-grid* (grid interface and implementation), *dune-istl* (iterative solver template library) and *dune-local functions* (interface for finite element shape functions).

The development of DUNE is a joint effort of five research groups located at German and English universities (Bastian et al., 2008a,b). Its user base is growing. DUNE is free software licensed under the GPL (version 2) (see http://www.dune-project.org/license.html) with a so called "runtime exception". Thus, it is possible to use DUNE even in proprietary software.

2.2. Multiphase/multicomponent systems

In the multiphase/multicomponent models, which could be illustrated with the example of water-NAPL-gas system (**Figure 3**), the phases are not only the matter of a single chemical substance. In general they are composed of several different constituents – *components*. In addition to the flow (diffusion, transport) equations, for each component the mass conservation is considered. The mass transfer between phases is allowed.

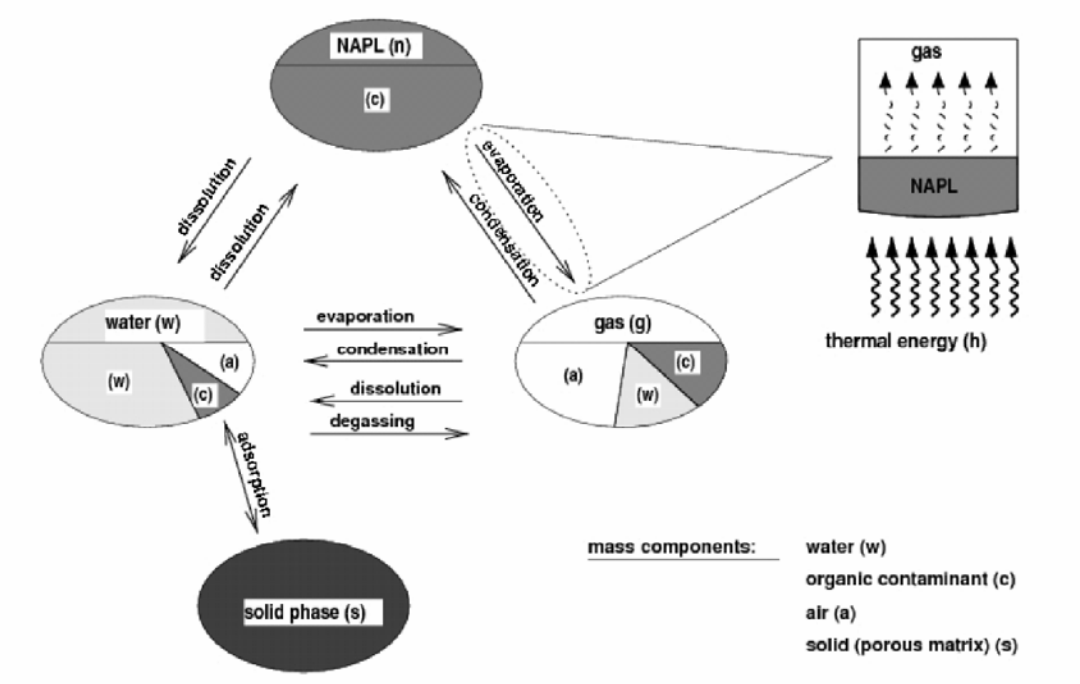

Figure 3: *Three-phase (water-NAPL-gas) three-component (water-air-contaminant) system - mass and energy transfer (Class et al., 2006)*

In the case of non-isothermal system, for the transfer of energy between the phases the thermal energy (heat) balance is added. According to the Gibbsian phase rule, the number of independent unknowns (degrees of freedom) should be equal to the number of components plus one. Thus supplementary constraints plus constitutive relations are also needed. Multiphase multicomponent models in porous media first appeared in the oil industry (extraction of oil and natural gas from fossil deposits) in the 1970s. Later, these concepts have extended to issues of groundwater protection and remediation (recovery of drinking water) as to the storage of CO_2 in deep geological formations.

2.3. Implemented numerical models

In DuMu^X two, fully coupled implicit and decoupled, the approaches for the solution of porous media problems are possible:

- Original strongly coupled balance equations could be solved fully-implicit. The following standard models which assume local thermodynamic equilibrium are implemented: One-phase, One-phase two-component, Two-phase, Non-isothermal two-phase, Two-phase two-component, Non-isothermal two-phase two-component, Three-phase tree-component, Non-isothermal three-phase tree-component, M-phase N-component, Richards, Two-component Stokes and Non-isothermal two-component Stokes. For all of them, the box method is used for the space discretization and implicit Euler method for the time discretization. For the resulting system of nonlinear algebraic equations Newton's solver is applied. In addition, several non-standard models are available.
- Balance equations of multi-phase flow are reformulated in one equation for pressure and one or more equations for transport (of phases, components. energy, etc.). Pressure equation is the sum of mass balance equations and describes the total flow of the fluid. The new set of equations is only weakly coupled with each other and thus sequential

IMPET (IMplicit Pressure Explicit Transport) scheme can be applied: first pressure equation is solved implicitly to get the flow field and then transport equations are solved explicitly. Standard Single phase, Immiscible two-phase, miscible two-phase and miscible three-phase models are available in DuMu^X. For the discretization cell-centred finite volumes with TPFA/MPFA (Two/Multi-Point-Flux-Approximation) and mimetic finite differences can be used in a combination with explicit Euler scheme. Time step size is calculated by CFL-like criteria.

Default parameters for each numerical model are implemented and can be changed for specific problem. DuMu^X includes some example applications.

The modularity of DuMu^X allows the combination of the above mentioned models in multiscale and/or multi-physics concepts, which allows the model complex processes occurring in the large scale domains. Multiscale couplings combine simulations on different length or time scales. They can be done in the context of classical numerical upscaling/downscaling methods or in the combination with multi-physics strategies. Multi-physics and multiscale modelling capabilities of DuMu^X are illustrated (Flemisch et al., 2011) on the CO_2 storage and permeability upscaling examples.

2.4. Newton's method

Newton's method is applied at each time step for solving the nonlinear system of algebraic equations, which appears to be a really difficult task in the fully coupled numerical models. For example, the following nonlinear equation

$$\phi \frac{\partial p_\alpha}{\partial t} - \mathrm{div}\left[\rho_\alpha \frac{k_{r\alpha}}{\mu_\alpha} \mathbf{K}(\mathrm{grad}\, p - \rho\, g) \right] - q_\alpha = 0 \ldots \mathbf{f}(\mathbf{u}) = 0 \qquad (1)$$

could be approximated in the neighbourhood of the value $\mathbf{u}^r$ by

$$\mathbf{f}(\mathbf{u}^r) + \mathbf{f}'(\mathbf{u}^r)(\mathbf{u}^{r+1} - \mathbf{u}^r) = 0 \qquad (2).$$

The Newton method can be formalized as follows:

$$\mathbf{u}^{r+1} = \mathbf{u}^r - (\mathbf{f}'(\mathbf{u}^r))^{-1} \mathbf{f}(\mathbf{u}^r) \Leftrightarrow \mathbf{f}'(\mathbf{u}^r)(\mathbf{u}^{r+1} - \mathbf{u}^r) = -\mathbf{f}(\mathbf{u}^r) \qquad (3)$$

where $\mathbf{u}$ is the vector of unknowns, exponents ^{r} and $^{r+1}$ denote last and current iteration respectively, $\mathbf{f}$ is the nonlinear vector valued function and $\mathbf{f}'(\mathbf{u}^r)$ is its Jacobian matrix. The last equation is the system of linear equations which could be written in the matrix form

$$\mathbf{f}'(\mathbf{u}^r)(\mathbf{u}^r - \mathbf{u}^{r+1}) = \mathbf{f}(\mathbf{u}^r) \Leftrightarrow \mathbf{A}\mathbf{x} = \mathbf{b} \qquad (4)$$

where the coefficient matrix $\mathbf{A} = \mathbf{f}'(\mathbf{u}^r)$ is the Jacobian matrix which could be obtained by numerical differentiation, the right hand side $\mathbf{b} = \mathbf{f}(\mathbf{u}^r)$ is known from the last iteration and $\mathbf{x} = \mathbf{u}^r - \mathbf{u}^{r+1}$ is the solution vector. Starting from the given initial vector the following two steps are iterated:

1) the linear system $\mathbf{A}\mathbf{x} = \mathbf{b}$ is solved;
2) the estimate of the solution of the nonlinear equation $\mathbf{f}(\mathbf{u}) = 0$ is updated $\mathbf{u}^{r+1} = \mathbf{u}^r - \mathbf{x}$;

until the desired accuracy is reached, i.e. until $\mathbf{x} = \mathbf{u}^r - \mathbf{u}^{r+1}$ is small enough. In close combination with Newton's method there is the control of the step length for the time discretization. If the convergence inside Newton's method gets worse, i.e. the number of iterations exceeds a specified threshold, the actual step length is discarded and replaced with halved time step. And if convergence gets better again, i.e. within less iterations, the time step is increased.

3. CONCLUSION

Among various porous media simulators only DuMu^{X} is released under the terms and conditions of the GNU General Public License (GPL) version 2 or later. "The free and open source idea provides a chance for sustainable software development in geosciences." (SIAM GS 2011 Mini Symposium). New contributions are welcome.

4. ACKNOWLEDGEMENT

I would like to thank Professor Mladen Jurak for the long lasting inspiration.

5. REFERENCES

BASTIAN, P., BLATT, M., DEDNER A., ENGWER, C., KLÖFKORN, R., OHLBERGER M. & SANDER. O. (2008a): A Generic Grid Interface for Parallel and Adaptive Scientific Computing. Part I: Abstract Framework, Computing, 82, 2-3, 103-119.

BASTIAN, P., BLATT, M., DEDNER A., ENGWER, C., KLÖFKORN, R., KORNHUBER, R., OHLBERGER M. & SANDER. O. (2008b): A Generic Grid Interface for Parallel and Adaptive Scientific Computing. Part II: Implementation and Tests in DUNE, Computing, 82, 2-3, 121-138.

FLEMISCH, B., DARCIS, M., ERBERTSEDER, K., FAIGLE, B., LAUSER, A., MOSTHAF, K., MÜTHING, S., NUSKE, P., TATOMIR, A., WOLFF, M. & HELMIG R. (2011): DuMu^X : DUNE for Multi-{Phase, Component, Scale, Physics, ...} Flow and Transport in Porous Media, Advances in Water Resources, 34, 9, 1102-1112.

FLEMISCH, B., FRITZ, J., HELMIG, R., NIESSNER, J. & WOHLMUTH B.I. (2007): DuMu^X: A multi-scale multi-physics toolbox for flow and transport processes in porous media. - In: IBRAHIMBEGOVIC, A. & DIAS, F. (eds.): ECCOMAS Thematic Conference on Multi-scale Computational Methods for Solids and Fluids, Paris, France, Proceedings, 82-87.

CLASS, H., HELMIG, R., NIESSNER, J. & ÖLMANN, U. (2006): Multiphase Processes in Porous Media. - In: Helmig, Rainer; Mielke, Alexander; Wohlmuth, Barbara I. (eds.): Multifield Problems in Solid and Fluid Mechanics, 28. Springer-Verlag, XI, 45-82.

Student part

(Reviewed papers)

Detection of invasive plants on the flood plain of river Tisza, using hyperspectral airborne imagery

Balint CSENDES

University of Szeged Department of Physical Geography and Geoinformatics, Egyetem u. 2-6. Szeged Hungary H-6722, bcsendes@geo.u-szeged.hu

Abstract: One of the most serious problems of Hungarian water resource and landscape management is raised by invasive plants, such as Amorpha fruticosa. These shrubs suppress the native plant communities and slow down the flow of water, thus increasing the risk of floods. The goal was to map these bushes using the wide spectral range of hyperspectral bands and the inherent dimensionality of the data, therefore atmospheric correction and data compression transformations (MNF or PCA) were needed. Pixels can be classified using known reference spectra (Spectral Angle Mapping, Binary Encoding, etc.) or using derived spectral endmembers. According to the Linear Mixture Theory, each pixel value is a linear combination of the spectral endmembers. The result of the analysis shows that the main land cover classes are well-separated in the spectral space. Abundance images of the endmembers may predict features that do not fill the entire pixel.

Key words: Hyperspectral remote sensing, vegetation monitoring, environmental issues, Amorpha fruticosa.

1. INTRODUCTION

One of the most serious problems of Hungarian water resource and landscape management is raised by invasive plants, such as Amorpha fruticosa. These shrubs suppress the native plant communities and slow down the flow of water, thus increasing the risk of floods. Airborne hyperspectral data have been used to investigate vegetation changes since

the 1990's, the first Hungarian attempts were performed in 2002 (Hargitai et al., 2006). In most cases, multispectral images also fulfill the spatial and spectral requirements of the analysis. However, if the spatial scale of the land covers types is lower than the geometric resolution, spectral mixing is obtainable. Amorpha fruticosa bushes often appear as narrow belts along canals or flood plains. In this study the plant communities of the flood plain of river Tisza were investigated. The goal was to map these locations using the wide spectral range of hyperspectral bands and the inherent dimensionality of the data (Boardman and Kruse, 1994), therefore atmospheric correction and data compression transformations (Minimum Noise Fraction or Principle Component Analysis) were needed. Pixels can be classified using known reference spectra (Spectral Angle Mapping, Binary Encoding, etc.) or using derived spectral endmembers. According to the Linear Mixture Theory, the spectral signature recorded at each pixel is a linear combination of the spectral endmembers (Singer and McCord, 1979). Abundance images of the endmembers may predict features that do not fill the entire pixel, hereby a complex mapping system can be formed using the identified land cover and vegetation types.

2. INVESTIGATED AREA

The area is located in the southeastern part of Hungary, ont he left bank of Tisza, near the confluence with river Maros (**Figure 1**). This region is also known for its oil fields, the agricultural areas are interspersed by several pipelines, oil and gas wells of the Hungarian Oil Company (MOL). Irrigation canals lead the water to the arable lands and those are responsable for the collection of inland excess water, too. However, due to neglect of upkeep, many of the canals are filled with plants. The flood plain of the Tisza is covered with Populus trees. Shrubs of the invasive Amorpha fruticosa plant appear between the forest belt and the dam in the illuminated areas.

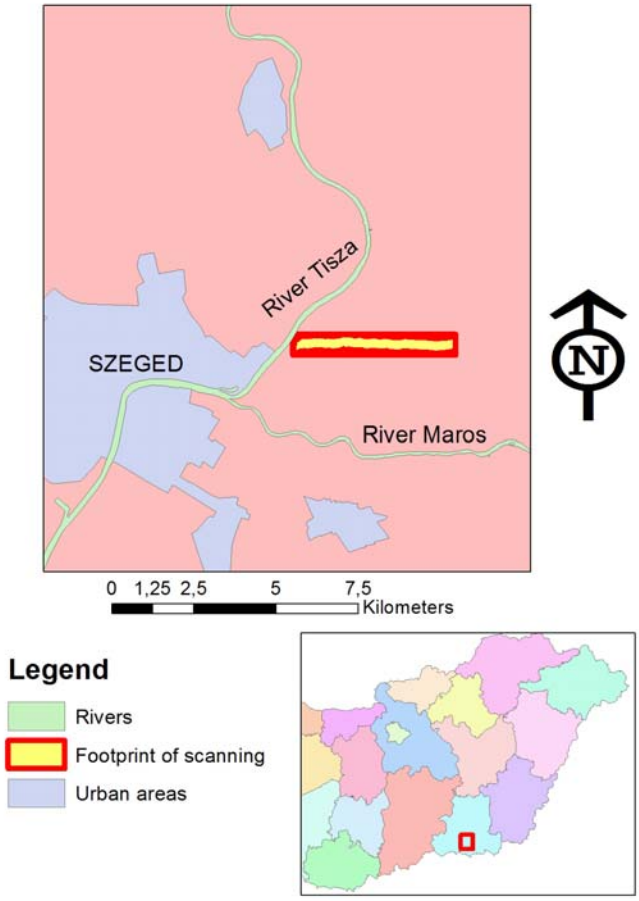

***Figure 1**: The location of the investigated area*

3. USED DATA AND METHODS

The hyperpectral survey over the investigated area was performed on 22nd September 2010. The imaging spectrometer measured reflectance in 359 bands from 400 to 2450 nanometres, the geometric resolution is 1.5 metres. 119 bands were neglected due to atmospheric noise. Atmospheric corrections were implemented using ground radiometric measurements (ASD). Twot types of transformations, Minimal Noise Fraction (MNF) and Principal Component Analysis (PCA) were performed to compress data and to suppress sensor noise. As previous studies have shown, Mixture tuned matched filtering is an appropriate method to map land cover features in cases when not all endmembers are known (Hestir et al., 2008; Andrew and Ustin, 2008; Parker Williams and Hunt, 2002). In this paper, the goal was to

map the endmembers of vegetation, and to separate them by species (**Figure 2**). Since the target, Amorpha fruticosa appears in narrow shrubs and under the canopy, abundance images were used to determine the locations of the plant. Derived endmembers were examined using Spectral Angle Mapping and Binary Encoding classifications.

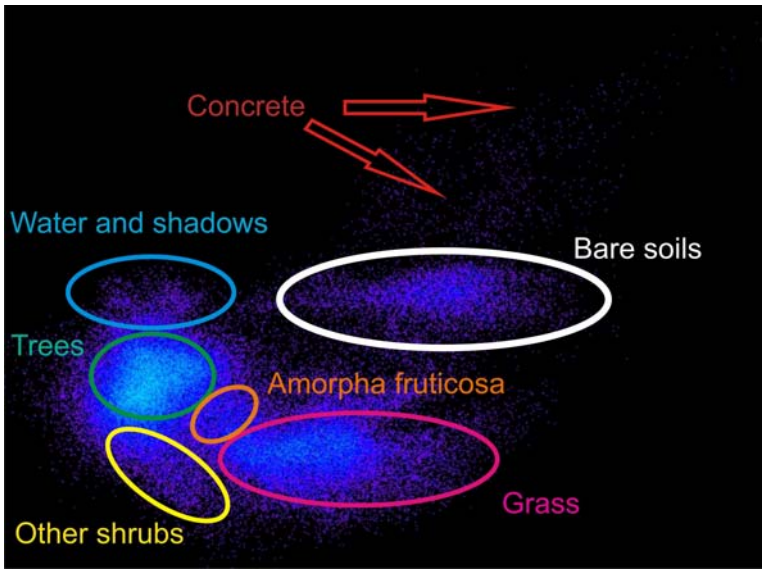

***Figure 2**: Derived classes in the spectral space*

4. DISCUSSION AND CONCLUSIONS

The locations of the Amorpha fruticosa are demonstrated on **Figure 3**. The spectral characteristics of the land cover features were identified using the mapped geographical location. **Figure 4** shows the spectral signature for these features. After defining the spectral endmembers Mixture Tuned Matched Filtering was performed to find the matching pixels. MTMF result consists of two images: a fractional abundance image called 'Matched filtering Score' and an Infeasibility image that rates the feasibility of the spectral mixture at the given pixel. Probable locations were determined using the values of these two images of the Amorpha fruticosa's spectral feature (**Figure 5**).

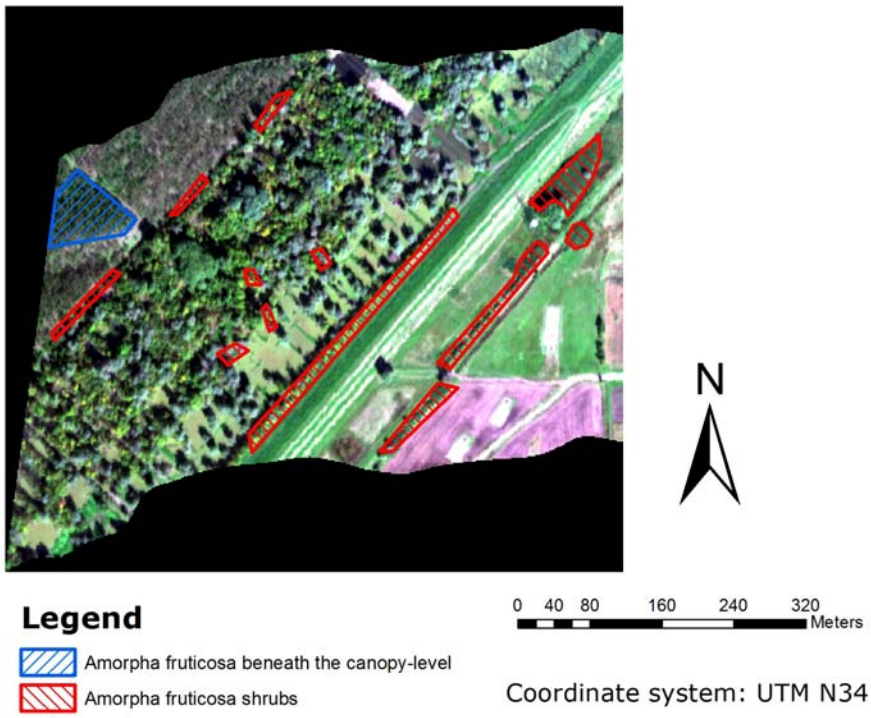

***Figure 3**: Location of Amorpha fruticosa plants*

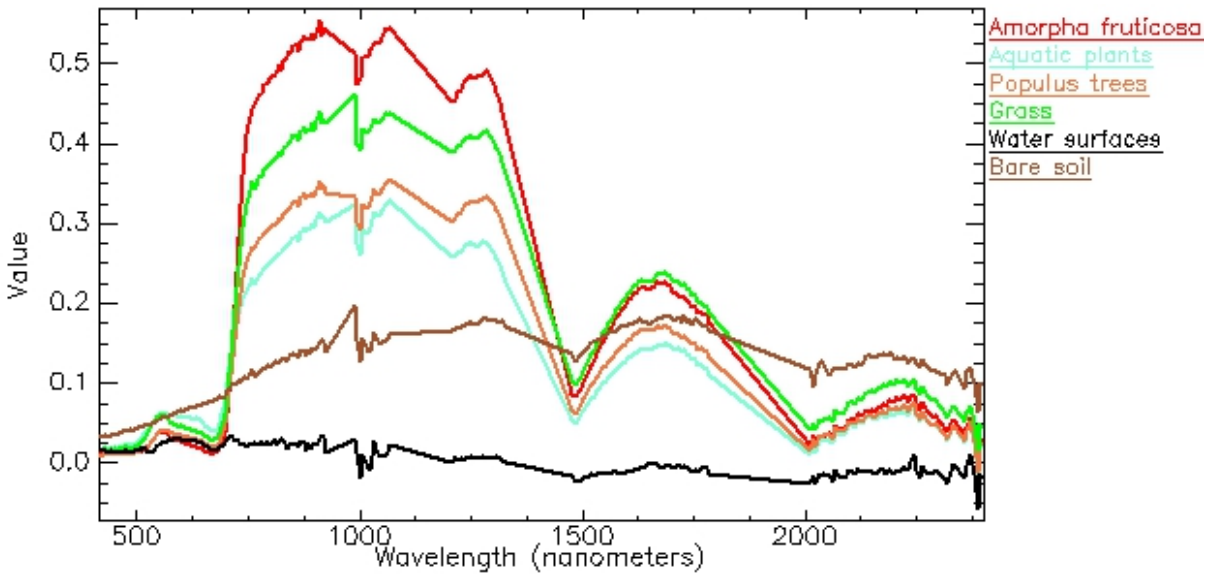

***Figure 4**: Spectral signatures of the main land cover types*

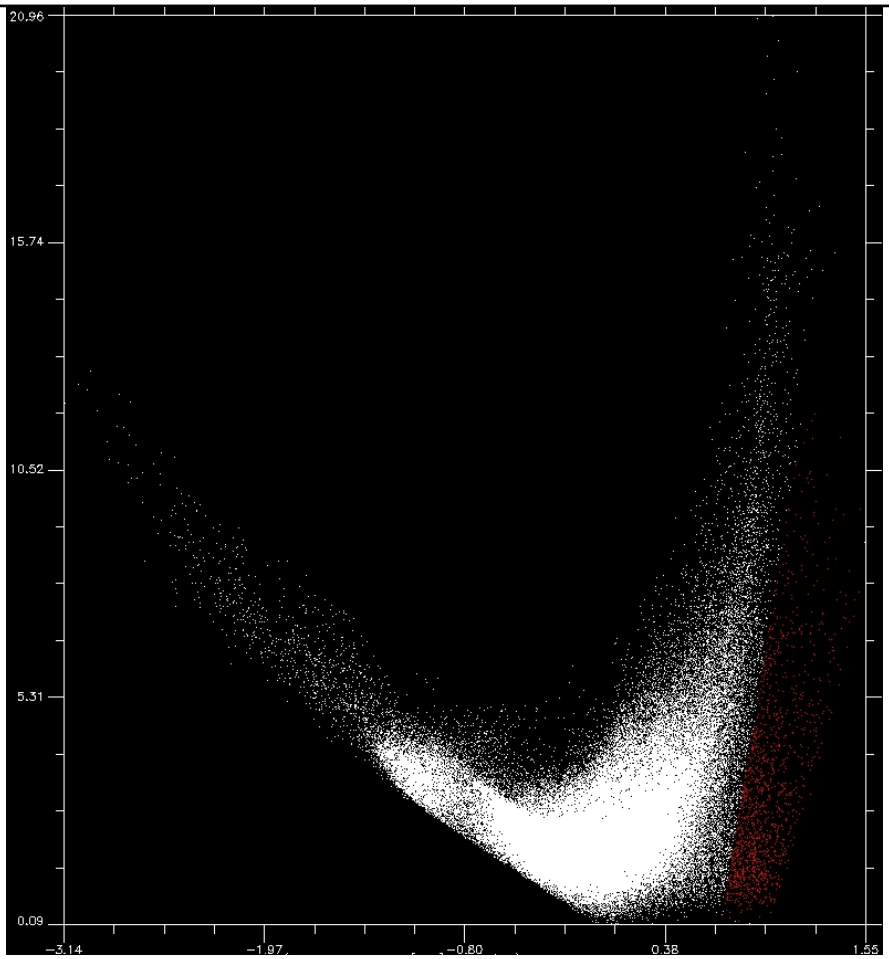

***Figure 5**: Pixels with high MF scores and low infeasibility are marked with red colour*

The marked region consists of 1326 pixels. After comparing with the ground truth data, 1178 belong to Amorpha fruticosa shrubs, it indicates user's accuracy of 89%. However, sparse plants and those that are under a closed canopy level didn't appear among the marked pixels (**Figure 6**).

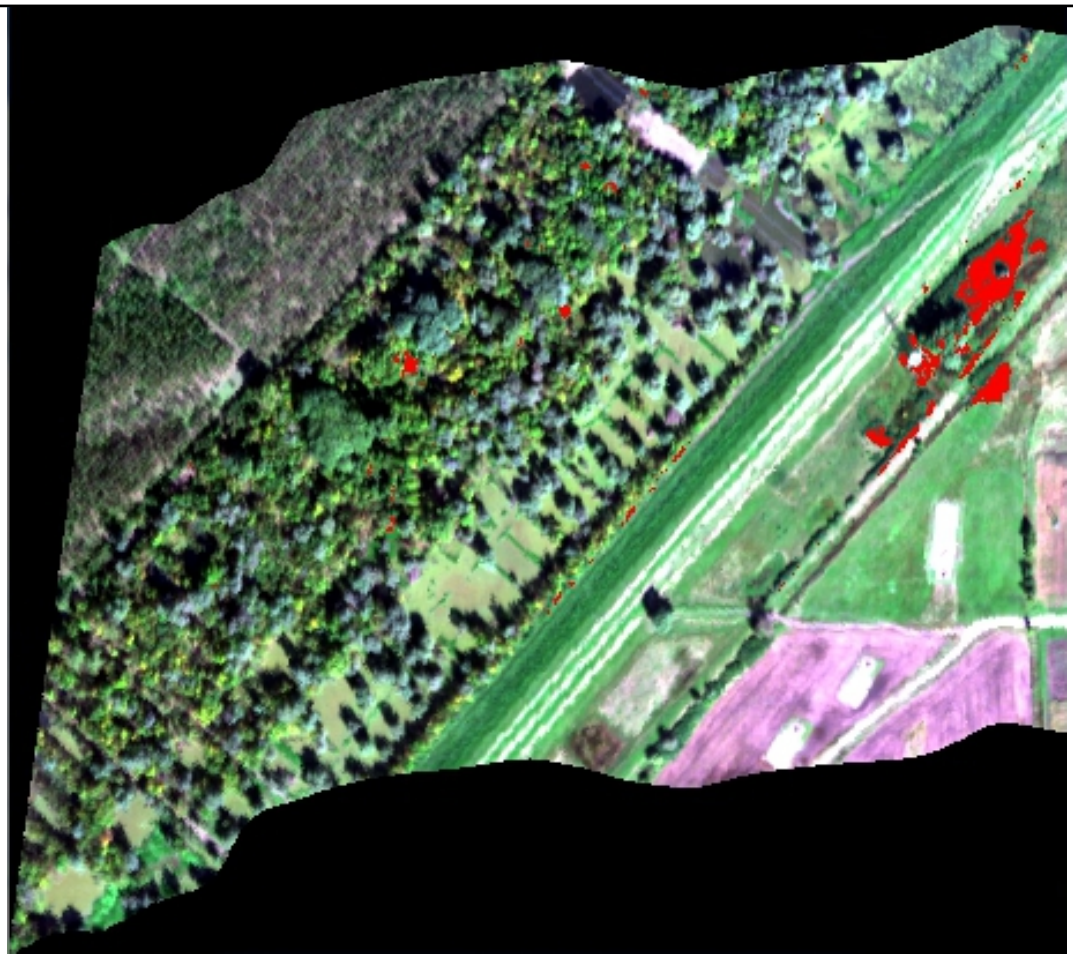

***Figure 6**: Pixels of Amorpha fruticosa derived from the result of MTMF*

REFERENCES

ANDREW, M. E. & USTIN, S. L. (2008): The role of environmental context in mapping invasive plants with hyperspectral image data. Remote Sensing of Environment, 112, 4301-4317.

BOARDMAN, J. W. & KRUSE, F. A. (1994): Automated spectral analysis: A geologic example using AVIRIS data, north Grapevine Mountains, Nevada. -In ARBOR, A. (ed.): Tenth Thematic Conference on Geologic Remote Sensing, Michigan, Proceedings, I-407-I-418.

HARGITAI, H., KARDEVÁN, P. & HORVÁTH, F. (2006): Az első magyarországi képalkotó spektrométeres repülés és adatainak elemzése erdőtípusok elkülönítésére. Geodézia és Kartográfia, LVIII, 9, 21-33.

HESTIR, E. L., KHANNA, S., ANDREW, M. E., SANTOS, M. J., VIERS, J. H., GREENBERG J. A., RAJAPAKSE, S. S. AND USTIN, S. L. (2008): Identification of invasive vegetation using hyperspectral remote sensing in the California Delta ecosystem. Remote Sensing of Environment, 112, 4034-4047.

PARKER WILLIAMS, A. & HUNT, E. R. (2002): Estimation of leafy spurge cover fromhyperspectral imagery using mixture tuned matched filtering. Remote Sensing of Environment, 82, 446–456.

SINGER, R. B. & MCCORD, T. B. (1979): Mars: Large scale mixing of bright and dark surface materials and implications for analysis of spectral reflectance. -In: Lunar and Planetary Science Conference - 10th, Houston, Proceedings, 1835-1848.

Analysis of geochemical and magnetic susceptibility data in the borehole of the Udvari-2A

Péter János KORONCZ

University of Szeged, Department of Geology and Palaeontology, 6722 Szeged, Egyetem utca 2-6., koroncz.peter@gmail.com

Abstract: The investigation was carried out on the upper 18 m of a vertical loess profile exposed in the borehole Udvari-2A. This location is situated in the central part at the Tolna Hegyhát hills (Transdanubian, Hungary). In the core description study there have been identified 3 paleosol horizons in the sequence. The core was divided into 25 cm sections. On the samples ignition loss at 550°C and 1000°C (called LOI), water extractable ion concentrations and magnetic susceptibility data were measured. Multivariate statistical techniques of chemical and magnetic susceptibility variables were used to reconstruct paleoenvironmental and diagenetical history of the sequence. The results of factor analysis suggested only one depositional mechanism controlling formation of the loess sequence. Cluster analysis showed a hierarchical group of core segments and discriminant analysis confirmed that 100 % of the samples were correctly classified. These findings indicated that the core sequence can be divided into 4 significantly different geochemical phases.

Keywords: Udvari-2A, Loess, LOI, Magnetic susceptibility, Multivariate statistical analysis.

1. INTRODUCTION

The borehole of Udvari-2A is located approximately in the center of Tolna Hegyhát hills (**Figure 1**), in the central part of the Carpathian basin (Transdanubian, Hungary). The drilling explored the thickest loess sequence

in Hungary. The thickness of the formation is more than 94 meters. This study is made as an attempt to reflect the reasons of the differences between macroscopical core description and geochemical bias.

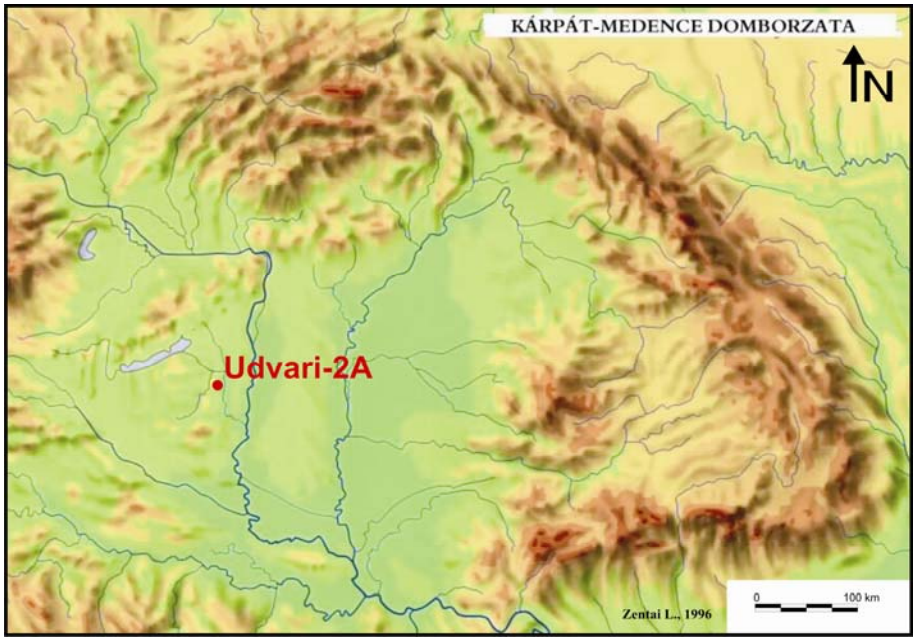

Figure 1: *Location of the borehole Udvari-2A*

2. SAMPLING AND METHODS

After macroscopical core description the core was divided into 25 cm sections. The organic matter and carbonate content has been determined by loss-on-ignition at 550°C for 1.5 hours and the carbonate content by the further loss-on-ignition at 1000°C for 1.5 hours (Dean, 1974; Bengtsson and Enell, 1986).

In a first reaction, organic matter is oxidised at 500-550 °C to carbon dioxid and ash. In a second reaction, carbon dioxid is produced from carbonate at 900-1000 °C, leaving oxide (Dean, 1974; Heiri et al., 2001). Magnetic susceptibility measurement was performed by a Bartington MS2 portable susceptibility meter. Measurements were carried out on dried and powdered samples with the same intervals. The results of the measurements by field instrument were carried out to get some further information about the main

elemental difference between the loess and paleosol horizons, which indicates the glacial (stadial) and interglacial (interstadial) periods of late Pleistocene (Galović et al., 2011).

Water extraction was carried out for unseparated samples. 100 ml distilled and purified water was added to 1.0 g samples and shaken for 1 hour. After decantation samples were analyzed as follows: K, Mg, Na, Ca, Fe, Mn, Zn, Cu, determined by an atomic absorption spectrophotometer.

3. STATISTICAL ANALYSIS

Cluster analysis (Within-groups method with Chebychew algorithm) was performed to obtain a grouping of samples, based on water extractable geochemical data. Discriminant analysis served to validate and supplement the cluster analysis.

Principal component analysis was employed to group associated variables into a few factors. It is based on the concentration profiles that acted as geochemical fingerprints. The factors were initially extracted using principal component analysis and then redistributed using the varimax rotation method.

4. DISCUSSION

Based on core description there have been identified 3 paleosol horizons in the sequence (**Figure 2**). Between 11.5-8.25 m at the section of the profile a double paleosol can be identified (U S1 and U SS2). On the upper part of the sequence (between 2.25-3.25 m) a third, weakly developed, light brown horizon can be defined (U SS1).

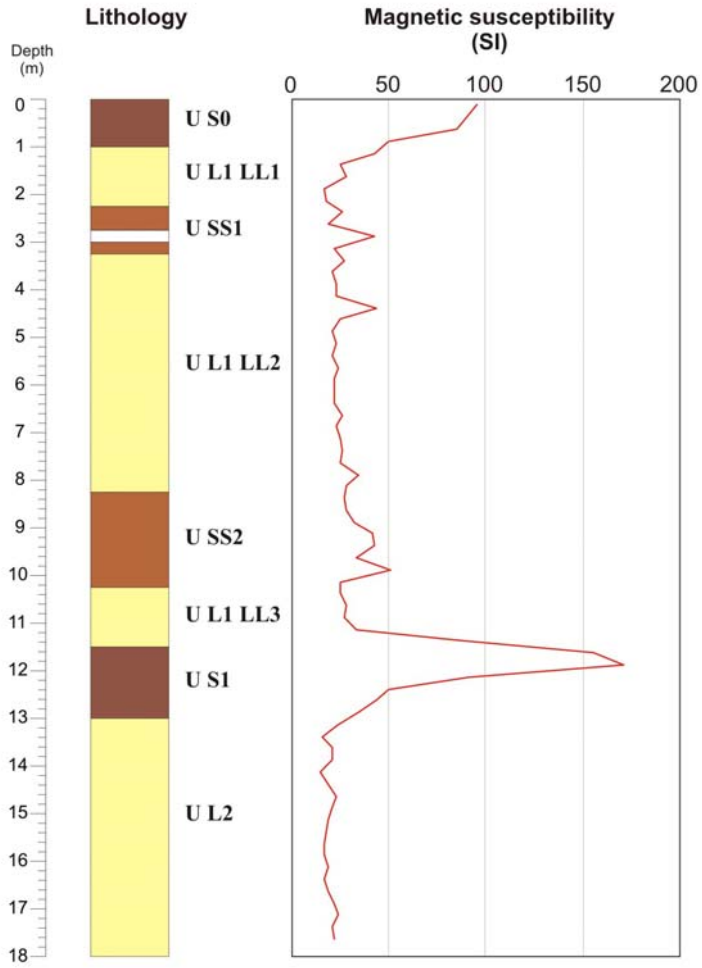

Figure 2: *Lithological and magnetic susceptibility profile of Udvari-2A*

The grouping with hierarchical clustering based on water extractable ion concentrations indicated that the core sequence can be divided into 4 significantly different geochemical phases (**Figure 3**). Adjacent samples of the same group membership can be considered as a core segment that represent a particular phase of environmental (depositional) or diagenetical history (Ng and King, 2004).

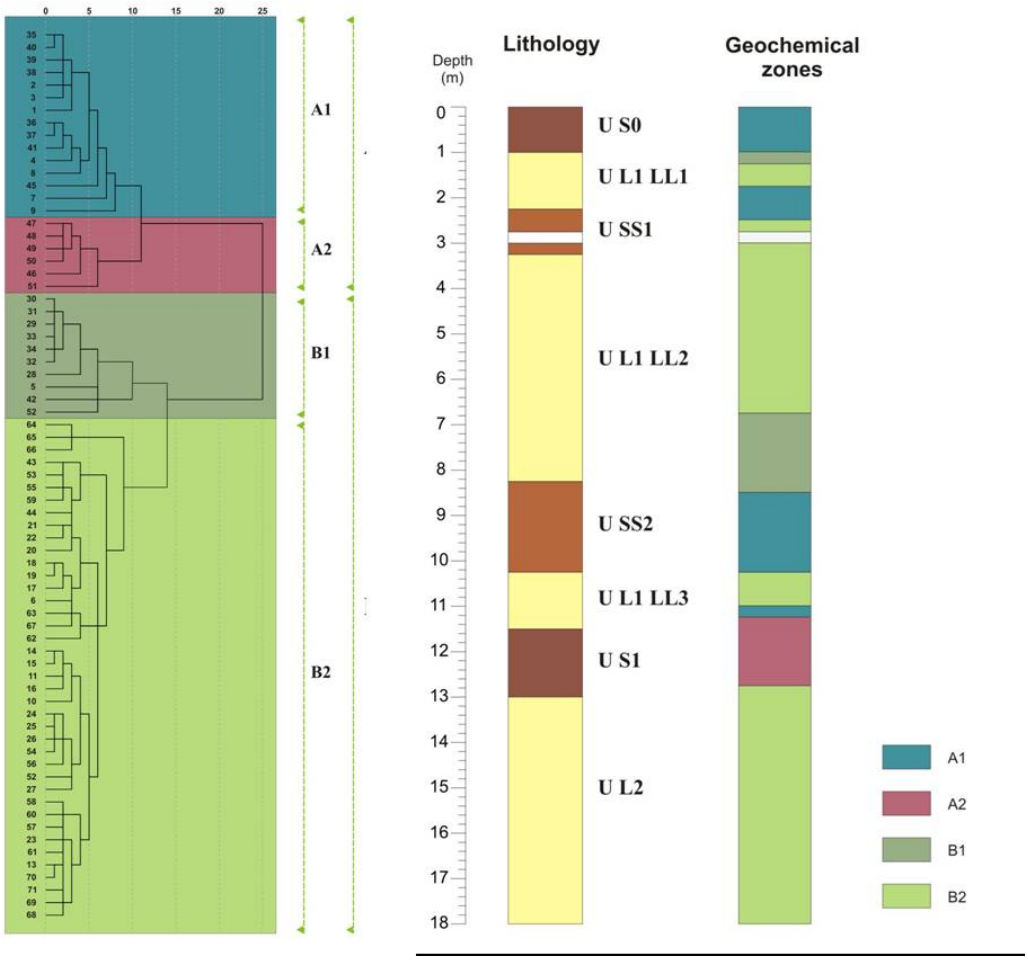

Figure 3: *Results of hierarchical clustering method*

5. ACKNOWLEDGEMENTS

The author would like to thank his mentors Pál Sümegi and János Geiger for the leading and all of their instructions. Special thanks to Bálint Csökmei for magnetic susceptibility measures and Janina Horváth for helping in statistical analysis.

6. REFERENCES

BENGTSSON L. & ENELL, M. (1986): Chemical analysis. -In: BERGLUND, B. E. (ed.): Handbook of Holocene Palaeoecology and Palaeohydrology, Blackburn Press, Chichester, 423–451.

DEAN, W. E. (1974): Determination of carbonate and organic matter in calcareous sediments and sedimentary rocks by loss on ignition: comparison with other methods. Journal of Sedimentary Petrology, 44, 242-248.

GALOVIĆ, L., FRECHEN M., PEH, Z., DURN, G. & HALAMIĆ, J. (2011): Loess/palaeosol section in Šarengrad, Croatia – A qualitative discussion on the correlation of the geochemical and magnetic susceptibility data. Quaternary International, 240, 1-13.

HEIRI, O., LOTTER, A. F. & LEMCKE, G. (2001): Loss on ignition as a method for estimating organic and carbonate content in sediments: reproducibility and comparability of results. Journal of Paleolimnology, 25, 101-110.

NG, S. L. & KING, R. H. (2004): Geochemistry of Lake Sediments as a Record of Environmental Change in a High Arctic Eatershed. Chemie der Erde, 64, 257-275.

Manipulation with spatial data to define neotectonic active faults in the Čačak – Kraljevo Basin (Serbia)

Ana MLADENOVIĆ, Dragana PETROVIĆ
University of Belgrade – Faculty of Mining and Geology, Đušina 7, 11000 Belgrade,
ana.mladenovic@rgf.bg.ac.rs, dragana.petrovic@rgf.bg.ac.rs

Abstract: Research has been done with the task of identifying structural and tectonic characteristics of the Čačak – Kraljevo basin, and in order to determine neotectonic active ruptures. In respect to defined tasks, mathematical transformations and analyses of different spatial data have been done. It was obtained that tectonic characteristics of the investigated area is complex, due to it's complex geotectonic setting. Four families of ruptures are dominating on the investigated area, with direction: NW-SE, WSW-ENE, NNW – SSE and N – S. Faults from the second and the fourth group are considered as neotectonic active.

Key words: neotectonics, Čačak-Kraljevo basin, morphometric maps, Landsat 7 imagery, map of temperatures.

1. INTRODUCTION

The aim of this research was to determine the tectonic fabric of the investigated area, using different types of transformed spatial data. The idea was to provide data about ruptures that can't be obtained by standard geological investigation. Pursuant to the order, the task was to identify neotectonic active ruptures on the investigated area, by analyzing Landsat 7 satellite image and map of temperatures derived from thermal bands of the satellite imagery, digital elevation model and morphometric maps, and map of vertical gradients of gravity acceleration.

Investigated area is located in western Serbia, in the Zapadna Morava Valley (**Figure 1**). The central part of the investigated area, Čačak – Kraljevo basin, is formed between mountain Jelica in the southwest, and dacite-andesite Kotlenik massif in the northeast. Southern parts of the terrain are in the area south of Ibar and Zapadna Morava and belong to the northern branches of the Goč and the Stolovi mountains. On the northwest, terrain extends to the southeastern parts of the Rudnik Mountain, which is connected to massif of the Kotlenik range.

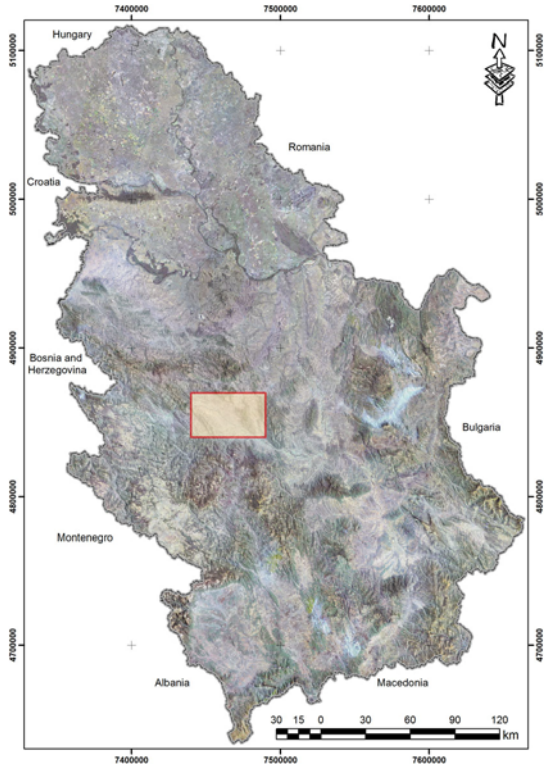

Figure 1: *Physical setting of the investigated area*

From the geological and geotectonic aspect, investigated area is situated in the complex area, which conditioned complex relationships between geological units in this area. In the geotectonic view, investigated area is situated on the contact of three big geotectonic units. According to Dimitrijević (2000), in the south-western parts of the investigation area Drina-Ivanjica Element (DIE) is situated, the central parts of the investigation area is dominated by Extern Vardar Zone (EVZ) and the

easternmost parts are in the Central Vardar Zone (CVZ). Two regional normal faults of the northwest-southeast direction, are dominating on the investigated area. On the end of Cretaceous, basin has been formed along to those faults (Novković and Terzin, 1957). Neotectonic evolution of this terrain was probably caused by several tectonic events, and the most important of them was extension during collapse of the Dinaride orogeny.

2. MATERIALS AND METHODS

Determining of tectonic fabric was done by combination of several different spatial bases. The main base was satellite imagery Landsat 7, with RGBI combination of spectral bands 4, 5, 7, 8. This satellite imagery passed through all stages of preprocessing and processing.

Also, a transformation of DN values of thermal bands in the relative values of temperature was obtained, using formulas in **Figure 2**.

X	Y	DN band 61
7513589,686	4780036,765	153
7513646,709	4780036,765	178
7513703,731	4780036,765	140
7513760,754	4780036,765	131
7513817,777	4780036,765	114
7513874,8	4780036,765	126
7513931,823	4780036,765	153
7513988,846	4780036,765	172

Radiance = ((LMAX-LMIN)/(QCALMAX-QCALMIN)) * (QCAL-QCALMIN) + LMIN

$QCAL_{MIN}$	= 1 (LPGS Products) = 0 (NLAPS Products)
$QCAL_{MAX}$	= 255
QCAL	= Digital Number

ETM+ Thermal Band Calibration Constants		
	Constant 1- K_1 watts/(meter squared * ster * μm)	Constant 2 - K_2 Kelvin
Landsat 7	666.09	1282.71

temperature:
$T=K_2/(\ln(K_1/L_\lambda+1))$

Figure 2: *Formulas used for temperature calculations*

Two neotectonic (morphometric) maps of this area have been formed – map of the relief energy and map of the relief anomalies. Detailed method was introduced by Marković et al. (2004). For purpose of this investigation, the original method was slightly modified. All calculations have been performed through PHP script (**Figure 3**). Formation of these maps consisted of

detailed analysis of digital elevation model for this area of research and calculations derived from pixel values (elevations). Calculations are very simple – for the defined matrix of pixels, one can calculate the highest and the lowest value. The relief energy map is derived by calculating difference between highest and lowest value of pixels in defined matrix and then normalising values in accordance to mean value of all pixels of DEM. During forming map of the relief anomalies, maximum value of pixels for defined matrix was calculated. Those values are substracted from the values of pixels for recent relief, and the result show what is the deviation between expected relief (model) and recent relief.

```
$f = file($argv[1]);
$what = $argv[2];
$window = intval($argv[3]);

foreach($f as $y => $line) {
    if(preg_match("/^[^0-9]/", $line)) continue;
    $line = strtr(rtrim($line), ",", ".");
    $line = explode(" ", $line);
    foreach($line as $x => $v) {
        $data[$y][$x] = floatval($v);
    }
}

$data = array_values($data);

//print_r($data);

$width = count($data[0]); $height = count($data);
$res = array();
for($y = 0; $y <= $height - $window; $y++) {
    for($x = 0; $x <= $width - $window; $x++) {
        $tmp = array();
        for($i = 0; $i < $window; $i++) {
            for($j = 0; $j < $window; $j++) {
                $tmp[] = $data[$y+$i][$x+$j];
            }
        }
        $res[$y][$x] = $what($tmp);
    }
}

$width = count($res[0]); $height = count($res);
foreach($res as $line) {
    echo strtr(implode(" ", $line), ".", ",") . "\n";
}
```

Figure 3: *PHP script used for calculations*

Second derivative of the gravity acceleration in the vertical direction, i.e. vertical gradient, was calculated. Second derivatives of the gravity acceleration have been calculated in order to delineate possible zones where vertical contacts of geological units can be located. These vertical contacts are often regarded as tectonic contacts. This method consisted of analyses of ruptures on different levels, in the way of calculating vertical gradients for different levels of analytical extended gravity field.

3. RESULTS AND INTERPRETATION

Two types of morphometric maps have been created: map of the relief energy and map of the relief anomalies. Both maps are derived by matrix analysis of digital elevation model data, whose resolution was 10 m. Dimension of matrix used was 9 times 9 pixels. Map of the relief energy is presented on the **Figure 4 - left**. Neotectonic active areas on this map are marked by extremely positive and extremely negative values, while neotectonic active ruptures are located between maximum and minimum values.

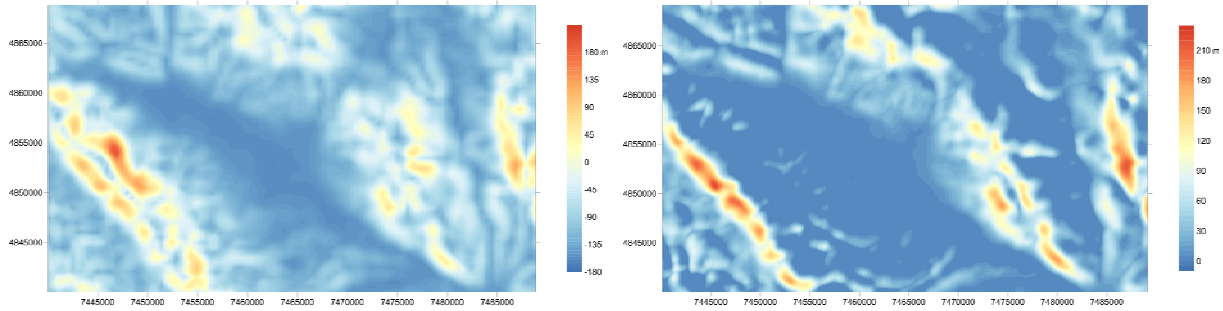

Figure 4: *Map of the relief energy, left; and Map of the relief anomalies, right*

Figure 4 – right shows map of the relief anomalies. Digital elevation model, which was input for matrix analysis had resolution of 10 m, while the matrix had dimension of 9 times 9 pixels. On the map of the relief anomalies, negative values are regarded as areas of relative inactivity, while neotectonic active areas are marked by positive values. Neotectonic active ruptures are located on the contacts between active and inactive areas.

Analysis and interpretation of all data used, was primarily focused on the determination of tectonic fabric of the investigated area. Interpretation of the tectonic fabric is shown on the **Figure 5**.

Map on **Figure 6 – left**, was obtained by a transformation of DN values in the relative values of temperature. Ruptures are located in areas where temperatures rapidly change their values. All ruptures couldn't be

determined by standard visual analyses of remote sensing. Based on the map of vertical gradients of gravity acceleration (**Figure 6 – right**), existence of other ruptures could be assumed, but it was necessary to confirm their existence in those places. Now, there are two maps which can confirm the existence of these ruptures in places, which are not highly visible on the satellite image in visual analysis.

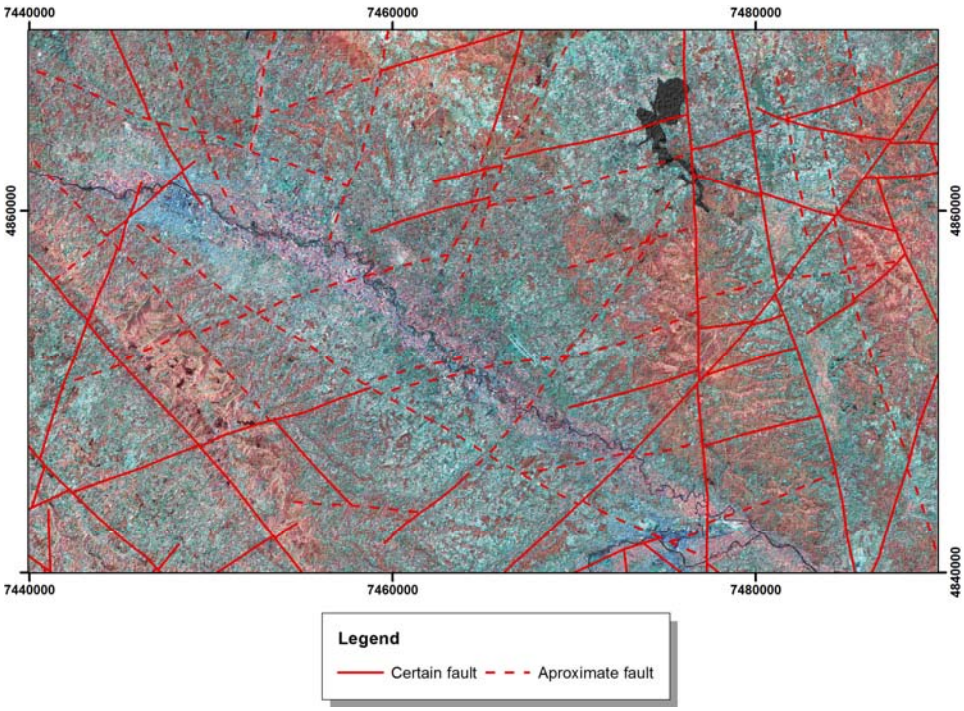

Figure 5: *Interpreted ruptures, shown on satellite imagery Landsat 7, combination of bands 4, 5, 7, 8*

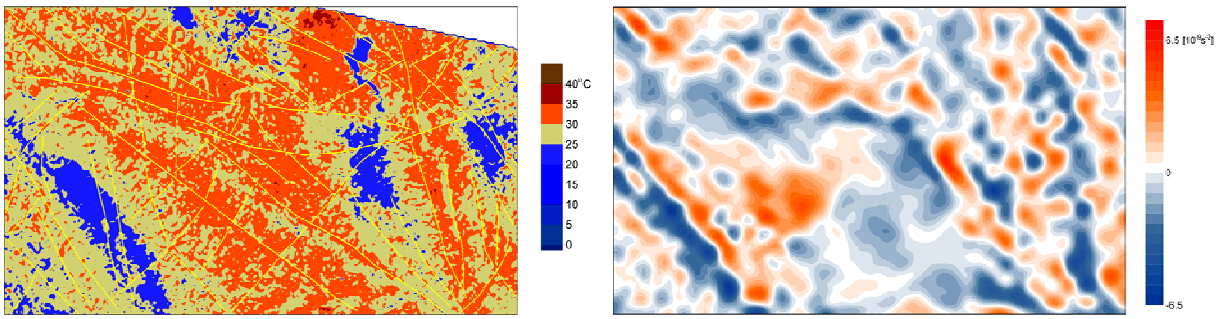

Figure 6: *Map of temperatures, left; and map of vertical gradients of gravity acceleration, right*

Interpretation of morphometric maps (**Figure 4**) is shown on the **Figure 7**. Here, neotectonic active faults are located. This is also confirmed by newest seismological data (Mladenović and Petrović, 2011).

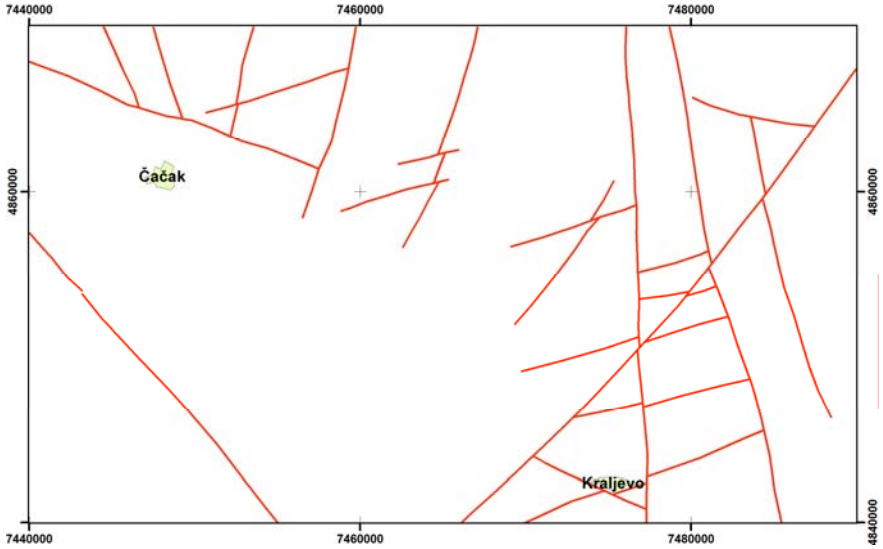

Figure 7: *Neotectonic active faults, according to morphometric maps*

Following group of ruptures can be seen on this interpretation:

- The oldest group of ruptures has NW-SE strike, and it can be seen in western edge of the basin. These are reverse faults, which were active during obduction of Vardar part of Tethys ocean, during Upper Cretaceous;
- Almost perpendicular to previous group, a group of ruptures with WSW-ENE strike is located. Considering map of vertical gradients of Bouguer anomalies, ruptures from this group can be interpreted as ruptures of subvertical to vertical dip, and as strike-slip faults;
- Čačak – Kraljevo basin was formed along faults of NNW – SSE strike. These are normal faults, activated in Campanian – Maastrichtian for the first time;
- Faults of N – S strike have been activated in Miocene. Along these faults, volcanic rocks from Borač – Kotlenik range have been extruded. Stress conditions during this volcanic episode were most probably extensional, because of collapse of Dinaride orogeny.

4. CONCLUSION

Tectonic characteristics of the investigated area are determined by designing, analysing and interpreting of different spatial data. Tectonic characteristics of the investigated area are complex, due to it's complex geotectonic setting. Kinematics and dip angles of the ruptures were obtained from the combination of standard visual methods and mathematically transformed standard spatial data. It is concluded that there are four main groups of ruptures were active on the investigated area. The oldest faults are formed in compressional conditions, and after this phase, most probably only extensional conditions were active in this area.

5. ACKNOWLEDGEMENT

Authors want to thank to Serbian Geological Society and it's president, Prof. Nenad Banjac, for help during preparation of this paper for the congress.

6. REFERENCES

1. DIMITRIJEVIĆ, M. (2000): Geology of Yugoslavia. -Geological Institute of Serbia, Belgrade, 187 p.
2. MARKOVIĆ, M., PAVLOVIĆ, R. & ČUPKOVIĆ, T. (2004): Geomorfologija. - Zavod za udžbenike i nastavna sredstva, Beograd, 461 p.
3. MLADENOVIĆ, A. & PETROVIĆ, D. (2011): Stress Condition Determination Based on Focal Mechanism Data: A Case Study on Kraljevo Earthquake. 6th Congress of Balkan Geophysical Society, Budapest, Proceedings, electronic edition (available through EAGE EarthDoc)
4. NOVKOVIĆ, M. & TERZIN, V. (1957): Geološki prikaz zapadno-moravskog tercijarnog basena. Fond stručne literature Zavoda za geološka i geofizička istraživanja, Beograd.

Geomathematical characterization of special and conventional core analyses in the Endrőd-II (Szarvas) Field

Katalin SÁRI, University of Szeged, Department of Geology and Palaeontology, 6722 Szeged, Egyetem utca 2-6., sarikatoca@gmail.com

Abstract: The Endrőd-II (Szarvas) Field is a hydrocarbon reservoir situated in the central part of the Pannonian basin. There are 37 boreholes in the field; core analyses and CT measurements are available. The purpose of this study was to build up small-scale genetic models of the reservoir by comparing the small and medium scale information derived from special and conventional core analyses, CT measurements and well logs. For the numerical solution several one and multivariable statistical methods were used to describe one and multidimensional similarities. Finally a multivariable identifying model summarizes the information gained in different scales. This model can be regarded as a tool for classifying new information according to the genetic hierarchy identified.

Key words: geomathematics, core analysis, CT measurement, well log.

1. INTRODUCTION

The Endrőd-II (Szarvas) Field is a hydrocarbon reservoir situated in the central part of the Pannonian basin. This field consists of several individual deep water fan-type rock bodies (Geiger et al., 2004).

The purpose of this study was to build up small-scale genetic models of the reservoir by comparing the small and medium scale information derived from special and conventional core analyses, CT measurements and well logs.

2. MATERIAL AND METHODS

There are 37 boreholes in the Endrőd-II (Szarvas) Field (**Figure 1**). Core measurements are available from twenty wells and CT measurements from three wells.

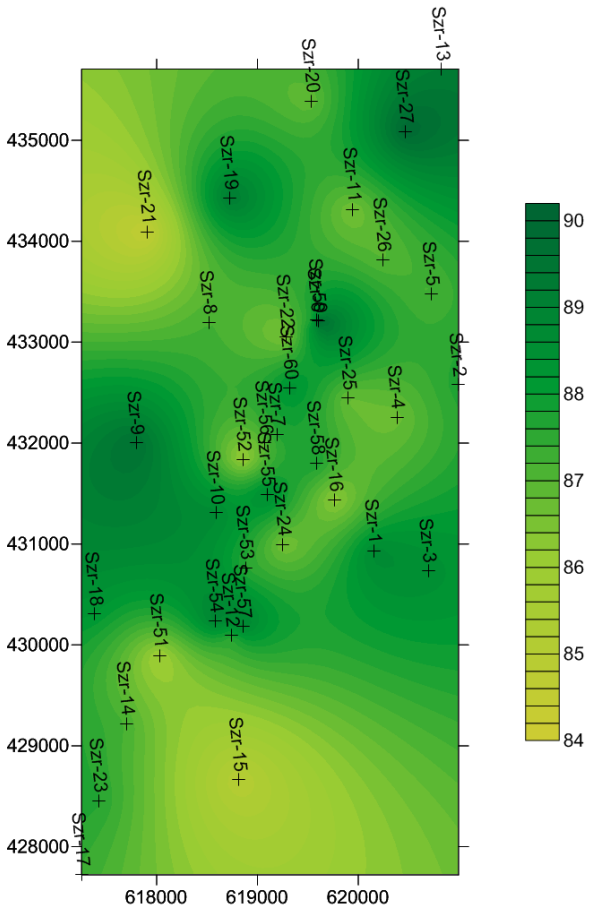

Figure 1: *Localization of the boreholes*

At first porosity and permeability was analysed for each rock type and rock body in dataset. The mean, confidence interval of mean, median, standard deviation, distribution, outliers and extremes were calculated and compared to other rock fields.

Mercury porosimetry results were also available. To analyse the pore size distribution, nine pore size intervals with quasi-equal frequency on a logarithmic scale were determined. The distribution, mean, standard deviation and mode were calculated for each rock type and rock body.

The following features were analysed by correlation, factor and cluster analyses for each rock type: porosity; horizontal and vertical permeability; the mean, standard deviation and mode of pore size distribution; the frequency of the nine pore size intervals. After these analyses the clusters were put back to the rock column. By explaining the well logs, a genetic model was built up. Connections were searched for between the electro facies, CT measurements and core analyses.

3. RESULTS

The analysis showed that the distribution of porosity in every rock type was asymmetric; see box plots on **Figure 2**. It also came out that distribution of sand and silt samples had two modes. Additionally, the horizontal and vertical permeabilities had very similar distribution, but the vertical one was always lower (**Figure 3**).

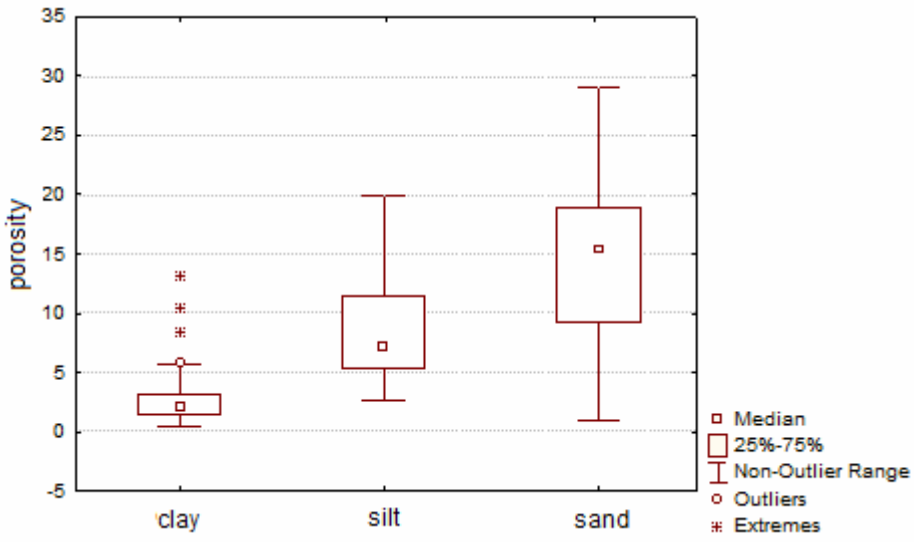

Figure 2: *Porosity for each rock type*

The porosity and permeability were analysed also for each rock body. The distributions of rock bodies were compared to each other and to all the samples. Not every rock type was represented in every rock body; this made the analysis more complicated.

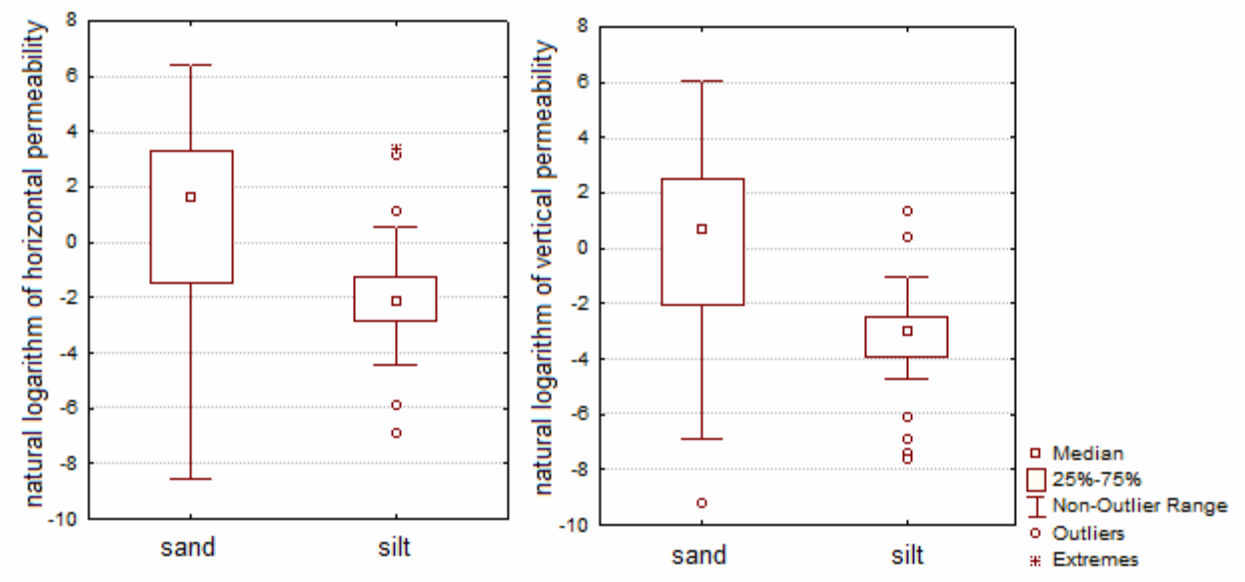

Figure 3: *Natural logarithm of permeability for each rock type*

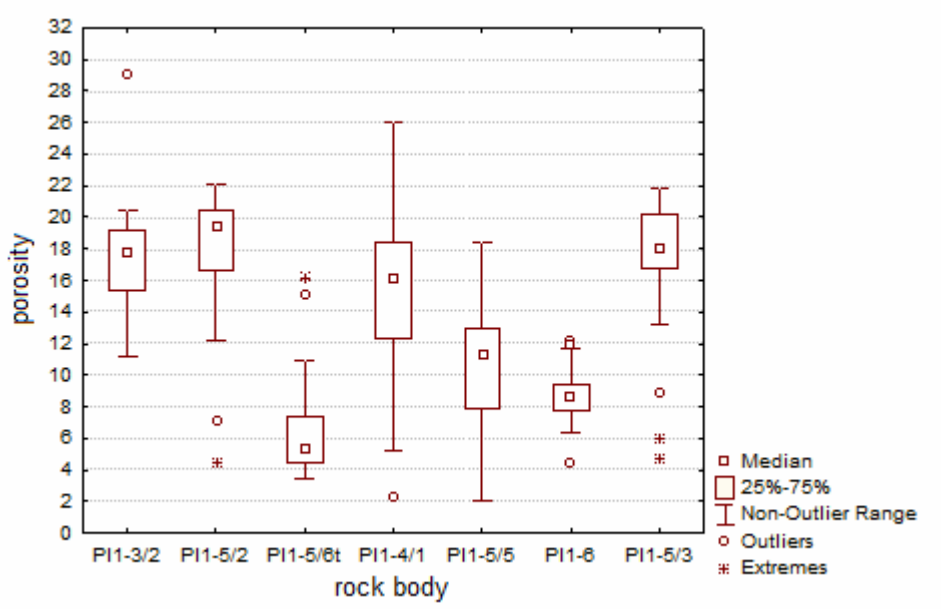

Figure 4: *Distribution of porosity of sand samples for each rock bodies*

While comparing the porosity and permeability of sand samples, three rock bodies (Pl1-3/2, Pl1-5/2 and Pl1-5/3) seemed to be similar (**Figure 4**), these belonged to the larger mode. Another three rock bodies form the smaller mode. Rock body Pl1-4/1 belonged to none of the modes. Additionally, by analysing the porosity of silts, similar rock bodies were

found. Clay samples were insufficient to analyse for each rock body. The pore size distributions of sands and silts had two modes (**Figure 5**), which were also represented in some rock bodies. This may be caused by different facies.

Correlation and factor analyses were only possible in case of sands. Parametric and non-parametric correlation were calculated and compared. Through the correlations came out that the porosity, permeability, the mean, mode and standard deviation of the pore size distribution were closely connected to each other. The smallest and the largest pores were also in a relationship with these and with each other but not with the medium size pores. In the result of the factor analysis, these medium size pores formed a distinct factor. A cluster analysis was carried out, then the clusters were put back to the rock column.

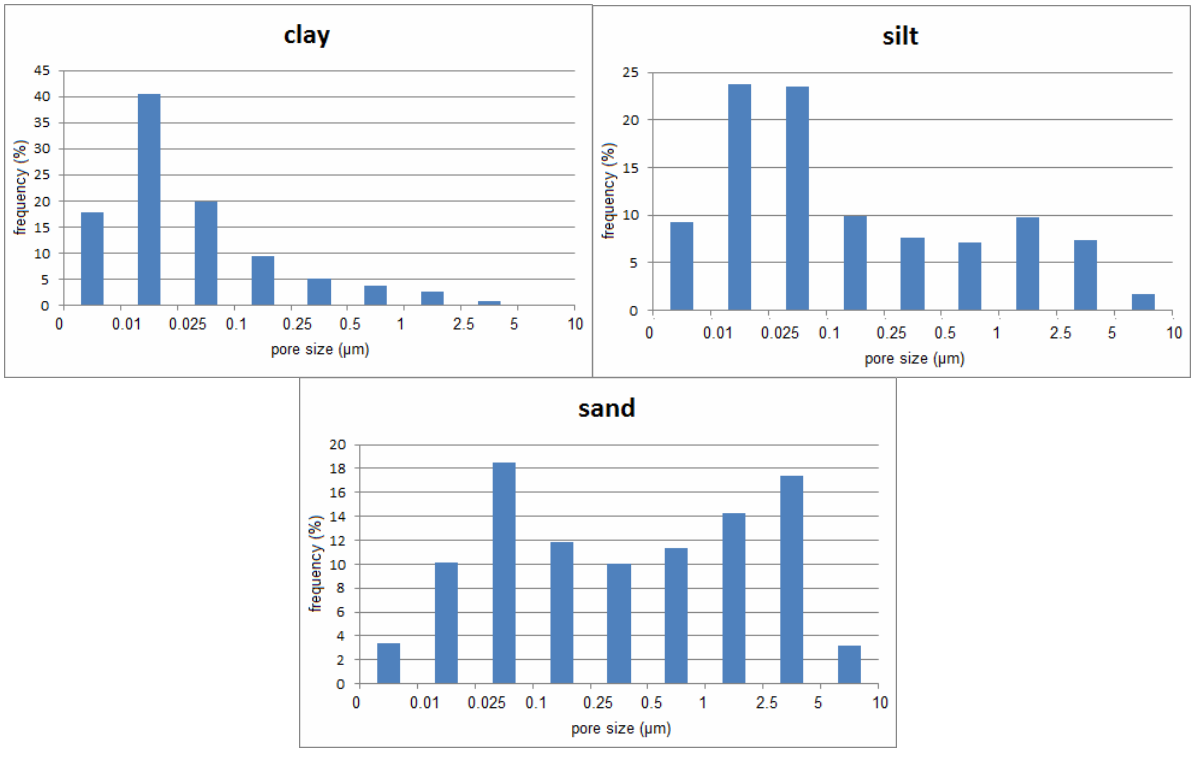

Figure 5: *Pore size distribution for each rock type*

4. CONCLUSIONS

For the numerical solution several one and multivariable statistical methods were used to describe one and multidimensional similarities. Finally a multivariable identifying model summarizes the information gained in different scales. This model can be regarded as a tool for classifying new information according to the genetic hierarchy identified.

5. ACKNOWLEDGEMENT

I would like to thank my supervisor, János Geiger.

6. REFERENCES

GEIGER, J., KORMOS, L. & POLLNER, L. (2004): Az Endrőd-II mező Pl1-2, Pl1-3, Pl1-4 és Pl1-5 kőzettestében levő telepek rezervoár geológiai reambulációja [*Reservoir geological reambulation of Pl1-2, Pl1-3, Pl1-4 and Pl1-5 rock bodies in Endrőd-II Field*] – MOL Open-File Report, Szeged.

3D facies analysis with combination of classic and stochastic sedimentological applications

Andrea WÁGENHOFFER

University of Szeged, Department of Geology and Palaeontology, 6722 Szeged, Egyetem utca 2-6., wagenhofferandrea@gmail.com

Abstract: The joint application of classic and stochastic sedimentological might bring a solution to 3D facies analysis. 13 boreholes can be found in the study area and several well logs were measured in these wells. One of the observed wells has a core, which core description occurred in a traditional sedimentological way. The analysis and the earlier studies suggested a beach area as depositional system. Dynamic and continuous sedimentation were found in this area. The geophysical dataset consists of spontaneous potential (SP) and gamma ray (GR) measurements. The porosity and the shale volume are calculated from these data. For identifying some electrolithological categories, the shale porosity correlation chart was used. Algorithms of Inverse Distance Weights and Lithobending were used to build a meaningful 3D porosity and lithological model correspondingly within the frame of RockWorks. The models showed a beach area with beach slopes.

Keywords: Beach profile, Porosity and lithological model, 3D facies analysis.

1. THE STUDY AREA

The area region is located in the southeastern part of Hungary, this is also known for its oil fields, oil and gas wells of the Hungarian Oil Company (MOL). This depositional system was beach area of the Lake Pannon. The tree zones within the profile that were subjected to rather different

conditions: backshore, foreshore and nearshore. The nearshore zone is characterized by rather continuous sand bars that are nearly parallel to the beach (Davis, R. A. Jr., 1978; Reading, H.G., 1978).

2. USED DATA AND METHODS

One of the observed wells has a core with 9.5 meter of thickness, which core description occurred in a traditional sedimentological way. The core consists of typical bedforms: massive structureless sandstone, parallel laminated silt and ripple cross-laminated silt. The observed structures indicate slides and slumps in the sequence.

Three main periods were identified in core a description study, which was caused by unbalanced character of erosion and sedimentation (**Figure 1**). In the first and the third cycles the sedimentation was more intense then the erosion, that is why thick massive sandstones were deposited. The second cycle indicates less intense sedimentation, which way reflected by typical silt and clay grain sizes (Geiger, J., verbal communication, 2012).

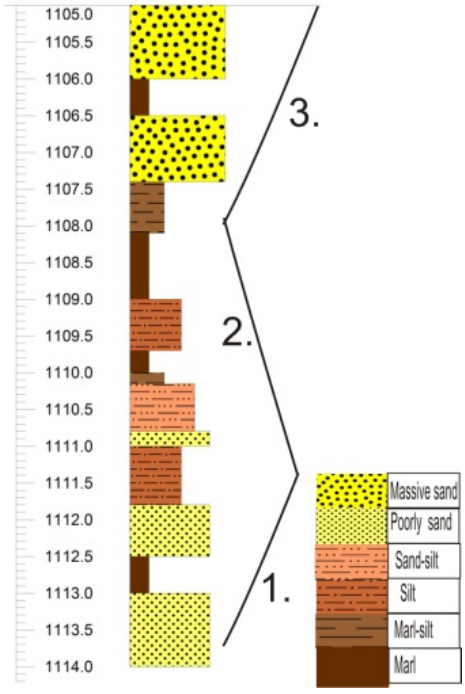

Figure 1: *Lithology of core with the three cycles*

The geophysical dataset consists of spontaneous potential (SP) and gamma ray (GR) measurements. The porosity and the shale volume are calculated from these data. For identifying some electrolithological categories, the shale porosity correlation chart was used. The corresponding electrolitholocal units were as follows: massive/clear sandstones, poorly sorted/dirty sandstones, silty-sandstones and marls.

To build a meaningful 3D porosity and lithological model algorithms of Inverse Distance Weights and Lithobending were used correspondingly within the frame of RockWorks. The volume rendering processed to visualize the 3D geometry of beach/sand bar and redeposited sand bodies (**Figure 2**).

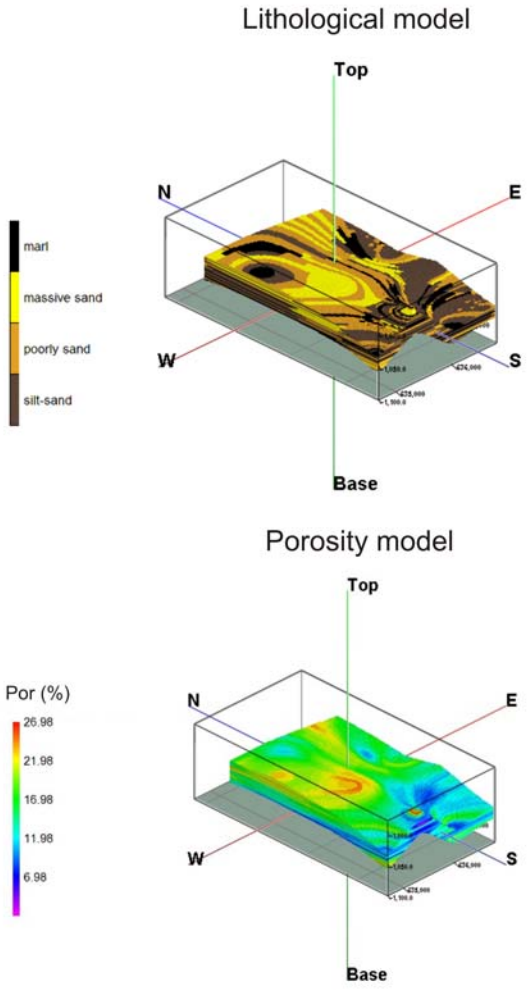

Figure 2: *3D porosity and lithological models*

3. DISCUSSION

The 3D models and the core analysis showed the depositional environment. Three main cycles were identified in core, the reason which was caused by unbalanced character of erosion and sedimentation. The beach development and the corresponding geometrical variations were demonstrated by 3D sections (**Figure 3)**.

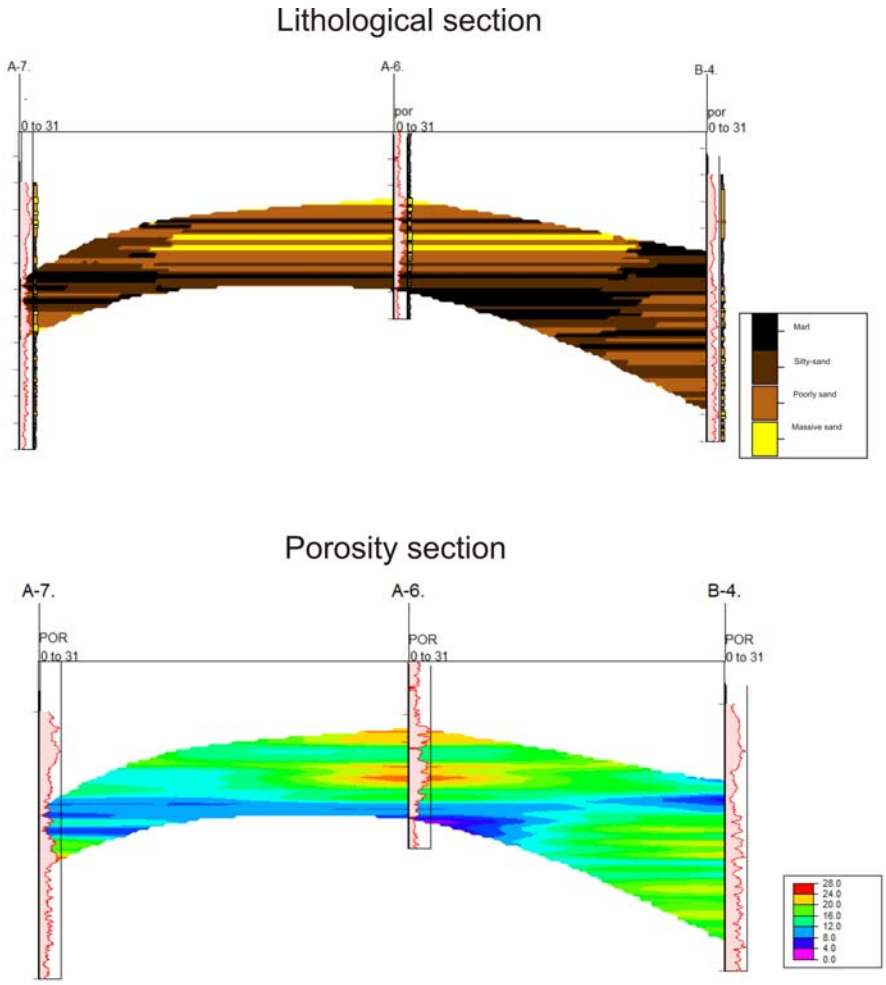

Figure 3: *Redeposited sandstones are in A-7. and B-4.boreholes and bar sandstone is in A-6.*

The results suggested that depositional strike of the beach was NW-SE, and the last reworking process happed on the beach slopes (**Figure 4**).

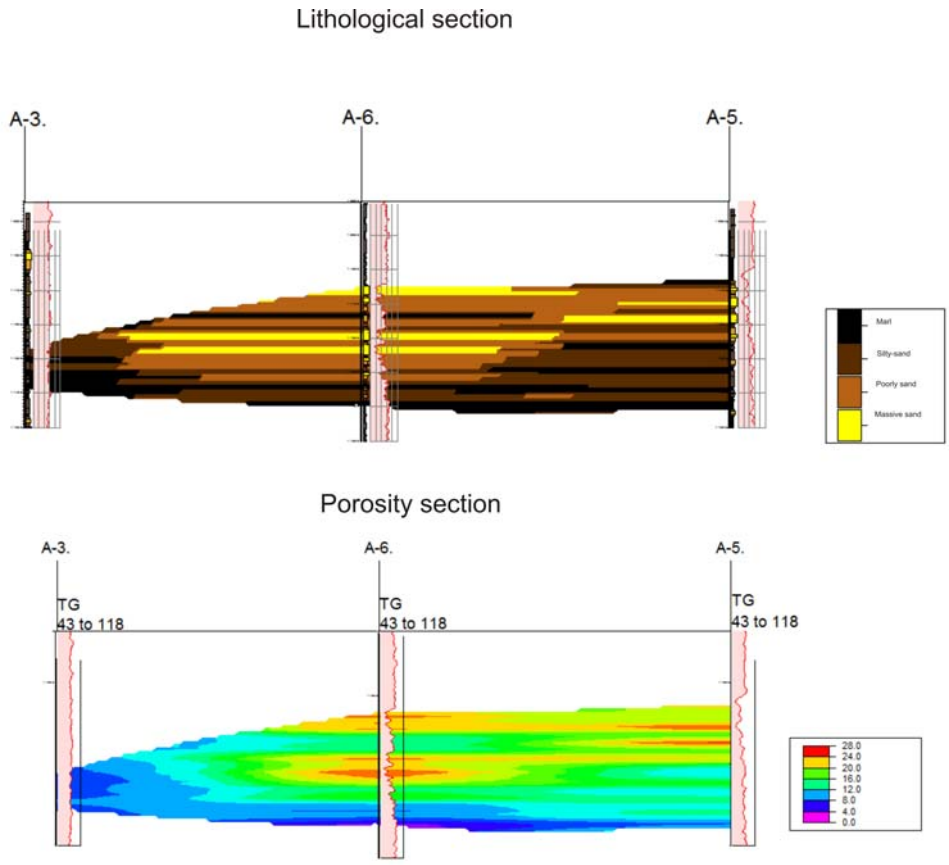

***Figure 4**: Beach slope is in A-3. and bar sandstones are in A-6 and A-5 boreholes*

4. ACKNOWLEDGMENT

The author would like to thank MOL Plc. for providing the data used in this study. Furthermore, I express my gratitude to János Geiger (from Department of Geology and Palaeontology, University of Szeged, Hungary) and Balázs Kiss (from MOL Plc.) for their useful suggestions.

5. REFERENCES

DAVIS R.A. Jr. (1978): Coastal Sedimentary Environment. Springer-Verlag.pp. 237-280.

READING H.G. (1978): Sedimentary Environments and Facies. Elsevier Press, New York, p. 557.

Appendix

(Submissions as pure abstracts)

Distribution of chemical elements in alkaline lake sediments at Fehér-Lake, Szeged, Hungary

Gábor BOZSÓ[1*], Elemér PÁL-MOLNÁR[1], László HALMOS[1],
Alexandra GÓDOR[1], Nóra CZIRBUS[1]
[1]Department of Mineralogy, Geochemistry and Petrology, University of Szeged, H-6701 Szeged, P.O. Box 651, Hungary
[*] corresponding author. Tel.: +36 62 544641; fax: +36 62 426479; e-mail: bozso.gabor@geo.u-szeged.hu

Abstract: The primary aim of the present research was to shed light on the distribution of chemical elements important from an environmental perspective in saline lake sediments (Fehér-Lake, Szeged, Hungary), characterised by similar geology but different hydrology and anthropogenic influence. It was proven – based on the results of the main component analysis - that the element distribution in the alkaline sediments of Lake Fehér is primarily determined by two background processes. The weathering of loess, forming the base rock of sediments, is the most significant factor in this respect. This process is the most relevant in the upper 100 cm zone of the sediment sequence where water table and pH fluctuation is the most intensive. The second background process (water level fluctuation and the migration of highly soluble weathering products) is in close relation with the previous one, and causes salt enrichment also in the upper zone.

Geochemical investigation of red clay rendzina soils (Aggtelek Karst, NE Hungary)

Nóra CZIRBUS[1], Tünde NYILAS[1], Lóránt BÍRÓ[1], Klaudia KISS[2], Magdolna HETÉNYI[1], Gábor BOZSÓ[1]

[1]University of Szeged, Department of Mineralogy, Geochemistry and Petrology H-6701, Szeged PO Box 651, Hungary

[2]Eötvös Lóránd University, Department of Environmental and Landscape Ecology H-1117 Budapest, Pázmány Péter prom. 1./c, Hungary

e-mail: czirbus.nora@geo.u-szeged.hu

Abstract: The organic and inorganic geochemical examination of soils allow us to study different soil-chemical processes and to determine geochemical boundaries. The aim of this work was to investigate mineral and organic geochemical characteristics of red clay rendzina soils and its soil of slope sediments. By combined interpretation of mineral composition and elemental distribution of the samples we show the effects of parent material and climatic conditions during pedogenesis. Using Rock-Eval pyrolysis the amount, quality and maturity of the soil organic matter and the turnover of biopolymers to humic substances were determined. Integration of geochemical data help us to point out geochemical lines in the soil profile. In addition, our results suggest that we can determine borders of the mining area by using statistics of geochemical data. The project was supported by the Hungarian National Science Foundation (K 81181).

Key words: red clay rendzina, Rock-Eval pyrolysis, XRF, XRD.

Uncertainty of porosity values calculated on the basis of He-pycnometry

Ferenc FEDOR

GEOCHEM Ltd., Hungary, fedor.ferenc@geochem-ltd.eu

Abstract: Porosity is one of the most important parameters of reservoir characterization. Estimation of porosity can be done in many different indirect ways such as from well logs, different laboratory measurements, etc. In the most cases the uncertainty of porosity cannot be estimated in an adequate way because of information gaps which originate from the different scales of estimation, the measurements and parameter calculation. In large (field) scale stochastic simulation can be applied to handle the uncertainty of porosity of different flow units and most of the time it is working. However, particularly in case of very tight reservoirs, like tight gas zones and geosituation of HLW repository that are more homogeneous rock bodies, the uncertainty and the estimated porosity are in the same scale. In these latter cases the role of laboratory analysis and estimation of porosity are up valued and the estimation of uncertainty should be realized. Generally, the estimation of matrix porosity can be achieved by He-pycnometry on the basis of the Boyle-Mariott Law. If the temperature is constant, the geometry of analysed core plugs are well defined and all the volumes used during the measurement including calibration standards are well known then the porosity of a given plug can be calculated. If the expected values of all parameters in this parameter field exist and so the standard deviation of all parameters can be calculated, then the absolute and relative error of porosity values can also be estimated.

Key words: porosity, uncertainty, He-pycnometry.

Nomen est omen: environment-constrained morphological variability of the endemic thalassoid planorbid *Gyraulus varians varians* (Fuchs) from ancient Lake Pannon, Hungary

Sándor GULYÁS[1] Pál SÜMEGI[1], Imre MAGYAR[2], Dana H. GEARY[3]

[1]University of Szeged, Department of Geology and Paleontology, H-6722 Szeged, Egyetem u.2-6. Hungary, gulyas-sandor@t-online.hu

[2]MOL Hungarian Petroleum Ltd, Budapest Hungary

[3]University of Wisconsin, Madison, USA

Abstract: The endemic Lake Pannon planorbid taxon *Gyraulus varians varians* is characterized by large scale morphological variety generally characteristic of marine specimens. This variety must reflect some special environmental adaptation. In order to understand this adaptation, the morphology must be quantitatively accurately assessed. For this purpose altogether 49 specimens deriving from 4 localities of Lake Pannon were photographed digitally in a lateral view. The main shape characteristics of the shells were assessed using geometric morphometric techniques relying on 12 landmark points of lateral shell views. The outline coordinates were transformed to Procrustes coordinates by removing position, size and rotation using the approach of least squares fit. The received Procrustes coordinates were taken to capture the morphology of the individual specimens and were subjected to further multivariate statistical analysis. The degree of distinction among morphotypes of the studied localities was assessed and displayed graphically using discriminant analysis and canonical variate analysis. Landmark warps were calculated to allow for the interactive plotting of shape deformations as a function of position along the discriminant axis as thin-plate spline deformations. This visualization also allowed for the interpretation of the biological meaning of morphotype shifts and separations along the discriminant axes. Size was calculated as centroid

size for each specimen (Euclidean norm of the distances from all landmarks to the centroid). Size comparisons were performed using non-parametric tests of variance. According to our findings the specimens of the younger Radmanest site differ significantly from those of the other older sites. Differences were linked to different hydraulic parameters of the habitats recorded in shell ultrastructures. Funding of grants TÁMOP-4.2.1/B-09/1/KONV-2010-0005 acknowledged.

Key words: geometric morphometrics, shape analysis, planorbids, Lake Pannon, Hungary.

Morphological variability of the invasive thermophylous mussel *Corbicula fluminalis* from the Pleistocene of Hungary using geometric morphometric techniques

Sándor GULYÁS[1], Pál SÜMEGI[1], Zoltán SZALÓKI[1]

[1]University of Szeged, Department of Geology and Paleontology, H-6722 Szeged, Egyetem u.2-6. Hungary, gulyas-sandor@t-online.hu

Abstract: The mussel taxon *Corbicula fluminea* is an invasive, thermophylous element recorded in the Lower Pleistocene fluvial deposits of the Carpathian Basin. Some specimens from the interglacials of the Upper Pleistocene have also been recorded. In order to see how this form adapted to the paleoenvironment of the ice age the morphology must be quantitatively accurately assessed. For this purpose ca. 180 specimens deriving from 2 Lower Pleistocene and 2 Upper Pleistocene localities were photographed digitally. The main shape characteristics of the shells were assessed using geometric morphometric techniques relying on Elliptical Fourier shape analysis of the shell outlines. The received harmonic components were taken to capture the morphology of the individual specimens and were subjected to further multivariate statistical analysis. The degree of distinction among morphotypes of the studied localities was assessed and displayed graphically using discriminant analysis and canonical variate analysis. Inverse fourier transform of the harmonic components were calculated to allow for the interactive plotting of shape deformations as a function of position along the discriminant axis. This visualization also allowed for the interpretation of the biological meaning of morphotype shifts and separations along the discriminant axes. Size was calculated as centroid size for each specimen (Euclidean norm of the distances from all landmarks to the centroid). Size comparisons were performed using non-parametric tests of variance (Kruskal-Wallis) with Mann-Whitney U pairwise comparison. According to our findings the specimens of the Younger Pleistocene differ

somewhat from those of the other older sites. Differences were seen in flatness of the shell and prosogyrousity of the beaks. Funding of grants TÁMOP-4.2.1/B-09/1/KONV-2010-0005 and TÉT_10-1-2011-0039 acknowledged.

Key words: geometric morphometrics, elliptical fourier shape analysis, mussels, Pleistocene, Hungary.

4th HR-HU and 15th HU geomathematical congress "Geomathematics as Geoscience" | 23-25 May, 2012

Applicability of PSD for numerical rock modelling

Szabina GRUND[1]*, Judit TÓTH Dr.[2], László GYŐRY[3]

[1] MOL Plc. EPD IFA Engineering & Technology Development, University of Szeged, Department of Geology and Palaentology (PhD studies)

[2] MOL Plc. EPD IFA Engineering & Technology Development

[3] MOL Plc. EPD IFA Exploration Laboratories

Abstract: Pore structure information of reservoir rocks are generally acquired from thin section investigation and mercury injection data. Obtaining SCAL data is highly expensive, the analyses and interpretation of the data take a lot of time. Consequently the numerical rock modelling techniques have gained considerable attention recently. Data for creating rock models can be gained by several methods, for example by processing of thin section description, XRD, CT, microCT, SEM, LSCM, MRI, PSD or log (e.g. porosity log) data. From these we present the applicability of PSD (Particle Size Distribution). Challenges of the method are derived from the irregular shape of grains and the selection of the appropriate rock sample disintegration technique.All different techniques have advantages and disadvantages, but the laser scattering method has an overall performance advantage in respect of analytical time and reproducibility. On the bases of the experiences, LALLS (Low Angle Laser Light Scattering) PSD analytical data can be applied for numerical rock models, thus for iCore model as a primary data source.We started PSD investigation of samples of AP-13 reservoir in order to complete the previous results.

Key words: PSD, numerical rock modelling, AP-13.

iCore – numerical rock and pore model

Laszlo GYORY[1], Gergely KRISTOF[2], Janos GEIGER[3]

[1]MOL Plc E&P IFA Exploration Laboratories, Korosi ut 84 Szolnok, Hungary, e-mail: lgyory@mol.hu

[2]Budapest University of Technology and Economics, Department of Fluid Mechanics, Bertalan Lajos u 4-6 Budapest, Hungary

[3]University of Szeged, Department of Geology and Paleontology. Egyetem u.2, Szeged, Hungary

Abstract: iCore as an R&D project itself looks back on two years preparatory and development work but is supported by many years of experience and expertise in core analyses, geological modeling and fluid mechanics. The basic idea of the project was conceived driven by the recognition of the elementary need especially in those situations when exploration and production developments are pushed towards the extremes and the lack of sufficient data might results in increasing risks of failure. Some parts of the projects are put on well established knowledge and concepts in geology and core analyses while other parts of it are brand new in our industrial practice therefore they require intensive applied research regarding its intentions and tools and applications. The development is realized by the cooperation of three organizations: MOL and two Hungarian universities, Budapest University of Technology and University of Szeged. The goal of the project is to develop a numerical rock and pore model and using this model that basically represents unconsolidated formations for describing its pore structure and flow simulations. The rock model is implemented by specifying the geological setting of the formation and creating the representative pattern of layers consisting of particles of specific shapes and size. These data are acquired by laboratory measurements using samples taken from the formation in question and CT measurements. The pattern is then filled up by these particles using a packing generating method based on computer algorithm developed by the project participants.

The pore structure is then extracted from the numerical rock model and various measurements can be performed on it to characterize its features using computer programs also developed by MOL and the participating universities. This pore structure is then the subject of pore size level flow simulations as well that is achieved using the lattice-Boltzmann method that has never been applied before in our industrial practice.

Key words: random packing, numerical modeling, particle size, pore size distribution, lattice-Boltzmann.

Handling of Uncertainties in Safety Assessment of Radioactive Waste Disposal Facilities

Zoltan NAGY
Public Limited Company for Radioactive Waste Management, HUNGARY

Abstract: Disposal of radioactive waste represents the final step in its management. The operator of the radioactive waste disposal facility is responsible for safety and must assess the safety of the facility. A key output from safety assessment is the identification of uncertainties that have the potential to undermine safety. Classification system of the uncertainties arises from the way safety assessment is implemented: (i) scenario uncertainties, (ii) model uncertainties, (iii) data/parameter uncertainties. The treatment of uncertainties related to future evolution of repository and future events passing off in the repository over long times (e.g. 1 000 000 years) represents a significant challenge for a post-closure safety case. For each specific scenario it is necessary to deal with uncertainties in the models and parameter values used. Although actions are undertaken to reduce uncertainties, there are always remaining uncertainties which have to be dealt with in such way that it is possible to draw conclusions from the results of the assessment and make decisions. The presentation gives an illustration of handling uncertainties in the safety assessment of the deep geological repository for radioactive waste set up in Bátaapáti 250 m below the surface in Hungary.

Complex examination of the effects of anthropogenic activity on wetlands

Gábor NAGY[1], András KIRÁLY[1], Tünde NYILAS[2], Lóránt Bíró[2]

[1] SoilChem Agricultural and Environmental Laboratory, H-6782 Mórahalom, Vállalkozók útja 1/b., e-mail: gabor.nagy@sclab.hu

[2] Department of Mineralogy Geochemistry and Petrology, University of Szeged H-6701 Szeged, PO Box: 651.

Abstract: Nowadays natural habitats are endangered because of human landscape-transformer processes and negative effects of climate change. Wetlands belong to the most vulnerable areas because low rate of anthropogenic effects can lead to significant and fast changes in these places. In the frame of the Hungary-Romania Cross-Border Co-operation Programme of the European Union we examined the dynamics of environmental processes and the anthropogenic effects in two watery habitats (a karst lake in Oradea, Romania and a salin lake near Mórahalom, Hungary). Paleoecological analysis, soil- and water-chemical measurements and geological examinations were carried out in the areas. The statistical analyses were based on the results of laboratory measurements and field studies. The presented examination is a part of a complex project that aims to classify ecological potential, to define the rate of degradation and to determine ecological function of the natural habitat.

Key words: wetland, factor analysis, environmental chemistry, karst lake, salin lake.

New paleoenvironmental data for the Middle and Late Pleistocene of the Carpathian Basin: preliminary results to the „longest" Danubian loess/paleosol sequence of modern Hungary: Udvari-2A

Pál SÜMEGI[1,2], Sándor GULYÁS[1], Gergő PERSAITS[1], Bálint CSÖKMEI[1]
[1]University of Szeged, Department of Geology and Paleontology, H-6722 Szeged, Egyetem u.2-6. Hungary, sumegi@geo.u-szeged.hu

Abstract: Predicting climate and environmental changes is one of the most significant challenges of current research in earth sciences. Long-term climatic changes at a resolution of several kys can be assessed by the careful investigation of various paleoarchives including terrestrial archives. Among terrestrial paleoarchives loess/paleosol sequences tend to be the most common and most prominent type of deposits of the Quaternary covering about 10-15% of the area of modern Hungary. A careful multiproxy analysis of loess/paleosol sequences yields us information about not only the fluctuations in past environmental components but a feedback of the local biota as well. Extensive loess sheets and loess plateus of several meters thickness accumulated in the Pannonian Basin, especially in its southern part, which present ideal archives of long-term macro and meso-scale fluctuations of the climate and environment for the Middle and Late Pleistocene. A recently published site of Udvari-2A located in the Tolna-Hegyhát (Tolna Hills) area of the Transdanubian Hills in SW Hungary is outstanding from this point as the borehole deepened in 1996 and originally described by Koloszár (1997) represents the thickest and probably most complete loess/paleosol sequence of Danubian loess from Hungary covering the past 1100 kys. According to the preliminary clay and carbonate mineral analysis of selected loess and paleosol samples by Földváry & Kovács-Pálffy

(2002), the sequence seems to be less weathered than other LP sequences studied from nearby Danubian sites of Hungary. In order to assess the degree of weathering for different sedimentary components marking fluctuations in the temperature and humidity and to shed light onto the nature of the paleosols and pedogenesis identified on the basis of macroscopic lithological description of the profile detailed geophysical (MS), geochemical, phytolith and malacological analyses of selected loess-paleosol samples of the sequence was carried out. This paper presents the initial results of this work. Funding of grants TÁMOP-4.2.1/B-09/1/KONV-2010-0005 and TÉT_10-1-2011-0039 acknowledged.

Key words Quaternary, paleoenvironment, multproxy analysis, multivariate statistics, Hungary.